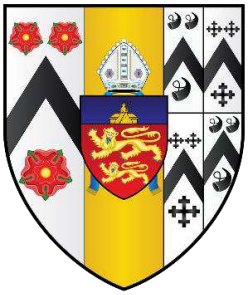
MECHANISMS OF INDUCTION OF TYPE I/III INTERFERONS IN CANCER CELLS BY IONIZING RADIATION AND THE ROLE OF TUMOUR CELL-DERIVED TYPE I IFN AND TYPE I IFN SIGNALLING IN ANTI-TUMOUR IMMUNE RESPONSE

Jianzhou Chen, M.D., M.S. (Hons)

Brasenose College



Thesis submitted to the Medical Sciences Division of the University of Oxford in partial fulfilment of the requirements for the degree of Doctor of Philosophy



CRUK/MRC Oxford Institute for Radiation Oncology

Department of Oncology

University of Oxford

Trinity 2018

Word count: 25803

Abstract

Mechanisms Of Induction Of Type I/III Interferons In Cancer Cells By Ionizing Radiation And The Role Of Tumour Cell-Derived Type I IFN And Type I IFN Signalling In Anti-Tumour Immune Response

Submitted for the degree of Doctor of Philosophy

Jianzhou Chen, Brasenose College, Trinity term 2018

Interferons (IFNs) are a group of cytokines that have been shown to play an important role in both radiotherapy and the anti-tumour immune response. How ionizing radiation (IR) induces IFNs in the tumour is still not fully understood. We found that IR directly induced dose- and time-dependent upregulation of I/III IFNs in cancer cells. This induction occurs via cytosolic DNA sensors-STING-TBK1-IRFs signalling axis and to less extent, the NF-κB pathway in colorectal cancer cells. Furthermore, Type I/III acts as a feedback loop to further enhance IFNs expression via upregulating key factors in the signalling axis.

In vivo, cancer cells not the immune cells actually have the greatest contribution to overall intratumoural production of type I IFN in the MC38 tumours. By using a variety of animal models, we demonstrated that tumour-derived type I IFN has critical contribution to the anti-tumour immune response at local site. Strikingly and unexpectedly, abrogation of type I IFN signalling via IFNAR1 KO in cancer cells led to remarkable improvement of tumour response to IR. This phenomenon is mainly driven by significantly enhanced susceptibility of cancer cells to CD8+ T cell-mediated killing via PD-L1/Galectin-9-independent mechanisms. Overall, these findings add another layer of complexity to the understanding of irradiation-induced anti-tumour immunity and cancer immune evasion, and may provide novel insights into combinational therapy of radiotherapy and immunotherapy.

In loving memory of my dear mother, Ruhua Xie,

and Grandma Liqing Zhuang

Acknowledgements

Firstly, I would like to thank my supervisors Profs. Ruth Muschel and Gillies MeKenna for their great guidance and support. I am very grateful for the precious opportunity they have given to me. It has been a great learning experience filled with challenges and inspirations. The knowledges and research principles that I have learnt from them will continue to guide and help me in my future career.

I sincerely appreciate my colleagues' kind supports. I did not have any laboratory experiences when I started my project. It's their support that help me go through all kind of issues and troubles: Dr. Yunhong Cao for general laboratory techniques and plasmid cloning, Drs. Su Yin Lim, Thomas Tapmeier, Chad McKee, Serena Lucotti, Pavitra Kannan and Jenny Vermeer for *in vitro* assays, Drs. Bostjan Markelc, Sally hill, Karla Watson, Ana Gil-bernabe and Jaehong Im for animal experiment. Drs. Graham Brown and Rhodri Wilson for imaging, Drs. Jonathan Webber, Andrew Worth and Mick Woodcock for flow cytometry.

I want to thank all members of Muschel's lab, all friends in the Department of Oncology and Colleges for making my life in Oxford happy and fruitful.

My sincere gratitude also goes to my family: my father Kaizhong, brothers Jianning and Jianze and my little sister Jingqi, my aunts and uncles. It's their caring and support along with my life journey that keeps me strong and reminds me the true meaning of life.

Lastly, all these would not have taken place without the funding support from Cancer Research UK, the Clarendon Scholarship and Brasenose College.

Specific acknowledgements

All works presented in this thesis were completed by the candidate with help for specific procedures from the following colleagues:

Dr. Yunhong Cao for CRISPR plasmid cloning.

Dr. Bostjan Markelc and Mr. Jacod Kappler for tumour inoculation in mice.

Dr. Bostjan Markelc for live-cell imaging.

Dr. Andrew Worth for cell sorting.

Contents

Abstract i

Acknowledgements iv

Specific acknowledgements v

List of Abbreviations xi

List of figures xiii

List of tables xv

Chapter 1 Introduction 1

1.1 Challenges in radiation treatment of cancer 2

1.2 Immune checkpoint blockade in cancer immunotherapy 6

1.2.1 Cancer immunotherapy 6

1.2.2 Cancer-immunity cycle 6

1.2.3 Cancer immune evasion 8

1.2.4 Immune checkpoint blockade in cancer treatment 8

1.3 Combing RT and immune checkpoint blockade: opportunities and challenges 11

1.4 IFNs 13

1.4.1 Subtypes of IFNs 13

1.3.2 Induction of IFNs and type I IFN signalling 14

1.4.3 Role of IFNs in anti-tumour immune response and RT 15

1.4.4 Key questions that remain to be answered 16

1.5 Research objectives 18

Chapter 2 Materials and Methods 19

2.1 Cells 20

2.2 Reagents 20

2.3 IR in tissue culture 22

2.4 RT-qPCR 22

2.4.1 RNA isolation 22

2.4.2 DNase treatment and cDNA synthesis 22

2.4.3 qPCR 23

2.4.5 Quality control of qPCR 23

2.4.6 Positive control of human IFNL1 24

2.5 Immunoblotting 27

2.6 NF-κB reporter assay 28

2.7 Gene knockdown using shRNA 28

2.8 Generation of knockout cell lines using CRISPR 29

2.8.1 CRISPR plasmid cloning 29

2.8.2 Plasmid transfection and generation of single cell clones 30

2.9 Fluorescent staining and confocal imaging 32

2.10 ELISA 32

2.11 Clonogenic assay 32

2.12 Cell proliferation assay 33

2.13 Assessment of Caspase 3/7 in cells via flow cytometry 34

2.14 Assessment of cell cycle in cell using propidium Iodide 34

2.15 Animal model 35

2.15.1 Mice 35

2.15.2 Subcutaneous tumour model 35

2.15.3 Irradiation treatment of subcutaneous tumours 35

2.16 Immune profiling using flow cytometry 36

2.17 Fluorescence-activated cell sorting (FACS) 39

2.18 CD8+ T cells or NK cells depletion in C57BL6 mice 39

2.19 In vitro killing of cancer cells by tumour-derived CD8+ T cells 40

2.20 Imaging assessment of apoptosis in cancer cells upon co-cultured with tumour-derived CD8+ T cells 40

2.21 Statistical analysis 41

Chapter 3 Mechanisms affecting type I/III IFN induction in cancer cells after exposure to IR 42

3.1 Introduction 43

3.1.1 IR triggers anti-tumour immune responses 43

3.1.2 IFNs as mediators in IR-induced immune response 43

3.1.3 Roles of tumour cells in IR-induced IFNs 44

3.1.4 Aims 44

3.2 Results 45

3.2.1 Induction of type I/III IFN in cancer cells after exposure to IR 45

3.2.2 TBK1 and NF-κB pathways contribute to IFN induction by IR. 50

3.3.3 Cytosolic DNA sensors-STING is the key signalling axis in induction of IFNs by IR 57

3.3.4 IR induction of IFNs was mediated by IRF1 in HT29 and IRF3 in MC38, respectively 65

3.3.5 IFNAR and IL-28R signalling pathways act in positive feedback loops to enhance induction of IFNs after IR 71

3.3.6 Model for IR-induced IFNs in cancer cells 82

3.4 Discussion 84

3.4.1 The findings and significances of current study 84

3.4.2 STING-TBK1 and NF-κB signalling pathways mediate induction of type I/III IFNs in cancer cells after IR 84

3.4.3 IRFs in induction of IFNs by IR 86

3.4.4 Type I/III IFN signalling pathways 87

3.4.5 IFNA 88

3.5 Conclusions 89

Chapter 4 Abrogation of type I IFN signalling in cancer cells led to remarkable improvement in irradiation-induced anti-tumour immunity 90

4.1 Introduction 91

4.2 Results 93

4.2.1 Abrogation of type I IFN signalling in cancer cells led to remarkable improvement of tumour response to IR, while genetic elimination of STING led to reduced tumour response to irradiation. These paradoxical outcomes were mediated by the host immune system. 93

4.2.2 Abolishing type I IFN signalling in cancer cells led to enhanced cytotoxic immune response in irradiated tumours 103

4.2.3 CD8+ T cells were the main effector cells that mediated the improved response of IFNAR1 KO MC38 tumours to IR 109

4.2.4 IFNAR1 KO MC38 cells were more susceptible to CD8+ T mediated cytolytic killing than WT MC38 cells 113

4.2.5 The increased vulnerability of IFNAR1 KO MC38 to CD8+ T cells is not mediated by either PD-L1 or Galectin-9 120

4.2.6 CD155 and H-2Kb are candidates to play a role in the enhanced susceptibility of IFNAR1 KO MC38 cells to CD8+ T cell-mediated killing 125

4.3 Discussion 129

4.3.1 Summary of findings in the current study 129

4.3.2 Role of tumour cell-derived type I IFN in anti-tumour immune response 129

4.3.3 Role of tumour cell-derived type I IFN signalling in anti-tumour immune response 131

4.3.4 PD-L1 and Galectin-9 132

4.3.5 CD155 133

4.3.6 H-2Kb 134

4.3.7 Endogenous resistant mechanisms 134

4.3.8 The role of NK cells in IFNAR1 KO MC38 tumours 135

4.3.9 Redundant contribution from type III IFN signalling 135

4.4 Conclusion 137

Reference 138

Appendix I Published paper

Appendix II Manuscript in preparation

List of Abbreviations

18s rRNA	18S ribosomal RNA
AP1	Activator protein 1
ATCC	American type culture collection
B2M	Beta-2-microglobulin
CD	Cluster of differentiation
cGAS	Cyclic GMP-AMP synthase
CRISPR	Clustered Regularly Interspaced Short Palindromic Repeats
Ct	Threshold cycle
cGAMP	cyclic guanosine monophosphate-adenosine monophosphate
CTLA4	Cytotoxic T-lymphocyte-associated protein 4 (also known as CD152)
DCs	Dendritic cells
DAMPs	Damage associate molecular patterns
DAPI	4′,6-diamidino-2-phenylindole
DNA	Deoxyribonucleic acid
DNA-PK	DNA-dependent protein kinase, catalytic subunit
DMEM	Dulbecco's Modified Eagle Medium
DMSO	Dimethyl sulfoxide
ELISA	Enzyme-linked immunosorbent assay
F	Fraction
FACS	Fluorescence-activated cell sorting
FDA	Food and Drug Adminstration
FMO	Fluorescence minus one
Gy	Gray
hMGFP	Humanized monster green fluorescent protein
HVEM	Herpesvirus entry mediator
IFNs	Interferons
IFN-α	Interferon alpha (IFNA)
IFN-β	Inteferon beta (IFNB)
IFN-γ	Interfeorn gamma (IFNG)
IFN-λ	Interfeorn lambda (IFNL)
IL	interleukin
IKK-α	Inhibitor of nuclear factor kappa-B kinase subunit alpha
IKK-β	Inhibitor of nuclear factor kappa-B kinase subunit beta
IR	Ionizing radiation
IRF	Interferon regulatory factor

ISGs	Interferon-stimulated genes
ISGF3	Interferon-stimulated gene factor 3
ISRE	Interferon stimulated response element
JAK	Janus tyrosine kinase
LDS	Lithium Dodecyl Sulfate
LLC	Lewis lung cancer
MAVS	Mitochondrial antiviral signaling
MHC	Major histocompatibility complex
NEMO	NF-kappa-B essential modulator
NF-κB	Nuclear factor kappa-light-chain-enhancer of activated B cells
NK	Natural killer
NSCLC	Non-small cell lung cancer
PBS	Phosphate buffered saline
PD-1	Programmed cell death protein 1 (also known as CD279)
PD-L1	Programmed death-ligand 1 (also known as CD274)
PD-L2	Programmed death-ligand 2 (also known as CD273)
Poly I:C	Polyinosinic:polycytidylic acid
qPCR	Quantitative polymerase chain reaction
RT-qPCR	Reverse-transcription qPCR
RIG-I	Retinoic acid-inducible gene 1
RIPA buffer	Radioimmunoprecipitation assay buffer
RLRs	RIG-I-like receptors
RNA	Ribonucleic acid
ROS	Reactive oxygen species
RT	Radiation therapy
RPMI1640	Roswell Park Memorial Institute 1640 medium
RT-qPCR	Quantitative reverse transcription polymerase chain
STAT	Signal Transducer and Activator of Transcription
TAK1	Transforming growth factor beta-activated kinase 1
TBK1	TANK-binding kinase 1
Tim-3	T-cell immunoglobulin and mucin-domain containing-3 (CD366)
TNFα	Tumor necrosis factor alpha
TLR	Toll-like receptor
TRIF	TIR-domain-containing adapter-inducing interferon-β
VACV	Vaccinia virus

List of figures

Chapter 1

Figure 1	The cancer-immunity cycle	7
Figure 2	Induction of type I IFNs and type I IFN signalling	14

Chapter 3

Figure 3	Induction of type I/III IFNs and ISGs in cancer cells after exposure to IR *in vivo* and *in vitro*	47
Figure 4	IR induced type I/III IFNs and ISGs in dose- and time-dependent manners	49
Figure 5	Activation of NF-κB pathway and TBK1 in HT29 cells following 6 Gy IR	51
Figure 6	TBK1 and NF-κB pathways contribute to type I/III IFN induction in cancer cells by IR	52
Figure 7	TBK1 and NF-κB pathways contribute to type I/III IFN induction in LOVO cells by IR	54
Figure 8	TLR3 knockdown did not reduce IR-induced type I/III IFNs in HT29 cells	58
Figure 9	Cytosolic DNA sensor-STING is the predominant signalling axis in IR induction of type I/III IFNs in HT29 cells	60
Figure 10	Cytosolic DNA sensor-STING is the predominant signalling axis in IR induction of IFNB in MC38 cells	62
Figure 11	IR induction of type I/III IFNs is mediated by IRF1 in HT29	65
Figure 12	IR induction of IFNB is mediated by IRF3 in MC38	67
Figure 13	Type I/III IFN signalling pathways act in positive feedback loops to enhance induction of type I/III IFNs in HT29 cells after irradiation	71
Figure 14	Type I IFN signalling act in a positive feedback loop to enhance induction of IFNB in MC38 cells after radiation	73
Figure 15	Validation of mechanisms model by assessing type I/III IFNs protein level in the supernatant of irradiated tumour cells	75
Figure 16	The impacts of type I/III IFN signalling pathways on the expression of key factors in IR-induced type I/III IFNs in tumour cells	76
Figure 17	NF-κB activity of cancer cells following stimulation	78
Figure 18	Model for induction of type I/III IFNs in cancer cells by IR	80

Chapter 4

Figure 19	Abrogation of type I IFN signalling in cancer cells led to improvement of tumour response to IR, while the treatment outcomes of irradiated tumours were significantly comprised with the abolishment of STING pathway in cancer cells. These paradoxical outcomes were mediated by the host immune system.	94
Figure 20	In vitro characterization of MC38 cell lines	96
Figure 21	Abrogation of type I IFN signalling in cancer cells led to improvement of tumour response to IR in KPC and LLC tumour models.	98
Figure 22	Flow cytometric profiling of cell populations in MC38 tumours with or without IR treatment	102
Figure 23	Proliferation and cytotoxic capacity of CD8+ T cells and NK cells in MC38 tumours with or without IR.	104
Figure 24	CD8+ T cells were the main effectors cells that mediated the improved response of IFNAR1 KO MC38 tumours to IR	108
Figure 25	IFNAR1 KO MC38 tumour cells are more susceptible to CD8+ T cells mediated killing	113
Figure 26	The increased vulnerability of IFNAR1 KO MC38 to CD8+ T cells is independent of PD-L1- and Galectin-9	118
Figure 27	In vivo expression of immunomodulators on the surface of MC38 tumour cells with or without IR	122

List of tables

Chapter 1

Table 1	Age-standardised 5-year net survival of patients (totally 37,513,025) diagnosed with cancers in 71 countries during 2000-2014	2
Table 2	Subtypes of interferons	13

Chapter 2

Table 3	Antibodies for immunoblotting and confocal imaging	21
Table 4	Primers for RT-qPCR	25
Table 5	Taqman primers/probes for RT-qPCR	27
Table 6	List of shRNA	29
Table 7	CRISPR gRNA sequences	31
Table 8	Antibodies used for flow cytometry experiments	37

Chapter 1

Introduction

1.1 Challenges in radiation treatment of cancer

Cancer is one of the leading causes of death in the world. Globally, there are approximately 14.1 million cases of newly diagnosed cancer and 8.2 million patients died of cancer in 2012 [2]. For solid tumours, a recently published study showed that the 5-year net survival of most cancer types was around 50% and worse in diseases arising from lung, liver, oesophagus and pancreas (**Table 1** [1]). Thus, more efficient therapeutics are warranted to improve the overall outcomes for cancer patients.

Organ origin of cancer disease	5-year net survival (%)
Breast	> 80
Prostate	70-100
Lung	10-30
Colon	50-70
Rectum	50-70
Cervix uteri	50-70
Stomach	20-40
Liver	5-30
Ovary	30-50
Oesophagus	10-30
Melanoma	60-90
Brain (adults)	20-40
Pancreas	5-15

Table 1. Age-standardised 5-year net survival of patients (totally 37,513,025) diagnosed with cancers in 71 countries during 2000-2014 [1].

Radiation therapy (RT), is one of the main treatment methods for cancers. More than half of cancer patients benefit from RT during their course of treatment [3]. About 40% of cancer patients, who are cured, include RT as a crucial part of curative regimens. Modern RT techniques deliver radical or high IR doses to tumour target volumes in precise and accurate fashions, while reducing IR doses to the surrounding normal tissues. This has led to significant reduction of radiation-induced toxicities and improvement of local-regional tumour control in some cancer types [4]. The development of RT in the past decades has been mainly driven by the advances of radiation physics and imaging techniques. Additional improvements may require greater considerations of cancer biology.

Firstly, the advantages of homogenous IR dose distribution achieved via modern techniques is undermined by the intra-tumour heterogeneity. The heterogeneous cancer cell clones within the tumour may have a wide range of sensitivity to RT and other therapeutics as well ([5], reviewed in [6]). Resistant clones can survive the initial treatment and lead to disease persistence or recurrence [7-10]. Secondly, distant metastasis has gradually become the main failure pattern following localized RT treatment in many cancer types. Adding systemic chemotherapy to RT has proved to be insufficient to eliminate all metastatic lesions [11-13]. Therefore, more specific and efficient therapeutics are required to cure or even prevent post-treatment metastasis. Last but not least, one of major unmet needs for cancer RT is to reduce RT-related toxicities and improve the quality of life of patients. Over the past two decades, significant progress has been achieved with the application of modern radiation therapy [14-18]. However, modern RT techniques cannot completely spare the irradiation of normal tissues, owing to physical limitations of RT delivery and tumour invasion of anatomical structures. Novel strategies are

warranted to expand the therapeutic window, which may allow RT dose de-escalation and therefore reduce radiation-induced toxicities.

In the classical model, ionizing radiation (IR) kills cancer cells via direct induction of lethal DNA damage. It is now well acknowledged that host immunity has a pivotal impact on the therapeutic outcomes of RT [19-21]. However, how IR interacts with host immune system is still poorly understood. On the one hand, there are data suggesting that IR leads to an immunosuppressive microenvironment due to the greater vulnerability of various immune cells to DNA damage [22-24]. For instance, whole body IR has been used to deplete the immune system before bone marrow transplant in clinic. It remains unknown whether local IR treatment might suppress the tumour-specific immune response. On the other hand, studies also show that IR has the potential to modify the tumour microenvironment, favouring the anti-tumour immune response [25-27]. Irradiated tumour cells can release a variety of immunomodulatory factors, including damage associate molecular patterns (DAMPs), cytokines and chemokines, resulting in an inflammatory microenvironment that may facilitate tumour-specific immunity. One well-acknowledged example, but extremely rare phenomenon in which localized IR treatment occasionally leads to the regression of out-of-field tumour, is termed the abscopal effect [28]. Harnessing the host immune system may help improve the efficacy of RT, but will require more comprehensive understanding on IR-induced immune response and cancer immune evasion.

To sum up, cancer is a leading cause of death globally. RT, one of the main therapeutic modalities, plays an important role in cancer management. Owing to the development of radiation physics and imaging techniques, modern RT has made significant progress in the improvement of tumour control and normal tissue

protection. However, there are still emerging challenges and unmet needs, including tumour heterogeneity, post-treatment metastasis and the need to further improve quality of life for survivors. Emerging data suggests that IR can trigger anti-tumour immune response, which has important impacts on the overall outcomes of RT. Better understanding of IR-induced immune response may help improve the therapeutic efficacy of RT via harnessing the host anti-tumour immunity.

1.2 Immune checkpoint blockade in cancer immunotherapy

1.2.1 Cancer immunotherapy

Historically, the main treatment methods for cancer include surgery, RT and chemotherapy, whereas immunotherapy has gradually emerged as the fourth modality, with promising clinical results. Resistance to immune surveillance, the primary defence against malignant diseases, is a hallmark of cancer [29, 30]. Cancer immunotherapy, aims to harness the host immune system to eliminate cancer cells in an efficient and specific fashion. The application of immunotherapy can be dated back to the 1890s, when Coley showed that immunostimulants, such as bacterial products, improved tumour control [31]. Since then, immunotherapy has been examined to treat cancer in the clinic via a variety of strategies in the last century. However, despite the enthusiasm, the outcomes of these studies were disappointing with limited efficacy, which is partially due to the poor understanding of cancer immune evasion [32]. The recent progress in the understanding of cancer-immunity cycle, especially the role of immune checkpoints in cancer immune evasion, has led to extraordinary development of cancer immunotherapy [33].

1.2.2 Cancer-immunity cycle

CD8+ T cells are one of the major effectors in cancer immunotherapy. Killing of cancer cells by CD8+ T cells is a fine tuned and multistage process, including : (1) Release of cancer cell antigens via a variety of mechanism; (2) Capture and processing of these antigens by antigen presenting cells (mainly dendritic cells), which then present antigen-derived peptides on their cellular surface together with MHC class I molecules; (3) Migration of antigen presenting cells to the draining lymph node, where they prime and activate CD8+ T cells; (4) Trafficking of activated

CD8+ T cells to tumours via blood vessels; (5) Infiltration of CD8+ T cells into the tumour; (6) Recognition of tumour cells that present the antigen-derived peptides by CD8+ T cells via peptide-specific TCR receptor; (7) Formation of an immune synapse between tumour cells and CD8+ T cells, followed by secretion of cytotoxic granules (compose of perforin and granzyme B), which enter tumour cells and activate the caspase pathway, resulting in their death (reviewed in [34]).

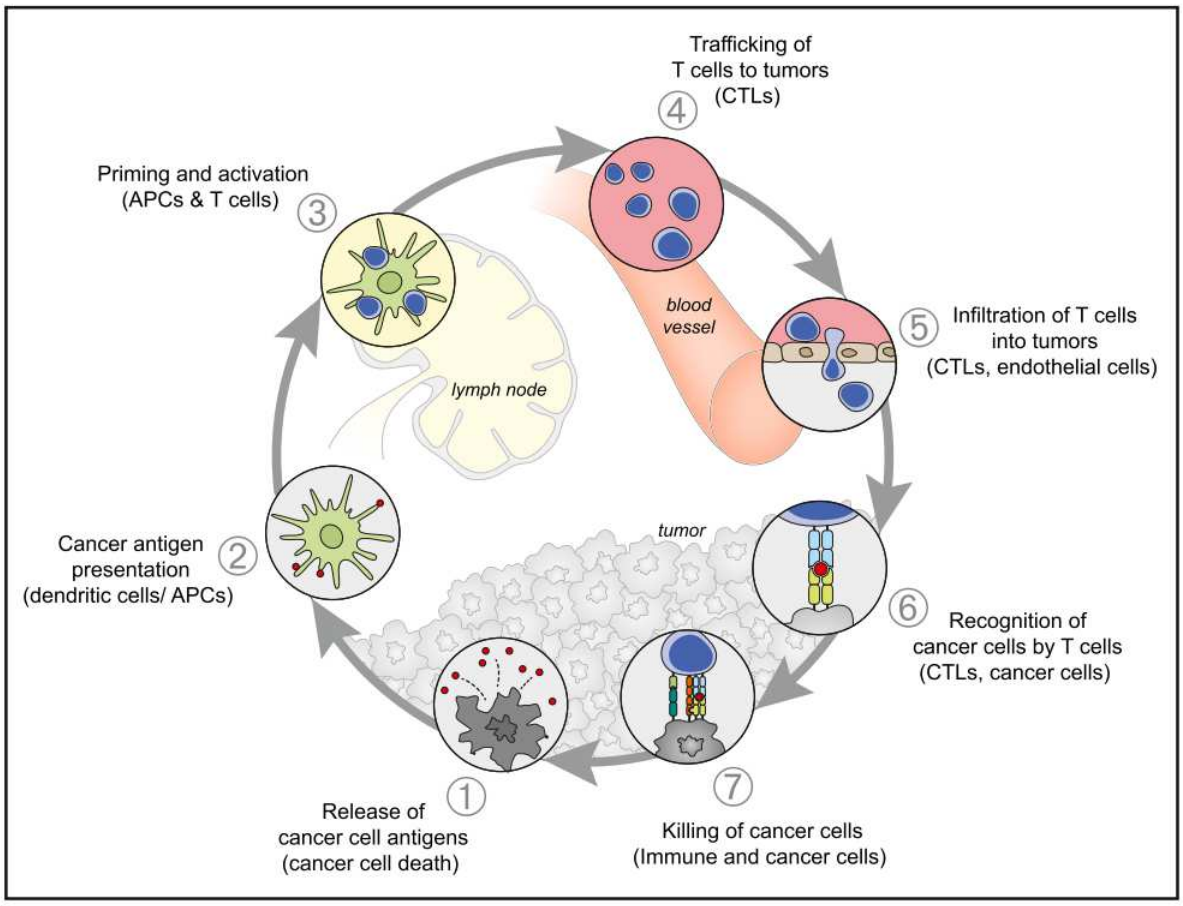


Figure 1. The cancer-immunity cycle ([34])

1.2.3 Cancer immune evasion

Cancer cells can jeopardize the anti-tumour immune response through various mechanisms. Firstly, cancer cells can impede immune recognition by downregulation of MHC class I molecules (reviewed in [29]), and loss of antigen as well [35, 36]. Lower visibility (less MHC-I and specific antigen) by CD8+ T cells provides cancer cells advantages to survive under the selection of immune editing and to become the predominant clone (reviewed in [37]). Secondly, cancer cells can upregulate a variety of suppressors, including immune inhibitory checkpoints (reviewed in [33, 38]), which can lead to blunting of the cytotoxic function of T cells and their exhaustion. Thirdly, the activation of dendritic cells and priming of CD8+ T cells is commonly subverted within the tumour immunosuppressive microenvironment, which is characterized with an imbalance between immunosuppressive and pro-inflammatory cytokines [39]. Lastly but not the least, tumours can establish an endothelial barrier, favouring infiltration of regulatory T cells instead of cytotoxic T cells, which could lead to tumour immune tolerance [40].

1.2.4 Immune checkpoint blockade in cancer treatment

Upregulation of immune checkpoints (e.g. CTLA4, PD-1, and Tim-3) and their ligands (e.g. PD-L1, PD-L2 and Galectin-9) in the tumour microenvironment is one of main mechanisms that cancer cells utilized to evade the host immune system. Immune checkpoint blockade has shown intriguing clinical results and been approved for the treatment of a variety of advanced cancer diseases, including melanoma, non-small cell lung cancer (NSCLC), renal cell carcinoma, head and neck squamous cell carcinoma and urothelial carcinoma [41, 42]. Moreover, its application has been expanded to settings other than advanced diseases. A recently study

published in NEJM showed that the administration of anti-PD-L1 (durvalumab) after definite chemoradiotheapy resulted in significant increase of disease-free survival, which led to the approval of durvalumab in stage III NSCLC by FDA [43]. Another study applied anti-PD-1 therapy in non-small lung cancer as neoadjuvant treatment before radical surgery and their results indicated that 45% of patients had major pathological response (<10% of viable cancer cells in tumours) [44]. Despite all these promising progress, challenges exists for immune checkpoint blockade.

To start with, only a minority of treated patients benefit from immune checkpoint blockade. The objective response rates were 19.0 ~ 57.6% in melanoma patients in response to single agent (anti-CTLA4 or anti-PD-1) or combination therapy of immune checkpoint blockade, and 15.0 ~ 29.0 % in non-small cell lung cancer after anti-PD-1 treatment [41, 45-47]. In colon cancer, benefits from anti-PD-1 were exclusively found in tumours with mismatch repair-deficient, which only accounts for around 6% of patients with colorectal adenocarcinoma [48, 49]. Most studies indicate that patients with existing anti-tumour immunity and the presence of immune checkpoint within the tumour are more likely to gain survival benefits from immune checkpoint blockade. How to boost its efficacy in patients with less immunogenic tumours has become one of the major challenges. Secondly, immune checkpoint blockade alone could not completely eradicate tumours in the majority of patients. Only 11.5% of patients with melanoma, one of the most immunogenic cancer diseases, experienced complete regression following treatment with anti-CTLA4 plus anti-PD-1 [41]. Thus, it is critical to combine immune checkpoint blockade with the main therapeutic modalities to achieve a cure. Lastly, there are increasing concerns of immune-related adverse events associated with immune checkpoint blockade, especially in combination [50, 51]. Fox example, following anti-

PD-1 (nivolumab), anti-CTLA-4 (ipilimumab), or these two in combination, 16.3%, 27.3% and 55.0% of melanoma patients experienced grade 3-4 adverse events [41]. A more selective approach may help reduce unnecessary treatment and increase the overall benefits.

1.3 Combing RT and immune checkpoint blockade: opportunities and challenges

Given the specific characteristics of each therapeutic modality, combining RT and immune checkpoint blockade may potentially lead to synergistically therapeutic effect in cancer. From the perspective of RT, immune checkpoint blockade can boost CD8+ T cell-mediated anti-tumour immune response, which has a potential to match the scale of tumour heterogeneity, as the estimated number of distinct TCR complex is up to 10^{18} in man [52]. Moreover, one of the main drivers of tumour heterogeneity is genetic mutations in cancer cells [53-57], which is also correlated with the abundance of neoantigens in the tumour [58, 59]. It is increasingly appreciated that tumours with higher antigenicity are more likely to benefit from immune checkpoint blockade [48, 49, 60-62]. Thus, the factor conferring the radioresistance of tumour cells, may actually sensitize them to immune checkpoint blockade. In addition, a systemic anti-tumour immune response has the potential to attack disseminated cells when combined with local RT. Lastly, RT and immunotherapy target the cancer cell via distinct mechanisms and have distinct toxicity profiles. Therefore, when in combination, they could help expand the therapeutic window, which may allow RT dose de-escalation and help improve the quality of life of cancer survivors.

From the perspective of immune checkpoint blockade, including RT may boost the overall anti-tumour immune response. Immune checkpoint blockade relies heavily on the presence of existing anti-tumour immunity within the tumour and their efficacy is limited in non-immunogenic tumours (‘‘cold tumours’’). Local RT can turn ‘‘cold tumours’’ into ‘‘hot tumours’’ via a variety of mechanisms. IR can enhance the expression of MHC class I molecules and expand the antigen peptide pool that are critical for the antigenicity of cancer cells [63]. More importantly, irradiated cancer

cells release a variety of immunomodulators, including cytokines and damage associated molecule patterns, resulting in an inflammatory microenvironment, which can help facilitate anti-tumour immune response. A recently published study showed that RT prior to anti-PD1 immunotherapy led to longer progression-free survival and overall survival [64]. Taken together, RT may augment the immunogenicity of cancer cells or alter the microenvironment in favour of inflammatory immune response, which may maximize the efficacy of immune checkpoint blockade and further improve the survival outcomes following either modality alone.

Despite the great potential of synergistic effect from the combination of RT and immune checkpoint blockade, the application of such combinational regimen in the clinic has been sluggish, owing to poor understanding of the interaction between these two modalities. It is still not fully understood how IR help facilitate anti-tumour immune response. Better understanding of the underlying mechanisms will help identify patients that would benefit from the combinational therapy or develop adjuvant therapeutics for non-responder patients. Second, although IR can trigger immune responses and there are case reports describing abscopal effects of IR, the overall incidence of this phenomenon is rare. Why IR fails to trigger an effective immune response in many cases in unclear. Lastly, there are a variety of immune checkpoints that could be found in the tumour microenvironment. The types of combinations and timings of administration of RT remain to be determined to achieve the maximum efficacy.

1.4 IFNs

1.4.1 Subtypes of IFNs

Interferons (IFNs) are a group of interleukins with the hallmark of antiviral function. There are three types of IFNs that can be defined by their binding to specific receptors, all of which consist of a pair of heterologous [65]. Type I IFNs bind to IFNAR1 & 2 and are subdivided into IFN-α (IFNA), β (IFNB), ω, ε, κ, δ, τ and ξ. Of them, only IFNA and IFNB are ubiquitously expressed. There is only one type II IFN, IFN gamma (IFNG) that binds to a different receptor complex, IFNGR-1 & 2. Type III IFN includes 4 homologous proteins, IFN lambda 1-4 (IFNL1-4), and utilizes a receptor complex of, IFNLR1, also called IL-28R, together with IL-10R2, a receptor subunit shared with IL-10, IL-22 and IL-26 [66, 67]. All cell types are capable of expressing type III IFN.

Types	Subtypes	Expression pattern	Receptors	Receptor distribution
I	α (IFNA), β (IFNB)	Ubiquitous	IFNAR1 & 2	Ubiquitous
	ω, ε, κ, δ, τ and ξ	Tissue-specific	IFNAR1 & 2	Ubiquitous
II	γ (IFNG)	Immune cells	IFNGR1 & 2	Ubiquitous
III	λ1 ~ λ4 (IFNL1-4)	Ubiquitous	IL-28R & IL-10R2	Epithelial cells Immune cells

Table 2. Subtypes of interferons

1.3.2 Induction of IFNs and type I IFN signalling

The transcription of type I IFNs is regulated by a complex network which comprises sensors, adaptors, transcriptional kinases and factors, IFNs themselves and their downstream genes. The number of members of this network is still increasing. Pathogens result in triggering IFN induction by the release of pathogen associated molecules patterns (PAMPs). An alternative pathway with a similar but distinctive mechanisms of IFN induction occur with damage associated molecules patterns (DAMPs) from irradiated cancer cells [68]. Cells recognize these molecules with specific sensors, such as TLRs (e.g. TLR4), RLRs (e.g. RIG-I) or DNA sensors (e.g. cGAS). This recognition in turn triggers different adaptors (e.g. TRIF, MAVS and STING) to phosphorylate their associated kinases (e.g. IKK and TBK1). These adaptors with or without the kinases then activate the transcriptional factors (e.g. IRF3), leading to IFN expression. When IFNs are secreted, they bind to their relevant receptors and activate the Jak-Stat pathway, resulting in the expression of interferon stimulated genes through transcriptional complex ISGF3 (phosphorylated STATs together with IRF9).

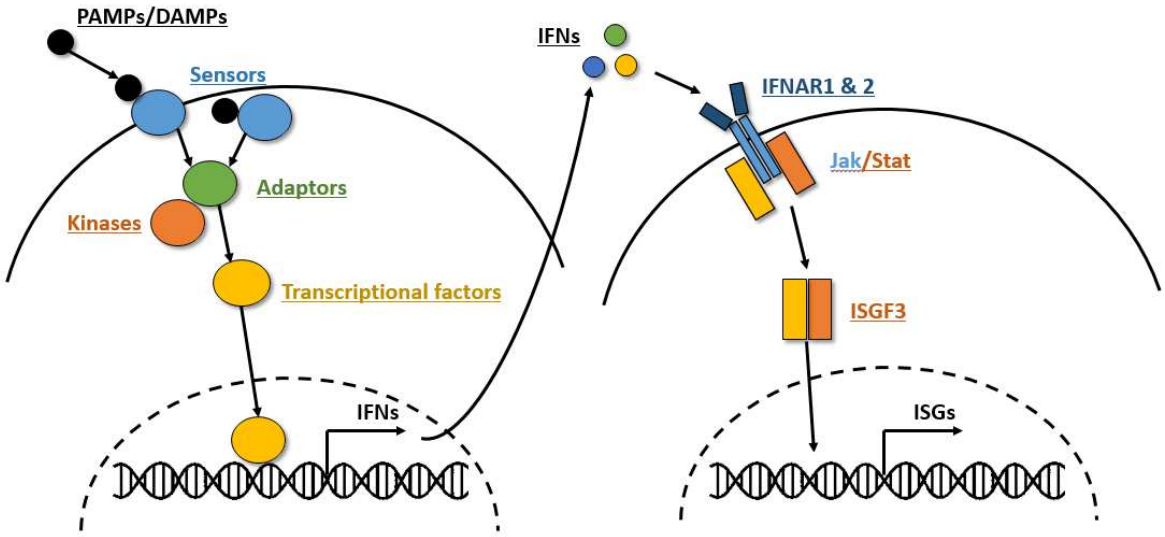


Figure 2. Induction of type I IFNs and type I IFN signalling

1.4.3 Role of IFNs in anti-tumour immune response and RT

IFNs have a hallmark of antiviral function. They also exhibit anti-tumour effects through direct induction of cell cycle arrest and apoptosis (reviewed in [69, 70]), and have been used as therapeutic agents or radiation sensitizers for decades in a number of diseases, including melanoma, lymphoma, leukaemia and sarcoma [71-74]. In addition to their direct anti-tumour effects, type I IFNs also act as immunomodulators and have a critical role in the cancer-immunity cycle. Type I IFN is selectively required, in comparison to type II IFN, for the initiation of anti-tumour immune response [75, 76]. An intact type I IFN signalling in dendritic cells is necessary for their migration, maturation and cross-priming. Moreover, activation of type I IFN signalling in CD8+ T cells can enhance their survival, clonal expansion, differentiation, cytotoxic function, memory formation and protect them from NK cell attack as well [77-81]. Indeed, a number of studies showed that genetic elimination of type I IFN receptors in host or systemic blockade of type I IFN signalling via antibody abrogated the anti-tumour immune response [75, 76, 82].

In the scenario of RT, emerging data suggests that IFN signalling pathways are involved in determining the therapeutic efficacy of RT. One study found that localized IR treatment not only induced lethal damage in cancer cells, but also promoted intratumoural production of IFNγ, which in turn altered the tumour microenvironment, leading to enhanced T cell infiltration and tumour target recognition [83]. Another study showed that the therapeutic efficiency of ablative IR treatment relied upon the type I IFN-dependent innate and adaptive immune response [82]. These studies suggest that IFNs are key mediators of IR induction of anti-tumour immune response. Better understanding the underlying mechanism may help improve the overall efficacy of RT.

1.4.4 Key questions that remain to be answered

IFNs have an important role in IR-induced anti-tumour response. However, one critical question that remains to be answered is how IR induces IFNs in tumours, especially type I IFNs, which could be expressed by all cell types. Previous studies suggested that the main produces of type I IFNs in tumours were dendritic cells, whereas emerging data indicates that cells of non-haematological origins, including cancer cells, could also be the source of type I IFN [19, 82, 84, 85]. Indeed, cancer cells are the main cellular component in the tumour microenvironment. Thus, it will be interesting to investigate their potential contribution to the overall induction of type I IFN after exposure to IR and the underlying mechanism as well. Additionally, type III IFN, the new member of IFN family, utilizes similar transcriptional factors to type I IFN, and presumably could be induced by the same stimulus. Whether IR can augment the expression of type III IFN in cancer cells remains unknown.

In regard to the role of type I IFN signalling, it is well established that activation of this pathway in dendritic cells and immune effectors cells is essential for the anti-tumour immune response. Nevertheless, data has emerged suggesting that the role of type I IFN signalling in tumours is more complicated than previously thought and can exhibit detrimental effect on tumour control (reviewed in [86]). For instance, activation of type I IFN signalling in cancer cells has been found to correlate with resistance to therapies, including RT, and worse outcomes in breast cancer patients [87-90]. In the scenario of chronic infection, studies suggested that activated type I IFN signalling could lead to upregulation of a number of immunosuppressors and hence dampened the anti-virus immune response, resulting in virus tolerance. Therefore, the role of cancer cell-derived type I IFN signalling in the therapeutic efficacy of RT is still elusive and needs to be investigated in a

context-dependent manner. More importantly, better understanding of how type I IFN signalling exerts its influence on the anti-tumour immune response will help determine the rational combination of radiotherapy and immune checkpoint blockade.

In addition to signalling in cancer cells, the therapeutic scheme of radiation including dose, fractionation and time, also has important impacts on the induced anti-tumour immunity. Samuel Strober, et al.'s study showed that ablative irradiation (30Gy x 1F in 1 day) led to significantly stronger CD8 T cell infiltrate, loss of MDSC and durable tumour remissions compared to extended fractionated radiation (3Gy x 10F in 10 days) [91]. Whilst a recently published study by Sandra Demaria et al. found that radiation dose higher than 12-18 Gy induced DNA exonuclease Trex1 which degraded cytosolic DNA and therefore attenuated the immunogenicity of cancer cells, preventing synergy with anti-CTLA4 or anti-PD-1 [92]. These studies together suggest that ablative irradiation scheme may provoke stronger immune response when applied alone in local tumours, whereas for systemic anti-tumour immunity, fractionated radiation with moderate fraction size leads to greater synergistic effects in combination with immune checkpoint blockade. Nonetheless, the optimized fraction size, interval time between fractions and timing in combination with various immunotherapy requires more comprehensive investigations in a context-dependent fashion. Determination of optimized therapeutic scheme is beyond the scope of this project and is not further discussed in this report.

1.5 Research objectives

This project contents two parts. The first part aimed to investigate the potentially direct induction of type I/III IFNs in cancer cells after exposure to IR and its underlying mechanisms as well. The second part was to determine the role of cancer cell-derived IFNs and IFN signalling in tumour response to IR.

Chapter 2.

Materials and Methods

2.1 Cells

The following cells lines were used in this study: HT29, LOVO and HCT116 (all human colorectal cancer cell lilnes), OE21 and OE33 (human esophageal cancer cell lines), MC38 (murine colorectal cancer cell line), LLC (Lewis lung carcinoma cell line), KPC and Pano2 (murine pancreatic cancer cell lines) and B16F10 (murine melanoma cell line). All cell lines used in this study were originally obtained from American Type Culture Collection (ATCC), with the exceptions of MC38 (a gift from Dr. Lee Gorden, Vanderbilt University), KPC (a gift from Dr. Owen Sansom, University of Glasgow), OE21 and OE33 (both are gifts from Dr. Ester Hammond, Oxford University). HT29 and B16F10 were grown in Roswell Park Memorial Institute 1640 medium (RPMI 1640). LOVO, HCT116, OE21, OE33, MC38, LLC, KPC and Pan02 were cultured in Dulbecco's Modified Eagle Medium (DMEM). All mediums were supplemented with 10% (v/v) of fetal bovine serum and 1% of penicillin-streptomycin (all from Sigma-Aldrich, St. Louis, MO). Cells were used with passage number < 8. Mycoplasma was routinely tested and negative.

2.2 Reagents

ML120B dihydrochloride (Bio-techne, Minneapolis, MN) was dissolved in dimethyl sulfoxide (DMSO) at 20 mM and used at 20 μM (when used in treatment, final DMSO concentration 0.1%). Universal Type I IFN alpha and human IL-29/IFN lambda 1 (PBL, Piscataway, NJ) were used at 1000 U/ml. Human TNF alpha (TNFα, from Bio-techne)) and Murine TNF alpha (ThermoFisher, Waltham, MA) were used at 100ng/ml. Lipofectamine 3000 (ThermoFisher) was used to deliver the following reagents to cells according to manufacturer's protocol: 2',3'-cyclic guanosine monophosphate-adenosine monophosphate (cGAMP), VACV-70, and PolyI:C HMW

(InvivoGen, San Diego, CA). Antibodies for immunoblotting and confocal imaging are listed in **Table 3**.

Table 3. Antibodies for immunoblotting and confocal imaging

Antibodies	Suppliers; catalogue No	Dilution
Anti-cGAS	Merck Millpore; ABF124	1:2000
Anti-STING	Abcam; ab82960	1:2000
Anti-IKKB	Abcam; ab124957	1:1000
Anti-TBK1	Abcam; ab109735	1:2000
Anti-Phospho-TBK1(Ser172)(D52C2)	NEB; 5483P	1:2000
Anti-TLR3	Abcam; ab62566	1:2000
Anti-Rig-I (D33H10)	NEB; 4200	1:2000
Anti-B-Actin (8H10D10)	CSL; 3700	1:5000
IRDye 800CW Goat Anti-Rabbit IgG (H+L)	Li-cor; 926-32211	1:10000
IRDye 680RD Goat Anti-Mouse IgG (H+L)	Li-cor; 926-68070	1:10000
Anti-IRF1 (D5E4)	NEB; 8478	1:200
Anti-IRF3 (FL-425)	Santa Cruz; 9082	1:100
Anti-IRF7	Abcam; ab109255	1:500
Rabbit (DA1E) Isotype Control	Cell Signalling; 3900	Accordingly
Goat anti-Rabbit IgG Alexa 488 secondary antibody	ThermoFisher; A-11034	1:500

2.3 IR in tissue culture

Cells were seeded in 6-well plates with a density of 0.5-5 x 10^4 cells/cm^2 and maintained at 37 °C with 5% of CO_2. Twenty-four hours later, cells were treated with gamma-rays at indicated time points. Gamma-rays treatment was delivered using a 137Cs-laboratory irradiator (IBL 637, CIS bio International, Saclay, France) which produces gamma-rays (0.662 MeV) at a dose rate of 0.81 Gy/minute. Fractionated radiation was delivered at 1 fraction (F) per day with a time interval of 24 hours.

2.4 RT-qPCR

2.4.1 RNA isolation

RNA was extracted from the cells using Trizol (Sigma-Aldrich) or RNeasy Mini Kit (Qiagen). All RNA were dissolved in RNase-free water and stored at -80 °C. Generally, a total amount of 5~50 ug of RNA was yielded from each sample in this study. Their quality and quantity were measured using a NanoDrop 2000 microvolume spectrophotometer (Thermo Fisher). RNA samples with the ratio of absorbance at 260 and 280 nm (A260/280) > 1.8 and A260/230 > 2.0 were proceeded to subsequent analysis. All cDNA were diluted with DNase-free water and stored at -20 °C.

2.4.2 DNase treatment and cDNA synthesis

All RNAs were treated with DNase prior to the cDNA synthesis using Turbo DNA-free™ Kit (Life technologies), or RNase-Free DNase Set (Qiagen) according to manufacturer's protocols. Approximately 2 ug of RNA for each sample was

transcribed into cDNA using the High-Capacity cDNA Reverse Transcription Kit (Thermo Fisher).

2.4.3 qPCR

qPCR was performed using SYBR green (Invitrogen or Promega) with specific primers (listed in **Table 4**) or Taqman primers/probes (ThermoFisher, listed in **Table 5**). Reactions were run on a Mx3005p (Agilent Technologies, Santa Clara, CA, USA) in a final volume of 25 uL with cDNA equivalent of 10 ng RNA and 2 umol/L of primers. The cycling conditions were as follow: a. 50ºC 2 min, 1 cycle; b. 95ºC 2 min, 1 cycle; c.95ºC 15 s -> 55 ºC 30 s -> 72 ºC 30 s, 40 cycles; d.72ºC 10 min, 1 cycle.

Following the amplification, the threshold cycle (Ct) values for target genes and reference genes were recorded. The fold induction was calculated using the ΔΔCt method. Firstly, the difference of Ct values (ΔCt) between the target gene and reference gene was calculated. Then, the difference of ΔCt (ΔΔCt) between the experimental sample and control sample was calculated. The mRNA fold induction of the target gene in the experimental samples was then equal to $2^{(-\Delta\Delta Ct)}$. The expression stability of B-Actin has been validated using two additional housekeeping genes: Beta-2-microglobulin (B2M) and 18S rRNA.

2.4.5 Quality control of qPCR

The following controls were used in this study: non-enzyme control (excluding reverse transcriptase in the step of cDNA synthesis) for each sample and non-target control (excluding cDNA in the step of PCR reaction) for each pair of primers. The Ct values of all controls in this study were > 35. All genes we investigated in this study

displayed single peak on melting curve analysis after the amplication of qPCR. Their specificity were further validated by gel electrophoresis of qPCR products.

2.4.6 Positive control of human IFNL1

Full-length human IFNL1 cDNA was amplified from the pCR4-TOPO vector (GE healthcare, Little Chalfont, UK) using forward (GGGGTACCATGGCTGCAGCTTGGACCGTG) and reverse (ATAGTTTAGCGGCCGCGGTGGACTCAGGGTGGGTTGAC) primers. The cDNA of IFNL1 was then inserted into the Not 1 and Kpn 1 sites of the pcDNA3 plasmid which, subsequently, was used to transfect HT29 cells with the FuGENE® HD kit (Roche diagnostics, Indianapolis, IN). The RNA was extracted 48 hours after transfection and used as a positive control for IFNL1.

The standard curves of IFNL1 and β-Actin were generated using the positive control or genomic cDNA. The amplification efficiency for them was 99% and 100%, respectively, with R^2 of both > 0.99.

Table 4. Primers for RT-qPCR

Gene	Accession number		Sequence (5' - 3')	Amplicon length
Human				
IFNL1	NM_172140	F	CGCCTTGGAAGAGTCACTCA	79
		R	GAAGCCTCAGGTCCCAATTC	
IFNL2/3	NM_172138	F	GGGCCAAAGATGCCTTAGAAGA	154
	NM_172139	R	TCCAGAACCTTCAGCGTCAG	
IFNA		F	CACACAGGCTTCCAGGCATTC	100
		R	TCTTCAGCACAAAGGACTCATCTG	
IFIT2	NM_001547	F	ACGGTATGCTTGGAACGATTG	114
		R	AACCCAGAGTGTGGCTGATG	
Beta Actin	NM_001101	F	GAGCTACGAGCTGCCTGACG	119
		R	GTAGTTTCGTGGATGCCACAG	
RIG-I	NM_014314	F	GGACGTGGCAAAACAAATCAG	133
		R	GCAATGTCAATGCCTTCATCA	
cGAS	NM_138441	F	CCCAAGCATGCAAAGGAAGG	146
		R	ACAATCTTTCCTGCAACATTTCT	
STING	NM_198282	F	CACCTGTGTCCTGGAGTACG	193
		R	CATCTGCAGGTTCCTGGTAGG	
TBK1	NM_013254	F	AGCGGCAGAGTTAGGTGAAA	124
		R	CCAGTGATCCACCTGGAGAT	
IRF1	NM_002198	F	GAACTCCCTGCCAGATATCGAG	145
		R	TGCTCTTAGCATCTCGGCTGGA	
IRF7	NM_001572.3	F	CTCCTGGAGAGGGACAAGAA	104
		R	AGGGTGACAGGTACGGCTCT	

To be continued in the next page

Gene	Accession number		Sequence (5’ - 3’)	Amplicon length
B2M	NM_004048.3	F	TGCTGTCTCCATGTTTGATGTATCT	85
		R	TCTCTGCTCCCCACCTCTAAGT	
18S rRNA	X03205	F	GTAACCCGTTGAACCCCATT	150
		R	CCATCCAATCGGTAGTAGCG	
Mouse				
IFNA		F	CCTGAGAGAGAAGAAACACAGCC	50
		R	TCTGCTCTGACCACYTCCCAG	
IFNB	NM_002176	F	CAGCTCCAAGAAAGGACGAAC	137
		R	GGCAGTGTAACTCTTCTGCAT	
IFNL2/3	NM_001024673	F	AGCTGCAGGCCTTCAAAAAG	243
	NM_177396	R	TGGGAGTGAATGTGGCTCAG	
B-Actin	NM_007393	F	CGGTTCCGATGCCCTGAGGCTCTT	99
		R	CGTCACACTTCATGATGGAATTGA	
IFIT2	NM_008332	F	GGAAAAAGAAAGCCCTCACC	106
		R	GTTCCCCAAACTCCTGACAA	
RIG-I	NM_172689.3	F	CCACCTACATCCTCAGCTACATGA	85
		R	TGGGCCCTTGTTGTTCTTCT	
cGAS	NM_173386.5	F	GAATCTTCCGGAGCAAAATG	122
		R	GGCAGTTTTCACATGGTAGGA	
STING	NM_001289591	F	CCTAGCCTCGCACGAACTTG	107
		R	CGCACAGCCTTCCAGTAGC	
TBK1	NM_019786.4	F	GAGAGCTGGAGGACGATGAG	120
		R	ACGGTAGCCCCGTACTTCTT	
IRF3	NM_016849.4	F	CAAGAGGCTTGTGATGGTCA	100
		R	GCAAGTCCACGGTTTTCAGT	

Table 5. Taqman primers/probes for RT-qPCR

Genes	Primers/probes
Murine IFIT1	Mm00515153_m1
Murine IFIT44	Mm00505670_m1
Murine B-Actin	Mm02619580_g1
Human IFIT1	Hs01911452_s1
Human IFI44	Hs00951349_m1
Human B-Actin	Hs01060665_g1

2.5 Immunoblotting

Cells were lysed in RIPA buffer (Sigma) containing cOmplete™ Mini protease inhibitors cocktail (Roche) and PhosSTOP (Sigma). Cell lysates were cleared by centrifugation at 12, 000 x g for 20 minutes. Protein concentration of cell lysates was determined using the Pierce™ BCA protein assay (ThermoFisher). Proteins were mixed with LDS loading buffer (Invitrogen) and dithiothreitol (5 mM), and heated at 70◦C for 10 minutes or 95◦C for 5 minutes. Denatured and reduced proteins (10-20 µg/well) were then separated on 4-12% SDS-PAGE gel (Novex) and transferred to a FL nitrocellulose membrane (Pierce Biotechnology). Membranes were blocked with Odessy blocking buffer for 1 hour and then reacted with indicated primary Abs overnight. Following washing, membranes were incubated with Fluorescence-tagged secondary antibodies (Li-cor), and imaged using Li-Cor Odyssey Imaging system (Li-Cor).

2.6 NF-κB reporter assay

Tumour cells were transfected with CignalTM lenti NF-κB hMGFP reporter (10 transducing units per cells) using SureENTRY (QIAGEN, Hilden, Germany, final concentration 8 μg/ml), and selected with puromycin (1.5 μg/ml) for 10-14 days. Human TNF-α was used as a positive control to activate NK-κB pathway in cells. NF-κB activity of the transfected cells was monitored and quantified using Attune flow cytometer (Thermo Fisher). The flow cytometry data was analyzed using FlowJo software (FlowJo, LLC, Ashland, USA). NF-κB activity was calculated as the percentage of hMGFP positive cells on histogram plot of FITC filter. Fold change of NF-κB activity was calculated as the ratio of NF-κB activity between experimental sample and control sample.

2.7 Gene knockdown using shRNA

Cells were transfected with shRNA lenti particles (Sigma) using SureENTRY reagent according to the manufacturer's protocol. Transfected tumour cells were selected with puromycin for 10-14 days. The efficiency of knockdown was assessed using immunoblot. The shRNA lenti-virus particles used in the study were listed in **Table 6**.

Table 6. List of shRNA

Genes	shRNA lenti-virus constructs from sigma
Human IKKB	TRCN0000018917
Human TBK1	TRCN0000314840
Human TLR3	TRCN0000056851
Murine TBK1	TRCN0000323444
Murine IRF1	TRCN0000077441
Non-target control	SHC002V

2.8 Generation of knockout cell lines using CRISPR

2.8.1 CRISPR plasmid cloning

Gene knockout cell lines were generated using the CRISPR technique. Nickase Cas9 plasmids, including pSpCas9n (BB)-2A-GFP (PX461) and pSpCas9n (BB)-2A-Puro (PX462), were gifts from Feng Zhang through Addgene (plasmids # 48140 and # 62987). A pair of gRNA primers targeting a region within exon 1-4 for each gene were designed using Feng Zhang lab's CRISPR Design (http://crispr.mit.edu/) (**Table 7**), and cloned into plasmid PX461 and PX462 respectively according to a published protocol [93]. Briefly, plasmids were digested with Bpil (ThermoFisher) and purified using GFX™ PCR DNA and Gel Band Purification Kit (GE Healthcare, Chicago, USA). The pair of gRNA oligos were phosphorylated, annealed and ligated with the digested plasmids. The ligation reaction was then treated with Plasmid-safe ATP-Dependent DNase (Cambio Ltd, Cambridge, UK) to prevent unwanted recombination products. The plasmid cloning

was verified by sequencing using the U6 primer (5'-GAGGGCCTATTTCCCATGATTCC-3').

2.8.2 Plasmid transfection and generation of single cell clones

Cells were then transfected with PX461-gRNA-1 and PX462-gRNA-2 plasmids simultaneously using Lipofectamine® 3000 Transfection Reagent (ThermoFisher). A total number of 0.5 x 10^5 cancer cells were seeded in 12-well plate and maintained in the incubator. Twenty-four hours later, the following reagent mixtures were prepared: (1) Lipofectamine 3000 dilution: Opti-MEM medium (ThermoFisher) 150 µl + lipofectamine 3000 4µl; (2) Master mix of DNA: OPti-MEM medium 150 µl + PX461-gRNA-1 1µg + PX462-gRNA-2 1µg + p3000 reagent 4 µl. Upon mixed well, the master mix of DNA was added to diluted Lipofectamine 3000 reagent and incubated in room temperature for 15 minutes. The DNA-lipid complex was then added to the cells and returned to the incubator for 24 hours. Following transfection, cells were washed with PBS for 2 times and cultured with medium containing puromycin (1.5 µg/ml) for 24-48 hours to select transfected cells. Cells remained alive after selection were proceeded to generate single cell clones via serial dilution or FACS (0.5 cell per well in 96-well plates). Single cell clones with biallelic gene knockout were selected and validated using western blots, fluorescent staining or functional assays.

Table 7 CRISPR gRNA sequences

Genes	gRNA pair	sequence (5' - 3')
Human cGAS	1	CAAAACCGCCCGGAGCTTCG
	2	GATGATATCTCCACGGCGGC
Human STING	1	CAACAGGGCCCCACGGCGGA
	2	TACTCCCTCCCAAATGCGGT
Human IFNAR1	1	CTAGGGTCGTCGCGCCCAGG
	2	GCTCGTCGCCGTGGCGCCAT
Human IL-28R	1	GGGAGAGCAGCGTCACATTC
	2	ACTTCAGCGTGTACCTGACA
Human IRF1	1	GATGCGCGGGACGAACATAG
	2	CCGAGTGTCAGCCCACGCGT
Murine cGAS	1	TCGAAGAAAGGCCGCGAAAA
	2	TTCTTTCCCGGACCGAAGAG
Murine STING	1	GTGGATCCTTTGCCACCCAA
	2	CACCTAGCCTCGCACGAACT
Murine IFNAR1	1	CCACATGTTCCCGTCTTGTC
	2	TCAGTTACACCATACGAATC
Murine IRF3	1	CAGCTAAGCCTCCGAGCGCT
	2	CGAGTCTCAGAACTACTGTT

2.9 Fluorescent staining and confocal imaging

From 1-4 x 10^4 Cells were seeded on 4 or 8-well chamber slides (VWR). Following treatment, cells were fixed with 4% (w/v) of paraformaldehyde in PBS for 15 minutes, permeabilized with 0.2% (v/v) Triton X-100 for 15 minutes, blocked with 5% of goat serum (Sigma) for an hour, and then incubated with primary antibodies containing 1% of goat serum at 4 ◦C overnight. After washing with PBS, they were incubated with anti-mouse IgG Alexa 488 fluorescence secondary antibodies (Life technologies) in dark for an hour. Following washing and removal of the chambers, the cells were incubated with mounting medium with DAPI (Molecular Probes) in the dark overnight. Coverslips were sealed with nail polish and slides were imaged using Leica SP8 inverted scanning confocal microscope.

2.10 ELISA

Cell culture supernatants were collected from HT29 or MC38 cells at 72 hours after mock or single dose IR (6Gy for HT29 and 10Gy for MC38). Human IFNL1 and mouse IFNB protein levels in these supernatants were measured using the Human IL-29 (IFN lambda 1) ELISA Ready-SET-Go kit (eBioscience) and the mouse IFN-beta ELISA Kit (R & D), respectively.

2.11 Clonogenic assay

Cancer cells (from 100 to 2000 with greater number plated proportional to the radiation dose) were plated in 6-well plates and incubated at 37 °C in 5% of CO_2 for 24 hours, to allow the cells to attach. They were then irradiated with a range of

doses: 0, 2, 4, 6, 8 and 10 Gy. After RT, they were maintained in the incubator for 2 or 3 weeks, until cells in the control plates had formed colonies suitable for counting. All colonies were stained using a mixture of 6.0% glutaradehyde and 0.5% crystal violet and dried on the bench top at room temperature. Finally, the colony number was counted on the GelCount^{TM} Tumour Colony Counter (Oxford Optronix Ltd, Oxford, UK). The plating efficiency (PE) and survival fraction (SF) were calculated using the following equations: PE= number of colonies formed in mock irradiated plates / seeding cell number x 100%; SF= number of colonies formed / seeding cell number x PE. The survival fraction data was then plotted on a $\log_{10}$ scale against the RT dose in a linear scale. The survival curves were fitted in Graphpad Prism 5 (GraphPad Software, Inc. San Diego, CA, USA) using the linear quadratic model: ln (SF) = - $\alpha D - \beta D^2$.

2.12 Cell proliferation assay

Cell proliferation was assessed using WST-1 (Sigma). A total number of 500 cells were seeded in 96-well plates and incubated at 37 °C in 5% of CO_2. At indicated time points, the medium was removed and 90 ul fresh complete medium plus 10 ul WST-1 reagent was added to each well. Following incubation at 37 °C in 5% of CO_2 for 1h, the absorbance of the samples at 450 nm minus the reference (690 nm) was measured using Infinite 200 Pro reader (TECAN).

2.13 Assessment of Caspase 3/7 in cells via flow cytometry

The presence of caspase 3/7 in cells was assessed using CellEvent™ Caspase-3/7 Green Detection Reagent (ThermoFisher). A total number of 10^5 cells were seeded in 6-well plates and incubated at 37 °C in 5% of CO_2 for 24 hours. Cells were then subjected to mock or 10Gy IR. At indicated time points following IR, cells were harvested, resuspended in PBS with 5% FBS, incubated with Caspase-3/7 green detection reagent (500 µm) at 37 °C for 30 minutes. Cells were then assessed in the BD FACS Calibur flow cytometer (BD Bioscience) using 488 nm laser and the FITC channel. The FACS data was analysed using Flowjo.

2.14 Assessment of cell cycle in cell using propidium lodide

The cell cycle distribution in cells was assessed using Propidium lodide Flow Cytometry kit (Abcam). A total number of 10^5 cells were seeded in 6-well plates and incubated at 37 °C in 5% of CO_2 for 24 hours. Cells were then subjected to mock or 10Gy IR. At indicated time points following IR, cells were harvested, resuspended in PBS, fixed with 66% ethanol at 4°C for at least 2 hours and stained with propidium iodide plus RNase at 37 °C for 30 minutes. Cells were then assessed in the BD FACS Calibur flow cytometer (BD Bioscience) using 488 nm laser and FL2 channel. The FACS data was analysed in Flowjo using the Cell Cycle function (Watson model).

.

2.15 Animal model

2.15.1 Mice

Female C576BL/6 and CD1-nude mice were purchased from Charles River Laboratories (Wilmington, USA). All mice were used at age 6-8 weeks and held under specific pathogen-free conditions with humidity and temperature control. Animal procedures were carried out in accordance with the UK Animal (Scientific Procedures) Act 1986 and local ethics reviews.

2.15.2 Subcutaneous tumour model

Cancer cells had medium refreshment one day prior to injection and were harvested while in log-growth phase (approximately 70% of confluency). A total number of 2.5 x 10^5 cells (resuspended in 100 µl PBS) were injected into the mouse subcutaneously on the right flank under inhalation anaesthesia with 3% isoflurane. For tumour rechallenge, 1 x 10^5 cancer cells were injected on the left flank. Tumour sizes were measured every other day using calipers. Tumour sizes were measured 3 times per week using callipers. Tumour volumes were calculated using the formula: Length x $Width^2/2$.

2.15.3 Irradiation treatment of subcutaneous tumours

Mice were subjected irradiation treatment when their tumour sizes reached 100 mm^3. X-ray radiation treatment (300 KV, dose rate 2.25 Gy per minute) was delivered to the xenograft tumours using a GulmayRS320 irradiation system (Gulmay Medical Ltd, Surrey, UK). Mice were shielded with only the tumour exposed under

anaesthesia. Following IR, Mice were observed for at least two months and culled when their tumour size exceeded 500 mm^3. Mice with tumour ulceration were culled and excluded from the analysis.

2.16 Immune profiling using flow cytometry

Tumour samples were cut into small pieces using scalpels and incubated in 5 ml of Hank's Balanced Salt solution with collagenase 2 (10mg/ml), DNase I (2 U/ml) and 1X protein transport inhibitor cocktail (ThermoFisher) with regular shaking at 37°C. Cell suspensions were then strained through 50 µm nylon strainer, treated with red blood cell lysis buffer and washed with ice cold PBS. Cells were blocked with anti-mouse CD16/32 antibodies for 5 minutes prior to the incubation with mixed antibodies at 4°C in the dark for 45 minutes. Antibodies used in this study were listed in **Table 8**. Following incubation, cells were washed and fixed for 40 minutes at room temperature using Foxp3/Transcription Factor Fixation/permeabilization working solution (ThermoFisher). Cells with intracellular markers in the panel were permeabilizated and incubated with antibodies in the dark for 45 minutes. Subsequently, these cells together with samples without intracellular markers in the panel were washed, resuspended in PBS and proceeded to the assessment in the flow cytometer.

Three types of control were prepared along with the samples: (1) isotype control: cells stained with viability dyes and mixed isotype control antibodies for each panel; (2) Fluorescence minus one (FMO) control: cells stained with all the flurochromes in the panel except the one being measured; (3) Singe stained controls: single stained controls for compensation were prepared using Amine Reactive

Compensation Bead Kit (ThermoFisher, for viability dye) and UltraComp eBeads ™ Compensatoin Beads (ThermoFisher, for all remaining flurochromes).

Flow cytometry analysis were performed using LSR II (BD Bioscience) or Attune (ThermoFisher). The flow cytometry data was analyzed using FlowJo software.

Table 8. Antibodies used for flow cytometry experiments

Antibodies (clone)	Isotype	Suppliers; Catalogue number
Rat anti-Mouse CD16/CD32 (Fc block)		BD Bioscience; 553141
Anti-CD8a (53-6.7) FITC	Rat IgG2a, κ	eBioscience; 11-0081-81
Anti-CD31 (390) FITC	Rat IgG2a, κ	eBioscience; 11-0311-82
Anti-CD140a (APA5) FITC	Rat IgG2a, κ	eBioscience; 11-1401-80
Anti-CEACAM1a (MAb-CC1) AF 488	Mouse IgG1, κ	BioLegend; 134525
Anti-CD11c (N418) PerCp-Cy5.5	Hamster IgG	BioLegend; 117327
Anti-Galectin-9 (RG9-35) PerCp-Cy5.5	Rat IgG2a, κ	BioLegend; 136111
Anti-PD-L2 (122) PerCP-eFluor 710	Rat IgG2a, κ	eBioscience; 46-9972-82
Anti-Ki67 (SolA15) PE	Rat IgG2a, κ	eBioscience; 12-5698-82
Anti-CD86 (B7-2) PE	Rat IgG2a, κ	eBioscience; 12-0862-81
Anti-F4/80 (BM8) PE	Rat IgG2a, κ	eBioscience; 12-4801-82
Anti-HVEM (HMHV-1B18) PE	hamster IgG	BioLegend; 136303
Anti-CD45 (30-F11) PE-Cy7	Rat IgG2b, κ	eBioscience; 25-0451-81
Anti-Granzyme B (NGZB) PE-Cy7	Rat IgG2a, κ	eBioscience; 25-8898-82
Anti-CD11b (M1/70) PE-Cy7	Rat IgG2b, κ	eBioscience; 25-0112-82
Anti-Galectin-9 (RG9-35) APC	Rat IgG2a, κ	BioLegend; 136109
Anti-Tim-3 (RMT3-23) APC	Rat IgG2a, κ	BioLegend; 119705

To be continued in the next page

Antibodies	Isotype	Suppliers; Catalogue number
Anti-H-2Kb (AF6-88.5.5.3) APC	Mouse IgG2a, κ	eBioscience; 17-5958-80
Anti-FOXP3 (FJK-16s) APC	Rat IgG2a, κ	eBioscience; 17-5773-80
Anti-NK1.1 (PK136) APC	Mouse IgG2a, κ	eBioscience; 17-5941-81
Anti-CD155 (TX56) PE-Cy7	Rat IgG2a, κ	BioLegend; 131512
Anti-CD45 (30-F11) Alexa Fluor® 700	Rat IgG2b, κ	eBioscience; 56-0451-82
Fixable Viability Dye eFluor® 780		eBioscience; 65-0865-14
Anti-PD-L1 (10F.9G2) BV421	Rat IgG2b, κ	BioLegend; 124315
Anti-PD-1 (29F.1A12) BV421	Rat IgG2a, κ	BioLegend; 135221
Anti-Qa-1(b) (6A8.6F10.1A6) BV421	Mouse IgG	BD Bioscience; 744385
Anti-NKp46 (29A1.4) APC	Rat IgG2a, κ	BioLegend; 137607
Anti-CD4 (RM4-5) BV510	Rat IgG2a, κ	BioLegend; 100553
Anti-CD3ε (145-2C11) BV510	Hamster IgG	BioLegend; 100353
Anti-I-A/I-E (M5/114.15.2) BV510	Rat IgG2b, κ	BioLegend; 107635
Anti-CD3ε (145-2C11) BV605	Hamster IgG	BioLegend; 100351
Anti-CD80 (16-10A1) BV650	Hamster IgG	BioLegend; 104731
Anti-CD4 (RM4-5) BV605	Rat IgG2a, κ	BioLegend; 100548
Anti-Gr-1 (RB6-8C5) BV711	Rat IgG2b, κ	BioLegend; 108443

2.17 Fluorescence-activated cell sorting (FACS)

Singe cell suspensions were prepared as described in **2.16** with the exception that the protein transport inhibitor was not included in the digestion solution. Cells were blocked with anti-mouse CD16/32 antibodies for 5 minutes prior to the incubation with mixed antibodies in the dark at 4 °C. Stained cell suspensions were sorted into designed populations using a MoFlo MLS High Speed Cell Sorter (Beckman Coulter Legacy).

2.18 CD8+ T cells or NK cells depletion in C57BL6 mice

For CD8+ T cells depletion experiment, mice received intraperitoneal injection (i.p.) of InVivoMab anti-mouse CD8 Alpha (clone 2.43) or Rat IgG2b isotype control (clone LTF-2) at a dose of 10 mg/Kg each time. InVivoMab anti-mouse NK1.1 (clone PK136) and mouse IgG2a isotype control (C1.18.4) at a dose of 20 mg/Kg were used for NK cells depletion. Antibodies were diluted in PBS at 1 μg/μl. Injections were performed 1 day before treatment and then twice per week. All antibodies for the depletion experiment were purchased from Bio X Cell (West Lebanon, NH, USA). The efficacy of cell depletion was validated in C57BL6 mice bearing MC38 tumours using flow cytometry. At 24 and 72 hours following i.p an single dose injection of anti-CD8α or NK1.1 Ab, tumours were harvested, disaggregated and assessed using flow cytometry with FITC-anti-CD8α (clone 53.67) and APC-anti-NKp46 (clone 29A1.4) antibody, respectively.

2.19 In vitro killing of cancer cells by tumour-derived CD8+ T cells

Cancer cells were seeded in 96-well plate (10^3 cells per well) 24 hours prior to co-culture. The number of cancer cells in the well was re-counted to take account of their proliferation during culture. CD8+ T cells were sorted by FACS from tumours in C57BL6 mice and added to the plated tumour cells and maintained in the incubator. Tumour cells cultured alone were used as controls. Co-cultured medium was RPMI medium supplemented with 10% of FBS, 1% of Penicillin/Streptomycin, 1mM L-Glutamine, 55 μM 2-mercaptoethanol and IL-2 (30 U/ml). Upon co-cultured for 48 hours, culture wells were washed extensively with PBS, fixed with 4% of PFA for 15 minutes and stained with Hoechst (1μg/ml) for 5 minutes. The numbers of remained cells in the well were then quantified in Celigo Imaging Cytometer (Nexcelom Bioscience, Massachusetts, USA). The killing percentage was calculated using the following formula: (cell number in control well – cell number in co-cultured well)/cell number in control well x 100.

2.20 Imaging assessment of apoptosis in cancer cells upon co-cultured with tumour-derived CD8+ T cells

Cancer cells were tagged with mCherry via lentivirus transfection (vector: pCDH-CMV-MCS-EF1α-Hygro, System Bioscience, Palo Alto, CA, USA) followed by FACS for bright population. These cells were irradiated with 10Gy IR, immediately seeded in μ-Slide VI 0.4 channel slides (ibidi, Munich, Germany) and returned to the incubator. Forty-eight house later, CD8+ T cells were isolated from WT or IFNAR1 KO MC38 tumours by FACS at day 4 after 10Gy IR, labelled with CMAC dye (ThermoFisher), and added to channel slides in an E: T ratio of 3:2. Culture media were supplemented with IL-2 (30 U/ml) and Caspase-3/7 Green detection reagent

(500 nM, ThermoFisher). Subsequently, channel slides were imaged every 15 minutes for up to 16 hours using Nikon ECLIPSE Ti-E Inverted Microscope. During the whole course of imaging, chamber slides were maintained at 37 °C with 5% CO2. The imaging data was transferred to Imaris station for analysis (Bitplane, Zurich, Switzerland). The percentage of caspase 3/7+ tumour cells was calculated using the following formula: the number tumour cells becoming caspase-3/7+ following interaction with CD8+ T cells/ the number of tumour cells interacted with CD8+ T cells x 100.

2.21 Statistical analysis

All values in this study represent means (M) and standard deviations (SD) with the exception that bars in the growth curves of tumours show means and the standard errors of the mean (SEM). More than one independent experiment was performed with at least three determines for each data. Comparisons were performed using Student's t-test (ns > 0.05, * P < 0.05, ** P < 0.01, *** P < 0.001). Survival time was measured from the beginning of IR treatment until the date of mice being culled. The survival curves for different groups of mice were generated using the Kaplan-Meier method. The log-rank test was used to compare the median survival time. All graphs were plotted using Graphpad Prism 5.

Chapter 3

Mechanism affecting type I/III IFN induction in cancer cells after exposure to IR

3.1 Introduction

3.1.1 IR triggers anti-tumour immune responses

In the classical model, IR kills cancer cells mainly by direct induction of lethal DNA damage. However, emerging data suggest that host immunity also plays an important role in the therapeutic outcome of radiation therapy [19, 20, 94]. Irradiated tumour cells can release a variety of immunomodulatory factors, including DAMPs, cytokines and chemokines, resulting in an inflammatory microenvironment with the potential to facilitate tumour-specific immunity. IR has been demonstrated to trigger an anti-tumour immune response at the local site and even systemically affecting distant sites [25, 95, 96]. The underlying mechanisms are still not fully understood.

3.1.2 IFNs as mediators in IR-induced immune response

IFNs have exhibited multiple antitumor effects and been used to treat a number of malignancies for decades [71]. New concepts have emerged suggesting that IFN signalling pathways are involved in determining the therapeutic efficacy of IR. One study found that localized IR treatment not only induced lethal damage in cancer cells, but also promoted intratumoural production of IFN-γ, which in turn altered the tumour microenvironment, leading to enhanced T cell infiltration and tumour target recognition [83]. Another study found that the therapeutic efficiency of ablative IR treatment relied upon type I IFN-dependent innate and adaptive immune responses [82]. These studies suggest that IFNs may help improve therapeutic efficacy by enhancing tumour-specific immune response.

3.1.3 Roles of tumour cells in IR-induced IFNs

One critical question that remains to be answered is how IR induces IFNs in tumours, especially type I/III IFNs, which in principle could be expressed by all cell types. Previous studies suggested that the main producers of type I IFN in tumour were immune cells, especially dendritic cells, whereas cancer cells, the main cellular component in tumours, did not show significant contributions [19, 82, 83]. However, emerging data indicates that cells of non-hematological origins, including cancer cells, may also have role in IR-induced IFNs. In fact, type I IFN expression is evident in cells of non-hematological origin following IR treatment [97]. Moreover, etoposide, a chemotherapeutic agent that like IR induces DNA double strand breaks, has been found to directly induce type I IFNs in cancer cells [84]. In our hands, we also found many IFN stimulated genes (ISGs) were upregulated in tumour xenografts after fractionated IR. Taken together, we hypothesized that IR could directly induce IFNs in cancer cells.

3.1.4 Aims

The current study aimed to answer the following two questions: (1) Could type I/III IFNs be directly upregulated in cancer cells by IR? (2) If they could, what is the underlying mechanism?

3.2 Results

3.2.1 Induction of type I/III IFN in cancer cells after exposure to IR

We first sought to determine whether IR induced type I IFN (IFNB and IFNA) in cancer cells *in vivo* in tumours. MC38 tumours grown in C57BL/6 were subjected to single dose (10 Gy /1 F), fractionated (2 Gy x 5 F, 1 F /day) or mock IR. At 120 hours after single dose IR or 24 hours after fractionated IR, respectively, tumours were harvested, disaggregated and separated into three main cellular populations, cancer cells, dendritic cells and other immune cells (**Figure 3A).** Cells other than cancer cells or immune cells were less than 1% of the total and therefore were discarded in the following analysis.

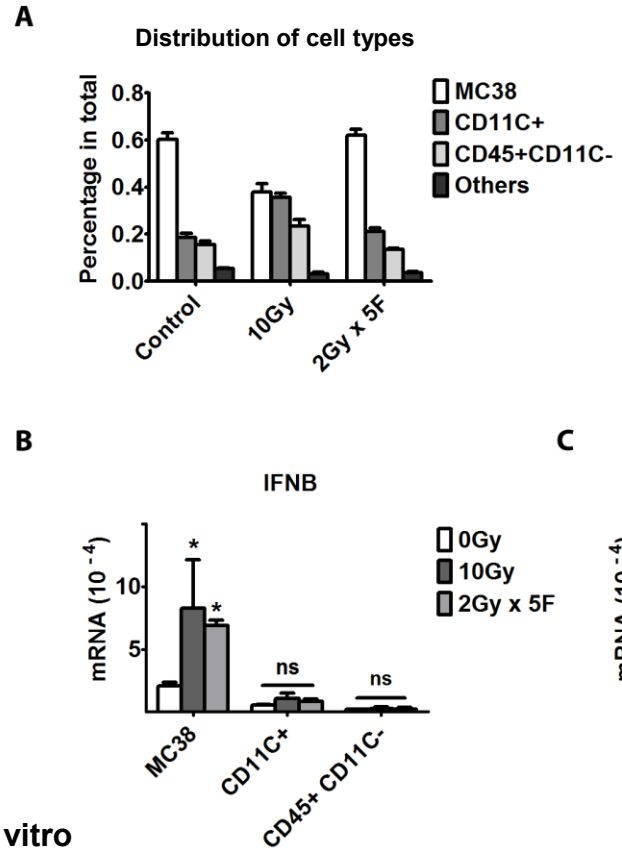
Type I IFN (IFNB and IFNA) expression in the three main cell populations was analysed by RT-qPCR. Strikingly, both single dose and fractionated IR led to robust upregulation of IFNB in MC38 cells (**Figure 3 B**). The IFNB expression level of cancer cells after 10 Gy x 1 F and 2 Gy x 5 F were 4.0 ± 1.9 fold and 3.3 ± 0.2 fold of that in control group. Whilst there was a trend toward increased expression of type I IFN in dendritic cells and other immune cells, these inductions were not statistically significant and of no more than 2 fold (**Figure 3 B and C**). Thus, clearly cancer cells are an important source of IFNB in irradiated tumours.

Similar results were found after irradiation of MC38 cells and HT29 cells in tissue culture (**Figure 3 D and E**). Interestingly, differences were also noted between *in vivo* and *in vitro* experiments. IFNA was induced by IR in MC38 in cell culture, whilst not in MC38 tumours (**Figure 3 C and D**). In HT29, IFNL1 and IFNL2/3, in addition to IFNB, were upregulated after IR (**Figure 3E**). As far as we know, this is

the first evidence that IR can directly induce type III IFN in cancer cells. IFNA was upregulated by less than 2 fold after the single dose and less than 3 fold after fractionated IR with very low absolute RNA levels in HT29. Type III (IFNL2/3) was barely detectable at the mRNA level in MC38. Therefore, induction of IFNA in HT29 and IFNLs in MC38 were not followed in subsequent experiments. IR treatment of several other human (**Figure 3F**) and murine (**Figure 3G**) cancer cell lines in tissue culture led to similar patterns of IFN induction. Collectively, these findings suggest that IR induction of type I/III IFNs in cancer cells is a general phenomenon and may have important contributions to their responses to IR. Further, induction of type III IFNs was limited to human cancer cells in our experiments.

Next, we sought to characterize the induction pattern of IFNs by IR in cancer cells. We irradiated HT29 cells with a range of IR doses (0 ~12 Gy) and assessed the gene expression levels of IFNs and ISGs. As displayed in **Figure 4 A** and **B**, IR-induced IFNs increased over time after IR treatment. Higher dose led to more IFNs induction with a trend of peaking at earlier time point. ISGs were induced at similar doses and times providing evidence of the induction of functional IFN (**Figure 4 C and D**). Taken together, these results suggest that IR induced IFNs in dose- and time-dependent fashions.

In vivo



In vitro

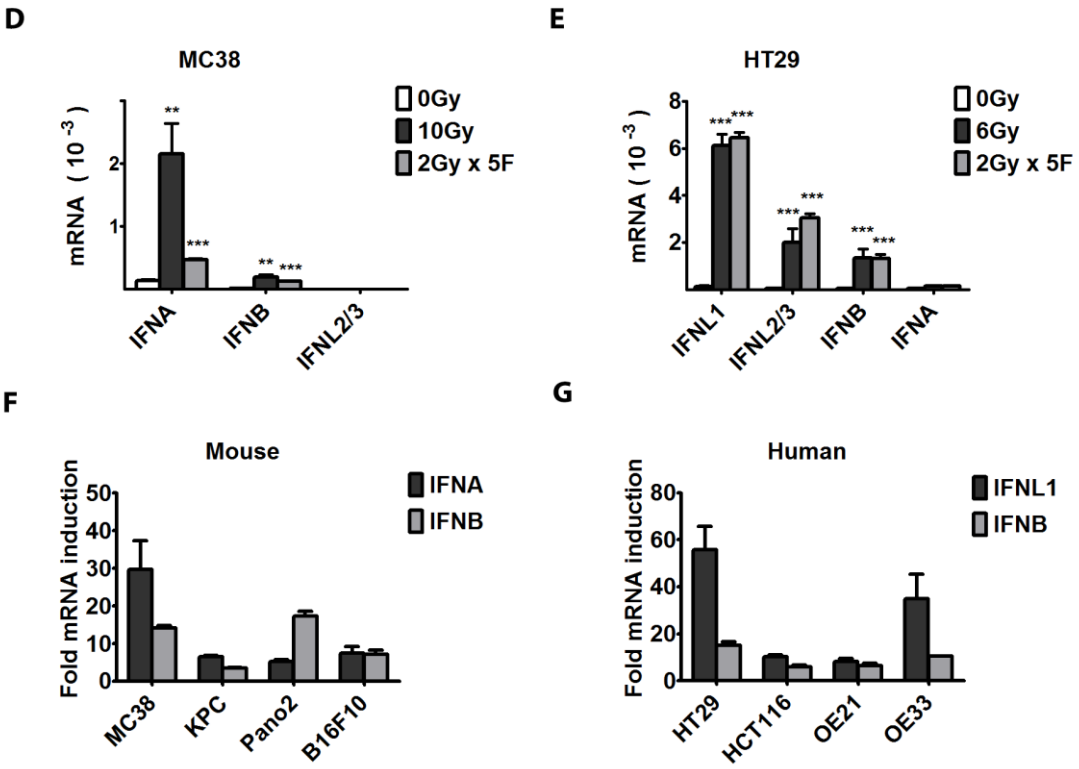


Figure 3. Induction of type I/III IFNs and ISGs in cancer cells after exposure to IR *in vivo* and *in vitro*

(**A**) Three different cell populations were sorted from MC38 tumour xenografts in C57BL/6 mice at 120 hours following mock or 10 Gray (Gy), or 24 hours after 2 Gy x 5 fractions (F) of ionizing radiation (IR). The percentage of each population in total live cells were summarized. N = 3.

RNA was extracted from these cells and transcribed to cDNA. IFNB (**B**) and IFNA (**C**) expression was then analysed by qPCR.

(**D**) IFN mRNA expressions in MC38 cells at 120 hours following mock or 10 Gy, or 24 hours after 2 Gy x 5 F IR *in vitro*.

(**E**) IFN mRNA expressions in HT29 cells at 120 hours following mock or 6 Gy, or 24 hours after 2 Gy x 5 F IR *in vitro*.

(**F**) Fold induction of IFN mRNA expression in a couple of murine cancer cell lines at 72 hours following 10 Gy IR.

(**G**) Fold induction of IFN mRNA expression in a several human cancer cell lines at 72 hours after 6 Gy IR.

All mRNA expression levels in vitro were normalized to beta actin (B-Actin). Gene mRNA fold induction following IR was normalized to expression level of control. All values in this study represent means and standard deviations of at least three determines in more than one independent experiment. Comparisons were performed using Student's t-test (ns > 0.05, * $P < 0.05$, ** $P < 0.01$, *** $P < 0.001$).

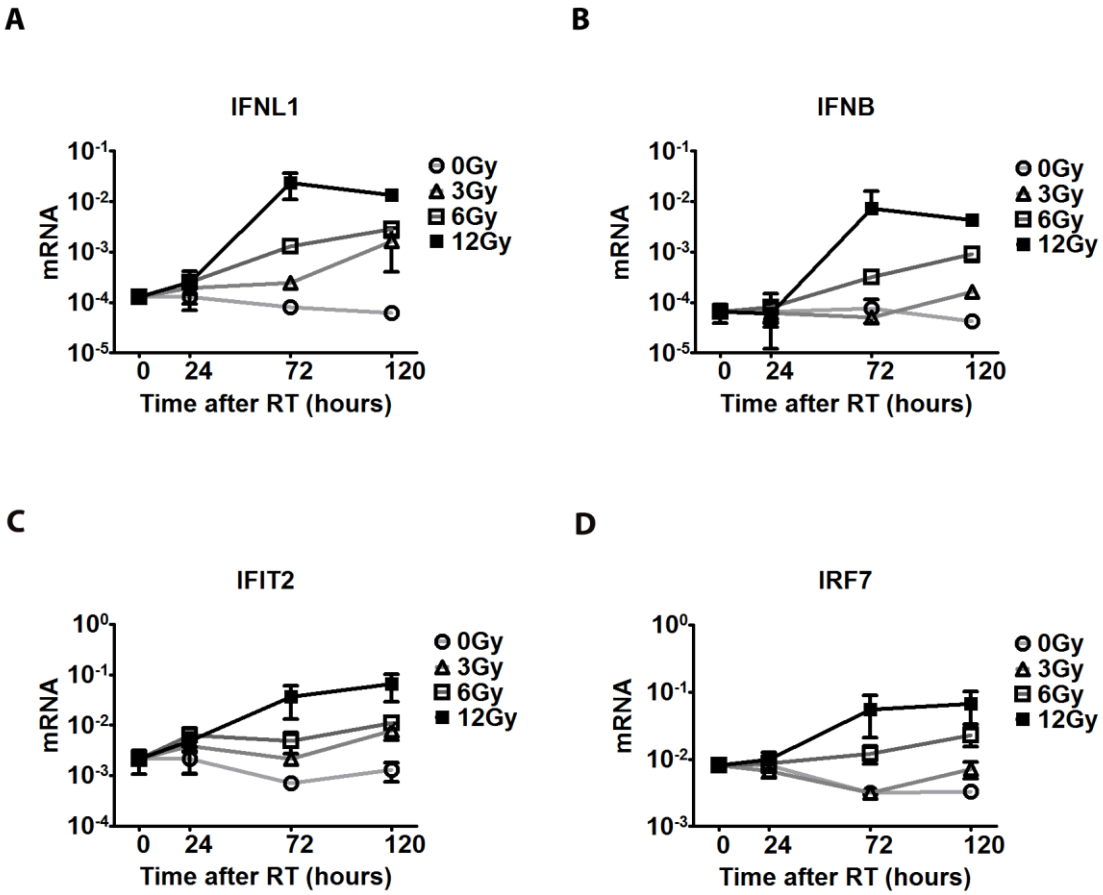


Figure 4. IR induced type I/III IFNs and ISGs in dose- and time-dependent manners.

HT29 cells were exposed to 0 ~ 12 Gy IR. Cells were harvested at indicated time points for the assessment of mRNA expression of IFNL1 (**A**), IFNB (**B**), IFIT2 (**C**) and IRF7 (**D**). Number (N) of replicates = 3.

3.2.2 TBK1 and NF-κB pathways contribute to IFN induction by IR.

The promoters of IFNB and IFNL1 genes have binding sites for both NF-κB transcriptional factors and IRFs which are regulated by their upstream kinases, IKKB and TBK1, respectively [98-100]. IR is known to induce NF-κB activity [99]. We transfected HT29 cells with a NF-κB hMGFP reporter, allowing cellular NF-κB activity to be monitored using flow cytometry. The efficacy of this reporter assay was validated with TNFα as a positive control (**Figure 5 A**). Following a single dose of 6 Gy IR, HT29 cells exhibited gradually increased NF-κB activity (**Figure 5B**). The enhanced NF-κB pathway activity in HT29 cells generated from either single dose or fractionated IR was significantly inhibited using ML120B, an IKKB specific inhibitor (**Figure 5C**). Meanwhile, we also found that IR resulted in oscillating activation of TBK1 (**Figure 5D**). Taken together, our results suggested that IR could activate both NF-κB and TBK1 pathways in HT29 cells.

To distinguish the contributions of these two pathways to induction of type I/III IFNs by IR, we down-regulated IKKB and TBK1 in HT29 using shRNA (**Figure 6 A and B**). Both reduced induction of IFNs, but to different extents. TBK1 KD significantly downregulated the expression of IFNs at both 72 and 120h after IR treatment, while IKKB KD only reduced IR-induced IFNs at the later 120h time point (**Figure 6 C-D**). Inhibiting both TBK1 and NF-κB pathways simultaneously completely abolished the induction of IFNs. Similarly results were found in LOVO. IFN induction was mainly mediated by TBK1, and to lesser extent, the NF-κB pathway (**Figure 7**). Thus both pathways play a role in mediating IFN induction with TBK1 having overall a greater effect.

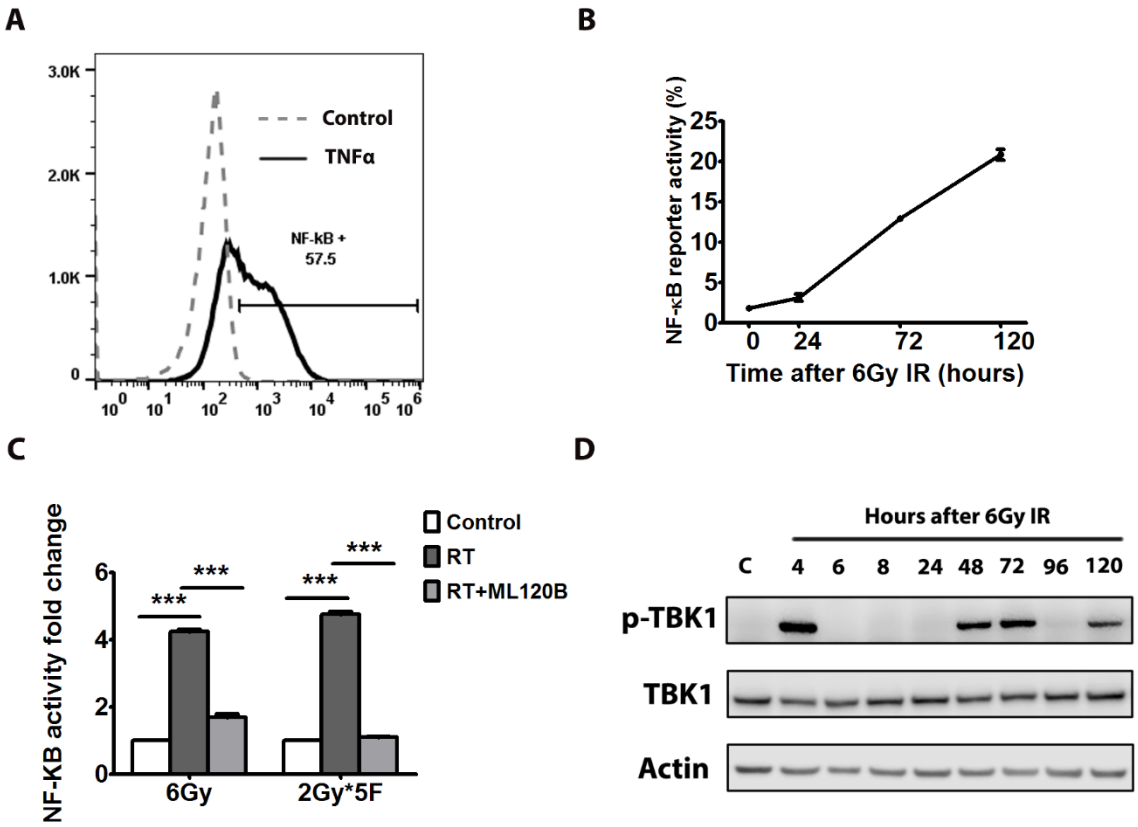

A
3.0K
2.0K
1.0K
0
Control
TNFα
NF-kB +
57.5
B
NF-κB reporter activity (%)
25
20
15
10
5
0
0
24
72
120
Time after 6Gy IR (hours)
C
NF-KB activity fold change
6
4
2
0
***
***
***
***
6Gy
2Gy*5F
Control
RT
RT+ML120B
D
Hours after 6Gy IR
C
4
6
8
24
48
72
96
120
p-TBK1
TBK1
Actin

Figure 5. Activation of NF-κB pathway and TBK1 in HT29 cells following 6 Gy IR.

(**A**) HT29 cells were transfected with NF-κB activity hMGFP reporter. NF-κB activity was assessed by flow cytometry with TNFα as a positive control.

(**B**) NF-κB activity in HT29 cells following 6 Gy IR in vitro. N = 3.

(**C**) NF-κB activity in HT29 cells at 120 hours after mock or 6 Gy, or 24 hours after 2 Gy x 5 F of IR, with or without ML120B (90 minutes of pre-incubation and remained in the medium through the experiment; final concentration 20 μm). N = 3.

(**D**) Phosphorylation of TBK1 in HT29 cells following 6 Gy IR.

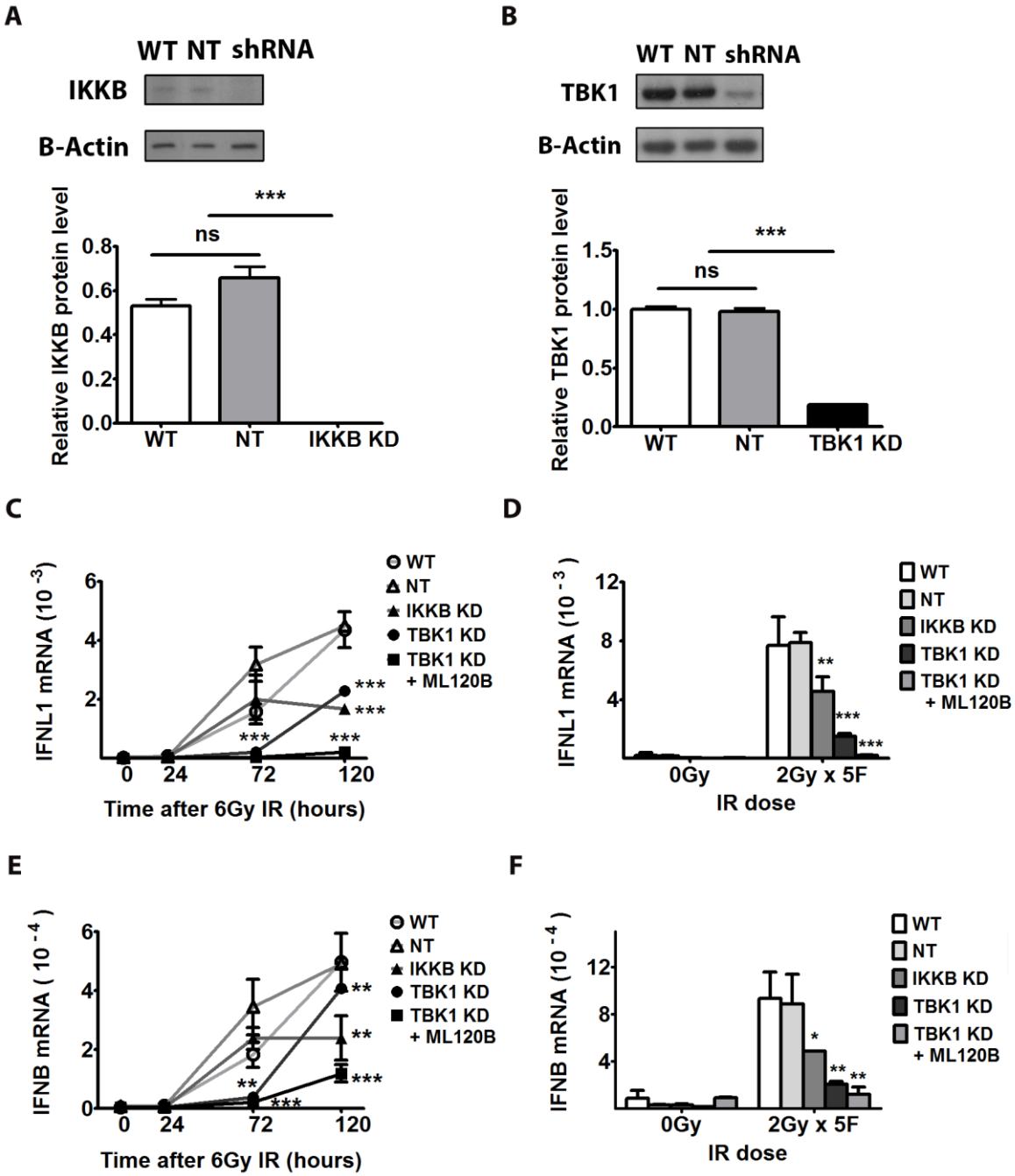

A
WT NT shRNA
IKKB
B-Actin
Relative IKKB protein level
***
ns
0.8
0.6
0.4
0.2
0.0
WT
NT
IKKB KD
B
WT NT shRNA
TBK1
B-Actin
Relative TBK1 protein level
***
ns
1.5
1.0
0.5
0.0
WT
NT
TBK1 KD
C
IFNL1 mRNA (10 -3)
6
4
2
0
24
72
120
Time after 6Gy IR (hours)
WT
NT
IKKB KD
TBK1 KD
TBK1 KD
+ ML120B
***
***
***
***
D
IFNL1 mRNA (10 -3)
12
8
4
0Gy
2Gy x 5F
IR dose
WT
NT
IKKB KD
TBK1 KD
TBK1 KD
+ ML120B
**
***
***
E
IFNB mRNA (10 -4)
6
4
2
0
24
72
120
Time after 6Gy IR (hours)
WT
NT
IKKB KD
TBK1 KD
TBK1 KD
+ ML120B
**
**
**
***
***
F
IFNB mRNA (10 -4)
12
8
4
0Gy
2Gy x 5F
IR dose
WT
NT
IKKB KD
TBK1 KD
TBK1 KD
+ ML120B
*
**
**

Figure 6. TBK1 and NF-κB pathways contribute to type I/III IFN induction in cancer cells by IR

The knockdown efficacies of IKKB (**A**) and TBK1 (**B**) in HT29 cells were assessed by western blot. N = 3.

IFNL1 expression in a panel of HT29 cells (WT *vs*. Non-target control (NT) *vs*. IKKB KD *vs*. TBK1 KD) following 6 Gy IR (**C**) or at 24 hours after 2 Gy x 5 F IR (**D**), with or without ML120B. N = 4.

IFNB expression in a panel of HT29 cells (WT *vs*. NT *vs*. IKKB KD *vs*. TBK1 KD) following 6 Gy IR (**E**) or at 24 hours after 2 Gy x 5 F IR (**F**), with or without ML120B. N = 4.

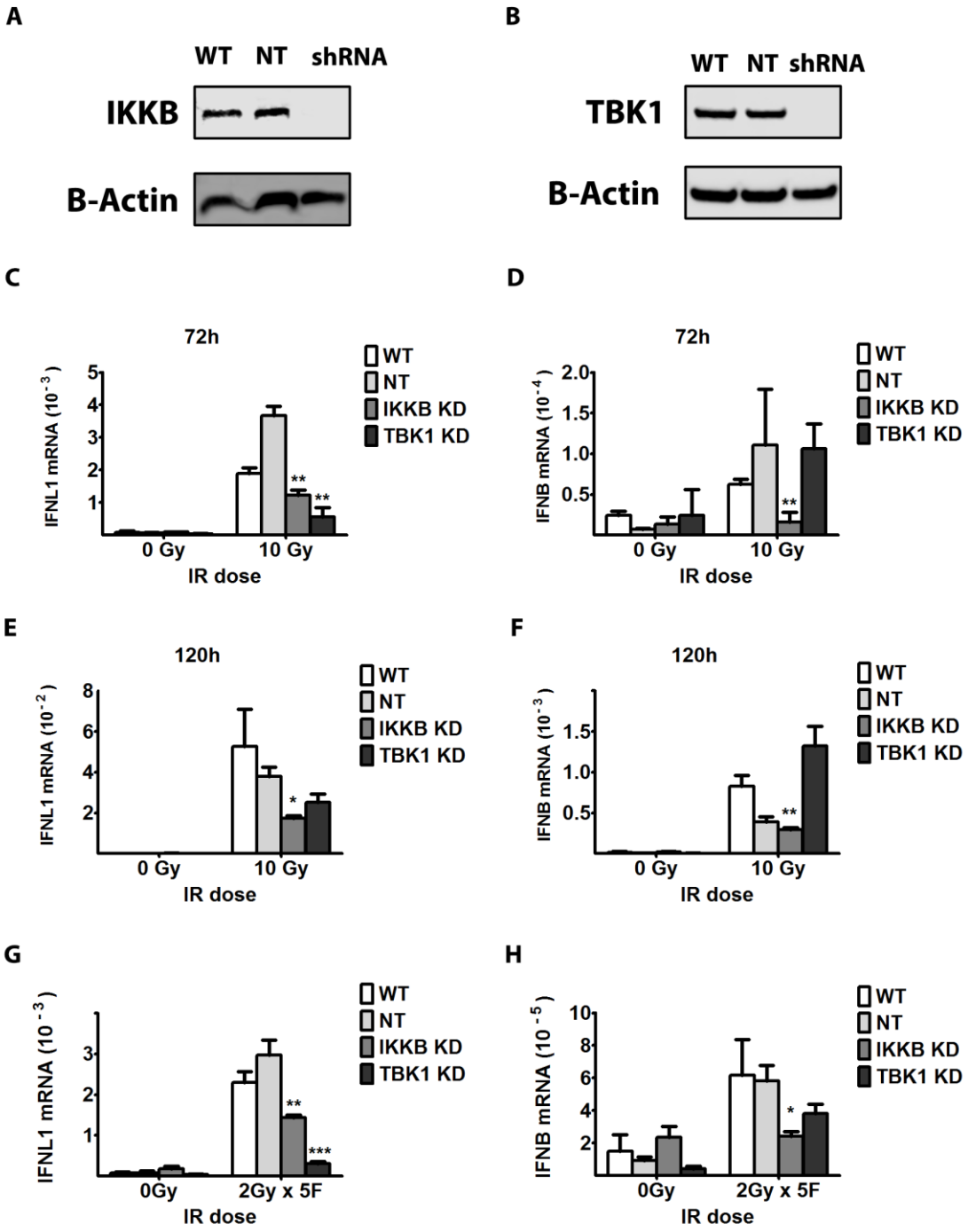

A
WT NT shRNA
IKKB
B-Actin
B
WT NT shRNA
TBK1
B-Actin
C
72h
IFNL1 mRNA (10-3)
WT
NT
IKKB KD
TBK1 KD
0 Gy
10 Gy
IR dose
D
72h
IFNB mRNA (10-4)
E
120h
IFNL1 mRNA (10-2)
F
120h
IFNB mRNA (10-3)
G
IFNL1 mRNA (10-3)
0Gy
2Gy x 5F
H
IFNB mRNA (10-5)

Figure 7. TBK1 and NF-κB pathways contribute to type I/III IFN induction in LOVO cells by IR.

The knockdown efficacies of IKKB (**A**) and TBK1 (**B**) in LOVO cells were assessed by western blot.

IFNL1 expression levels in LOVO cells (WT *vs*. NT *vs*. IKKB KD *vs*. TBK1 KD) at 72 hours and 120 hours after mock or 10 Gy (**C** and **E**), or 24 hours following 2 Gy x 5 F (**G**) IR were assessed by RT-qPCR. N = 3.

IFNB expression levels in LOVO cells (WT *vs*. NT *vs*. IKKB KD *vs*. TBK1 KD) at 72 hours and 120 hours after mock or 10 Gy (**D** and **F**), or 24 hours following 2 Gy x 5 F (**H**) IR. N = 3.

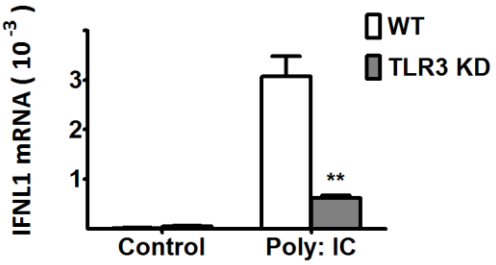
3.3.3 Cytosolic DNA sensors-STING is the key signalling axis in induction of IFNs by IR

TBK1 can be activated by a variety of sensors (e.g. TLRs, RLRs and CDRs) in cooperation with their adaptors. Of the sensors, TLR3 and RIG-I have been found to mediate or be related to type I IFN expression in cancer cells [97, 101]. Interestingly, in contrast to previous reports, we found that TLR3 downregulation actually resulted in more IFN expression in HT29 after IR (**Figure 8**). In the cell lines that we used we could barely detect RIG-I by immunoblot, although its mRNA level increased overtime after a single dose IR (data not shown). Thus, it is less likely that RIG-I initiates the induction of after IR, though its role cannot be totally excluded.

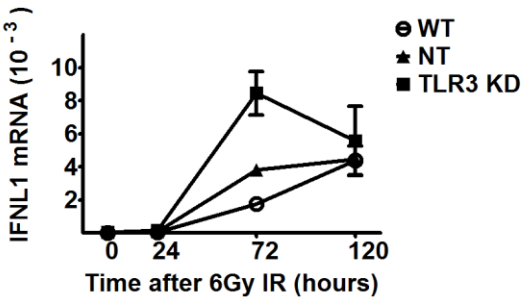
To further delineate the pathways leading to activation of TBK1, We turned to consideration of cytosolic DNA sensors, as recently published studies indicated that STING-dependent cytosolic DNA sensing mediated the induction of type I interferon in dendritic cells from untreated or irradiated tumours [102, 103]. To assess the roles of STING, we eliminated expression of this gene using CRISPR (validated in **Figure 9A**). Strikingly, STING KO completely abrogated IFNL1 and IFNB expression in HT29 after fractionated or single dose IR (**Figure 9 C-F**). In MC38, STING KO greatly reduced IFNB induction after 10Gy and reduced induction by about 50% after fractionated IR treatment as well (**Figure 10 C and D**). IFNA was less affected with almost no reduction after 10Gy and no discernible effect after fractionated IR (**Figure 10 E and F**). Thus, our evidence places STING as an adaptor in IR induction of type I/III IFN to variable extent. To further explore this signalling pathway, we evaluated the effects of genetic elimination of cGAS (validated in **Figure 9B** and **Figure 10B**, respectively), one of the upstream sensors of STING. In HT29, cGAS KO decreased FNB by 50% or less, indicating that other CDRs may be involved (**Figure 9 C-F**). In

MC38, cGAS KO even increased IFNA but reduced IFNB to approximately the same extent as STING KO (**Figure 11 E and F**).

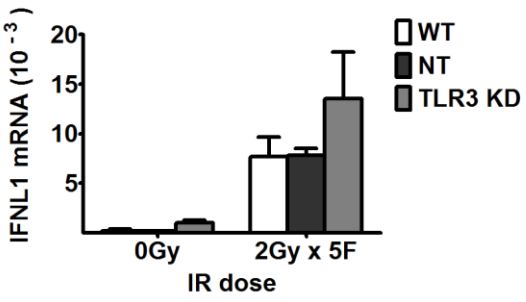
A


IFNL1 mRNA (10 -3)
WT
TLR3 KD
3
2
1
**
Control
Poly: IC

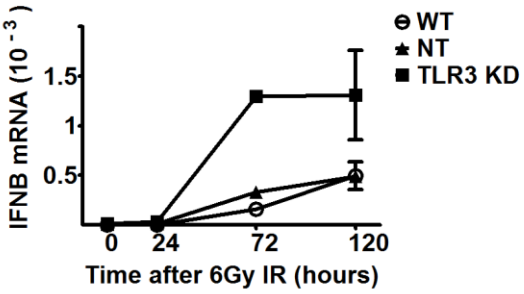
B


IFNL1 mRNA (10 -3)
WT
NT
TLR3 KD
10
8
6
4
2
0
24
72
120
Time after 6Gy IR (hours)

C


IFNL1 mRNA (10 -3)
WT
NT
TLR3 KD
20
15
10
5
0Gy
2Gy x 5F
IR dose

D


IFNB mRNA (10 -3)
WT
NT
TLR3 KD
1.5
1
0.5
0
24
72
120
Time after 6Gy IR (hours)

E

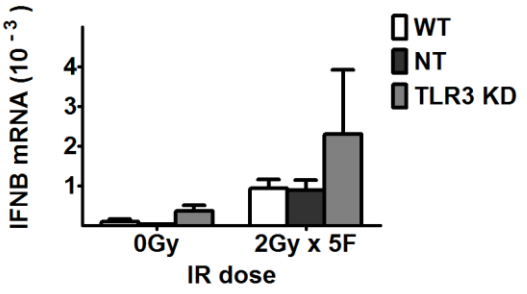

IFNB mRNA (10 -3)
WT
NT
TLR3 KD
4
3
2
1
0Gy
2Gy x 5F
IR dose

Figure 8. TLR3 knockdown did not reduce IR-induced type I/III IFNs in HT29 cells.

(**A**) IFNL1 expression in WT and TLR3 KD HT29 cells following treatment with a TLR agonist, Poly I:C (10 μg/ml).

IFNL1 expression in HT29 cells (WT *vs*. NT *vs*. TLR3 KD) at 24, 72 and 120 hours after mock or 6 Gy (**B**), or 24 hours after 2 Gy x F (**C**) IR were assessed by RT-qPCR. N = 3.

IFNB expression in HT29 cells (WT *vs*. NT *vs*. TLR3 KD) at 24, 72 and 120 hours after mock or 6 Gy (**D**), or 24 hours after 2 Gy x F (**E**) IR. N = 3.

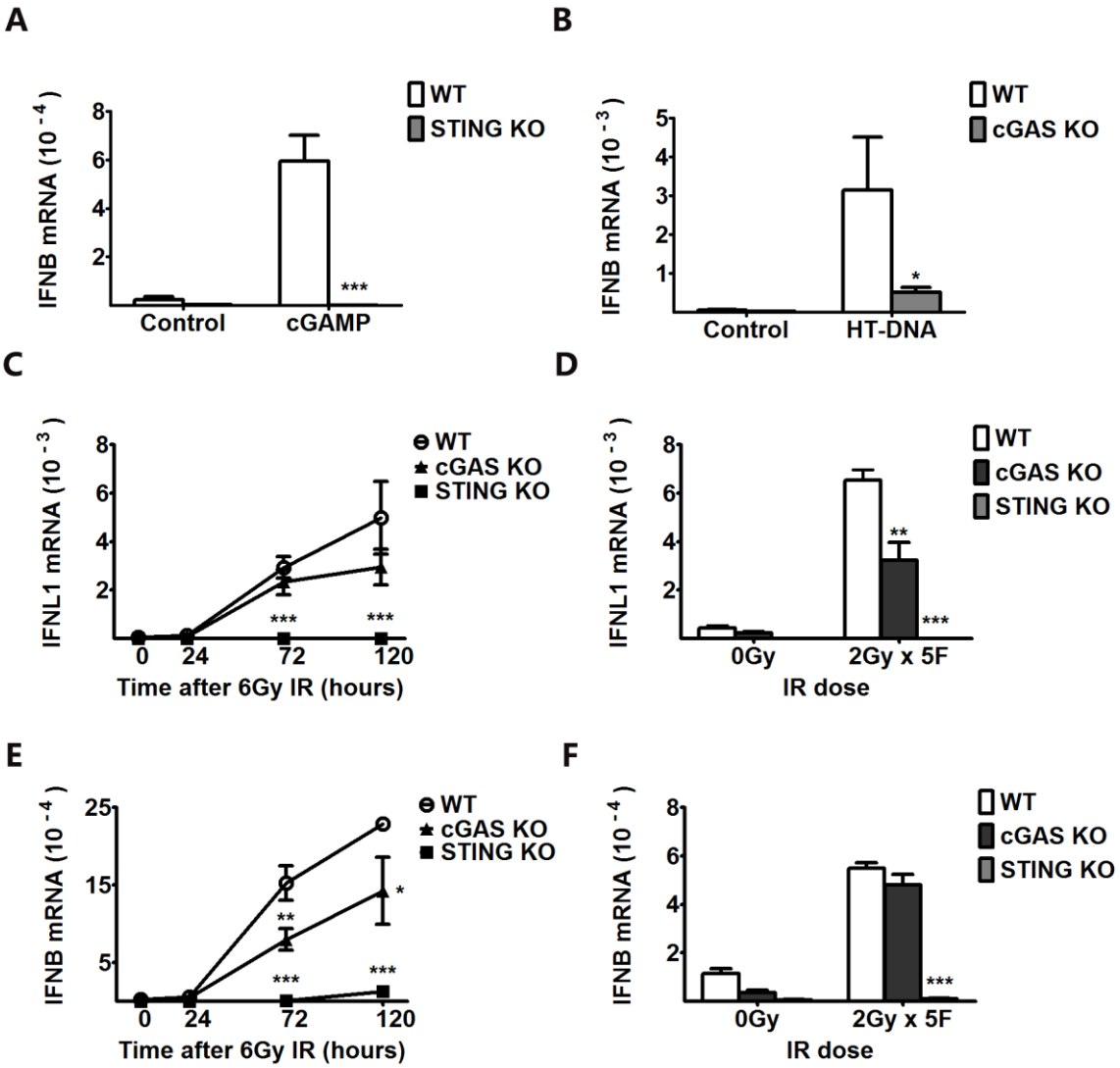

A
IFNB mRNA (10 -4)
WT
STING KO
***
Control
cGAMP
B
IFNB mRNA (10 -3)
WT
cGAS KO
*
Control
HT-DNA
C
IFNL1 mRNA (10 -3)
WT
cGAS KO
STING KO
***
***
0
24
72
120
Time after 6Gy IR (hours)
D
IFNL1 mRNA (10 -3)
WT
cGAS KO
STING KO
**
***
0Gy
2Gy x 5F
IR dose
E
IFNB mRNA (10 -4)
WT
cGAS KO
STING KO
**
*
***
***
0
24
72
120
Time after 6Gy IR (hours)
F
IFNB mRNA (10 -4)
WT
cGAS KO
STING KO
***
0Gy
2Gy x 5F
IR dose

Figure 9. Cytosolic DNA sensor-STING is the predominant signalling axis in IR induction of type I/III IFNs in HT29 cells.

(**A**). IFNB mRNA expression of HT29 (WT *vs*. STING KO) at 6 hours after cGAMP (5 μg/ml) treatment. N = 3.

(**B**). IFNB mRNA expression of HT29 (WT *vs*. cGAS KO) at 6 hours after HT-DNA treatment (5 μg/ml). N = 3.

IFNL1 expression in HT29 cells (WT *vs*. cGAS KO *vs*. STING KO) at 24, 72 and 120 hours after mock or 6 Gy (**C**) or 24 hours after 2 Gy x 5 F (**D**) IR were assessed by RT-qPCR. N = 4.

IFNB expression in HT29 cells (WT *vs*. cGAS KO *vs*. STING KO) at 24, 72 and 120 hours after mock or 6 Gy (**E**) or 24 hours after 2 Gy x 5 F (**F**). N = 4.

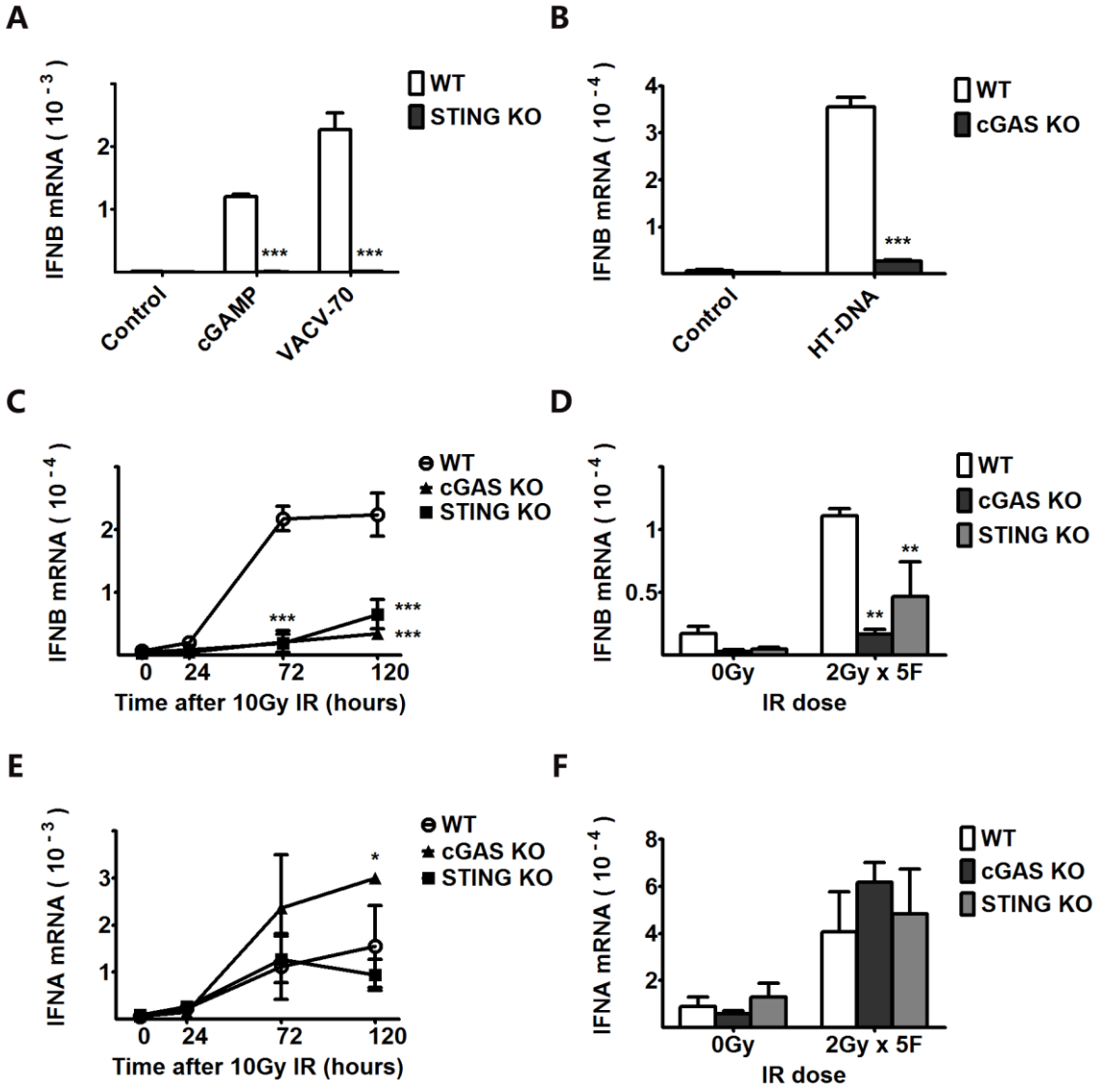

A
IFNB mRNA (10 -3)
WT
STING KO
***
***
Control
cGAMP
VACV-70
B
IFNB mRNA (10 -4)
WT
cGAS KO
***
Control
HT-DNA
C
IFNB mRNA (10 -4)
WT
cGAS KO
STING KO
***
***
***
0
24
72
120
Time after 10Gy IR (hours)
D
IFNB mRNA (10 -4)
WT
cGAS KO
STING KO
**
**
0Gy
2Gy x 5F
IR dose
E
IFNA mRNA (10 -3)
WT
cGAS KO
STING KO
*
0
24
72
120
Time after 10Gy IR (hours)
F
IFNA mRNA (10 -4)
WT
cGAS KO
STING KO
0Gy
2Gy x 5F
IR dose

Figure 10. Cytosolic DNA sensor-STING is the predominant signalling axis in IR induction of IFNB in MC38 cells.

(**A**). IFNB mRNA expression of MC38 (WT *vs*. STING KO) at 6 hours after cGAMP (5 μg/ml) or VACV-70 (5 μg/ml) treatment. N = 3.

B. IFNB mRNA expression of MC38 (WT *vs*. cGAS KO) at 6 hours after HT-DNA treatment (5 μg/ml).

IFNB expression in MC38 cells (WT *vs*. cGAS KO *vs*. STING KO) at 24, 72 and 120 hours after mock or 10 Gy (**C**) or 24 hours after 2 Gy x 5 F (**D**) IR were assessed by RT-qPCR. N = 3.

IFNA expression in MC38 cells (WT *vs*. cGAS KO *vs*. STING KO) at 24, 72 and 120 hours after mock or 10 Gy (**E**) or 24 hours after 2 Gy x 5 F (**F**). N = 3.

3.3.4 IR induction of IFNs was mediated by IRF1 in HT29 and IRF3 in MC38, respectively

We next asked which IRFs act in response to IR to induce IFNs transcription. IRFs are mainly localized in the cytoplasm when in a latent state and translocate to the nucleus following activation. Of the 9 members of IRFs, IRF1, IRF3, IRF5 and IRF7 positively regulate IFN expression with only IRF3 and IRF7 shown to be essential [104]. Since we also found robust induction of IRF1 in irradiated cancer cells, consistent with previous reports, we decided to focus on IRF1, in addition to IRF3 and IRF7 [105, 106]. To determine the subtype of IRFs mediating IR induction of IFNs, we examined the translocation of IRF 1, 3 and 7 from cytoplasm to nucleus in HT29. As shown in **Figure 11A**, IRF1, but neither IRF3 nor IRF7 translocated to the nucleus after IR. Genetic deletion of IRF1 (validated in **Figure 11A**) abrogated IR induction of type I/III IFN (**Figure 11 B-E**). On the other hand, both IRF1 and IRF3 accumulated in the nucleus of irradiated MC38 cells (**Figure 12A**). However, only IRF3 KO significantly reduced IFNB induction at 72h and 120h after a single dose of IR (**Figure 12D**). Neither IRF1 KD nor IRF3 KO individually reduced IFNA induction to substantial extents in MC38 (**Figure 12 F and G**).

This page intentionally left blank.

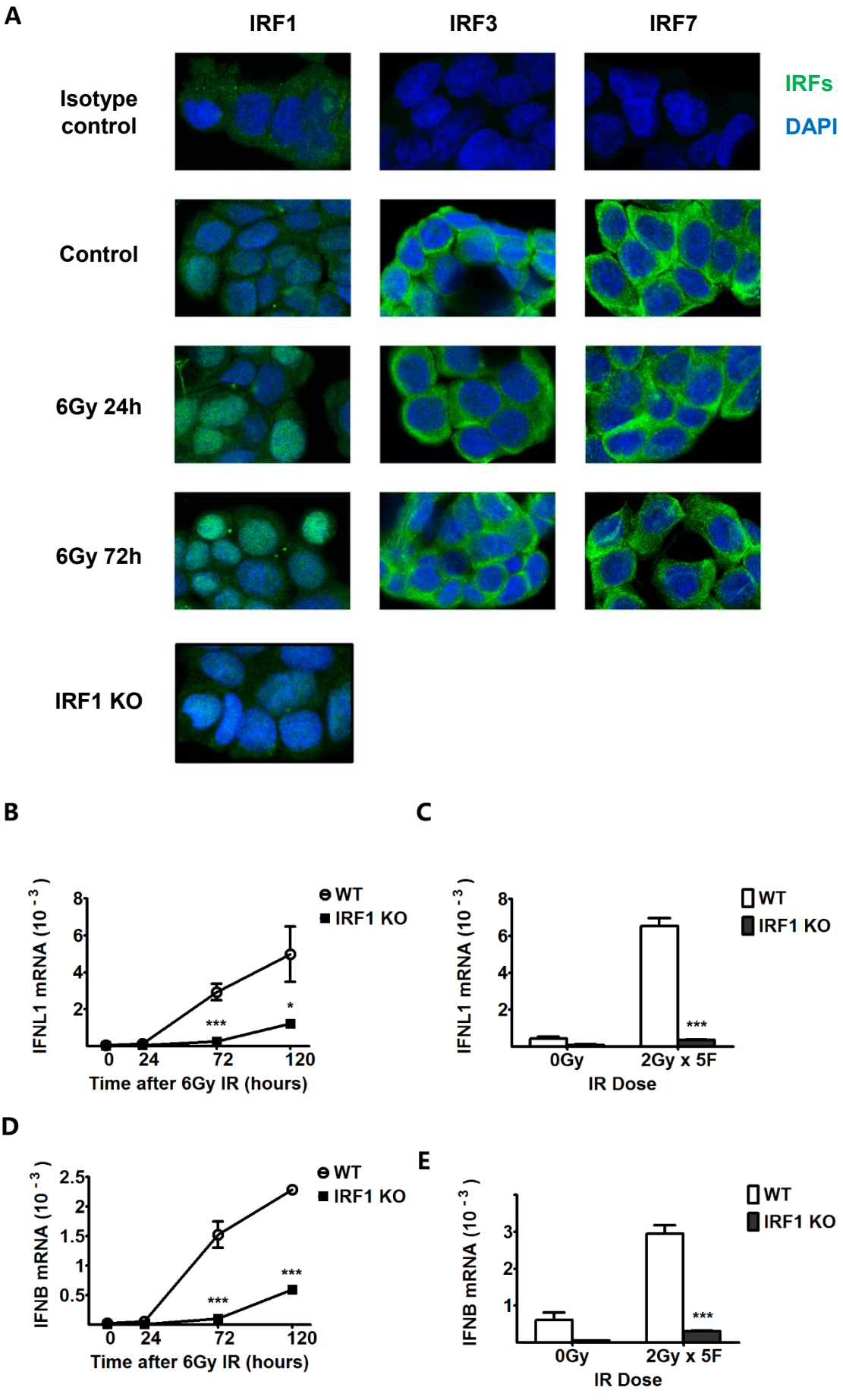

A
IRF1
IRF3
IRF7
Isotype control
Control
6Gy 24h
6Gy 72h
IRF1 KO
IRFs
DAPI
B
IFNL1 mRNA (10 -3)
WT
IRF1 KO
***
*
0
24
72
120
Time after 6Gy IR (hours)
C
IFNL1 mRNA (10 -3)
WT
IRF1 KO
***
0Gy
2Gy x 5F
IR Dose
D
IFNB mRNA (10 -3)
WT
IRF1 KO
***
***
0
24
72
120
Time after 6Gy IR (hours)
E
IFNB mRNA (10 -3)
WT
IRF1 KO
***
0Gy
2Gy x 5F
IR Dose

Figure 11. IR induction of type I/III IFNs is mediated by IRF1 in HT29.

(**A**) Distribution of IRF1, IRF3 and IRF7 within HT29 cells at 24 hours following mock (second row), 24 or 72 hours following 6 Gy IR (third and fourth row). Irradiated cells stained with isotype control Abs were shown in the first row. IRF1 KO validation was also illustrated on the fifth row.

IFNL1 expression in HT29 cells (WT *vs*. IRF1 KO) at 24, 72 and 120 hours following mock or 6 Gy (**B**), or 24 hours after 2 Gy x 5 F (**C**) IR was assessed by RT-qPCR. N = 3.

IFNB expression in HT29 cells (WT *vs*. IRF1 KO) at 24, 72 and 120 hours following mock or 6 Gy (**D**), or 24 hours after 2 Gy x 5 F (**E**) IR. N = 3.

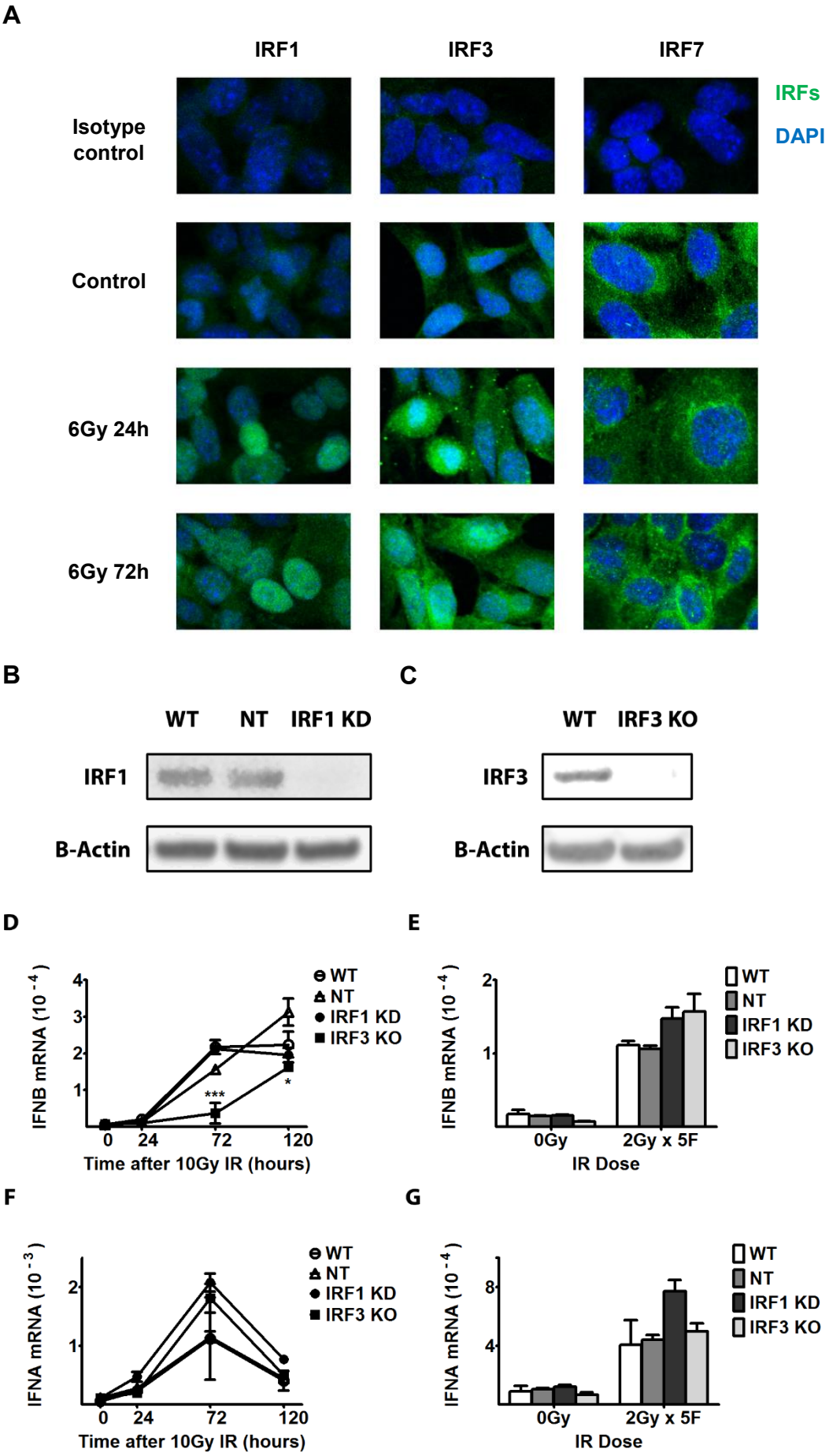

A
IRF1
IRF3
IRF7
IRFs
DAPI
Isotype control
Control
6Gy 24h
6Gy 72h
B
WT
NT
IRF1 KD
IRF1
B-Actin
C
WT
IRF3 KO
IRF3
B-Actin
D
IFNB mRNA (10 -4)
WT
NT
IRF1 KD
IRF3 KO
***
*
Time after 10Gy IR (hours)
E
IFNB mRNA (10 -4)
WT
NT
IRF1 KD
IRF3 KO
0Gy
2Gy x 5F
IR Dose
F
IFNA mRNA (10 -3)
WT
NT
IRF1 KD
IRF3 KO
Time after 10Gy IR (hours)
G
IFNA mRNA (10 -4)
WT
NT
IRF1 KD
IRF3 KO
0Gy
2Gy x 5F
IR Dose

Figure 12. IR induction of IFNB is mediated by IRF3 in MC38.

(**A**) Distribution of IRF1, IRF3 and IRF7 within MC38 cells at 24 hours following mock (second row), 24 or 72 hours following 6 Gy IR (third and fourth row). Irradiated cells stained with isotype control Abs were shown in the first row.

The knockdown or knockout efficacy of IRF1 (**B**) and IRF3 (**C**) in MC38 cells were assessed by western blot.

IFNB expression in MC38 cells (WT *vs*. IRF1 KD *vs*. IRF3 KO) at 24, 72 and 120 hours following mock or 10 Gy (**D**), or 24 hours after 2 Gy x 5 F (**E**) IR was assessed by RT-qPCR. N = 3.

IFNA expression in MC38 cells (WT *vs*. IRF1 KD *vs*. IRF3 KO) at 24, 72 and 120 hours following mock or 10 Gy (**F**), or 24 hours after 2 Gy x 5 F (**G**) IR. N = 3.

3.3.5 IFNAR and IL-28R signalling pathways act in positive feedback loops to enhance induction of IFNs after IR

Binding of IFNs to their receptors in autocrine or paracrine fashion leads to upregulation of ISGs. We found robust induction of ISGs after IR treatment in HT29 cells (**Figure 4 C and D**). Activation of type I/III IFN signalling pathway may further enhance IFN expression by a positive feedback loop. To test this possibility, we genetically eliminated IFNAR1 and IL-28R (IFNLR) to abrogate type I and III IFN signalling pathways in HT29 cells, respectively (**Figure 13 A and B**). Remarkably, we found either IFNAR1 KO or IL-28R KO significantly reduced IFN induction in HT29 cells (**Figure 13 C-F**). In MC38, IFNB induction was also almost completely abolished with IFNAR1 KO, whilst IFNA was unaffected (**Figure 14 C-F**). Consistent with our mRNA results, IR led to substantial induction of IFNL1 and IFNB proteins in the supernatant of irradiated WT HT29 and MC38 cells. This induction was completed abrogated by knockout of STING, and to lesser extent by knockout of type I/III receptors (**Figure 15 A and B**).

In further experiments, we found that abrogation of either type I and type III signalling pathway significantly reduced the expression of key factors involved in induction of IFNs, including cGAS, STING, TBK1 and IRFs (**Figure 16**). Taken together, these findings document a critical role for positive feedback loops by type I/III signalling pathways in induction of IFNs by IR.

We found no evidence of crosstalk between NF-κB pathway and STING-TBK1 signalling axis, in contrast to previous reports in other systems [107, 108]. Neither triggering STING-TBK1 via cGAMP nor activating IFNAR1 singling pathway with type I IFN directly led to increased NF-κB activities (**Figure 17 A**). Furthermore, activation of NF-κB pathway after IR was unaltered by either STING KO or IFNAR1 KO (**Figure**

17 B). These data suggest that NK-κB pathway is neither a downstream of STING nor a component of the IFN-receptor positive feedback loop.

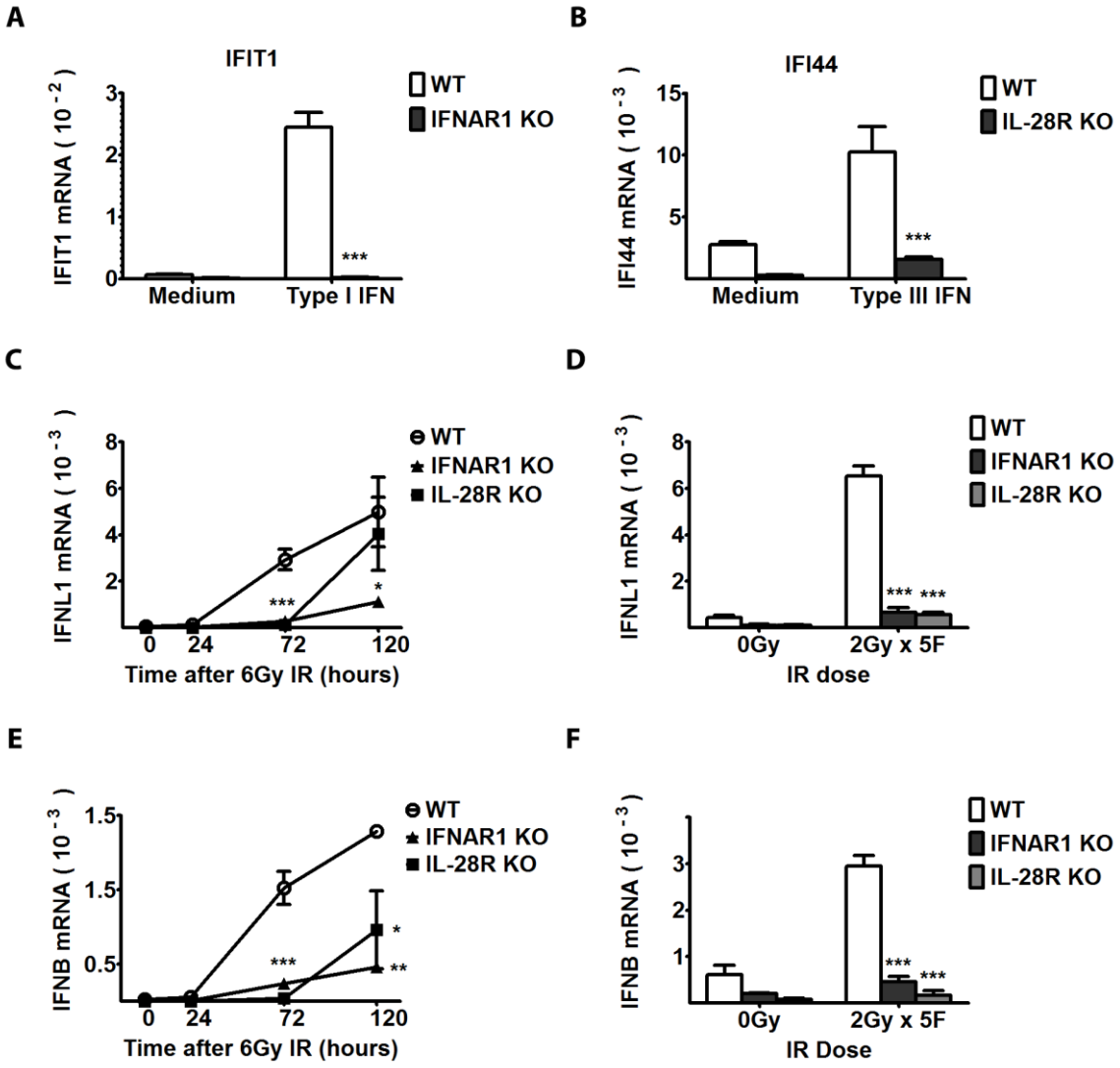

A
IFIT1
IFIT1 mRNA (10 -2)
WT
IFNAR1 KO
***
Medium
Type I IFN
B
IFI44
IFI44 mRNA (10 -3)
WT
IL-28R KO
***
Medium
Type III IFN
C
IFNL1 mRNA (10 -3)
WT
IFNAR1 KO
IL-28R KO
***
*
Time after 6Gy IR (hours)
D
IFNL1 mRNA (10 -3)
WT
IFNAR1 KO
IL-28R KO
*** ***
0Gy
2Gy x 5F
IR dose
E
IFNB mRNA (10 -3)
WT
IFNAR1 KO
IL-28R KO
***
*
**
Time after 6Gy IR (hours)
F
IFNB mRNA (10 -3)
WT
IFNAR1 KO
IL-28R KO
*** ***
0Gy
2Gy x 5F
IR Dose

Figure 13. Type I/III IFN signalling pathways act in positive feedback loops to enhance induction of type I/III IFNs in HT29 cells after irradiation.

(**A**). IFIT1 mRNA expression in HT29 cells (WT *vs*. IFNAR1 KO) at 3.5 hours after universal type I IFN treatment (1000 U/ml).

(**B**). IFI44 mRNA expression in HT29 (WT *vs*. IL-28R KO) at 3.5 hours after IFNL1 treatment (1000 U/ml).

IFNL1 expression in HT29 cells (WT *vs*. IFNAR1 KO *vs*. IL-28R KO) at 24, 72 and 120 hours after mock or 6 Gy (**C**), or 24 hours after 2 Gy x 5 F (**D**) IR was assessed by RT-qPCR. N = 3.

IFNB expression in HT29 cells (WT *vs*. IFNAR1 KO *vs*. IL-28R KO) at 24, 72 and 120 hours after mock or 6 Gy (**C**), or 24 hours after 2 Gy x 5 F (**D**) IR. N = 3.

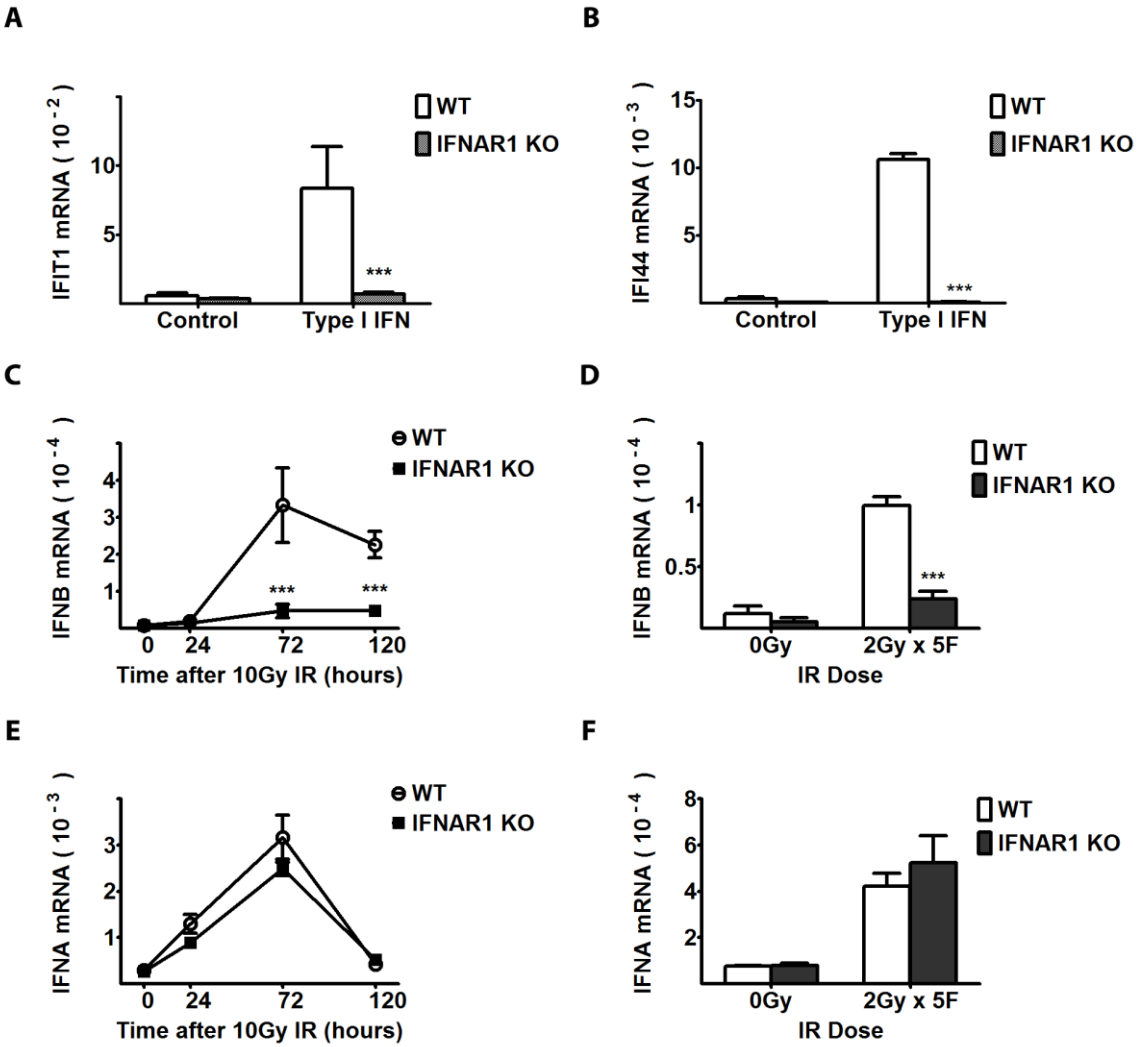

A
IFIT1 mRNA (10 -2)
10
5
WT
IFNAR1 KO
***
Control
Type I IFN
B
IFI44 mRNA (10 -3)
15
10
5
WT
IFNAR1 KO
***
Control
Type I IFN
C
IFNB mRNA (10 -4)
4
3
2
1
WT
IFNAR1 KO
***
***
0
24
72
120
Time after 10Gy IR (hours)
D
IFNB mRNA (10 -4)
1
0.5
WT
IFNAR1 KO
***
0Gy
2Gy x 5F
IR Dose
E
IFNA mRNA (10 -3)
3
2
1
WT
IFNAR1 KO
0
24
72
120
Time after 10Gy IR (hours)
F
IFNA mRNA (10 -4)
8
6
4
2
WT
IFNAR1 KO
0Gy
2Gy x 5F
IR Dose

Figure 14. Type I IFN signalling act in a positive feedback loop to enhance induction of IFNB in MC38 cells after radiation.

IFIT1 (**A**) and IFI44 (**B**) expression in MC38 cells (WT *vs*. IFNAR1 KO) at 3.5 hours after universal type I IFN treatment (1000 U/ml).

IFNB expression in MC38 cells (WT *vs*. IFNAR1 KO) at 24, 72 and 120 hours after mock or 10 Gy (**C**), or 24 hours after 2 Gy x 5 F (**D**) IR was assessed by RT-qPCR. N = 3.

IFNA expression in MC38 cells (WT *vs*. IFNAR1 KO) at 24, 72 and 120 hours after mock or 10 Gy (**E**), or 24 hours after 2 Gy x 5 F (**F**) IR. N = 3.

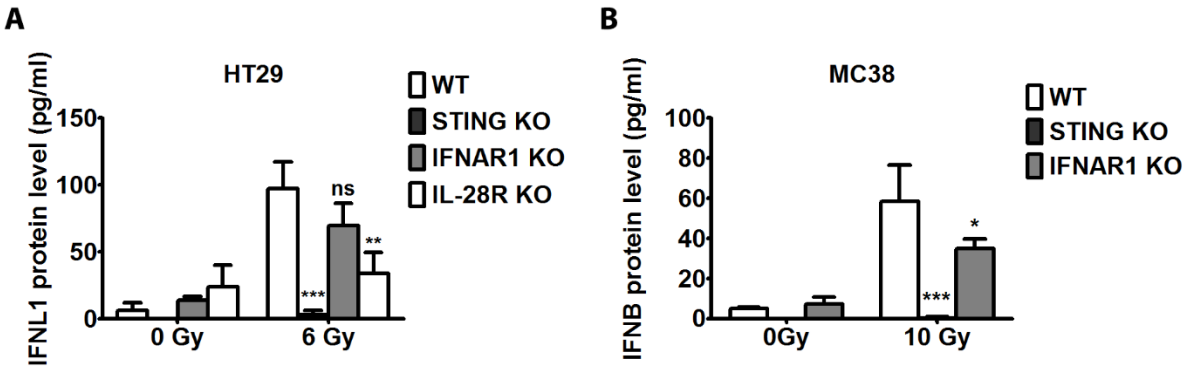


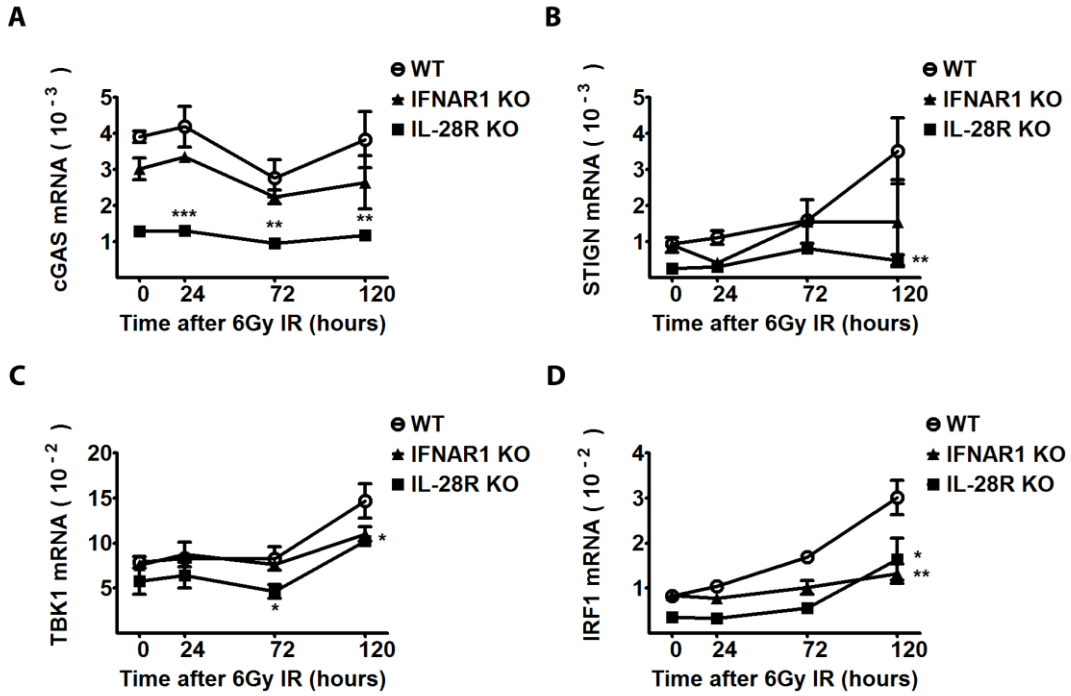
Figure 15. Validation of mechanisms model by assessing type I/III IFNs protein level in the supernatant of irradiated tumour cells.

(**A**). IFNL1 protein level in tissue culture supernatants of HT29 cells (WT *vs*. STING KO *vs*. IFNAR1 KO *vs*. IL-28R KO) was measured by ELISA at 72 hours after mock or 6 Gy IR. N = 4.

(**B**). IFNB protein level in tissue culture supernatants of MC38 cells (WT *vs*. STING KO *vs*. IFNAR1 KO) was measured by ELISA at 72 hours after mock or 10 Gy IR. N = 4.

This page intentionally left blank.

HT29


A
B
C
D
WT
IFNAR1 KO
IL-28R KO
cGAS mRNA (10 -3)
STIGN mRNA (10 -3)
TBK1 mRNA (10 -2)
IRF1 mRNA (10 -2)
Time after 6Gy IR (hours)
0 24 72 120

MC38

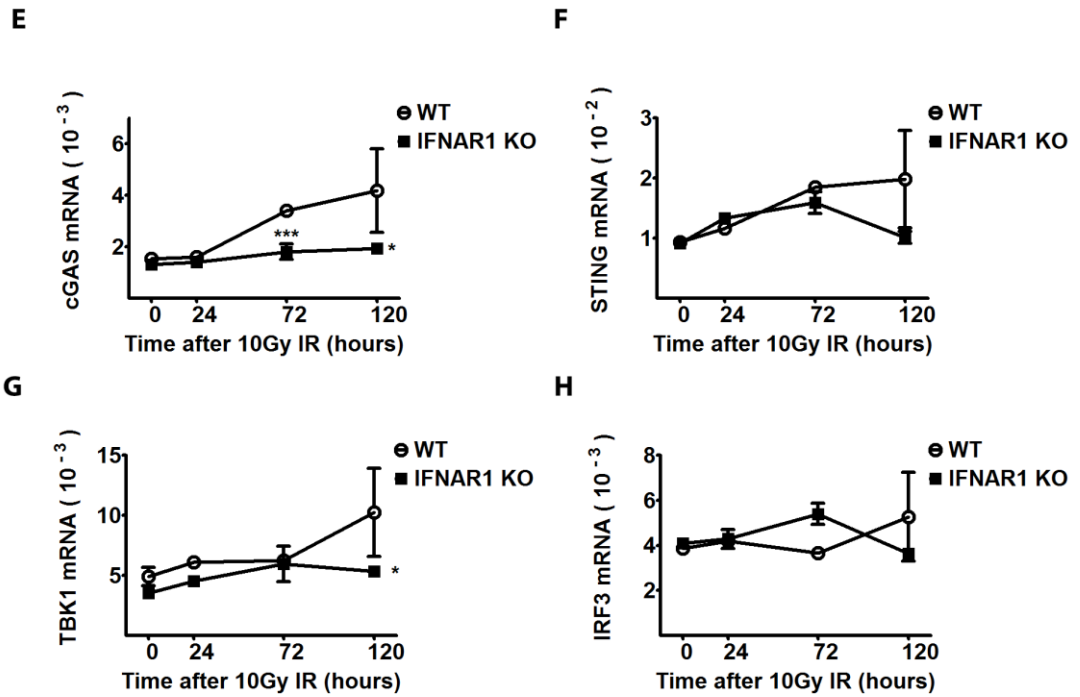

E
F
G
H
WT
IFNAR1 KO
cGAS mRNA (10 -3)
STING mRNA (10 -2)
TBK1 mRNA (10 -3)
IRF3 mRNA (10 -3)
Time after 10Gy IR (hours)
0 24 72 120

Figure 16. The impacts of type I/III IFN signalling pathways on the expression of key factors in IR-induced type I/III IFNs in tumour cells.

HT29 cells were exposed to 6 Gy IR. Cells were harvested at indicated time points for the assessment of mRNA expression of cGAS (**A**), STING (**B**), TBK1 (**C**) and IRF1 (**D**). N = 3.

MC38 cells were exposed to 10 Gy IR. Cells were harvested at indicated time points for the assessment of mRNA expression of cGAS (**E**), STING (**F**), TBK1 (**G**) and IRF3 (**H**). N = 3.

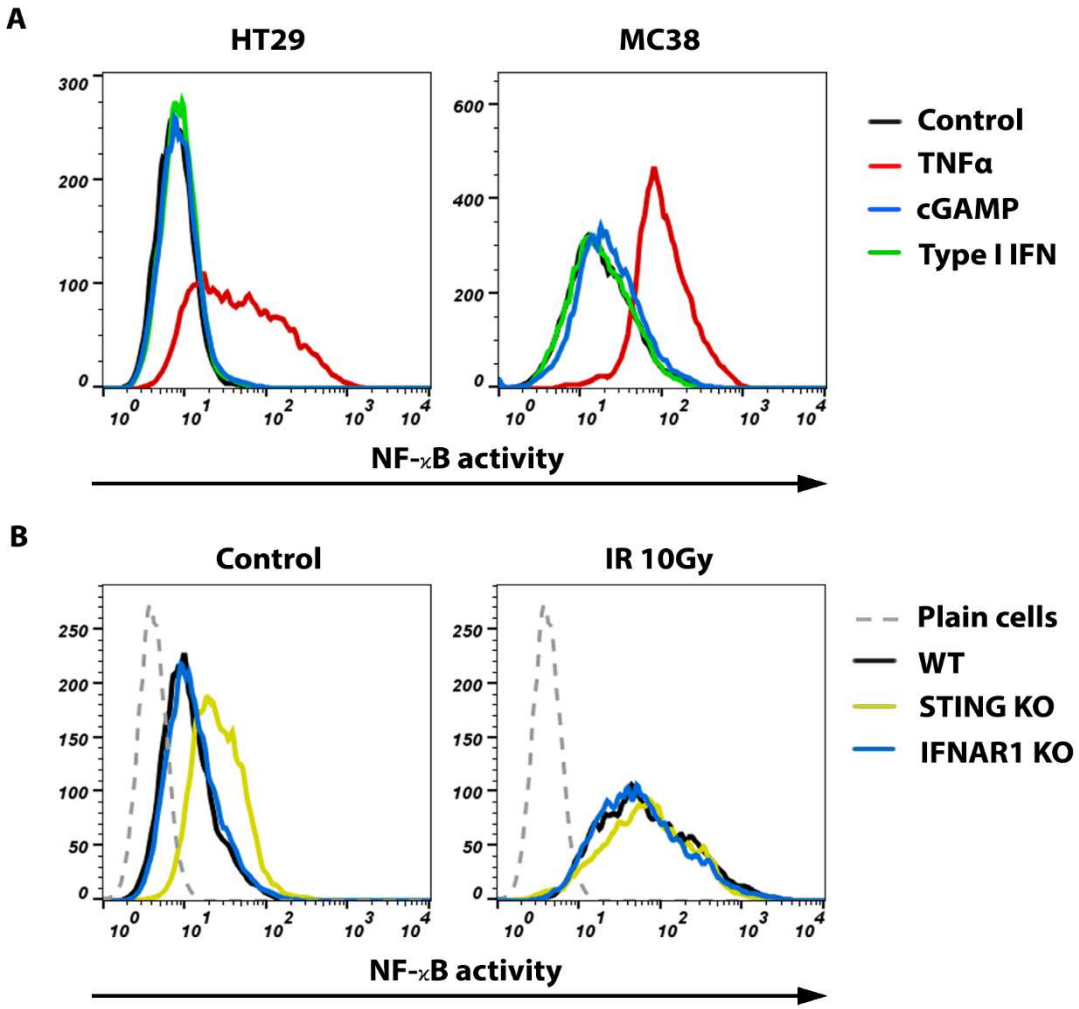


Figure 17. NF-κB activity of cancer cells following stimulation.

(**A**) HT29 and MC38 cells were exposed to control medium, TNFα (40 ng/ml), cGAMP (5 μg/ml) and type I IFN (1000 U/ml), respectively and 18 hours later, their NF-κB activity was quantified using flow cytometry.

(**B**) MC38 cells were exposed to mock or 10 Gy IR, and 96 hours later, their NF-κB activity was quantified using flow cytometry.

3.3.6 Model for IR-induced IFNs in cancer cells

Based on our findings, we propose a model for induction of type I/III IFNs in cancer cells by IR. As shown in **Figure 18**, DNA damages induced by IR activates STING-TBK1-IRF signalling and NF-κB pathway as well, leading to induction of type I/III IFNs. These induced IFNs then bind to their relevant receptors. Signalling through both type I and III IFN receptors acts as a feedback loop to further enhance IFNs expression via upregulation of kinases in the cytosolic DNA signalling pathways.

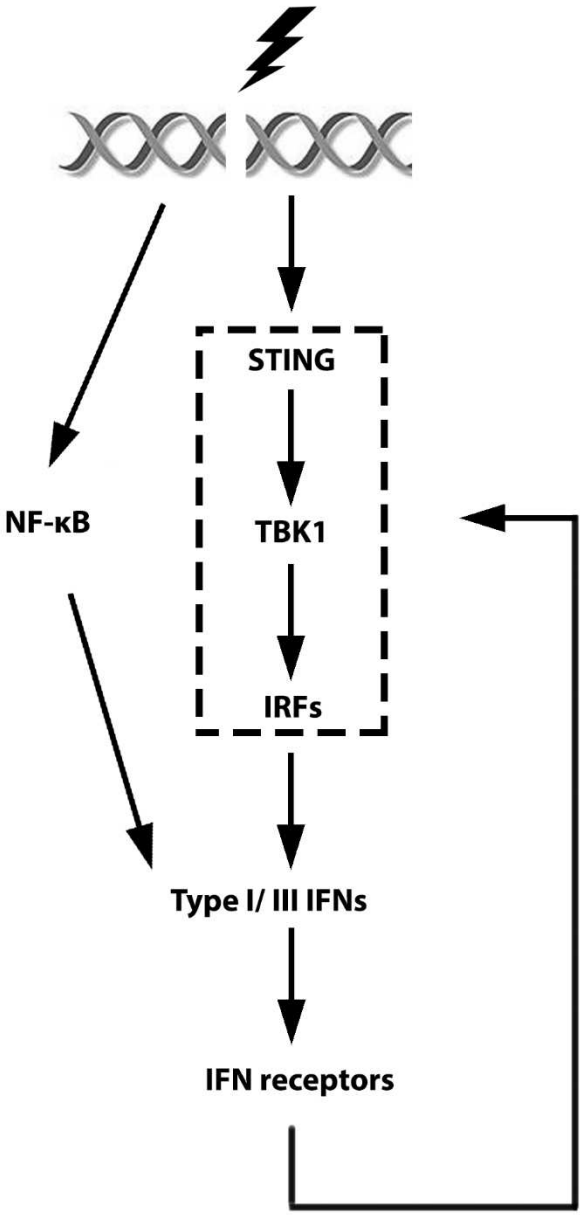


Figure 18. Model for induction of type I/III IFNs in cancer cells by IR.

3.4 Discussion

3.4.1 The findings and significances of current study

Type I IFNs have been implicated in enabling anti-tumour immune responses after radiation therapy. Here we show that cancer cells as well as immune cells are sources of type I IFNs after IR and that STING-TBK1 signalling and to a lesser extent NF-κB mediates IFNs induction. Of type I IFNs, IFNB was induced in both the human and murine cell lines tested, but IFNAs only in the murine cell lines. Moreover, for the first time, we demonstrate that IR also led to significant induction of type III IFN in human cell lines via similar signalling pathways. The induction of type I/III IFNs occurs over days with maximum levels of mRNA at 3 ~ 5 days after a single dose of IR consistent with recent findings showing a requirement of mitosis after a G2 delay for the formation of micronuclei, an important source of cytosolic DNA [109-111] .

3.4.2 STING-TBK1 and NF-κB signalling pathways mediate induction of type I/III IFNs in cancer cells after IR

While both STING-TBK1 and NF-κB signalling pathways can trigger Type I and III IFNs, NF-κB proved to have a lesser contribution in the cancer cell lines we tested and at most times. Consistent with our results, Vanpouille-Box et al., recently showed that knockdown of cGAS or STING completely abrogated type I IFN induction in several cell lines, though they did not look at type III IFN [92]. Notably, despite our data suggesting that STING is indispensable in induction of IFNs after IR, reduced IFN induction was still found upon inhibition of NF-κB pathway. It has been indicated in a number of studies that activating STING pathway via dsDNA

transfection can directly trigger NF-κB pathway in both normal and malignant cell lines, which involves TBK1, NEMO and IKKβ [107, 112-115]. However, in the cell lines we used in this study, we did not found apparently enhanced NF-κB activity upon the activation of STING pathway. Indeed, our results suggest that NF-κB pathway mediate IFN induction independently of STING, in agreement with previous studies showing that the NF-κB pathway is required for maximum levels of IFN gene expression and could upregulate IFN in an IRF-independent manner [92, 116, 117] . Nevertheless, our results suggest that induction of type I/III IFNs in general is mainly driven by STNG-TBK1 after radiation, but this is not universal and redundancy with NF-κB exists.

The STING pathway is triggered by a variety of cytosolic sensors following detection of DNA fragments [85, 118, 119]. Potential sources of these DNA fragments include the nuclear genome, mitochondrial DNA, exosomes released by neighbouring cells, micronuclei, and uptake of debris after cell death [103, 109-111, 118, 120, 121]. Many cytosolic DNA sensors have been identified, including cGAS, IFI16, DDX41, DNA-PK and Ku70 [122-126]. While we have not comprehensively sought to identify the cytosolic sensors, cGAS elimination abrogated IFNB induction in irradiated MC38 cells, but only partially reduced IFN upregulation in HT29. Clearly multiple redundant mechanisms are present.

Many human colorectal carcinoma cell lines have defective STING signalling [127]. These cell lines may rely solely on NF-κB pathway to express Type I/III IFNs in response to IR, and may have relatively less induction. These defects in STING may also lead to reduced anti-tumour immune responses. Cells with deficiencies in key kinases of the DNA damage machinery elicited dramatically increased presence of cytosolic DNA, resulting in type I IFN induction via the STING pathway [100, 128].

Under basal conditions, cytosolic DNA can be quickly degraded by Trex1, a master DNA exonuclease in the cytoplasm, and hence would be cleared before activation of the STING pathway [129]. Patients with mutated Trex1 exhibit high basal levels of type I IFN presumably resulting from the accumulation of cytosolic DNA [130, 131]. It has been shown that oxidative modification of DNA by ROS confers resistance to Trex1 degradation, resulting in STING-dependent IFN production [132]. Further, micronuclei induced by IR also trigger cGAS-STING-TBK1. Whether Trex1 has any impact on micronuclei is unknown. These factors will clearly add additional heterogeneity to the induction of IFNs after radiation in cancer cells.

3.4.3 IRFs in induction of IFNs by IR

Type III IFN expression could be mediated by a variety of IRFs, depending on the cell type and the activated upstream signalling. There was heterogeneity of response with activation of IRF1 as indicated by nuclear localization observed in HT29 and MC38, but IRF3 only in MC38 cells. Consistent with the isolated activation of IRF1 in HT29, genetic elimination of IRF1 strongly abrogated the induction of IFNs in those cells. But in MC38 cells, IRF1 elimination did not affect IFN induction, whilst IRF3 KO only reduced IR-induced IFNB at one time point, indicating involvement of redundant mechanisms.

Induction via RIG-I or TLR signalling has been suggested to be mediated by both IRF3 and IRF7, whereas IRF1 was also found to play an important role in IFNL upregulation mediated by peroxisomal MAVS and in human airway epithelial cells in response to RNA virus infection [133-136]. Increased type I/III IFN expression in a murine fibroblast cell line following treatment with etoposide, a chemotherapeutic

agent that like IR induces DNA double strand breaks, requires the presence of IRF1 and IRF7 as well [84]. In our hands, induction of type I/III IFNs in HT29 cells was solely mediated by IRF1 and clearly IRF1 is an important downstream mediator of the STING-TBK1 pathway. Consistent with our results, a recently published study indicated that STING-mediated type III IFN production in HEK 293 cells, in response to exogenous DNA, required IRF1, IRF3 and IRF7 [126]. Collectively, these results suggest that IRF1 is an important transcriptional factor for cytosolic DNA sensing-mediated type I/III IFN production.

3.4.4 Type I/III IFN signalling pathways

Positive feedback loops using IFNARs are known to augment IFN levels. We demonstrated feedback by preventing IFN signalling through either IRNAR1 or IL-28 leading to reduced induction of IFN by IR. One consequence of the removal of either IFN receptor was decreased transcription of some of the components in the TBK1-STING pathway. The literature shows that inhibition of IFNAR1 using a blocking antibody to reduce IFN signalling in host cells reduced anti-tumour immunity [102]. Our work establishes that induction of IFN can be reduced by blocking positive feedback loops mediated through IFNAR1 and IL-28 in tumour cells.

Type III and I IFNs induce a similar profile of ISGs, however, the induction magnitudes and temporal patterns differ [137, 138]. More importantly, whilst almost all cell types respond to type I IFN, response to type III IFN is restricted to epithelial tissues and a subset of immune cells [139, 140]. Since our results suggest that type III IFN signalling plays a pivotal role in enhancing induction of type I/III IFN in a positive feedback loop, the impacts of type III IFN on IR-induced immune response

may be more profound in cancer of epithelial origins. The consequences of IR-induced type III IFN in cancer cells remain to be determined.

3.4.5 IFNA

IR elicited upregulation of IFNB in both human and murine cells lines, whereas IR-induced IFNA was only found in murine cell lines, suggesting that the induction of IFNA may be mediated by a species-specific mechanism. The only known transcriptional factors for IFNA are IRFs, however, none of the IRFs (IRF1, IRF3 and IRF7) we tested in this study appeared to mediate IFNA induction. Although IFNA and IFNB share a common receptor and downstream signalling pathway, they have distinguishable functions in some situations [141-144]. Structural studies suggest that these functional differences may be related to differential binding affinities towards receptor subunits [145, 146]. Whether they may have different roles in IR-induced anti-tumour response still needs to be investigated.

3.5 Conclusions

Our results suggest that type I/III IFNs can be upregulated in cancer cell lines following IR treatment. This induction occurs via cytosolic DNA sensors-STING-TBK1-IRFs signalling axis and to less extent, the NF-κB pathway. Furthermore, Type I/III acts as a feedback loop to further enhance IFNs expression via upregulating key factors in the signalling axis. These findings add another layer of complexity to the understanding of irradiation-induced anti-tumour immunity and may provide novel insights into IFN-based cancer treatment.

Chapter 4

Abrogation of type I IFN signalling in cancer cells led to remarkable improvement in irradiation-induced anti-tumour immunity

4.1 Introduction

Clinical results of immunotherapy in cancer are promising, yet mixed as most patients fail to be cured [42, 147-150]. This failure may be due to inadequate immunogenicity of tumours [48, 60, 61, 151, 152]. Radiation therapy has been shown to enhance tumour immunogenicity and may hence facilitate anti-tumour immune response [63, 153, 154]. Thus, combing radiotherapy with immunotherapy may have a synergistic effect and result in better outcomes. However, it is still unclear what combination will be the most beneficial to patients, due to poor understanding of the complex interactions between radiotherapy and host anti-tumour immune response.

Interferons (IFNs) are a group of cytokines that have been shown to play an important role in anti-tumour immune response. It is well acknowledged that generation of anti-tumour immunity requires type II IFN [83, 155-158], whereas emerging evidence also suggests that type I IFNs have a critical contribution to the anti-tumour immune response [75, 76, 159-161]. Abrogation of type I IFN signalling in the host impairs multiple steps of the cancer-immunity cycle, including recruitment of antigen presenting cells and activation of effector cells [159, 162-164]. However, this is not universal. Studies indicate that activation of the IFN/STAT1 signalling pathway in tumours could also lead to immunosuppression in different settings and has been associated with tumour therapeutic resistance and poor survival outcomes [87, 165-167]. Thus, type I IFN signalling can exhibit both pro-inflammatory and immunosuppressive activities in anti-tumour immunity. What determines the outcome of this pathway is still not well understood, which needs to be investigated in a context-dependent fashion.

The contribution of host immune immunity to tumour response to IR has been increasingly appreciated [19, 20, 94]. Moreover, data has emerged suggesting that

this IR-induced immune response is mediated by type I IFN [82, 102]. In a study from University of Chicago, Ralph Weichselbaum and colleagues showed that following IR, type I IFN induction in tumour infiltrated dendritic cells via the STING pathway and the activation of type I IFN signalling in these cells was crucial for radiation-induced anti-tumour immunity in immunogenic tumours [102]. Interestingly, we and others also found that IR directly induced type I IFN and type I IFN signalling in tumour cells *in vivo* [168]. More importantly, cancer cells not the immune cells actually have the greatest contribution to the overall intratumoural production of type I IFN in our model. Therefore, we asked whether tumour cell-derived type I IFN and type I IFN signalling had a role in tumour response to IR.

By using a variety of animal models, here we demonstrated that tumour-derived type I IFN has important contribution to the anti-tumour immune response at the local site. Strikingly and unexpectedly, abrogation of type I IFN signalling via genetic elimination of IFNAR1 in cancer cells led to remarkable improvement of tumour response to IR. This phenomenon is mainly driven by significantly enhanced susceptibility of cancer cells to CD8+ T cell-mediated killing through PD-L1/Galectin-9-independent mechanisms. How abrogation of type I IFN signalling in cancer cells augment their vulnerability to cytotoxic killing remains to be determined.

4.2 Results

4.2.1 Abrogation of type I IFN signalling in cancer cells led to remarkable improvement of tumour response to IR, while genetic elimination of STING led to reduced tumour response to irradiation. These paradoxical outcomes were mediated by the host immune system.

As demonstrated in **Chapter 3**, IR-induced type I IFN and type I IFN signalling could be abrogated by genetic deletion of STING and IFNAR1, which allowed us to test their roles in tumour response to IR. STING deletion reduced the production of type I IFN in tumours after IR, whereas IFNAR1 KO would eliminate cellular response to type I IFN. Tumours derived from WT, STING KO or IFNAR1 KO MC38 cells, grew at comparable rates in C57BL6 mice without treatment (**Figure 19A**). Following a single dose of 10 Gy IR (day 0), WT MC38 tumours displayed a temporal retardation of tumour growth and started to regrow at day 12 ~ 32. A similar growth delay was found in STING KO MC38 tumours, but on average for a much shorter period of time: 8 ~ 22 days (tumour volume at day 12: 267.8 ± 156.5 mm^3 *vs*. 142.3 ± 98.86 mm^3, $P = 0.0080$). On the other hand, IFNAR1 KO MC38 tumours substantially regressed in comparison to WT tumours (tumour volume at day 12: 60.3 ± 83.6 mm^3 *vs*. 142.3 ± 98.9 mm^3, $P = 0.0094$), with, strikingly, 50% of mice remaining tumour-free over 90 days of observation when the experiment was terminated. Kaplan Meier survival analysis also revealed comparable differences. In consistent with tumour growth results, mice bearing all 3 types of control tumours were indistinguishable. A single dose of 10Gy IR improved the median time for tumours to reach the ethical limit in C57BL6 mice harbouring WT MC38 tumours from 6 days to 24 days (**Figure 19C**, 95% CI: 18-30 days, $P < 0.001$). In contrast, significantly lesser median survival

(16 days, 95% CI: 13-19 days, $P = 0.03$) was found in mice bearing STING KO MC38 tumours after IR, whilst mice with IFNAR1 KO MC38 tumours had substantial improvement in survival, with a median survival of 44 days (insufficient number of events to estimate 95% CI, $P < 0.001$). Overall, our results suggest cancer cell-derived type I IFN is required for optimized tumour control induced by IR, whereas, paradoxically, abrogation of type I IFN signalling in cancer cells leads to significant improvement of therapeutic outcomes.

Roles of type I IFN in anti-tumour immune response have been well investigated, yet how type I IFN signalling in cancer cells influence tumour response to IR treatment is less understood. Abrogation of type I IFN signalling could alter the expression of hundreds of ISGs in tumour cells, which may ultimately impact their fate following IR treatment. To investigate the underlying mechanisms, we first examined several radiobiological parameters in vitro, including: proliferation, radiosensitivity, IR-induced apoptosis and cell cycle arrest. As shown in **Figure 20 A** and **B**, all these cell lines were equivalent in proliferation and radiosensitivity in vitro, except that IFNAR1 KO MC38 cells had a slight but significant faster growth in tissue culture compared with the other two. IFNAR1 KO MC38 cells also showed a minor but significant reduction (46 ± 1% *vs*. 60 ± 1%, $P < 0.001$) of cellular apoptosis at later times after 10 Gy IR (**Figure 20 C**). Both cell lines exhibited similar patterns of cell cycle arrest after IR (**Figure 20 D**). Collectively, no significant growth retardation or enhanced radiosensitivity was found in IFNAR1 KO MC38 cells in vitro, removing these as possible explanations for the improved response of IFNAR1 KO MC38 tumours to IR.

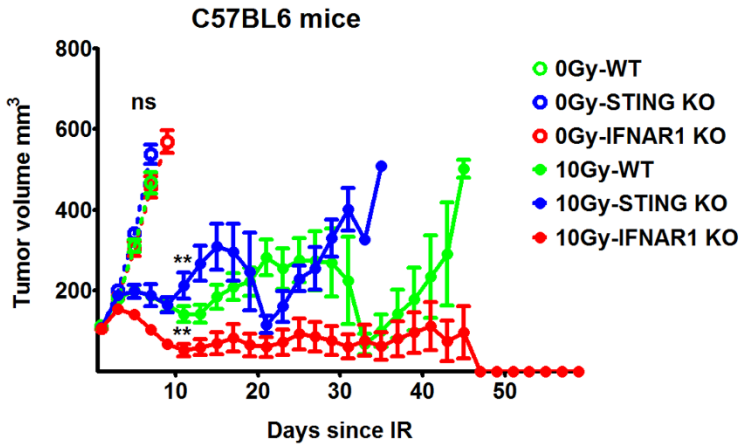
In addition to tumour cells themselves, type I IFN signalling in cancer cells may also impact other cellular components in the tumour, including immune cells. To

test whether the host immune response might play a role in these responses to IR, we performed an analogous experiment in immune incompetent host: CD1-nude mice. WT MC38 tumours exhibited notable but much less profound growth retardation following IR in CD1-nude mice (**Figure 19 B**) compared with that in C57BL6 mice, which translated into a reduced median survival in these mice of more than 50% (10 days *vs*. 24 days, $P < 0.001$) (**Figure 19 D)**. Clearly, the host immune system has an important contribution to IR induced tumour control in this model. Similar tumour control compromise and survival reduction were found in CD1-nude mice bearing either STING KO or IFNAR1 KO MC38 tumours after IR (**Figure 19 B** and **D**). More importantly, no significant difference of either tumour control or host survival was found among WT, STING KO or IFNAR1 KO MC38 tumours in the immunocompromised mice, suggesting that their discrepant outcomes are predominantly mediated by the host immune system.

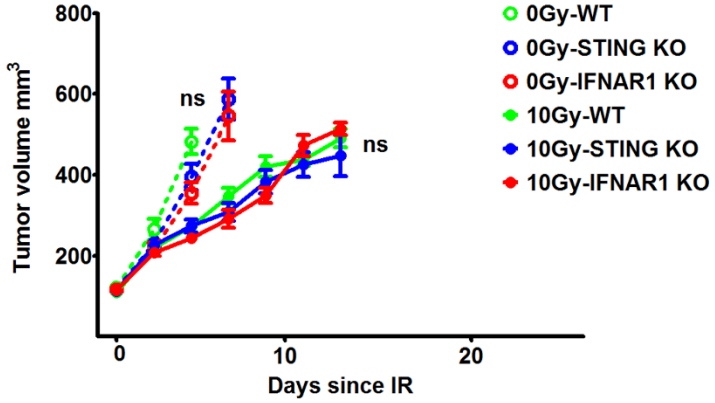
The improved tumour control in IFNAR1 KO in cancer cells is unexpected. To evaluate its generality, we tested IFNAR1 KO in another two cell lines: KPC (murine pancreatic cancer cell line) and LLC (murine lewis lung carcinoma cell line). In the KPC model, similarly, IFNAR1 KO tumours displayed significantly improved response after IR compared with WT tumours, though complete tumour complete regression was not found in these mice at the dose used (**Figure 21 A and B**). In the LLC model, interestingly, while no significant tumour growth retardation was observed in WT tumours after 10 Gy IR treatment, IFNAR1 KO tumours still exhibited notable regression after IR (**Figure 21 C and D**). In each model, abrogation of type I IFN signalling in cancer cells resulted in a greater tumour growth delay after IR, albeit to different extents. Without IR, no growth differences were observed. Moreover, consistent with MC38, these two cell lines did not exhibit significant differences in

terms of proliferation and radiosensitivity between WT and IFNAR1 KO cells *in vitro* (**Figure 21 E-H**).

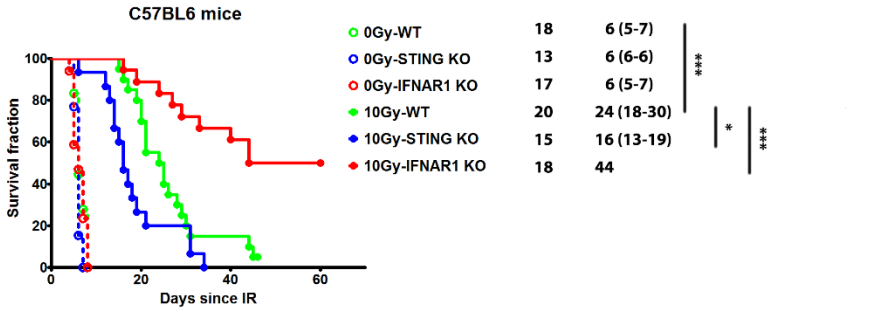
A


C57BL6 mice
Tumor volume mm3
800
600
400
200
ns
**
**
10
20
30
40
50
Days since IR
0Gy-WT
0Gy-STING KO
0Gy-IFNAR1 KO
10Gy-WT
10Gy-STING KO
10Gy-IFNAR1 KO

B


CD1-nude mice
Tumor volume mm3
800
600
400
200
ns
ns
0
10
20
Days since IR
0Gy-WT
0Gy-STING KO
0Gy-IFNAR1 KO
10Gy-WT
10Gy-STING KO
10Gy-IFNAR1 KO

C


C57BL6 mice
Survival fraction
100
80
60
40
20
0
0
20
40
60
Days since IR
0Gy-WT
0Gy-STING KO
0Gy-IFNAR1 KO
10Gy-WT
10Gy-STING KO
10Gy-IFNAR1 KO
No
Median survival days (95% CI)
18
6 (5-7)
13
6 (6-6)
17
6 (5-7)
20
24 (18-30)
15
16 (13-19)
18
44
***
*
***

D

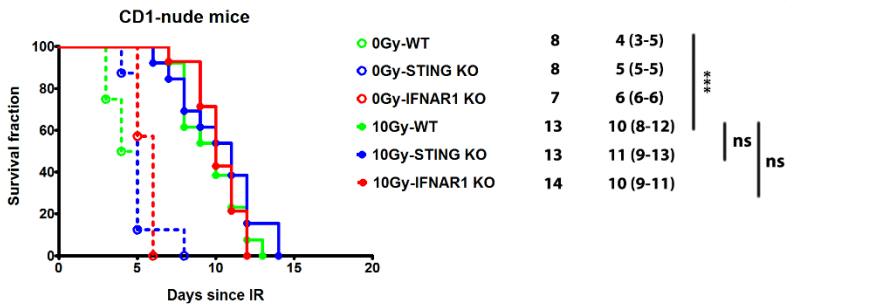

CD1-nude mice
Survival fraction
100
80
60
40
20
0
0
5
10
15
20
Days since IR
0Gy-WT
0Gy-STING KO
0Gy-IFNAR1 KO
10Gy-WT
10Gy-STING KO
10Gy-IFNAR1 KO
No
Median survival days (95% CI)
8
4 (3-5)
8
5 (5-5)
7
6 (6-6)
13
10 (8-12)
13
11 (9-13)
14
10 (9-11)
***
ns
ns

Figure 19. Abrogation of type I IFN signalling in cancer cells led to improvement of tumour response to IR, while the treatment outcomes of irradiated tumours were significantly comprised with the abolishment of STING pathway in cancer cells. These paradoxical outcomes were mediated by the host immune system.

Following ionizing radiation (IR), mice were followed up for a minimal of 90 days. All tumour volumes were measured every other day.

(**A**) MC38 tumour (derived from WT, STING KO and IFNAR1 KO cell lines, respectively) growths in C57BL6 mice following 0 Gy or 10 Gy IR.

(**B**) MC38 tumour (derived from WT, STING KO and IFNAR1 KO cell lines, respectively) growths in CD1-nude mice following 0 Gy or 10 Gy IR.

(**C**) Kaplan-Meier survival curves of C57BL6 mice from Figure A, along with numbers (No) and median survivals (95% CI) for each subgroup of mice.

(**D**) Kaplan-Meier survival curves of C57BL6 mice from Figure B, along with numbers and median survivals (95% CI) for each subgroup of mice.

Survival comparison between groups in this study were performed using log-rank's test. Student's t test was used to compared means of tumour volume (ns: $P > 0.05$, * $P < 0.05$, ** $P< 0.01$, *** $P< 0.001$)

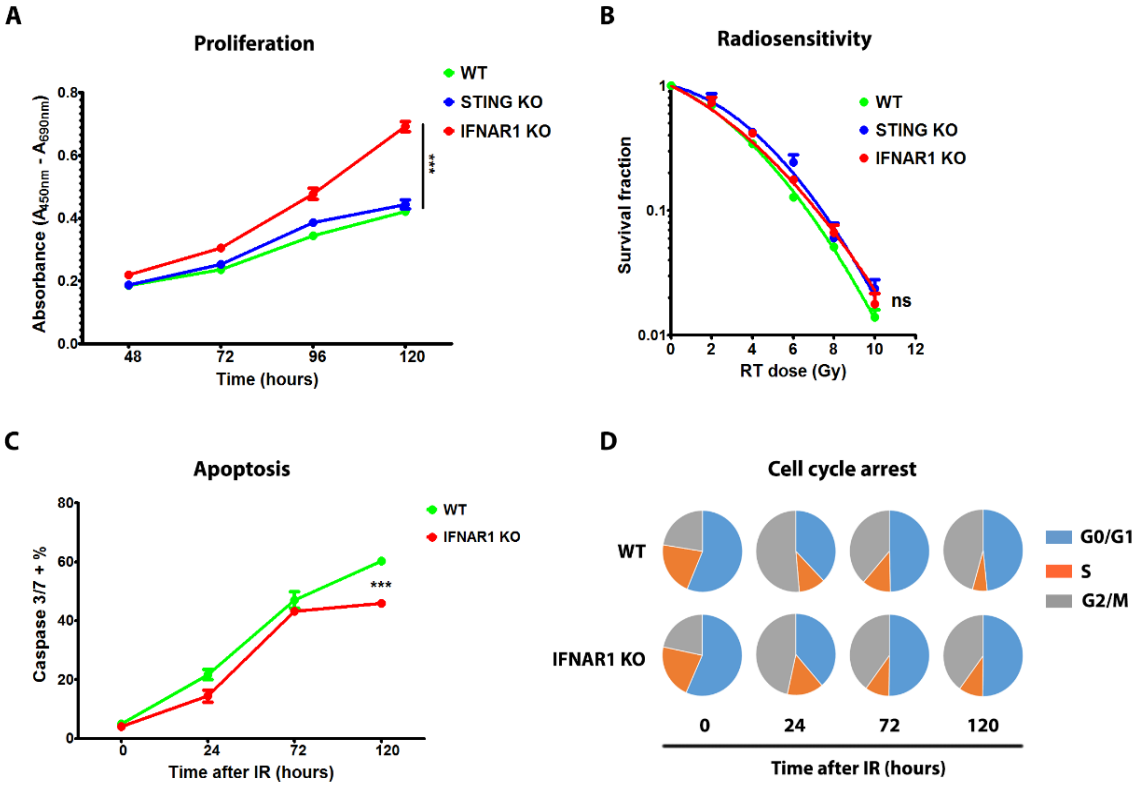

A
Proliferation
WT
STING KO
IFNAR1 KO
Absorbance (A450nm - A690nm)
0.0
0.2
0.4
0.6
0.8
48
72
96
120
Time (hours)
***
B
Radiosensitivity
WT
STING KO
IFNAR1 KO
Survival fraction
1
0.1
0.01
0
2
4
6
8
10
12
RT dose (Gy)
ns
C
Apoptosis
WT
IFNAR1 KO
Caspase 3/7 + %
0
20
40
60
80
0
24
72
120
Time after IR (hours)
***
D
Cell cycle arrest
WT
IFNAR1 KO
G0/G1
S
G2/M
0
24
72
120
Time after IR (hours)

Figure 20. In vitro characterization of MC38 cell lines

(**A**) Proliferation of MC38 cells (WT *vs*. STING KO *vs*. IFNAR1 KO) in vitro, evaluated by WST-1 assay. N = 8.

(**B**) Radiosensitivity of MC38 cells (WT *vs*. STING KO *vs*. IFNAR1 KO), assessed by clonogenic assay. N = 3.

(**C**) Percentages of apoptotic tumours cells (WT MC38 *vs*. IFNAR1 KO MC38) at indicated time points following 10 Gy IR, determined by flow cytometry with Caspase 3/7-FITC staining. N = 3.

(**D**) Distribution of cell cycle phases (G0/G1, S and G2/M phases) in MC38 cells (WT *vs*. IFNAR1 KO) at indicated time points following 10 Gy IR. Cell cycles were determined using flow cytometry with Propidium Iodide (PI) staining.

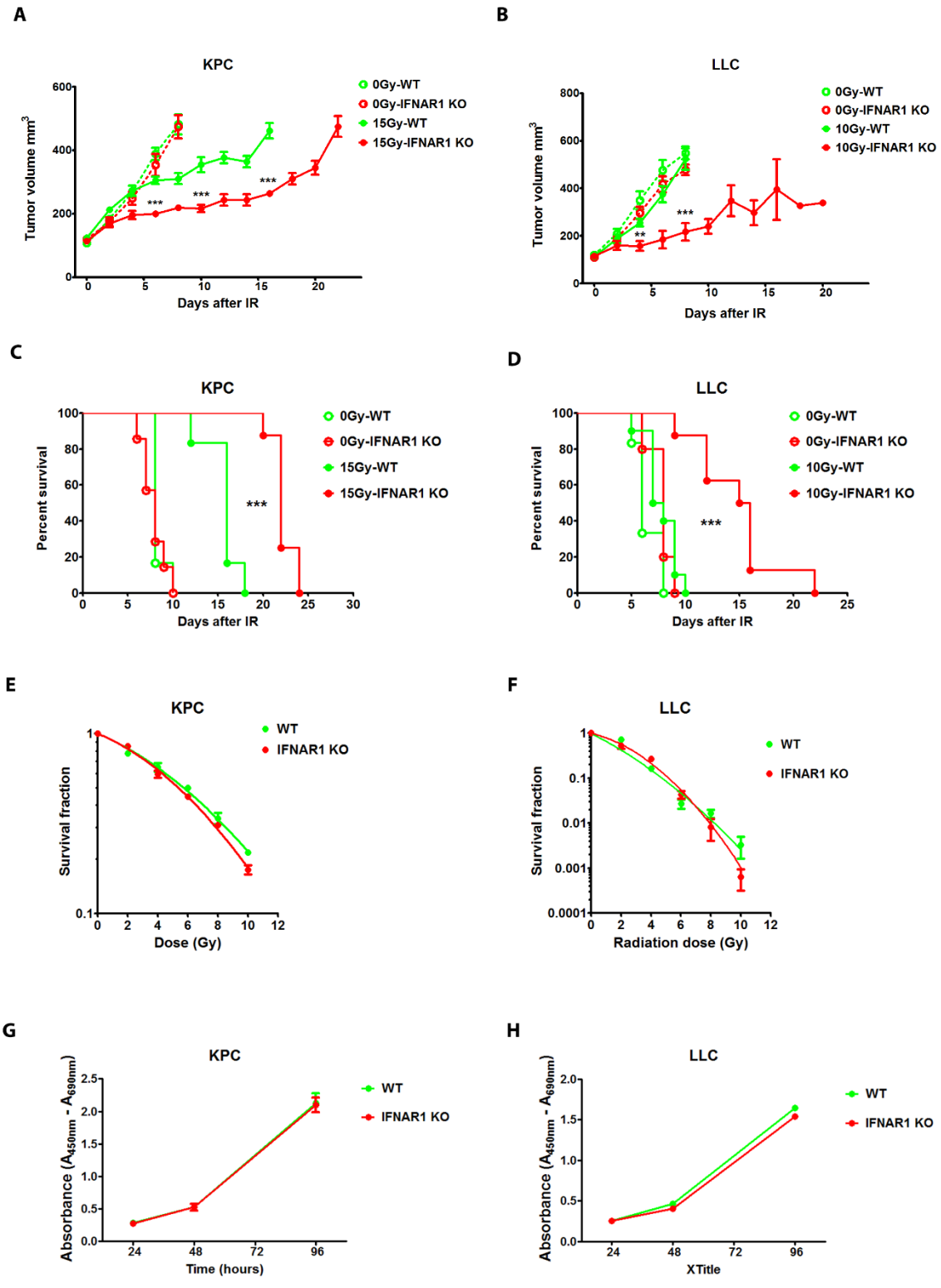

A
KPC
Tumor volume mm3
Days after IR
0Gy-WT
0Gy-IFNAR1 KO
15Gy-WT
15Gy-IFNAR1 KO
***
B
LLC
Tumor volume mm3
Days after IR
0Gy-WT
0Gy-IFNAR1 KO
10Gy-WT
10Gy-IFNAR1 KO
**
***
C
KPC
Percent survival
Days after IR
0Gy-WT
0Gy-IFNAR1 KO
15Gy-WT
15Gy-IFNAR1 KO
***
D
LLC
Percent survival
Days after IR
0Gy-WT
0Gy-IFNAR1 KO
10Gy-WT
10Gy-IFNAR1 KO
***
E
KPC
Survival fraction
Dose (Gy)
WT
IFNAR1 KO
F
LLC
Survival fraction
Radiation dose (Gy)
WT
IFNAR1 KO
G
KPC
Absorbance (A450nm - A690nm)
Time (hours)
WT
IFNAR1 KO
H
LLC
Absorbance (A450nm - A690nm)
XTitle
WT
IFNAR1 KO

Figure 21. Abrogation of type I IFN signalling in cancer cells led to improvement of tumour response to IR in KPC and LLC tumour models.

(**A**) KPC tumour (WT *vs*. IFNAR1 KO) growths in C57BL6 mice following 0 Gy or 15 Gy IR. The number of mice for each subgroup was as follows: 0 Gy-WT (n= 6), 0 Gy-IFNAR1 KO (n = 8), 15 Gy-WT (n = 6) and 15 Gy-IFNAR1 KO (n= 8).

(**B**) LLC tumour (WT *vs*. IFNAR1 KO) growths in C57BL6 mice following 0 Gy or 10 Gy IR. The number of mice for each subgroup was as follows: 0 Gy-WT (n = 6), 0 Gy-IFNAR1 KO (n = 6), 10 Gy-WT (n= 10) and 10 Gy-IFNAR1 KO (n = 8).

Kaplan-Meier survival curves of C57BL6 mice from Figure A and B were plotted in **(C)** and **(D)**.

Proliferation of KPC cells **(E)** and LLC cells **(F)** in vitro, evaluated by WST-1 assay.

N = 5.

Radiosensitivity of MC38 cells **(G)** and LLC cells **(H)** assessed by clonogenic assay.

N = 3.

4.2.2 Abolishing type I IFN signalling in cancer cells led to enhanced cytotoxic immune response in irradiated tumours

As suggested in **Figure 19**, the more favourable outcome of IFNAR1 KO MC38 tumours over WT MC38 tumours after IR treatment is mediated by the host immune system. The cancer-immunity cycle is a complex, multistage and tightly regulated process. At each stage, a variety of immune cells are involved, including dendritic cells (as APCs) for priming of T cells, CD8+ T cells and NK cells as effector cells killing tumour cells, regulatory T cells (Tregs), macrophages and myeloid-derived suppressor cells (MDSC) acting as regulators. To explore the underlying mechanisms, we first sought to describe the immune cell landscape of these MC38 (WT *vs*. IFNAR1 KO) tumours using flow cytometry.

At baseline (day 0), the distribution of various cell populations were similar between WT and IFNAR1 KO MC38 tumours, with the exception that IFNAR1 KO tumours had slightly but significantly more macrophages (**Figure 22G**, 28.6 ± 2.4% *vs*. 20.4 ± 2.7%, $P < 0.001$) and less regulatory T cells (**Figure 22F**, 1.0 ± 0.3% *vs*. 2.0 ± 0.6%, $P = 0.0042$). Following 10 Gy IR, the percentage of CD45+ cells increased gradually as the percentage of cancer cells in both WT and IFNAR1 KO MC38 tumours declined (**Figure 22 A** and **B**). However, although not statistically significant, IFNAR1 KO tumours had a much smaller percentage of cancer cells compared with WT tumours at day 6 (2.5 ± 0.4% *vs*. 20.0 ± 14.5%, $P = 0.0521$), which is consistent with the decreased tumour volumes of IFNAR1 KO tumour after IR compared to WT (**Figure 19A**).

Activated effector cells, including CD8+ T cells and NK cell, are generally responsible for the elimination of cancer cells in tumours. They utilize granzyme and perforin packaged in cytotoxic granules to kill cancer cells. They also tend to have

augmented proliferation. Therefore, the presence of these cells together with proliferation (e.g. Ki67) and cytotoxic molecules could reflect the extent of cytotoxic immune response within tumour. Whilst the In the MC38 model, IFNAR1 KO tumours had increased infiltration of NK cells (2.7 ± 0.4% *vs*. 1.5 ± 0.6%, $P = 0.0066$) at day 4 and CD8+ T cells (7.8 ± 2.3% *vs*. 4.2 ± 1.8%, $P = 0.0338$) at day 6 after IR treatment compared with WT tumours (**Figure 22 C** and **D**). More importantly, the proliferation of these cells in IFNAR1 KO tumours is much greater than that in WT tumours with the exception of CD8+ T cells at day 4 (**Figure 23A, B** and **E**). The presence of Granzyme B also peaked at day 4, with significantly higher percentages found in IFNAR1 KO tumours (**Figure 23 A, C** and **F**). Taken together, there were significantly more Ki67 & Granzyme B double positive CD8+ T cells (**Figure 23D**, 31.8 ± 4.4% *vs*. 18.0 ± 4.0%, $P = 0.0008$) and NK cells (**Figure 23G**, 51.0 ± 7.0% *vs*. 5.8 ± 5.3%, $P < 0.0001$) in IFNAR1 KO tumours. There results suggested that following IR, IFNAR1 KO tumours had a stronger immune response compared with WT tumours.

Both tumours exhibited similar distribution of other immune populations before and after IR treatment, including dendritic cells, Tregs, macrophages and MDSC (**Figure 22 E-H**).

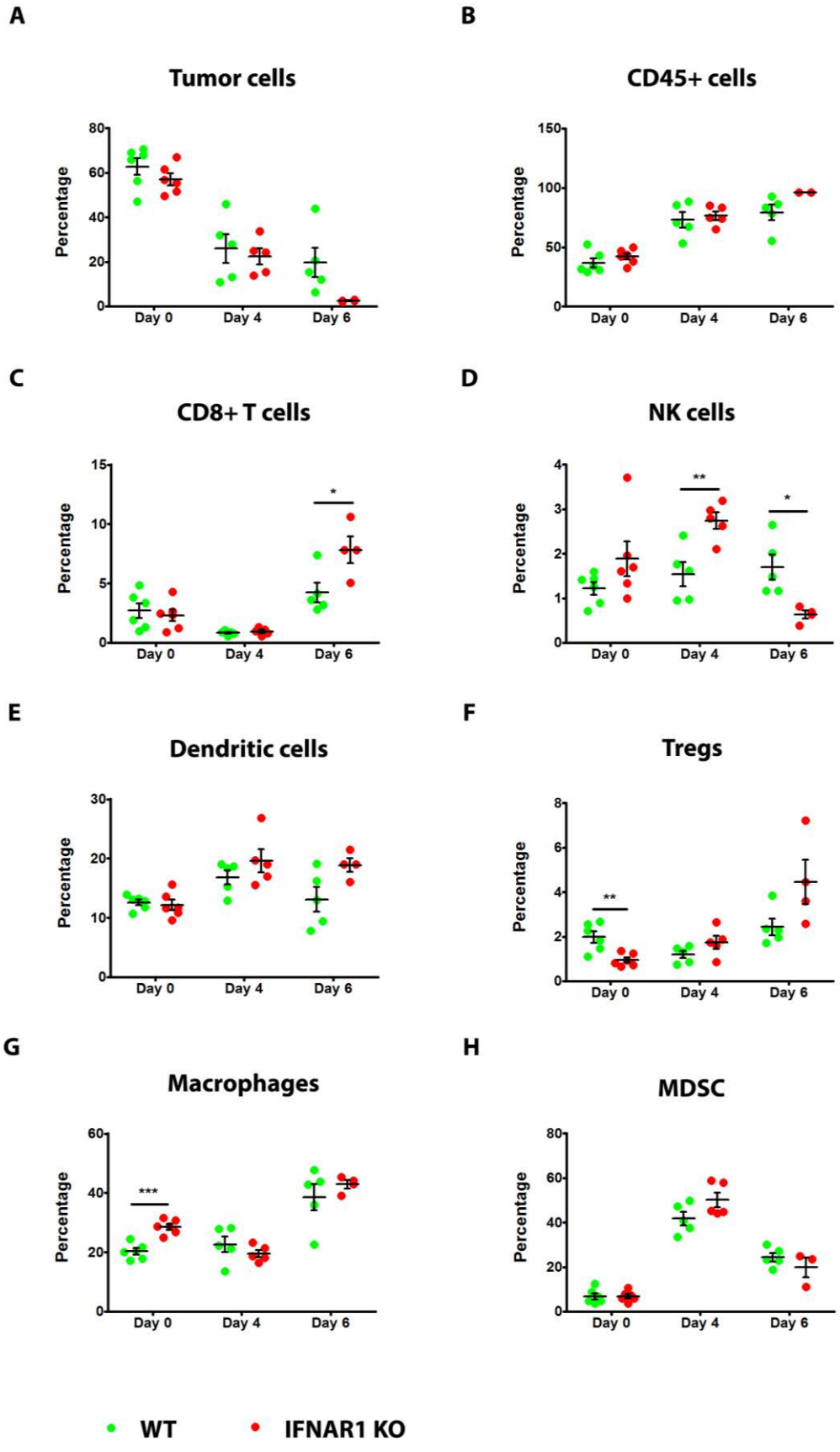

A
Tumor cells
Percentage
80
60
40
20
0
Day 0
Day 4
Day 6
B
CD45+ cells
Percentage
150
100
50
0
Day 0
Day 4
Day 6
C
CD8+ T cells
Percentage
15
10
5
0
*
Day 0
Day 4
Day 6
D
NK cells
Percentage
4
3
2
1
0
**
*
Day 0
Day 4
Day 6
E
Dendritic cells
Percentage
30
20
10
0
Day 0
Day 4
Day 6
F
Tregs
Percentage
8
6
4
2
0
**
Day 0
Day 4
Day 6
G
Macrophages
Percentage
60
40
20
0
***
Day 0
Day 4
Day 6
H
MDSC
Percentage
80
60
40
20
0
Day 0
Day 4
Day 6
WT
IFNAR1 KO

Figure 22. Flow cytometric profiling of cell populations in MC38 tumours with or without IR treatment

C57BL6 mice bearing either WT MC38 (green dots) or IFNAR1 KO (red dots) tumours were subjected to 0 Gy or 10 Gy IR. At day 0 (control without IR), 4 and 6 after IR, tumours were harvested and disaggregated for cell type profiling using flow cytometry: tumor cells (**A**), CD45+ cells (**B**), CD8+ T cells (**C**), NK cells (**D**), dendritic cells (**E**), Regulatory T cells (Tregs, **F**), macrophages (**G**), myeloid-derived suppressor cells (MDSC, **H**).

Percentage in the graphs for each population represents the fraction of this population in total live cells. Specific cell populations were gated out from live singlets (excluding cellular debris) with additional markers:

Tumor cells: CD45-, GFP+

CD45+ cells: CD45+

CD8+ T cells: CD45+, CD3+, CD8+

NK cells: CD45+, CD3-, NK1.1+

Dendritic cells: CD45+, CD11c+, MHC-II +

Tregs: CD45+, CD4+, Foxp3+

Macrophages: CD45+, CD11b+, F4/80+

MDSC: CD45+, CD11b+, Gr-1+

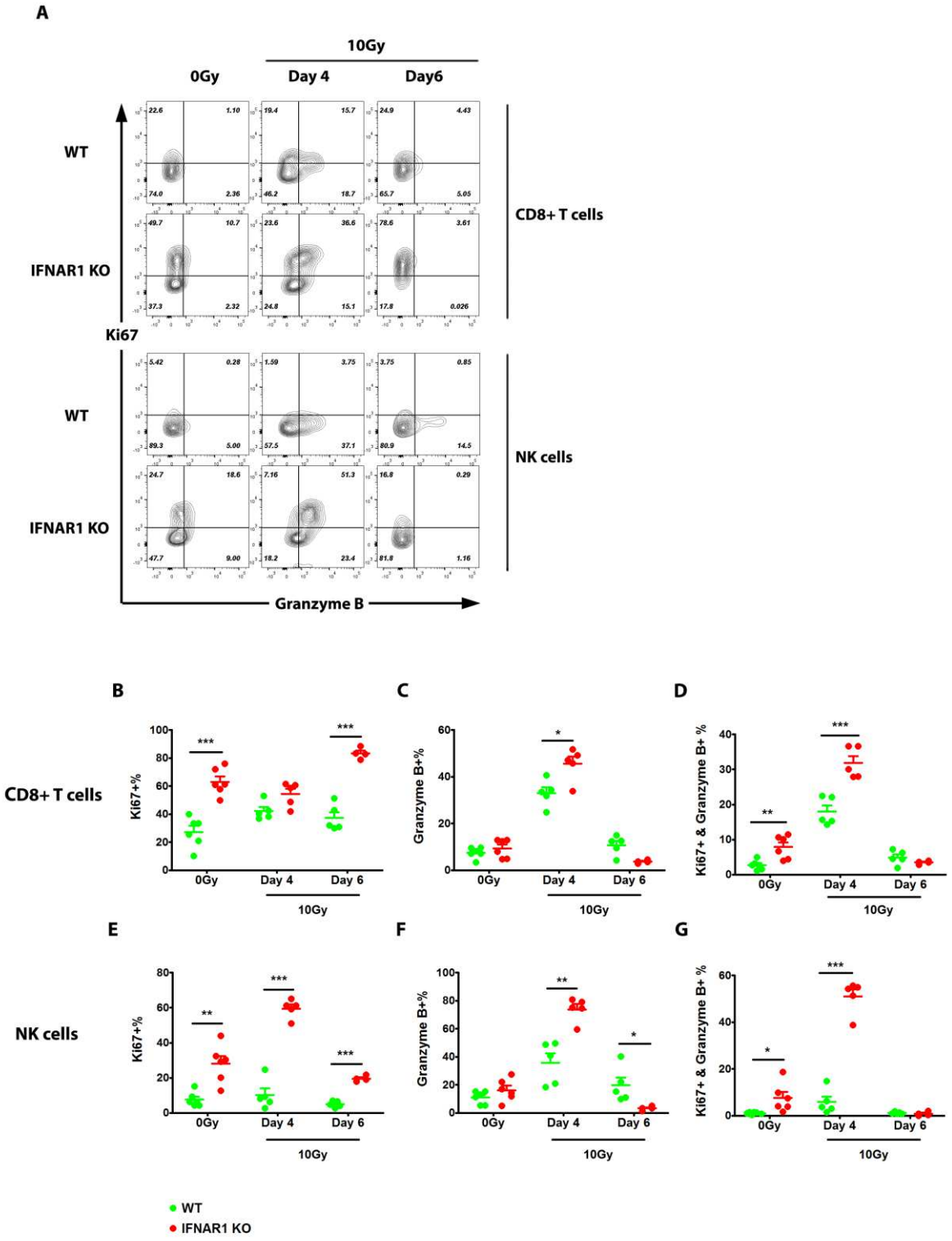

A
10Gy
0Gy
Day 4
Day6
WT
IFNAR1 KO
CD8+ T cells
NK cells
Ki67
Granzyme B
B
C
D
E
F
G
CD8+ T cells
NK cells
Ki67+%
Granzyme B+%
Ki67+ & Granzyme B+ %
0Gy
Day 4
Day 6
10Gy
WT
IFNAR1 KO

Figure 23. Proliferation and cytotoxic capacity of CD8+ T cells and NK cells in MC38 tumours with or without IR.

C57BL6 mice bearing MC38 tumours (WT *vs*. IFNAR1 KO) were subjected to 0Gy or 10 Gy IR. Control and irradiated tumours (day 4 and day 6, respectively) were collected, disaggregated and assessed by flow cytometry for the characterization of CD8+ T cells and NK cells. Percentage in the graphs for each population represents the fraction of this population in total CD8+ T cells or NK cells.

(**A**) An example plot for the characterization of CD8+ T cells (upper panel) and NK cells (lower panel), with Ki67 on X axis against Granzyme B on Y axis.

Percentage of Ki67+, Granzyme B+, and Ki67+ & Granzyme B+ CD8+ T cells in WT (green dots) or IFNAR1 KO (red dots) tumours with or without IR were summarized in (**B**), (**C**), and (**D**), respectively. N = 6 for control groups and 5 for treatment groups, respectively.

Percentage of Ki67+, Granzyme B+, and Ki67+ & Granzyme B+ NK cells in WT or IFNAR1 KO tumours with or without IR were summarized in (**E**), (**F**), and (**G**), respectively. N = 6 for control groups and 5 for treatment groups, respectively.

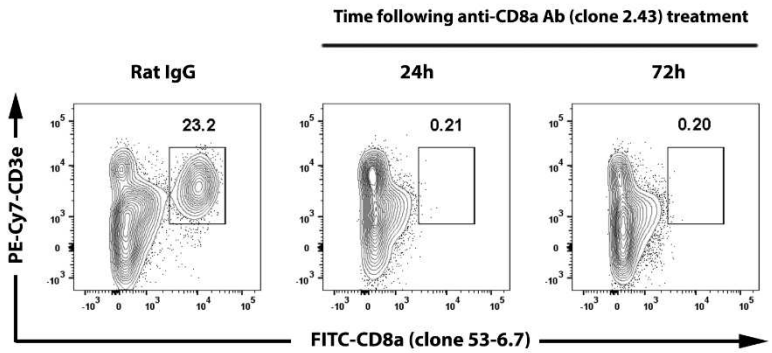
4.2.3 CD8+ T cells were the main effector cells that mediated the improved response of IFNAR1 KO MC38 tumours to IR

Enhanced cytotoxic function was found in tumour infiltrated CD8+ T cells and NK cells as well following IR in our MC38 tumour model. To determine their proportional contribution to the overall tumour response to IR, we depleted them using specific Ab. The depletion efficacy of CD8+ T cells or NK cells was validated by flow cytometry. A single intraperitoneal (i.p.) injection of Ab (anti-CD8α for CD8+ T cells and anti-NK1.1 for NK cells depletion) eliminated 99% of CD8+ T cells (**Figure 24A**) and 94% of NK cells (**Figure 24B**) in subcutaneous tumours for up to 72 hours. We then evaluated the growth of MC38 tumours following 10 Gy IR with or without the depletion of either population. Consistent with results in **Figure 19A**, 10 Gy IR plus isotype Ab treatment led to significant retardation of tumour growth in both WT and IFNAR1 KO tumours (**Figure 24 C** and **D,** lines with solid triangles). With CD8+ T cell depletion, growth delay in response to IR was significantly compromised in WT MC38 tumours and almost completely abolished in IFNAR1 KO tumours (**Figure 24 C** and **D**, lines with solid circles). More importantly, the enhanced response found in IFNAR1 KO tumours over WT tumours was abrogated with the elimination of CD8+ T cells, suggesting that CD8+ T cells were the main effector cells that mediating the improved outcomes of IFNAR1 KO tumours (**Figure 24E**). In contrast, no notable effect was found with NK cell depletion in addition to IR in IFNAR1 KO tumours, though there was a minor reduction of tumour response in WT MC38 tumours (**Figure 24 C** and **D,** lines with hollow squares). Consistently, IFNAR1 KO tumours with NK cell depletion still display substantially greater response to IR compared to WT tumours (**Figure 24E**). Taken together, our results suggest the improved

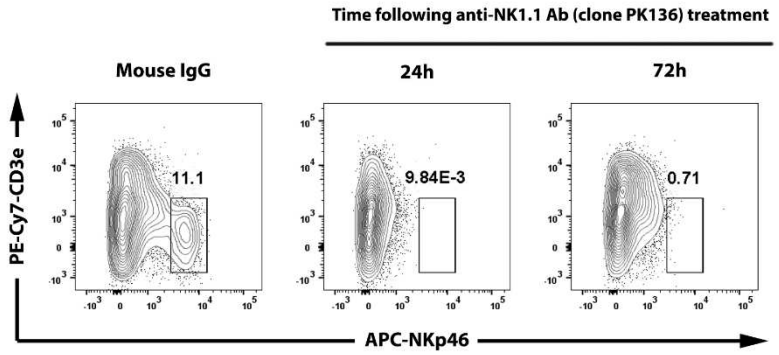
outcome in irradiated IFNAR1 KO MC38 tumours is predominantly mediated by CD8+ T cells.

We now asked whether mice in which IFNAR1 KO MC38 tumors had regressed retained systemic anti-tumor immunity to challenge with either WT or IFNAR1 KO cancer cells. Notably, neither WT nor IFNAR1 KO MC38 cells grew in mice that had previously rejected IFNAR1 KO tumors (**Figure 24F**). These data indicate that rejection was a systemic response involving memory. They also suggest that rejection was not due to recognition of a novel antigen presented by the Ifnar1 KO cells.

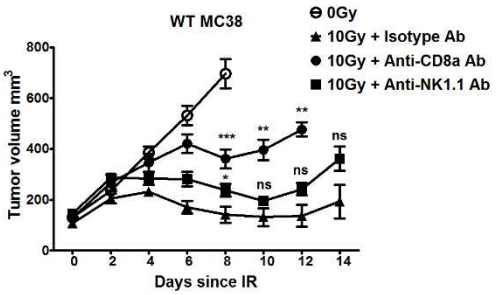
A


Time following anti-CD8a Ab (clone 2.43) treatment
Rat IgG
24h
72h
23.2
0.21
0.20
PE-Cy7-CD3e
FITC-CD8a (clone 53-6.7)

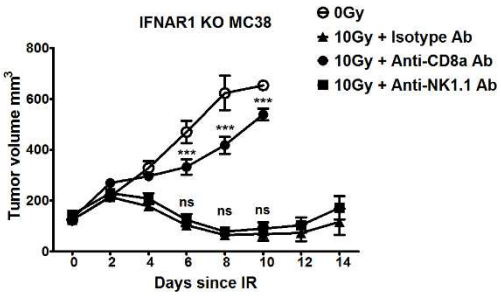
B


Time following anti-NK1.1 Ab (clone PK136) treatment
Mouse IgG
24h
72h
11.1
9.84E-3
0.71
PE-Cy7-CD3e
APC-NKp46

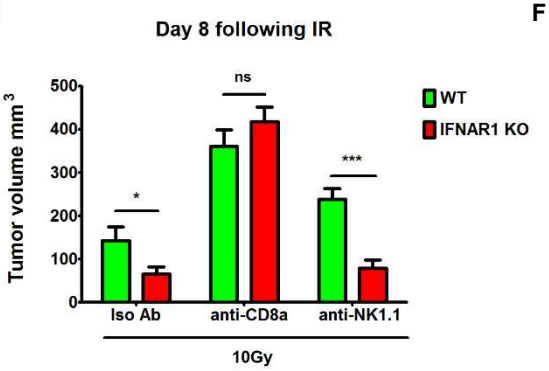
C


WT MC38
0Gy
10Gy + Isotype Ab
10Gy + Anti-CD8a Ab
10Gy + Anti-NK1.1 Ab
Tumor volume mm3
Days since IR

D


IFNAR1 KO MC38
0Gy
10Gy + Isotype Ab
10Gy + Anti-CD8a Ab
10Gy + Anti-NK1.1 Ab
Tumor volume mm3
Days since IR

E


Day 8 following IR
WT
IFNAR1 KO
Tumor volume mm3
Iso Ab
anti-CD8a
anti-NK1.1
10Gy

F

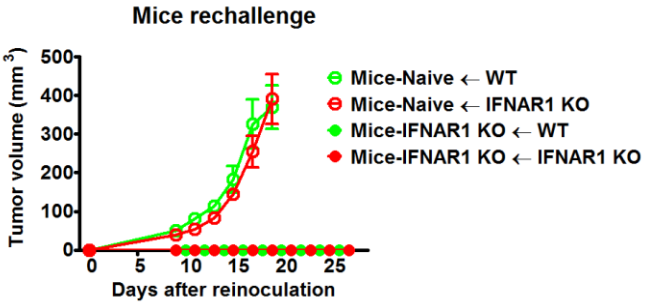

Mice rechallenge
Mice-Naive ← WT
Mice-Naive ← IFNAR1 KO
Mice-IFNAR1 KO ← WT
Mice-IFNAR1 KO ← IFNAR1 KO
Tumor volume (mm3)
Days after reinoculation

Figure 24. CD8+ T cells were the main effectors cells that mediated the improved response of IFNAR1 KO MC38 tumours to IR.

(**A**) The percentage of CD8+ T cells in MC38 tumours in C57BL6 mice at 24 and 72 hours following i.p injection of rat IgG2b isotype control antibody (Ab, clone LTF-2) or anti-mouse CD8α Rat IgG2b Ab (clone 2.43).

(**B**) The percentage of NK cells in MC38 tumours in C57BL6 mice at 24 and 72 hours following i.p injection of mouse IgG2a isotype control Ab (clone C1.18.4) or anti-mouse NK1.1 mouse IgG2a Ab (clone PK136).

C57BL7 mice bearing subcutaneous WT MC38 (**C**) or IFNAR1 KO (**D**) MC38 tumours were subjected to the following treatments: (1) 0 Gy IR; (2) 10 Gy IR on day 0 plus i.p. injection of rat and mouse isotype control Ab; (3) 10 Gy IR plus i.p. injection of anti-CD8α Ab; (4) 10Gy IR plus anti-NK1.1 Ab. Ab was administrated on day -1, 2, 5, 8 and 11. Following IR, tumour volumes were measured every other day using callipers. Tumours with either CD8+ T cells or NK cells depleted were compared with tumours receiving isotype Ab treatment.

(**E**) Tumour (WT *vs*. IFNAR1 KO) volume at day 8 following 10 Gy with i.p inection of isotype Ab, anti-CD8α Abs or anti-NK1.1 Ab (data from **C** and **D**).

(**F**). C57BL/6 mice, with completely regressed IFNAR1 KO MC38 tumors after IR were rechallenged with 1 x 10^5 WT or IFNAR1 KO MC38 cell on the other flank. The growth of tumors following reinoculation was plotted in (F). N = 4-6.

4.2.4 IFNAR1 KO MC38 cells were more susceptible to CD8+ T mediated cytolytic killing than WT MC38 cells

In **Figure 19A**, we showed that IFNAR1 KO MC38 tumours exhibited substantially improved response to IR over WT tumours (complete regression: 50% *vs*. 0%, $P < 0.0001$) mediated by tumour infiltrating CD8+ T cells. However, the total number of CD8+ T cells were indistinguishable between these two groups of tumours at day 4 following IR when Granzyme B expression was the highest. Moreover, there was only a moderate increase of the percentage of Granzyme B+ CD8+ T cells in IFNAR1 KO tumours compared to the WT (45.5 ± 6.9% *vs*. 33.1 ± 5.7%, $P = 0.0140$). To ask how this moderately enhanced cytotoxic capacity in effector cells could lead to such a dramatically enhanced tumour response, we evaluated susceptibility of the cancer cells to cytotoxicity by CD8+ T cells.

We co-cultured WT and IFNAR1 KO MC38 cells with sorted CD8+ T cells from either WT or IFNAR1 KO MC38 tumours with or without IR, respectively. The killing of tumours by CD8+ T cells was evaluated 48 hours later. As shown in **Figure 25 A**, there was greater killing of IFNAR1 KO cells than WT cells (67.0 ± 1.0% *vs*. 29.7 ± 7.0%, $P = 0.0008$) after they were co-cultured with CD8+ T cells from WT tumours. Similarly, there was also greater killing (41.7 ± 1.5% *vs*. 9.3 ± 5.5%, $P = 0.0006$) when the IFNAR1 KO tumour cells were incubated with CD8+ T cells from IFNAR1 KO tumours. These data indicate that IFNAR1 KO MC38 cells were more vulnerable to CD8+ T cell-mediated killing at baseline *in vitro*. CD8+ T cells from IFNAR1 KO tumours were less effective in this assay than those from WT. Since the cytotoxic immune response and its enhancement in IFNAR1 KO MC38 tumours only became evident after IR, we asked whether irradiated IFNAR1 KO MC38 cells also had greater susceptibility to CD8+ T cell-mediated killing. We examined cellular

apoptosis of irradiated tumours cells following co-culture with CD8+ T cells derived from irradiated tumours. In order to distinguish CD8+ T cell-mediated killing from radiation-induced killing, we used real-time imaging to capture the interaction between CD8+ T cells and tumour cells, and the initial of caspase-3/7 activation in tumour cells. In consistent with the results in Figure 22A, there was significantly more apoptosis in irradiated IFNAR1 KO MC38 cells compared with WT MC38 when co-cultured with CD8+ T cells derived from either WT MC38 (44.3 ± 8.4% *vs*. 13.8 ± 8.5%, $P = 0.0022$) or IFNAR1 KO MC38 (35.2 ± 11.2% *vs*. 18.0 ± 6.0%, $P = 0.0402$) tumours (**Figure 25B**).

We asked which tumour cell type, IFNAR1 KO or WT, would survive after radiation treatment in the same immune microenvironment *in vivo*. MC38 cells transfected with lentivirus particles to express GFP in WT cells and mCherry in IFNAR1 KO cells, were co-injected into C57BL6 mice subcutaneously at 1:1 ratio. As shown in **Figure 25C**, these mixed tumours retained the same ratio of cell types after growth in syngeneic mice. Following 10 Gy IR, mixed tumours initially showed growth pattern similar to IFNAR1 KO tumours, but later grew to volumes similar to WT MC38 tumours (**Figure 25D**). There were equivalent proportions of WT-GFP and IFNAR1 KO-mCherry tumour cells in total CD45- cells at approximately 100 mm^3 before treatment (WT *vs*. IFNAR1 KO: 53.3 ± 6.6% *vs*. 46.0 ± 6.5%, $P > 0.05$) (**Figure 25 E** and **F**). Following IR, IFNAR1 KO-mCherry cells were almost completely absent from tumours (< 5% of total CD45- live cells) at day 3, 5 and 25. WT-GFP cells were the majority of CD45- cells. To determine whether CD8+ T cells were responsible for the disparity of IFNAR1 KO cell survival after IR, we depleted CD8+ T cells. This partially restored the proportion of IFNAR1 KO cells to 80%. Depletion of NK cells had no effect (**Figure 25 G** and **H**). Thus, in *vivo* as in *in vitro*, IFNAR1 KO MC38 cells

displayed greater susceptibility to cytotoxic CD8+ T cell-mediated killing compared with WT MC38 cells after irradiation. Moreover, these results make it less plausible that the susceptibility is mediated by secreted factors. This also suggest that the susceptibility may be determined by molecules on the cell surface or within the cell.

Taken together, our results suggest that IFNAR1 KO tumours are more vulnerable to CD8+ T cells cytotoxic killing both *in vitro* and *in vivo*. Additionally, experiments mixing both the WT and the IFNAR1 KO cells indicate that this enhanced killing is more likely mediated by intrinsic mechanisms.

This page intentionally left blank.

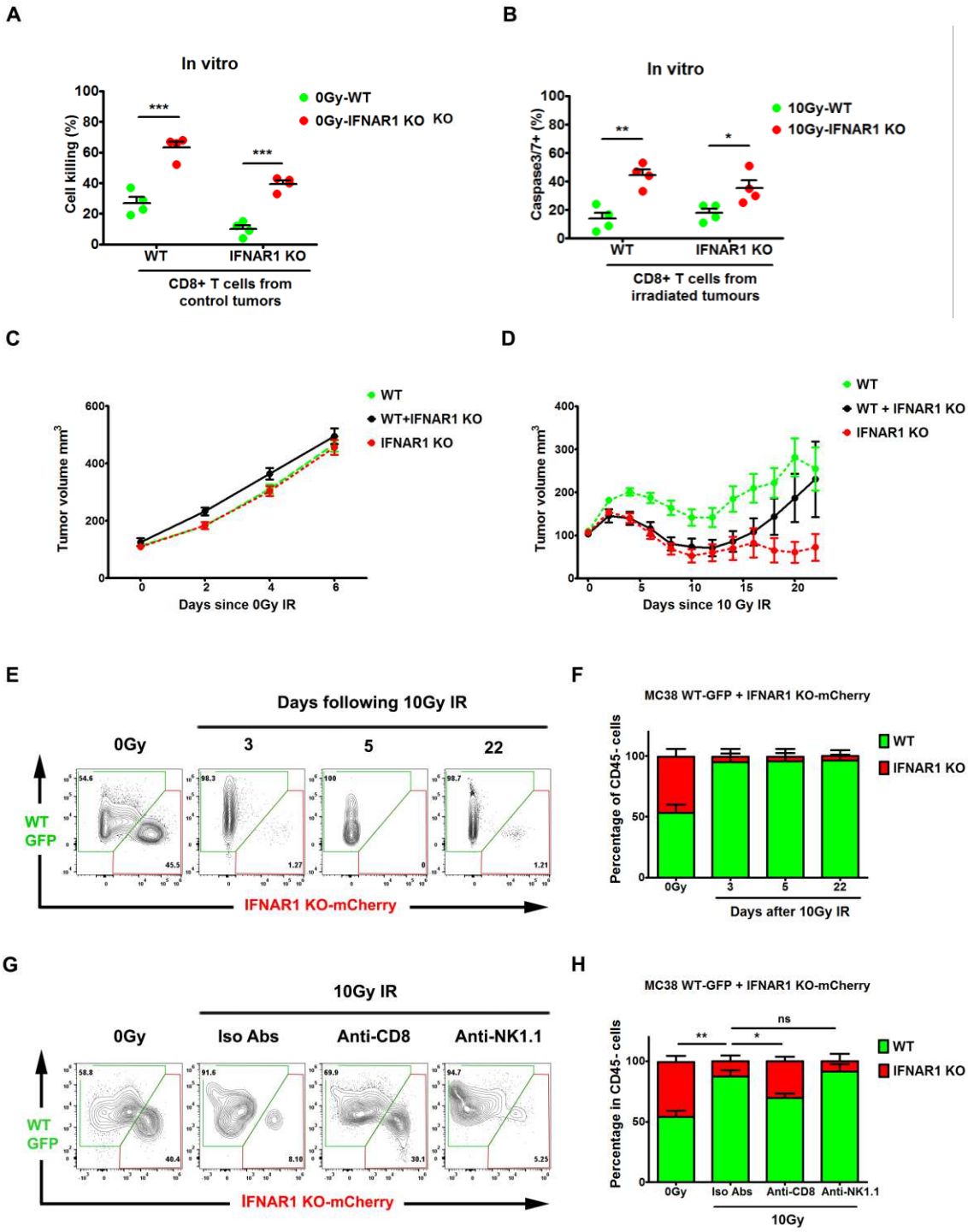

A
In vitro
Cell killing (%)
0Gy-WT
0Gy-IFNAR1 KO
KO
***
***
WT
IFNAR1 KO
CD8+ T cells from
control tumors
B
In vitro
Caspase3/7+ (%)
10Gy-WT
10Gy-IFNAR1 KO
**
*
WT
IFNAR1 KO
CD8+ T cells from
irradiated tumours
C
Tumor volume mm3
WT
WT+IFNAR1 KO
IFNAR1 KO
Days since 0Gy IR
D
Tumor volume mm3
WT
WT + IFNAR1 KO
IFNAR1 KO
Days since 10 Gy IR
E
Days following 10Gy IR
0Gy
3
5
22
WT
GFP
IFNAR1 KO-mCherry
F
MC38 WT-GFP + IFNAR1 KO-mCherry
Percentage of CD45- cells
WT
IFNAR1 KO
0Gy
3
5
22
Days after 10Gy IR
G
10Gy IR
0Gy
Iso Abs
Anti-CD8
Anti-NK1.1
WT
GFP
IFNAR1 KO-mCherry
H
MC38 WT-GFP + IFNAR1 KO-mCherry
Percentage in CD45- cells
ns
**
*
WT
IFNAR1 KO
0Gy
Iso Abs
Anti-CD8
Anti-NK1.1
10Gy

Figure 25. IFNAR1 KO MC38 tumour cells are more susceptible to CD8+ T cells mediated killing.

(A) WT and IFNAR1 KO MC38 cells were co-cultured with CD8+ T cells derived from either WT or IFNAR1 KO MC38 tumours at a CD8+ T cells (effector cells, E): tumour cells (targeted cells, T) ratio of 3:2 for 48 hours. The number of remained cells were quantified and the killing percentage was calculated using the following formula: (cell number in control well – cell number in co-cultured well)/cell number in control well x 100. WT and IFNAR1 KO MC38 cells were in green and red lines, respectively. N = 4.

(B) Irradiated MC38 cells (WT *vs*. IFNAR1 KO) were co-cultured with CD8+ T cells derived from irradiated WT or IFNAR1 KO MC38 tumours in an E: T ratio of 3:2. Culture media was supplemented with Caspase-3/7 Green detection reagent. Cells were maintained at 37 °C with 5% CO2 and imaged using Nikon Ti-E microscope. The percentage of tumour cells becoming caspase 3/7+ following interaction with CD8+ T cells was assessed in Imaris station. N = 4.

(C) GFP-tagged WT MC38 cells were mixed with mCherry-tagged IFNAR1 KO MC38 cells at a ratio of 1:1 and injected into C57BL6 mice subcutaneously. Established tumours were subjected to 0 Gy **(C)**, N = 5 or 10 Gy IR **(D)**, N = 6, and their volumes were then measured every other day. The growth of these mixed cells-derived tumours (in black solid line) were plotted along with the growth of tumours derived solely from either WT MC38 cells (in green dash line) or IFNAR1 KO MC38 cells (in red dash line) (data from **Figure 19A**).

(E) Tumours, derived from mixed MC38 WT-GFP and IFNAR1 KO-mCherry cells, were subjected to 0 Gy or 10 Gy IR at day 0. At day 3, 5 and 22 (only for irradiated tumours), they were collected, disaggregated and assessed by flow cytometry. An example of the proportions of WT-GFP against IFNAR1 KO cells in CD45- live cells were plotted.

(F) Summary of **(E)**. N = 4 in each subgroup.

(G) Tumours with mixed cells (MC38 WT-GFP + IFNAR1-mCherry) were subjected to the following treatment: 0Gy, 10 Gy (day 0) + isotype Abs, 10 Gy + anti-CD8 Abs and 10 Gy + anti-NK1.1 Abs, respectively. Abs were administrated on day -1 as described in Figure 21. At day 3, tumours were harvested, disaggregated and assessed by flow cytometry. The distribution of WT-GFP *vs*. IFNAR1 KO-mCherry MC38 cells in CD45- live cells was plotted.

(H) Summary of **(G)**. N = 3 in each subgroup.

4.2.5 The increased vulnerability of IFNAR1 KO MC38 to CD8+ T cells is not mediated by either PD-L1 or Galectin-9

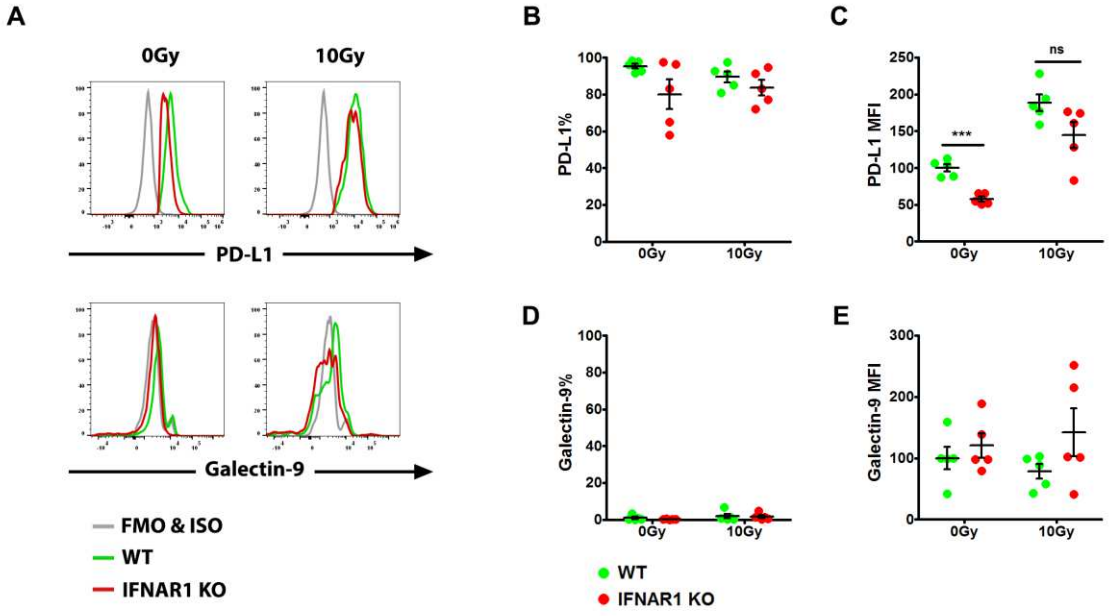
Cytotoxic T cell response is tightly regulated by a complex and hierarchical system, including inhibitory immune checkpoint molecules, which act as negative regulators to constrain the range of targeting cells and the extent of response as well. Cancer cells expressing these molecules on their surface could trigger co-inhibitory pathways in the cytotoxic T cells they encounter, resulting in functional compromise and even exhaustion (reviewed in [33]). Reversely, blockades of these molecules may enhance their susceptibility to cytotoxic immune response and potentially lead to them being completely eradicated by the host immune system (reviewed in [169]).

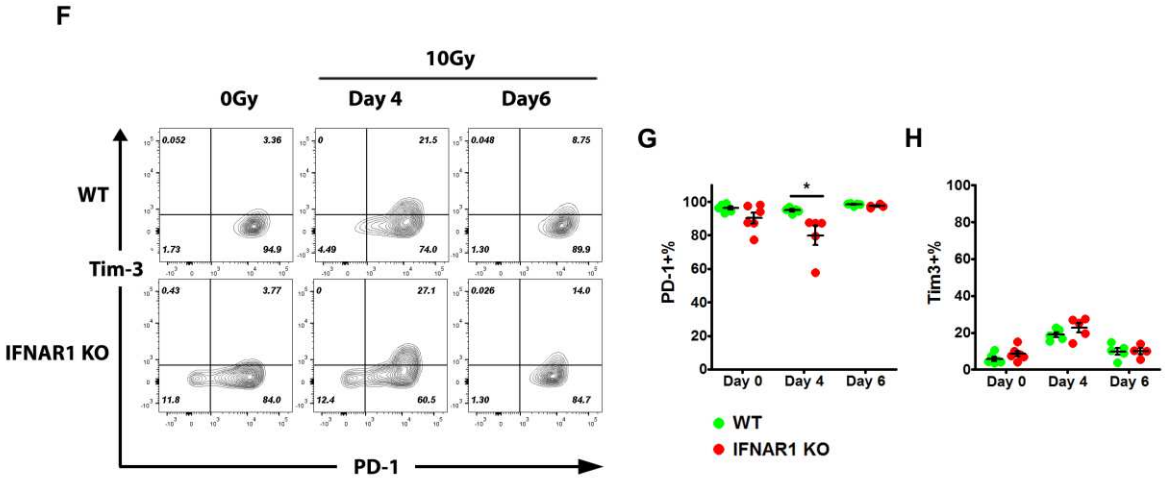
The known inhibitory immune checkpoint ligands expressed on cancer cells include PD-L1, Galectin-9, CD155, HVEM and CEACM1. To ask whether differential expression of the inhibitory ligands accounted for the augmented susceptibility of IFNAR1 KO cells, we first evaluated the expression of PD-L1 and Galectin-9 on cancer cells *in vivo*. The majority of both WT and IFNAR1 KO MC38 cells expressed PD-L1 in the tumour microenvironment with (89.5 ± 6.6% *vs*. 83.6 ± 9.5%, $P > 0.05$) or without IR (95.3 ± 3.0% *vs*. 80.0 ± 18.1%, $P > 0.05$) (**Figure 26A** and **B**). At baseline, the intensity of PD-L1 staining (MFI) was significantly less in IFNAR1 KO MC38 cells compared to WT MC38 cells at base line (**Figure 26C**, 57.7 ± 7.2 *vs*. 100.0 ± 11.4, $P = 0.0001$). However, following 10 Gy IR, both tumour cells exhibited upregulation of PD-L1 to comparable levels (144.5 ± 39.4 *vs*. 188.5 ± 25.5, $P > 0.05$). It seems less likely that PD-L1 would lead to the significantly discrepant tumour response. Very few WT or IFNAR1 KO cells expressed Galectin-9 on their surface

(**Figure 26 A** and **D**, < 10% in all samples), indicating that it is unlikely to play an important role in the susceptibility of IFNAR1 KO cells.

We also examined the expression status of PD-1 and Tim-3 (receptors for PD-L1 and Galectin-9, respectively) in tumour infiltrated CD8+ T cells. Interestingly, the majority of CD8+ T cells were PD-1 positive in both WT and IFNAR1 MC38 tumours, with the exception of a transient decrease at day 4 in IFNAR1 KO tumours (**Figure 26F** and **G**, 95.0 ± 1.6% *vs*. 79.9 ± 12.7%, $P = 0.0313$). To determine whether the transient downregulation of PD-1 may contribute to the enhanced cytotoxic activity of CD8+ T cells in irradiated IFNAR1 KO MC38 tumours. We analysed the correlation between the expression status of PD-1 and Ki67 or Granzyme B in IFNAR1 KO MC38 tumour-derived CD8+ T cells. In comparison to PD-1- CD8+ T cells, PD-1+ CD8+ T cells had a substantially higher percentage of Ki67+ cells at baseline (**Figure 26 I** and **J**, 63.7 ± 10.0% *vs*. 36.0 ± 16.6%, $P = 0.0058$) and more Ki67+ (**Figure 26 I** and **J,** 58.0 ± 9.1% *vs*. 38.7 ± 8.8%, $P = 0.0090$) and Granzyme B+ cells (**Figure 26 I** and **K**, 51.5 ± 7.7% *vs*. 19.5 ± 10.1%, $P = 0.0005$) after irradiation. Indeed, the majority (91.7 ± 9.3%) of Ki67 and Granzyme B double positive CD8+ T cells were PD-1+. Therefore, in our model, the presence of PD-1 is associated with active cytotoxic function, instead of functional compromise of CD8+ T cells, at the time point we examined. The percentage of CD8+ T cells expressing Tim-3 is much smaller than those expressing PD-1, with a temporary elevation at day 4 in both groups of tumours (**Figure 26 F** and **H**). Taken together, our results suggest that neither the PD-L1-PD1, nor the Galectin9-Tim-3 signalling axis confers the enhanced vulnerability of IFNAR1 MC38 cells to cytotoxic killing, though their contribution cannot be completely excluded.

This page intentionally left blank.


A
0Gy
10Gy
PD-L1
Galectin-9
FMO & ISO
WT
IFNAR1 KO
B
PD-L1%
C
PD-L1 MFI
ns
***
D
Galectin-9%
E
Galectin-9 MFI
WT
IFNAR1 KO


F
10Gy
0Gy
Day 4
Day6
WT
IFNAR1 KO
Tim-3
PD-1
G
PD-1+%
Day 0
Day 4
Day 6
WT
IFNAR1 KO
H
Tim3+%

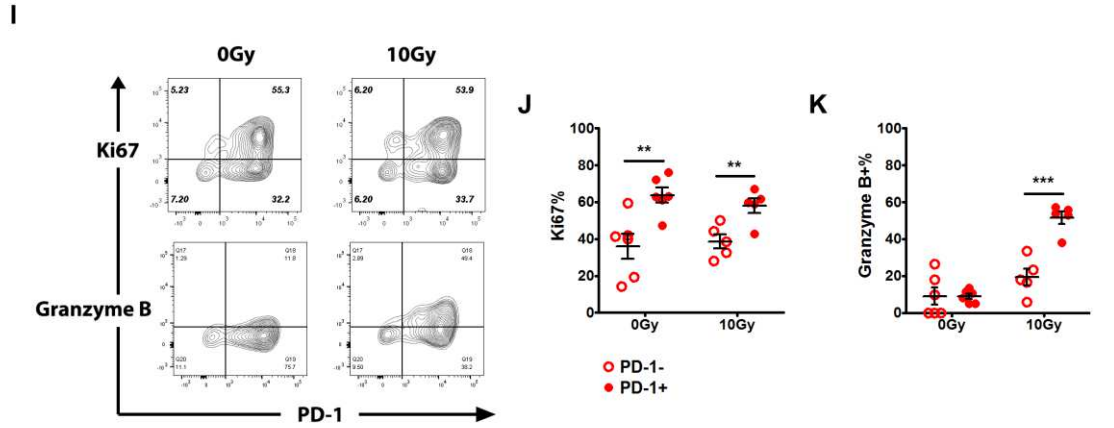

I
0Gy
10Gy
Ki67
Granzyme B
PD-1
J
Ki67%
PD-1-
PD-1+
K
Granzyme B+%

Figure 26. The increased vulnerability of IFNAR1 KO MC38 to CD8+ T cells is independent of PD-L1- and Galectin-9.

(A) C57BL6 mice bearing WT or IFNAR1 KO MC38 (plain cells) tumours were subjected to 0 Gy or 10 Gy IR (day 0), respectively. At day 4 following IR, tumours were harvested, disaggregated, and assessed by flow cytometry. Tumour cells were gated as Alexa Fluor 700-CD45-, APC-CD31-, APC-CD140a- live cells (APC-Cy7-). BV421-PD-L1 and PerCp-Cy5.5-Galectin-9 expression on tumours were examined on histogram plots, respectively (representative graph A). Cells stained with FMO & isotype control Abs were used as negative controls (grey line). WT and IFNAR1 KO MC38 cells were in green and red lines, respectively.

The percentage of PD-L1+ tumour cells and the MFI of these cells from (A) were summarized in **(B)** and **(C)**, respectively. N = 5. The percentage of Galectin-9+ tumours cells and the MFI of these cells from (A) were summarized in **(D)** and **(E)**, respectively. N = 5.

(F) C57BL6 mice bearing WT or IFNAR1 KO MC38 tumours without a fluorescent tag were subjected to 0 Gy or 10 Gy IR (day 0), respectively. At day 4 and day 6 following IR, tumours were harvested, disaggregated, and assessed by flow cytometry, respectively. CD8+ T cells were gated as Alexa Fluor 700-CD45+, BV510-CD3+, BV711-CD8+ live cells. BV421-PD-1 and APC-Tim-3 expression on CD8+ T cells were examined on dot plots (representative graph A). The percentage of PD-1+ or Galectin-9+ CD8+ T cells in tumours were summarized in **(G)** and **(H)**, respectively. N = 6 for control samples and 5 for irradiated samples, respectively.

(I) Expression of Ki67 and granzyme B in CD8+ T cells from IFNAR1 KO MC38 tumours (samples from **(F)**) at day 4 following 0Gy or 10Gy IR were analysed by flow cytometry, respectively. BV421-PD-1 was plotted on X-axis against PE-Ki67 and PE-Cy7-Granzyme B on Y-axis, respectively. Expression of Ki67 and granzyme B in PD-1+ or PD-1- CD8+ T cells were summarized in **(J)** and **(K)**, respectively. N = 6 for control samples and 5 for irradiated samples, respectively.

4.2.6 CD155 and H-2Kb are candidates to play a role in the enhanced susceptibility of IFNAR1 KO MC38 cells to CD8+ T cell-mediated killing

In addition to PD-L1 and Galectin-9, a number of surface immune modulators also have been found to regulate the function of cytotoxic CD8+ T cells or NK cells in tumours. These include CD155, H-2Kb, HVEM, CEACAM1, CD80, CD86, Mult-1 and Qa-1b (reviewed in [33, 170]). In an attempt to dissect the underlying mechanisms of IFNAR1 KO cells' susceptibility to CD8+ T cells cytotoxicity, we examined the expression of these molecules in MC38 cells *in vivo*. We would expect IFNAR1 KO cells to express less of the candidate molecules than WT after IR.

CD155, the receptor for polivirus (PVR), has dual roles in immune regulation. It leads to immune suppression via interacting with the counter-receptor TIGIT or activation when engages with DNAM-I (CD226) on CD8+ T cells and NK cells. At baseline, the majority of MC38 cells, both WT and IFNAR1 KO, were CD155 positive (**Figure 27 A** and **B**, 85.1 ± 9.0% and 90.1 ± 11.9%, respectively). Following 10 Gy IR, the percentage of CD155+ cells decreased to 66.3 ± 16.3% and 56.6 ± 7.9%, respectively. The intensity of CD155 in IFNAR1 KO cells is only one third of that in WT cells at both baseline (34.0 ± 11.0 *vs*. 100 ± 22.1, $P = 0.0003$) and after irradiation (45.8 ± 9.3 *vs*. 139.0 ± 39.4, $P = 0.0009$) (**Figure 27 A** and **C**). The significant downregulation of CD155 in IFNAR1 KO MC38 cells made it a candidate as a molecule involved in the enhanced vulnerability of IFNAR1 KO cells to CD8+ T cells.

H-2Kb, the major histocompatibility complex class I (MHC-I) molecule, is important for anti-tumour immunity, owing to its obligatory role in antigen

presentation. Only when cancer cells present tumour antigens via H-2Kb on their surface, can they be recognized by antigen-specific cytotoxic CD8+ T cells. Downregulation of H-2Kb is an important strategy that tumour cells utilize for immune escape, whilst upregulation of H-2Kb may potentially boost the anti-tumour immune response. In our hands, H-2Kb was present on both MC38 cells with or without IR (**Figure 27 D** and **E**, >98% in all samples). Surprisingly, as shown in **Figure 27 D** and **F**, the MFI of H-2Kb in IFNAR1 KO MC38 cells was notably higher than that in WT MC38 cells with (190.6 ± 21.6 *vs*. 95.4 ± 5.8, $P < 0.0001$) or without IR (176.7 ± 15.5 *vs*. 100 ± 11.7, $P < 0.0001$). It is unclear that to what extent does the upregulation of H-2Kb in IFNAR1 KO MC38 cells contribute to their increased susceptibility to cytotoxic killing.

Both WT and IFNAR1 KO MC38 tumour cells demonstrated upregulation of CEACAM1 and CD80, and downregulation of HVEM as well after IR (**Figure 27 G-O**). The percentage and MFI of these markers did not shown any significant differences between these two tumour cells. No notable expression of CD86, Mult-1 and Qa-1b was found in both tumour cells (data not shown).

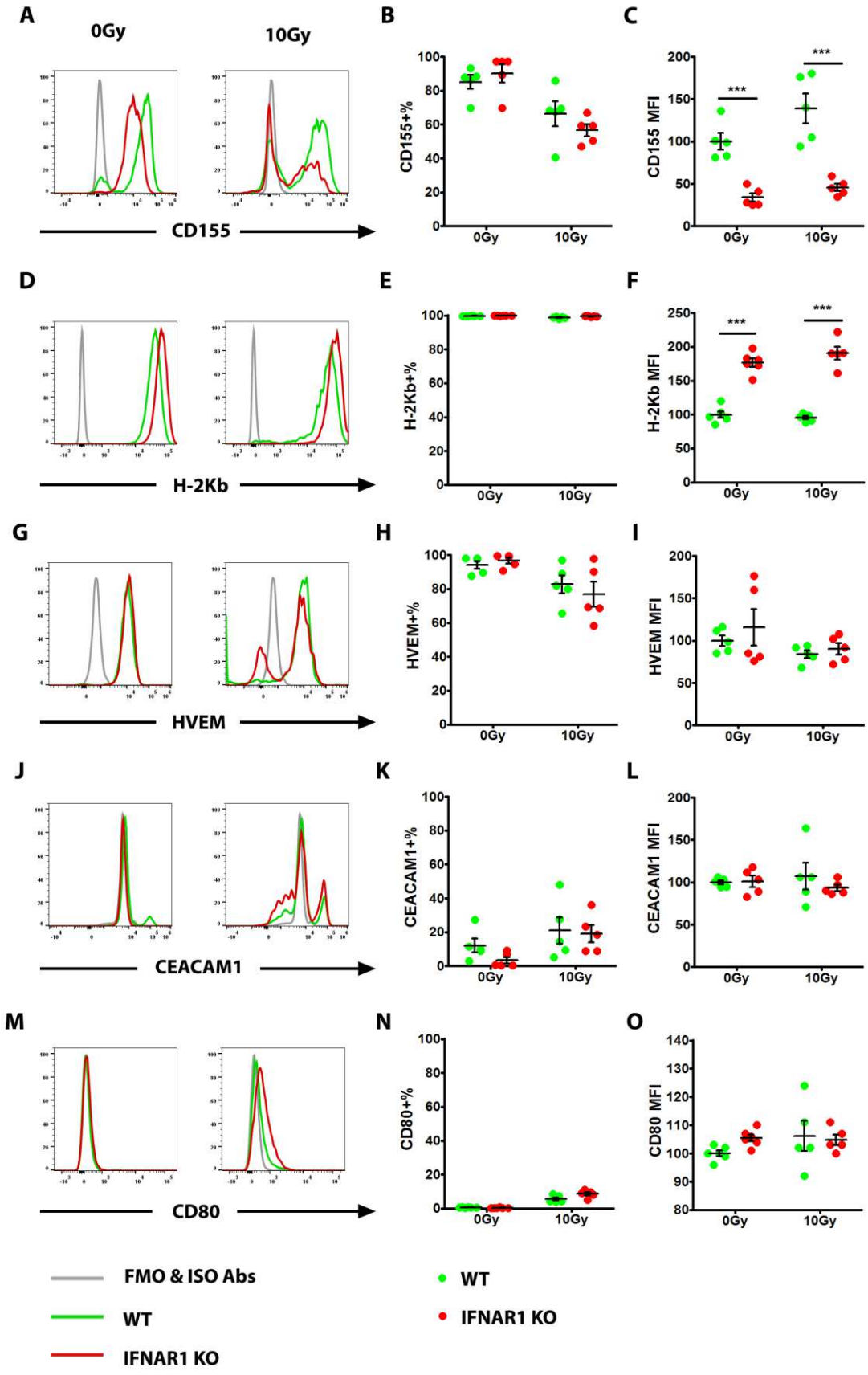

A
0Gy
10Gy
CD155
B
CD155+%
C
CD155 MFI
***
D
H-2Kb
E
H-2Kb+%
F
H-2Kb MFI
G
HVEM
H
HVEM+%
I
HVEM MFI
J
CEACAM1
K
CEACAM1+%
L
CEACAM1 MFI
M
CD80
N
CD80+%
O
CD80 MFI
FMO & ISO Abs
WT
IFNAR1 KO

Figure 27. In vivo expression of immunomodulators on the surface of MC38 tumour cells with or without IR.

WT or IFNAR1 KO MC38 (plain cells) tumours in C57BL6 mice were subjected to 0 Gy or 10 Gy IR (day 0). At day 4 following IR, tumours were harvested, disaggregated, and assessed by flow cytometry. N = 5 for each group.

Tumour cells were gated as Alexa Fluor 700-CD45-, APC-CD31-, APC-CD140a- live cells (APC-Cy7-). The expression level of immunomodulators were examined on histogram plots, including PE-Cy7-CD155, PE-Cy7-H-2Kb, PE-HVEM, FITC-CEACAM1, BV650-CD80, PE-CD86, PE-Mult-1 and BV421-Qa-1b.7. Cells stained with FMO control Abs were used as negative controls (grey line). WT MC38 cells in green line and IFNAR1 KO MC38 in red line, respectively.

The percentage of positive cells and the MFI of these positive cells were also summarized on the side of each representative graph. All MFIs were normalized to the mean MFI (designated as 100) of control WT MC38 tumours (0 Gy). Green dots: WT tumour cells; Red dots: IFNAR1 KO tumour cells.

(A), **(B)** and **(C)**: CD155

(D), **(E)** and **(F)**: H-2Kb

(G), **(H)** and **(I)**: HVEM

(J), **(K)** and **(L)**: CEACAM1

(M), **(N)**, and **(O)**: CD80

4.3 Discussion

4.3.1 Summary of findings in the current study

How IR leads to an anti-tumour immune response and how cancer cells develop resistance to cytotoxic killing is not fully understood. In this study, we investigated the role of cancer cell-derived STING pathway, a key pathway mediating type I IFN induction in cancer cells by IR, and type I IFN signalling pathway in IR-induced anti-tumour immune response. Consistent with previous literature, the host immune response made an important contribution to the tumour control following IR. This benefit was significantly comprised with the abolishment of STING pathway in tumour cells, suggesting its crucial role in facilitating anti-tumour immune response and consistent with researches showing that IFN induction after IR facilitates anti-tumour immune response. On the other hand, abrogation of type I IFN signalling in three different cancer cell lines led to remarkable improvement of the tumour response to IR. Moreover, for MC38, this reduction in tumour growth occurred predominantly via CD8+ T cell-mediated killing. The expression patterns of both PD-L1 and Galectin-9 make them unlikely to mediate the augmented vulnerability of IFNAR1 KO tumour cells to cytotoxic killing. Other potential candidates include CD155 and H-2Kb.

4.3.2 Role of tumour cell-derived type I IFN in anti-tumour immune response

Although it is increasingly acknowledged that cancer cells are an important source of type I IFN within tumours following IR, their contribution to the tumour response has been unclear. In this study, we found that elimination of the STING

pathway in cancer cells led to a compromise in anti-tumour immunity after IR. To our knowledge, this is first report demonstrating that cancer cell-derived type I IFN plays a crucial role in immune response triggered by IR at local site. In a recently published study, Vanpouille-Box and colleagues also investigated the role of tumour cell-derived type I IFN. Interestingly, they found that elimination of tumour-derived type I IFN via cGAS or STING KO did not affect tumour response to hypofractionated IR (8 Gy x 3F), but dampened systemic immune response to untreated tumours in the circumstance of immune checkpoint blockade [92]. It is very difficult to compare these results and ours, owing to different experimental designs, which includes tumour models, IR schemes and the use of immune checkpoint blockade. Nonetheless, both suggest that tumour-derived type I IFN has a critical role in IR-induced tumour-specific immune response, though the extent of contribution seems to be context-dependent.

To better determine the significance of this phenomenon, it is important to understand its underlying mechanisms. Type I IFNs have pivotal roles in multiple steps of cancer-immunity cycle that lead to substantial anti-tumour immune response [171, 172]. It is unclear if type I IFNs derived from different cellular components may have different roles in the immune response. A previous study suggest that IR induction of type I IFN within tumours has a critical role in the activation of dendritic cells activation and cross-priming of CD8+ T cells [75]. This is further supported by Vanpouille-Box, et al's study that an intact STING pathway in cancer cells is required for the recruitment and activation of dendritic cells in the early phase of anti-tumour immune response. Thus, it is possible that IR induction of type I IFN in tumour cell acts as the initial trigger to recruit dendritic cells, which then further amply the

production of type I IFN via the STING pathway, resulting in full activation of immune response.

Genetic elimination of cGAS or STING has been used as a means to investigate the role of tumour cell-derived type IFN. However, aside from mediating IFN induction, STING and its downstream transcriptional factors also regulate a number of genes in an IFN-independent manner [173, 174]. For instance, a recently published study suggested that activation of cGAS-STING pathway, in response to chromosomal instability-derived cytosolic micronuclei, triggers neither TBK1-IRFs-IFN nor canonical NF-κB pathway, but the noncanonical NF-κB pathway, resulting in augmented cellular invasion and metastasis [175]. Thus, we could not exclude the involvement of other mechanisms in the STING-mediated anti-tumour immune response.

4.3.3 Role of tumour cell-derived type I IFN signalling in anti-tumour immune response

Activation of type I IFN signalling in cancer cells has been considered as beneficial for tumour control due to its antiproliferative activity. In addition to this direct effect, emerging evidence suggests that tumour cell-derived type I IFN signalling also has a role in anti-tumour immune response. A recently published study showed that cancer cell autocrine type I IFN signalling was required to induced an immune response and contributed to response to anthracycline treatment in murine tumours [101]. Moreover, colorectal cancer patients with lower expression level of IFNAR1 in either stromal cells or tumour cells are associated with poor outcomes and loss of IFNAR1 leads to the generation of immune-privileged niche

[176]. These results indicate that an intact type I IFN signalling in cancer cells is favourable to substantial anti-tumour immune response at certain conditions.

In contrast to some of these reports, we found that abrogation of type I IFN signalling in cancer cells significantly enhanced the cytotoxic immune response in tumours following IR, resulting in significant improvement in tumour control. We further demonstrated that this phenomenon is mediated by enhanced susceptibility of the cancer cells to CD8+ T cell-mediated killing. Clearly, cancer cells can exploit type I IFN signalling as an important strategy to escape from CD8+ T cells immune surveillance in our model. In a recently published study from University of Pennsylvania, Andy Minn and colleagues found that prolonged type II IFN signalling renders cancer cells resistant to immune checkpoint blockade (anti-CTLA4) with or without radiotherapy [177]. They also showed that type I IFN signalling during immune activation phase has a minor contribution to this resistance. These results and ours suggest that activation of type I/II IFN signalling pathway can play a pivotal role in the immune resistance of tumour cells. The extent of contribution from either pathway may vary greatly, depending on the immunogenicity of tumour cells, animal model and treatment scheme.

4.3.4 PD-L1 and Galectin-9

Our results suggest that activation of type I IFN signalling in cancer cells render them more resistant to CD8+ T cell-mediated killing via non-secreted factors. PD-L1 is a cell surface molecule and is well acknowledged for its role in immune suppression. Galectin-9 is another potent co-inhibitory ligand, though it is also present in the cytoplasm and serum, in addition to the cell surface. Evidence has just

emerged, linking type I IFN signalling to these immune co-inhibitory molecules. One study indicated that type I IFN treatment induced PD-L1 in the tumour microenvironment and blocking of PD-L1 led to complete eradication of established tumours [178]. Minn's study suggests that cancer cell-derived type II and I IFN signalling elicits their immunosuppressive effect mainly via PD-L1 and Galectin-9, respectively. In our model, although abrogation of type I IFN in tumour cells led to less expression of PD-L1 at baseline, it did not affect its significant upregulation after IR, which presumably is mediated by the remaining intact type II IFN signalling pathway. We also found little galectin-9 on MC38 cells and on IFNAR1 KO cells, with very few positive cells, making it less plausible to be a major mediator. Thus, our results suggest that mediators other than PD-L1 or Galectin-9 are likely to play an important role in the adaptive immune resistance of cancer cells.

4.3.5 CD155

One of the potential candidates arising from our flow cytometry screen is CD155. CD155, originally discovered as the poliovirus receptor [179], has been shown to play an important role in anti-tumour immunity (reviewed in [180]). CD155 binds to TIGIT, an immune co-inhibitory receptor expressed on CD8+ T cells and NK cells, and inhibits their cytotoxic function [181-186]. Blockade of CD155-TIGIT signalling enhances anti-tumour immune response [184, 187]. Overexpression of CD155 has been found in a variety of cancer diseases and is associated with worse outcomes [184, 188, 189]. In this study, CD155 is also highly expressed in MC38 cells but substantially downregulated upon abrogation of type I IFN signalling. Therefore, CD155 is a potent mediator for the enhanced susceptibility of cancer cells to CD8+ T cells, which remains to be tested.

4.3.6 H-2Kb

Tumour specific immune responses require MHC class I molecules. IR can upregulate MHC class I molecules in cancer cells and hence enhance anti-tumour immune response [63]. Studies suggest that activation of type I/II signalling can lead to upregulation of MHC-I [190-194]. In this study, we did not find apparent induction of H-2Kb (MHC class I alloantigen in C57BL6 origin) in either WT or IFNAR1 KO MC38 cells after IR *in vivo*, however, IFNAR1 KO MC38 cells exhibited significantly higher expression level of H-2Kb than WT MC38 cells. The upregulation of H-2Kb in IFNAR1 KO MC38 cells may have a role in the enhanced cytotoxic immune response, though its extent of contribution will need to be examined.

4.3.7 Endogenous resistant mechanisms

Apart from the various immunomodulators found on the cell surface, endogenous resistant mechanisms exist and have been shown to impede cytotoxic immune response. Cancer cells acquire resistance to cytotoxic killing via undergoing autophagy [195-198], which can be directly induced in cancer cells by type I IFN [199, 200]. Thus, it is possible that cancer cells hijack the type I IFN signalling to undergo autophagy and become resistant to cytotoxic killing. Upregulation of serine protease inhibitors, such as PI-9 (human) or SPI-CI and SPI-6 (murine), is another mechanism that cancer cells utilize to escape from effector cell-mediated cytotoxicity, though it is unclear whether they are regulated by type I IFN signalling [201, 202]. It will be interesting to investigate the potential contribution of these endogenous resistant mechanisms in our model.

4.3.8 The role of NK cells in IFNAR1 KO MC38 tumours

NK cells are important effector cells in cancer immune surveillance. In our model, NK cells partially contribute to the overall response of WT MC38 tumour after IR, whereas in contrast, they did not show any apparent impact on the growth retardation of IFNAR1 KO tumours, despite the increased percentage of NK cells that expressed Granzyme B compared to WT tumours. The cytotoxic function of NK cells is determined by a balance between activation and inhibitory signalling (reviewed in [203]). The inhibitory signalling may outweigh the activation signalling in IFNAR1 KO tumours due to an altered profile of ligands on cancer cells, such as the downregulation of CD155 and upregulation of H-2Kb. CD155 can enhance the cytotoxic function of NK cells via interaction with DNAM-I: the activation receptor on NK cells [204-208]. Downregulation of CD155 in cancer cells may hence impede the cytotoxic capability of DNMA-I+ NK cells they encountered. Similarly, it is also possible that the upregulation of H-2Kb in IFNAR1 KO cancer may restrict the activation of tumour infiltrating NK cells. NK cells recognise and kill cells with deficient MHC-I molecules [209, 210]. Binding of MHC-I molecules to their relevant receptors on the surface of NK cells activates inhibitory pathways, leading to the tolerance of NK cells ([211], also reviewed in [212]). Thus, the cytotoxic function of NK cells may be compromised in a tumour microenvironment with more abundance of MHC-I molecules.

4.3.9 Redundant contribution from type III IFN signalling

In the current study, we focus mainly on the role of type I IFN signalling in cancer cells, whereas redundant contribution from type III IFN signalling could not be excluded. The IR induction of type III IFN (IFNL2/3) in the murine cell lines we

examined was not significant with much lower expression level at baseline compared to type I IFN. However, type III IFNs derived from the host in the tumour microenvironment may still prompt the signalling pathway in cancer cells, leading to upregulation of ISGs. Type III IFNs have been found to exhibit anti-tumour effects in both human and murine cancer cells via direct induction of cell cycle arrest and apoptosis and boosting anti-tumour immunity as well [213-220]. Whether activation of this signalling in cancer cells could also confer their resistance to cytotoxic immunity like we found with type I IFN signalling remains to be examined.

4.4 Conclusion

The essential requirement of adequate tumour immunogenicity for successful cancer immunotherapy and the capability of IR to enhance tumour immunogenicity provide a great opportunity to combine them for a synergistic effect and better outcomes. However, the development of such combinational therapy has been slow due to poor understanding of the complex interactions between radiotherapy and host anti-tumour immune responses. Interferons are a group of cytokines that have been shown to play an important role in both radiotherapy and the anti-tumour immune response. Many previous studies focused on the role of tumour infiltrating dendritic cells, whereas we found that IR also directly induced type I IFN and type I IFN signalling in tumour cells *in vivo*. More importantly, cancer cells not the immune cells actually have the greatest contribution to overall intratumoural production of type I IFN in our model. Therefore, we asked whether tumour cell-derived type I IFN and type I IFN signalling has a role in tumour response to IR. By using a variety of animal models, we demonstrated that tumour-derived type I IFN has critical contribution to the anti-tumour immune response at local site. Strikingly and unexpectedly, abrogation of type I IFN signalling via IFNAR1 KO in cancer cells led to remarkable improvement of tumour response to IR. This phenomenon is mainly driven by significantly enhanced susceptibility of cancer cells to CD8+ T cell-mediated killing via PD-L1/Galectin-9-independent mechanisms. How elimination of type I IFN signalling in cancer cells augment their vulnerability to cytotoxic killing remains to be determined.

Reference

1. Allemani, C., et al., *Global surveillance of trends in cancer survival 2000-14 (CONCORD-3): analysis of individual records for 37 513 025 patients diagnosed with one of 18 cancers from 322 population-based registries in 71 countries.* Lancet, 2018. **391**(10125): p. 1023-1075.
2. Ferlay, J., et al., *Cancer incidence and mortality worldwide: Sources, methods and major patterns in GLOBOCAN 2012.* International Journal of Cancer, 2015. **136**(5): p. E359-E386.
3. Delaney, G., et al., *The role of radiotherapy in cancer treatment: estimating optimal utilization from a review of evidence-based clinical guidelines.* Cancer, 2005. **104**(6): p. 1129-37.
4. Connell, P.P. and S. Hellman, *Advances in radiotherapy and implications for the next century: a historical perspective.* Cancer Res, 2009. **69**(2): p. 383-92.
5. Yaes, R.J., *Tumor heterogeneity, tumor size, and radioresistance.* Int J Radiat Oncol Biol Phys, 1989. **17**(5): p. 993-1005.
6. Dagogo-Jack, I. and A.T. Shaw, *Tumour heterogeneity and resistance to cancer therapies.* Nat Rev Clin Oncol, 2018. **15**(2): p. 81-94.
7. Jamal-Hanjani, M., et al., *Tracking the Evolution of Non-Small-Cell Lung Cancer.* N Engl J Med, 2017. **376**(22): p. 2109-2121.
8. Juric, D., et al., *Convergent loss of PTEN leads to clinical resistance to a PI(3)Kalpha inhibitor.* Nature, 2015. **518**(7538): p. 240-4.
9. Zaretsky, J.M., et al., *Mutations Associated with Acquired Resistance to PD-1 Blockade in Melanoma.* N Engl J Med, 2016. **375**(9): p. 819-29.
10. Sequist, L.V., et al., *Genotypic and histological evolution of lung cancers acquiring resistance to EGFR inhibitors.* Sci Transl Med, 2011. **3**(75): p. 75ra26.
11. Chen, L., et al., *Concurrent chemoradiotherapy plus adjuvant chemotherapy versus concurrent chemoradiotherapy alone in patients with locoregionally advanced nasopharyngeal carcinoma: a phase 3 multicentre randomised controlled trial.* Lancet Oncol, 2012. **13**(2): p. 163-71.
12. Ahn, J.S., et al., *Multinational Randomized Phase III Trial With or Without Consolidation Chemotherapy Using Docetaxel and Cisplatin After Concurrent Chemoradiation in Inoperable Stage III Non-Small-Cell Lung Cancer: KCSG-LU05-04.* Journal of Clinical Oncology, 2015. **33**(24): p. 2660-U124.
13. Burt, B.M., et al., *Utility of Adjuvant Chemotherapy After Neoadjuvant Chemoradiation and Esophagectomy for Esophageal Cancer.* Ann Surg, 2017. **266**(2): p. 297-304.
14. Lee, N., et al., *Intensity-modulated radiotherapy in the treatment of nasopharyngeal carcinoma: an update of the UCSF experience.* Int J Radiat Oncol Biol Phys, 2002. **53**(1): p. 12-22.
15. Wolden, S.L., et al., *Intensity-modulated radiation therapy (IMRT) for nasopharynx cancer: update of the Memorial Sloan-Kettering experience.* Int J Radiat Oncol Biol Phys, 2006. **64**(1): p. 57-62.
16. Miralbell, R., A. Lomax, and M. Russo, *Potential role of proton therapy in the treatment of pediatric medulloblastoma/primitive neuro-ectodermal tumors: spinal theca irradiation.* Int J Radiat Oncol Biol Phys, 1997. **38**(4): p. 805-11.
17. Mendenhall, N.P., et al., *Early outcomes from three prospective trials of image-guided proton therapy for prostate cancer.* Int J Radiat Oncol Biol Phys, 2012. **82**(1): p. 213-21.
18. Sejpal, S., et al., *Early findings on toxicity of proton beam therapy with concurrent chemotherapy for nonsmall cell lung cancer.* Cancer, 2011. **117**(13): p. 3004-13.
19. Apetoh, L., et al., *Toll-like receptor 4-dependent contribution of the immune system to anticancer chemotherapy and radiotherapy.* Nat Med, 2007. **13**(9): p. 1050-9.
20. Lee, Y., et al., *Therapeutic effects of ablative radiation on local tumor require CD8+ T cells: changing strategies for cancer treatment.* Blood, 2009. **114**(3): p. 589-95.

21. Swann, J.B. and M.J. Smyth, *Immune surveillance of tumors.* J Clin Invest, 2007. **117**(5): p. 1137-46.
22. Lara, P.C., et al., *Direct and bystander radiation effects: A biophysical model and clinical perspectives.* Cancer Lett, 2013.
23. Mauch, P., et al., *Hematopoietic stem cell compartment: acute and late effects of radiation therapy and chemotherapy.* Int J Radiat Oncol Biol Phys, 1995. **31**(5): p. 1319-39.
24. Eric Hall, A.G., *Radiobiology for radiobiologist 7th edion.* Lippincott Williams & Wilkins. , 2011: p. 334-335
25. Frey, B., et al., *Antitumor immune responses induced by ionizing irradiation and further immune stimulation.* Cancer Immunol Immunother, 2014. **63**(1): p. 29-36.
26. Weichselbaum, R.R., et al., *Radiotherapy and immunotherapy: a beneficial liaison?* Nat Rev Clin Oncol, 2017. **14**(6): p. 365-379.
27. Formenti, S.C. and S. Demaria, *Systemic effects of local radiotherapy.* Lancet Oncol, 2009. **10**(7): p. 718-26.
28. Postow, M.A., et al., *Immunologic Correlates of the Abscopal Effect in a Patient with Melanoma.* New England Journal of Medicine, 2012. **366**(10): p. 925-931.
29. Hicklin, D.J., F.M. Marincola, and S. Ferrone, *HLA class I antigen downregulation in human cancers: T-cell immunotherapy revives an old story.* Mol Med Today, 1999. **5**(4): p. 178-86.
30. Hanahan, D. and R.A. Weinberg, *Hallmarks of cancer: the next generation.* Cell, 2011. **144**(5): p. 646-74.
31. Nauts, H.C., G.A. Fowler, and F.H. Bogatko, *A review of the influence of bacterial infection and of bacterial products (Coley's toxins) on malignant tumors in man; a critical analysis of 30 inoperable cases treated by Coley's mixed toxins, in which diagnosis was confirmed by microscopic examination selected for special study.* Acta Med Scand Suppl, 1953. **276**: p. 1-103.
32. Kirkwood, J.M., et al., *Immunotherapy of cancer in 2012.* Ca-a Cancer Journal for Clinicians, 2012. **62**(5): p. 309-335.
33. Pardoll, D.M., *The blockade of immune checkpoints in cancer immunotherapy.* Nat Rev Cancer, 2012. **12**(4): p. 252-64.
34. Chen, D.S. and I. Mellman, *Oncology meets immunology: the cancer-immunity cycle.* Immunity, 2013. **39**(1): p. 1-10.
35. Uyttenhove, C., J. Maryanski, and T. Boon, *Escape of Mouse Mastocytoma P815 after Nearly Complete Rejection Is Due to Antigen-Loss Variants Rather Than Immunosuppression.* Journal of Experimental Medicine, 1983. **157**(3): p. 1040-1052.
36. Maeurer, M.J., et al., *Tumor escape from immune recognition - Lethal recurrent melanoma in a patient associated with downregulation of the peptide transporter protein TAP-1 and loss of expression of the immunodominant MART-1/Melan-A antigen.* Journal of Clinical Investigation, 1996. **98**(7): p. 1633-1641.
37. Dunn, G.P., et al., *Cancer immunoediting: from immunosurveillance to tumor escape.* Nat Immunol, 2002. **3**(11): p. 991-8.
38. Wherry, E.J. and M. Kurachi, *Molecular and cellular insights into T cell exhaustion.* Nature Reviews Immunology, 2015. **15**(8): p. 486-499.
39. Lippitz, B.E., *Cytokine patterns in patients with cancer: a systematic review.* Lancet Oncol, 2013. **14**(6): p. e218-28.
40. Motz, G.T., et al., *Tumor endothelium FasL establishes a selective immune barrier promoting tolerance in tumors.* Nat Med, 2014. **20**(6): p. 607-15.
41. Larkin, J., et al., *Combined Nivolumab and Ipilimumab or Monotherapy in Untreated Melanoma.* N Engl J Med, 2015. **373**(1): p. 23-34.
42. Robert, C., et al., *Pembrolizumab versus Ipilimumab in Advanced Melanoma.* N Engl J Med, 2015. **372**(26): p. 2521-32.

43. Antonia, S.J., et al., *Durvalumab after Chemoradiotherapy in Stage III Non-Small-Cell Lung Cancer.* N Engl J Med, 2017. **377**(20): p. 1919-1929.
44. Forde, P.M., et al., *Neoadjuvant PD-1 Blockade in Resectable Lung Cancer.* N Engl J Med, 2018.
45. Herbst, R.S., et al., *Pembrolizumab versus docetaxel for previously treated, PD-L1-positive, advanced non-small-cell lung cancer (KEYNOTE-010): a randomised controlled trial.* Lancet, 2016. **387**(10027): p. 1540-50.
46. Fehrenbacher, L., et al., *Atezolizumab versus docetaxel for patients with previously treated non-small-cell lung cancer (POPLAR): a multicentre, open-label, phase 2 randomised controlled trial.* Lancet, 2016. **387**(10030): p. 1837-46.
47. Rizvi, N.A., et al., *Activity and safety of nivolumab, an anti-PD-1 immune checkpoint inhibitor, for patients with advanced, refractory squamous non-small-cell lung cancer (CheckMate 063): a phase 2, single-arm trial.* Lancet Oncol, 2015. **16**(3): p. 257-65.
48. Le, D.T., et al., *PD-1 Blockade in Tumors with Mismatch-Repair Deficiency.* N Engl J Med, 2015. **372**(26): p. 2509-20.
49. Le, D.T., et al., *Mismatch repair deficiency predicts response of solid tumors to PD-1 blockade.* Science, 2017. **357**(6349): p. 409-413.
50. Moslehi, J.J., et al., *Increased reporting of fatal immune checkpoint inhibitor-associated myocarditis.* Lancet, 2018. **391**(10124): p. 933.
51. Postow, M.A., R. Sidlow, and M.D. Hellmann, *Immune-Related Adverse Events Associated with Immune Checkpoint Blockade.* N Engl J Med, 2018. **378**(2): p. 158-168.
52. Davis, M.M. and P.J. Bjorkman, *T-cell antigen receptor genes and T-cell recognition.* Nature, 1988. **334**(6181): p. 395-402.
53. Klein, C.A., et al., *Genetic heterogeneity of single disseminated tumour cells in minimal residual cancer.* Lancet, 2002. **360**(9334): p. 683-9.
54. Gerlinger, M., et al., *Intratumor heterogeneity and branched evolution revealed by multiregion sequencing.* N Engl J Med, 2012. **366**(10): p. 883-892.
55. Xu, X., et al., *Single-cell exome sequencing reveals single-nucleotide mutation characteristics of a kidney tumor.* Cell, 2012. **148**(5): p. 886-95.
56. Patel, A.P., et al., *Single-cell RNA-seq highlights intratumoral heterogeneity in primary glioblastoma.* Science, 2014. **344**(6190): p. 1396-401.
57. Gerlinger, M., et al., *Genomic architecture and evolution of clear cell renal cell carcinomas defined by multiregion sequencing.* Nat Genet, 2014. **46**(3): p. 225-233.
58. Rooney, M.S., et al., *Molecular and genetic properties of tumors associated with local immune cytolytic activity.* Cell, 2015. **160**(1-2): p. 48-61.
59. Brown, S.D., et al., *Neo-antigens predicted by tumor genome meta-analysis correlate with increased patient survival.* Genome Res, 2014. **24**(5): p. 743-50.
60. Snyder, A., et al., *Genetic basis for clinical response to CTLA-4 blockade in melanoma.* N Engl J Med, 2014. **371**(23): p. 2189-2199.
61. Rizvi, N.A., et al., *Cancer immunology. Mutational landscape determines sensitivity to PD-1 blockade in non-small cell lung cancer.* Science, 2015. **348**(6230): p. 124-8.
62. Yarchoan, M., A. Hopkins, and E.M. Jaffee, *Tumor Mutational Burden and Response Rate to PD-1 Inhibition.* N Engl J Med, 2017. **377**(25): p. 2500-2501.
63. Reits, E.A., et al., *Radiation modulates the peptide repertoire, enhances MHC class I expression, and induces successful antitumor immunotherapy.* J Exp Med, 2006. **203**(5): p. 1259-71.
64. Shaverdian, N., et al., *Previous radiotherapy and the clinical activity and toxicity of pembrolizumab in the treatment of non-small-cell lung cancer: a secondary analysis of the KEYNOTE-001 phase 1 trial.* Lancet Oncol, 2017. **18**(7): p. 895-903.
65. Takaoka, A. and H. Yanai, *Interferon signalling network in innate defence.* Cell Microbiol, 2006. **8**(6): p. 907-22.

66. Kotenko, S.V., et al., *IFN-lambdas mediate antiviral protection through a distinct class II cytokine receptor complex.* Nat Immunol, 2003. **4**(1): p. 69-77.
67. Sheppard, P., et al., *IL-28, IL-29 and their class II cytokine receptor IL-28R.* Nat Immunol, 2003. **4**(1): p. 63-8.
68. Platanias, L.C., *Mechanisms of type-I- and type-II-interferon-mediated signalling.* Nat Rev Immunol, 2005. **5**(5): p. 375-86.
69. Kotredes, K.P. and A.M. Gamero, *Interferons as Inducers of Apoptosis in Malignant Cells.* Journal of Interferon and Cytokine Research, 2013. **33**(4): p. 162-170.
70. Chawla-Sarkar, M., et al., *Apoptosis and interferons: Role of interferon-stimulated genes as mediators of apoptosis.* Apoptosis, 2003. **8**(3): p. 237-249.
71. Wadler, S. and E.L. Schwartz, *New Advances in Interferon Therapy of Cancer.* Oncologist, 1997. **2**(4): p. 254-267.
72. Sims, T.L., et al., *IFN-beta restricts tumor growth and sensitizes alveolar rhabdomyosarcoma to ionizing radiation.* Mol Cancer Ther, 2010. **9**(3): p. 761-71.
73. Syljuasen, R.G., et al., *Sensitization of renal carcinoma to radiation using alpha interferon (IFNA) gene transfection.* Radiat Res, 1997. **148**(5): p. 443-8.
74. Gruninger, L., et al., *Sensitizing human cervical cancer cells In vitro to ionizing radiation with interferon beta or gamma.* Radiat Res, 1999. **152**(5): p. 493-8.
75. Diamond, M.S., et al., *Type I interferon is selectively required by dendritic cells for immune rejection of tumors.* Journal of Experimental Medicine, 2011. **208**(10): p. 1989-2003.
76. Fuertes, M.B., et al., *Host type I IFN signals are required for antitumor CD8(+) T cell responses through CD8 alpha(+) dendritic cells.* Journal of Experimental Medicine, 2011. **208**(10): p. 2005-2016.
77. Le Bon, A., et al., *Direct stimulation of T cells by type I IFN enhances the CD8+ T cell response during cross-priming.* J Immunol, 2006. **176**(8): p. 4682-9.
78. Marrack, P., J. Kappler, and T. Mitchell, *Type I interferons keep activated T cells alive.* J Exp Med, 1999. **189**(3): p. 521-30.
79. Kolumam, G.A., et al., *Type I interferons act directly on CD8 T cells to allow clonal expansion and memory formation in response to viral infection.* J Exp Med, 2005. **202**(5): p. 637-50.
80. Curtsinger, J.M., et al., *Type I IFNs provide a third signal to CD8 T cells to stimulate clonal expansion and differentiation.* J Immunol, 2005. **174**(8): p. 4465-9.
81. Crouse, J., et al., *Type I interferons protect T cells against NK cell attack mediated by the activating receptor NCR1.* Immunity, 2014. **40**(6): p. 961-73.
82. Burnette, B.C., et al., *The efficacy of radiotherapy relies upon induction of type i interferon-dependent innate and adaptive immunity.* Cancer Res, 2011. **71**(7): p. 2488-96.
83. Lugade, A.A., et al., *Radiation-induced IFN-gamma production within the tumor microenvironment influences antitumor immunity.* J Immunol, 2008. **180**(5): p. 3132-9.
84. Brzostek-Racine, S., et al., *The DNA damage response induces IFN.* J Immunol, 2011. **187**(10): p. 5336-45.
85. Hartlova, A., et al., *DNA damage primes the type I interferon system via the cytosolic DNA sensor STING to promote anti-microbial innate immunity.* Immunity, 2015. **42**(2): p. 332-43.
86. Snell, L.M., T.L. McGaha, and D.G. Brooks, *Type I Interferon in Chronic Virus Infection and Cancer.* Trends Immunol, 2017. **38**(8): p. 542-557.
87. Weichselbaum, R.R., et al., *An interferon-related gene signature for DNA damage resistance is a predictive marker for chemotherapy and radiation for breast cancer.* Proceedings of the National Academy of Sciences of the United States of America, 2008. **105**(47): p. 18490-18495.
88. Boelens, M.C., et al., *Exosome transfer from stromal to breast cancer cells regulates therapy resistance pathways.* Cell, 2014. **159**(3): p. 499-513.

89. Erdal, E., et al., *A prosurvival DNA damage-induced cytoplasmic interferon response is mediated by end resection factors and is limited by Trex1.* Genes & Development, 2017. **31**(4): p. 353-369.
90. Post, A.E.M., et al., *Interferon-stimulated genes are involved in cross-resistance to radiotherapy in tamoxifen-resistant breast cancer.* Clin Cancer Res, 2018.
91. Filatenkov, A., et al., *Ablative Tumor Radiation Can Change the Tumor Immune Cell Microenvironment to Induce Durable Complete Remissions.* Clinical Cancer Research, 2015. **21**(16): p. 3727-3739.
92. Vanpouille-Box, C., et al., *DNA exonuclease Trex1 regulates radiotherapy-induced tumour immunogenicity.* Nat Commun, 2017. **8**: p. 15618.
93. Ran, F.A., et al., *Genome engineering using the CRISPR-Cas9 system.* Nature Protocols, 2013. **8**(11): p. 2281-2308.
94. Yoshimoto, Y., et al., *Radiotherapy-induced anti-tumor immunity contributes to the therapeutic efficacy of irradiation and can be augmented by CTLA-4 blockade in a mouse model.* PLoS One, 2014. **9**(3): p. e92572.
95. Gorin, J.B., et al., *Antitumor immunity induced after alpha irradiation.* Neoplasia, 2014. **16**(4): p. 319-28.
96. Ahmed, M.M., et al., *Immunobiology of radiotherapy: new paradigms.* Radiat Res, 2014. **182**(2): p. 123-5.
97. Widau, R.C., et al., *RIG-I-like receptor LGP2 protects tumor cells from ionizing radiation.* Proc Natl Acad Sci U S A, 2014. **111**(4): p. E484-91.
98. Ivashkiv, L.B. and L.T. Donlin, *Regulation of type I interferon responses.* Nat Rev Immunol, 2014. **14**(1): p. 36-49.
99. Brach, M.A., et al., *Ionizing radiation induces expression and binding activity of the nuclear factor kappa B.* J Clin Invest, 1991. **88**(2): p. 691-5.
100. Hartlova, A., et al., *DNA Damage Primes the Type I Interferon System via the Cytosolic DNA Sensor STING to Promote Anti-Microbial Innate Immunity.* Immunity, 2015. **42**(2): p. 332-343.
101. Sistigu, A., et al., *Cancer cell-autonomous contribution of type I interferon signaling to the efficacy of chemotherapy.* Nat Med, 2014. **20**(11): p. 1301-9.
102. Deng, L., et al., *STING-Dependent Cytosolic DNA Sensing Promotes Radiation-Induced Type I Interferon-Dependent Antitumor Immunity in Immunogenic Tumors.* Immunity, 2014. **41**(5): p. 843-52.
103. Woo, S.R., et al., *STING-dependent cytosolic DNA sensing mediates innate immune recognition of immunogenic tumors.* Immunity, 2014. **41**(5): p. 830-42.
104. Honda, K., A. Takaoka, and T. Taniguchi, *Type I interferon [corrected] gene induction by the interferon regulatory factor family of transcription factors.* Immunity, 2006. **25**(3): p. 349-60.
105. Tanaka, N., et al., *Cooperation of the tumour suppressors IRF-1 and p53 in response to DNA damage.* Nature, 1996. **382**(6594): p. 816-8.
106. Pamment, J., et al., *Regulation of the IRF-1 tumour modifier during the response to genotoxic stress involves an ATM-dependent signalling pathway.* Oncogene, 2002. **21**(51): p. 7776-85.
107. Abe, T. and G.N. Barber, *Cytosolic-DNA-mediated, STING-dependent proinflammatory gene induction necessitates canonical NF-kappaB activation through TBK1.* J Virol, 2014. **88**(10): p. 5328-41.
108. Yang, C.H., et al., *IFNalpha/beta promotes cell survival by activating NF-kappa B.* Proc Natl Acad Sci U S A, 2000. **97**(25): p. 13631-6.
109. Mackenzie, K.J., et al., *cGAS surveillance of micronuclei links genome instability to innate immunity.* Nature, 2017. **548**(7668): p. 461-465.
110. Harding, S.M., et al., *Mitotic progression following DNA damage enables pattern recognition within micronuclei.* Nature, 2017. **548**(7668): p. 466-470.
111. Bartsch, K., et al., *Absence of RNase H2 triggers generation of immunogenic micronuclei removed by autophagy.* Hum Mol Genet, 2017. **26**(20): p. 3960-3972.

112. Ishikawa, H. and G.N. Barber, *STING is an endoplasmic reticulum adaptor that facilitates innate immune signalling.* Nature, 2008. **455**(7213): p. 674-U74.
113. Ahn, J., et al., *STING manifests self DNA-dependent inflammatory disease.* Proc Natl Acad Sci U S A, 2012. **109**(47): p. 19386-91.
114. Xia, T., H. Konno, and G.N. Barber, *Recurrent Loss of STING Signaling in Melanoma Correlates with Susceptibility to Viral Oncolysis.* Cancer Res, 2016. **76**(22): p. 6747-6759.
115. Fang, R., et al., *NEMO-IKK beta Are Essential for IRF3 and NF-kappa B Activation in the cGAS-STING Pathway.* Journal of Immunology, 2017. **199**(9): p. 3222-3233.
116. Yie, J.M., K. Senger, and D. Thanos, *Mechanism by which the IFN-beta enhanceosome activates transcription.* Proceedings of the National Academy of Sciences of the United States of America, 1999. **96**(23): p. 13108-13113.
117. Panne, D., T. Maniatis, and S.C. Harrison, *An atomic model of the interferon-beta enhanceosome.* Cell, 2007. **129**(6): p. 1111-1123.
118. Shen, Y.J., et al., *Genome-derived cytosolic DNA mediates type I interferon-dependent rejection of B cell lymphoma cells.* Cell Rep, 2015. **11**(3): p. 460-73.
119. Parkes, E.E., et al., *Activation of STING-Dependent Innate Immune Signaling By S-Phase-Specific DNA Damage in Breast Cancer.* J Natl Cancer Inst, 2017. **109**(1).
120. West, A.P., et al., *Mitochondrial DNA stress primes the antiviral innate immune response.* Nature, 2015. **520**(7548): p. 553-7.
121. Kitai, Y., et al., *DNA-Containing Exosomes Derived from Cancer Cells Treated with Topotecan Activate a STING-Dependent Pathway and Reinforce Antitumor Immunity.* J Immunol, 2017. **198**(4): p. 1649-1659.
122. Cai, X., Y.H. Chiu, and Z.J. Chen, *The cGAS-cGAMP-STING pathway of cytosolic DNA sensing and signaling.* Mol Cell, 2014. **54**(2): p. 289-96.
123. Unterholzner, L., et al., *IFI16 is an innate immune sensor for intracellular DNA.* Nat Immunol, 2010. **11**(11): p. 997-1004.
124. Zhang, Z., et al., *The helicase DDX41 senses intracellular DNA mediated by the adaptor STING in dendritic cells.* Nat Immunol, 2011. **12**(10): p. 959-65.
125. Ferguson, B.J., et al., *DNA-PK is a DNA sensor for IRF-3-dependent innate immunity.* Elife, 2012. **1**: p. e00047.
126. Sui, H., et al., *STING is an essential mediator of the Ku70-mediated production of IFN-lambda1 in response to exogenous DNA.* Sci Signal, 2017. **10**(488).
127. Xia, T., et al., *Deregulation of STING Signaling in Colorectal Carcinoma Constrains DNA Damage Responses and Correlates With Tumorigenesis.* Cell Rep, 2016. **14**(2): p. 282-97.
128. Curtin, N.J., *DNA repair dysregulation from cancer driver to therapeutic target.* Nat Rev Cancer, 2012. **12**(12): p. 801-17.
129. Mazur, D.J. and F.W. Perrino, *Identification and expression of the TREX1 and TREX2 cDNA sequences encoding mammalian 3 '-> 5 ' exonucleases.* Journal of Biological Chemistry, 1999. **274**(28): p. 19655-19660.
130. Crow, Y.J., et al., *Mutations in the gene encoding the 3 '-5 ' DNA exonuclease TREX1 cause Aicardi-Goutieres syndrome at the AGS1 locus.* Nature Genetics, 2006. **38**(8): p. 917-920.
131. Grieves, J.L., et al., *Exonuclease TREX1 degrades double-stranded DNA to prevent spontaneous lupus-like inflammatory disease.* Proc Natl Acad Sci U S A, 2015. **112**(16): p. 5117-5122.
132. Gehrke, N., et al., *Oxidative Damage of DNA Confers Resistance to Cytosolic Nuclease TREX1 Degradation and Potentiates STING-Dependent Immune Sensing.* Immunity, 2013. **39**(3): p. 482-495.
133. Osterlund, P.I., et al., *IFN regulatory factor family members differentially regulate the expression of type III IFN (IFN-lambda) genes.* J Immunol, 2007. **179**(6): p. 3434-42.
134. Odendall, C., et al., *Diverse intracellular pathogens activate type III interferon expression from peroxisomes.* Nat Immunol, 2014. **15**(8): p. 717-26.

135. Siegel, R., J. Eskdale, and G. Gallagher, *Regulation of IFN-lambda1 promoter activity (IFN-lambda1/IL-29) in human airway epithelial cells.* J Immunol, 2011. **187**(11): p. 5636-44.
136. Ueki, I.F., et al., *Respiratory virus-induced EGFR activation suppresses IRF1-dependent interferon lambda and antiviral defense in airway epithelium.* J Exp Med, 2013. **210**(10): p. 1929-36.
137. Dumoutier, L., et al., *Role of the interleukin (IL)-28 receptor tyrosine residues for antiviral and antiproliferative activity of IL-29/interferon-lambda 1: similarities with type I interferon signaling.* J Biol Chem, 2004. **279**(31): p. 32269-74.
138. Zhou, Z., et al., *Type III interferon (IFN) induces a type I IFN-like response in a restricted subset of cells through signaling pathways involving both the Jak-STAT pathway and the mitogen-activated protein kinases.* J Virol, 2007. **81**(14): p. 7749-58.
139. Sommereyns, C., et al., *IFN-lambda (IFN-lambda) is expressed in a tissue-dependent fashion and primarily acts on epithelial cells in vivo.* PLoS Pathog, 2008. **4**(3): p. e1000017.
140. Pulverer, J.E., et al., *Temporal and spatial resolution of type I and III interferon responses in vivo.* J Virol, 2010. **84**(17): p. 8626-38.
141. da Silva, A.J., et al., *Comparison of gene expression patterns induced by treatment of human umbilical vein endothelial cells with IFN-alpha 2b vs. IFN-beta 1a: understanding the functional relationship between distinct type I interferons that act through a common receptor.* J Interferon Cytokine Res, 2002. **22**(2): p. 173-88.
142. Jost, E., et al., *Response of pancreatic cancer cells treated with interferon-alpha or beta and co-exposed to ionising radiation.* Int J Radiat Biol, 2010. **86**(9): p. 732-41.
143. Ng, C.T., et al., *Blockade of interferon Beta, but not interferon alpha, signaling controls persistent viral infection.* Cell Host Microbe, 2015. **17**(5): p. 653-61.
144. Westcott, M.M., et al., *Interferon Beta and Interferon Alpha 2a Differentially Protect Head and Neck Cancer Cells from Vesicular Stomatitis Virus-Induced Oncolysis.* J Virol, 2015. **89**(15): p. 7944-54.
145. Jaks, E., et al., *Differential receptor subunit affinities of type I interferons govern differential signal activation.* J Mol Biol, 2007. **366**(2): p. 525-39.
146. Piehler, J., et al., *Structural and dynamic determinants of type I interferon receptor assembly and their functional interpretation.* Immunol Rev, 2012. **250**(1): p. 317-34.
147. Topalian, S.L., et al., *Survival, durable tumor remission, and long-term safety in patients with advanced melanoma receiving nivolumab.* J Clin Oncol, 2014. **32**(10): p. 1020-30.
148. Schadendorf, D., et al., *Pooled Analysis of Long-Term Survival Data From Phase II and Phase III Trials of Ipilimumab in Unresectable or Metastatic Melanoma.* J Clin Oncol, 2015. **33**(17): p. 1889-94.
149. Gettinger, S.N., et al., *Overall Survival and Long-Term Safety of Nivolumab (Anti-Programmed Death 1 Antibody, BMS-936558, ONO-4538) in Patients With Previously Treated Advanced Non-Small-Cell Lung Cancer.* J Clin Oncol, 2015. **33**(18): p. 2004-12.
150. Reck, M., et al., *Pembrolizumab versus Chemotherapy for PD-L1-Positive Non-Small-Cell Lung Cancer.* N Engl J Med, 2016. **375**(19): p. 1823-1833.
151. Van Allen, E.M., et al., *Genomic correlates of response to CTLA-4 blockade in metastatic melanoma.* Science, 2015. **350**(6257): p. 207-211.
152. Gubin, M.M., et al., *Checkpoint blockade cancer immunotherapy targets tumour-specific mutant antigens.* Nature, 2014. **515**(7528): p. 577-81.
153. Lugade, A.A., et al., *Local radiation therapy of B16 melanoma tumors increases the generation of tumor antigen-specific effector cells that traffic to the tumor.* Journal of Immunology, 2005. **174**(12): p. 7516-7523.
154. Garnett, C.T., et al., *Sublethal irradiation of human tumor cells modulates phenotype resulting in enhanced killing by cytotoxic T lymphocytes.* Cancer Res, 2004. **64**(21): p. 7985-94.

155. Dighe, A.S., et al., *Enhanced in vivo growth and resistance to rejection of tumor cells expressing dominant negative IFN gamma receptors.* Immunity, 1994. **1**(6): p. 447-56.
156. Kaplan, D.H., et al., *Demonstration of an interferon gamma-dependent tumor surveillance system in immunocompetent mice.* Proc Natl Acad Sci U S A, 1998. **95**(13): p. 7556-61.
157. Ogawa, M., et al., *Multiple roles of interferon-gamma in the mediation of interleukin 12-induced tumor regression.* Cancer Res, 1998. **58**(11): p. 2426-32.
158. Nakajima, C., et al., *A role of interferon-gamma (IFN-gamma) in tumor immunity: T cells with the capacity to reject tumor cells are generated but fail to migrate to tumor sites in IFN-gamma-deficient mice.* Cancer Res, 2001. **61**(8): p. 3399-405.
159. Dunn, G.P., et al., *A critical function for type I interferons in cancer immunoediting.* Nat Immunol, 2005. **6**(7): p. 722-9.
160. Critchley-Thorne, R.J., et al., *Impaired interferon signaling is a common immune defect in human cancer.* Proceedings of the National Academy of Sciences of the United States of America, 2009. **106**(22): p. 9010-9015.
161. Demaria, O., et al., *STING activation of tumor endothelial cells initiates spontaneous and therapeutic antitumor immunity.* Proc Natl Acad Sci U S A, 2015. **112**(50): p. 15408-13.
162. Swann, J.B., et al., *Type I IFN contributes to NK cell homeostasis, activation, and antitumor function.* J Immunol, 2007. **178**(12): p. 7540-9.
163. Mizutani, T., et al., *Conditional IFNAR1 ablation reveals distinct requirements of Type I IFN signaling for NK cell maturation and tumor surveillance.* Oncoimmunology, 2012. **1**(7): p. 1027-1037.
164. Bidwell, B.N., et al., *Silencing of Irf7 pathways in breast cancer cells promotes bone metastasis through immune escape.* Nat Med, 2012. **18**(8): p. 1224-31.
165. Teichmann, J.V., et al., *Immunosuppressive effects of recombinant interferon-alpha during long-term treatment of cancer patients.* Cancer, 1989. **63**(10): p. 1990-3.
166. Beatty, G.L. and Y. Paterson, *IFN-gamma can promote tumor evasion of the immune system in vivo by down-regulating cellular levels of an endogenous tumor antigen.* Journal of Immunology, 2000. **165**(10): p. 5502-5508.
167. Duarte, C.W., et al., *Expression Signature of IFN/STAT1 Signaling Genes Predicts Poor Survival Outcome in Glioblastoma Multiforme in a Subtype-Specific Manner.* Plos One, 2012. **7**(1).
168. Ranoa, D.R., et al., *Cancer therapies activate RIG-I-like receptor pathway through endogenous non-coding RNAs.* Oncotarget, 2016. **7**(18): p. 26496-515.
169. Topalian, S.L., C.G. Drake, and D.M. Pardoll, *Immune checkpoint blockade: a common denominator approach to cancer therapy.* Cancer Cell, 2015. **27**(4): p. 450-61.
170. Morvan, M.G. and L.L. Lanier, *NK cells and cancer: you can teach innate cells new tricks.* Nature Reviews Cancer, 2016. **16**(1): p. 7-19.
171. Zitvogel, L., et al., *Type I interferons in anticancer immunity.* Nat Rev Immunol, 2015. **15**(7): p. 405-14.
172. Parker, B.S., J. Rautela, and P.J. Hertzog, *Antitumour actions of interferons: implications for cancer therapy.* Nat Rev Cancer, 2016. **16**(3): p. 131-44.
173. Chen, H.H., et al., *Activation of STAT6 by STING Is Critical for Antiviral Innate Immunity.* Cell, 2011. **147**(2): p. 436-446.
174. Noyce, R.S., S.E. Collins, and K.L. Mossman, *Identification of a novel pathway essential for the immediate-early, interferon-independent antiviral response to enveloped Virions.* Journal of Virology, 2006. **80**(1): p. 226-235.
175. Bakhoum, S.F., et al., *Chromosomal instability drives metastasis through a cytosolic DNA response.* Nature, 2018. **553**(7689): p. 467-472.
176. Katlinski, K.V., et al., *Inactivation of Interferon Receptor Promotes the Establishment of Immune Privileged Tumor Microenvironment.* Cancer Cell, 2017. **31**(2): p. 194-207.
177. Benci, J.L., et al., *Tumor Interferon Signaling Regulates a Multigenic Resistance Program to Immune Checkpoint Blockade.* Cell, 2016. **167**(6): p. 1540-1554 e12.

178. Yang, X., et al., *Targeting the tumor microenvironment with interferon-beta bridges innate and adaptive immune responses.* Cancer Cell, 2014. **25**(1): p. 37-48.
179. Mendelsohn, C.L., E. Wimmer, and V.R. Racaniello, *Cellular receptor for poliovirus: molecular cloning, nucleotide sequence, and expression of a new member of the immunoglobulin superfamily.* Cell, 1989. **56**(5): p. 855-65.
180. Anderson, A.C., N. Joller, and V.K. Kuchroo, *Lag-3, Tim-3, and TIGIT: Co-inhibitory Receptors with Specialized Functions in Immune Regulation.* Immunity, 2016. **44**(5): p. 989-1004.
181. Yu, X., et al., *The surface protein TIGIT suppresses T cell activation by promoting the generation of mature immunoregulatory dendritic cells.* Nat Immunol, 2009. **10**(1): p. 48-57.
182. Joller, N., et al., *Cutting Edge: TIGIT Has T Cell-Intrinsic Inhibitory Functions.* Journal of Immunology, 2011. **186**(3): p. 1338-1342.
183. Stanietsky, N., et al., *The interaction of TIGIT with PVR and PVRL2 inhibits human NK cell cytotoxicity.* Proc Natl Acad Sci U S A, 2009. **106**(42): p. 17858-63.
184. He, W., et al., *CD155T/TIGIT Signaling Regulates CD8(+) T-cell Metabolism and Promotes Tumor Progression in Human Gastric Cancer.* Cancer Res, 2017. **77**(22): p. 6375-6388.
185. Chauvin, J.M., et al., *TIGIT and PD-1 impair tumor antigen-specific CD8(+) T cells in melanoma patients.* J Clin Invest, 2015. **125**(5): p. 2046-58.
186. Johnston, R.J., et al., *The immunoreceptor TIGIT regulates antitumor and antiviral CD8(+) T cell effector function.* Cancer Cell, 2014. **26**(6): p. 923-937.
187. Inozume, T., et al., *Melanoma Cells Control Antimelanoma CTL Responses via Interaction between TIGIT and CD155 in the Effector Phase.* J Invest Dermatol, 2016. **136**(1): p. 255-63.
188. Masson, D., et al., *Overexpression of the CD155 gene in human colorectal carcinoma.* Gut, 2001. **49**(2): p. 236-40.
189. Nishiwada, S., et al., *Clinical significance of CD155 expression in human pancreatic cancer.* Anticancer Res, 2015. **35**(4): p. 2287-97.
190. Atta, M.S., et al., *Enhanced expression of MHC class I molecules on cultured human thyroid follicular cells infected with reovirus through induction of type 1 interferons.* Clin Exp Immunol, 1995. **101**(1): p. 121-6.
191. Keskinen, P., et al., *Regulation of HLA class I and II expression by interferons and influenza A virus in human peripheral blood mononuclear cells.* Immunology, 1997. **91**(3): p. 421-9.
192. Ljunggren, G. and D.J. Anderson, *Cytokine induced modulation of MHC class I and class II molecules on human cervical epithelial cells.* Journal of Reproductive Immunology, 1998. **38**(2): p. 123-138.
193. Martini, M., et al., *IFN-gamma-mediated upmodulation of MHC class I expression activates tumor-specific immune response in a mouse model of prostate cancer.* Vaccine, 2010. **28**(20): p. 3548-57.
194. Wan, S., et al., *Chemotherapeutics and radiation stimulate MHC class I expression through elevated interferon-beta signaling in breast cancer cells.* PLoS One, 2012. **7**(3): p. e32542.
195. Noman, M.Z., et al., *Blocking hypoxia-induced autophagy in tumors restores cytotoxic T-cell activity and promotes regression.* Cancer Res, 2011. **71**(18): p. 5976-86.
196. Akalay, I., et al., *Epithelial-to-mesenchymal transition and autophagy induction in breast carcinoma promote escape from T-cell-mediated lysis.* Cancer Res, 2013. **73**(8): p. 2418-27.
197. Baginska, J., et al., *Granzyme B degradation by autophagy decreases tumor cell susceptibility to natural killer-mediated lysis under hypoxia.* Proc Natl Acad Sci U S A, 2013. **110**(43): p. 17450-5.
198. Messai, Y., et al., *ITPR1 protects renal cancer cells against natural killer cells by inducing autophagy.* Cancer Res, 2014. **74**(23): p. 6820-32.
199. Schmeisser, H., et al., *Type I interferons induce autophagy in certain human cancer cell lines.* Autophagy, 2013. **9**(5): p. 683-96.
200. Ambjorn, M., et al., *IFNB1/interferon-beta-induced autophagy in MCF-7 breast cancer cells counteracts its proapoptotic function.* Autophagy, 2013. **9**(3): p. 287-302.

201. Medema, J.P., et al., *Blockade of the granzyme B/perforin pathway through overexpression of the serine protease inhibitor PI-9/SPI-6 constitutes a mechanism for immune escape by tumors.* Proceedings of the National Academy of Sciences of the United States of America, 2001. **98**(20): p. 11515-11520.
202. Bots, M., et al., *SPI-CI and SPI-6 cooperate in the protection from effector cell-mediated cytotoxicity.* Blood, 2005. **105**(3): p. 1153-61.
203. Guillerey, C., N.D. Huntington, and M.J. Smyth, *Targeting natural killer cells in cancer immunotherapy.* Nat Immunol, 2016. **17**(9): p. 1025-36.
204. Chan, C.J., et al., *DNAM-1/CD155 interactions promote cytokine and NK cell-mediated suppression of poorly immunogenic melanoma metastases.* J Immunol, 2010. **184**(2): p. 902-11.
205. El-Sherbiny, Y.M., et al., *The requirement for DNAM-1, NKG2D, and NKp46 in the natural killer cell-mediated killing of myeloma cells.* Cancer Res, 2007. **67**(18): p. 8444-9.
206. Bottino, C., et al., *Identification of PVR (CD155) and nectin-2 (CD112) as cell surface ligands for the human DNAM-1 (CD226) activating molecule.* Journal of Experimental Medicine, 2003. **198**(4): p. 557-567.
207. Tahara-Hanaoka, S., et al., *Tumor rejection by the poliovirus receptor family ligands of the DNAM-1 (CD226) receptor.* Blood, 2006. **107**(4): p. 1491-6.
208. Castriconi, R., et al., *Natural killer cell-mediated killing of freshly isolated neuroblastoma cells: critical role of DNAX accessory molecule-1-poliovirus receptor interaction.* Cancer Res, 2004. **64**(24): p. 9180-4.
209. Karre, K., et al., *Selective rejection of H-2-deficient lymphoma variants suggests alternative immune defence strategy.* Nature, 1986. **319**(6055): p. 675-8.
210. Ljunggren, H.G. and K. Karre, *In search of the 'missing self': MHC molecules and NK cell recognition.* Immunol Today, 1990. **11**(7): p. 237-44.
211. Kim, S., et al., *Licensing of natural killer cells by host major histocompatibility complex class I molecules.* Nature, 2005. **436**(7051): p. 709-713.
212. Orr, M.T. and L.L. Lanier, *Natural killer cell education and tolerance.* Cell, 2010. **142**(6): p. 847-56.
213. Lasfar, A., et al., *Characterization of the mouse IFN-lambda ligand-receptor system: IFN-lambdas exhibit antitumor activity against B16 melanoma.* Cancer Res, 2006. **66**(8): p. 4468-77.
214. Tezuka, Y., et al., *Potential anti-tumor effect of IFN-lambda 2 (IL-28A) against human lung cancer cells.* Lung Cancer, 2012. **78**(3): p. 185-192.
215. Zitzmann, K., et al., *Novel interferon-lambdas induce antiproliferative effects in neuroendocrine tumor cells.* Biochem Biophys Res Commun, 2006. **344**(4): p. 1334-41.
216. Hui, X.W., et al., *Antitumor activities of recombinant human interferon (IFN)-lambda 1 in vitro and in xenograft models in vivo for colon cancer.* Cancer Letters, 2011. **311**(2): p. 141-151.
217. Sato, A., et al., *Antitumor activity of IFN-lambda in murine tumor models.* J Immunol, 2006. **176**(12): p. 7686-94.
218. Li, Q., et al., *Interferon-lambda induces G1 phase arrest or apoptosis in oesophageal carcinoma cells and produces anti-tumour effects in combination with anti-cancer agents.* Eur J Cancer, 2010. **46**(1): p. 180-90.
219. Numasaki, M., et al., *IL-28 elicits antitumor responses against murine fibrosarcoma.* J Immunol, 2007. **178**(8): p. 5086-98.
220. Abushahba, W., et al., *Antitumor activity of type I and type III interferons in BNL hepatoma model.* Cancer Immunol Immunother, 2010. **59**(7): p. 1059-71.

Appendix I Published paper

International Journal of Radiation Oncology biology • physics

www.redjournal.org

Biology Contribution

STING-Dependent Interferon-λ1 Induction in HT29 Cells, a Human Colorectal Cancer Cell Line, After Gamma-Radiation

Jianzhou Chen, MD, MS,[*,†,‡] Bostjan Markelc, PhD,[*,†] Jakob Kaeppler, MS,[*,†] Vivian M.L. Ogundipe, MS,[*,†,§] Yunhong Cao, PhD,[*,†] W. Gillies McKenna, MD, PhD,[*,†] and Ruth J. Muschel, MD, PhD[*,†]

**CRUK/MRC Oxford Institute for Radiation Oncology, and [†]Department of Oncology, University of Oxford, Oxford, United Kingdom; [‡]Department of Radiation Oncology, Cancer Hospital of Shantou University Medical College, Shantou, China; and [§]Swammerdam Institute for Life Sciences, University of Amsterdam, Amsterdam, The Netherlands*

Received Nov 13, 2017, and in revised form Jan 17, 2018. Accepted for publication Jan 23, 2018.

Summary

Induction of type I and II interferons (IFNs) in irradiated tumors has been extensively documented, whereas the role of type III IFNs in tumors remains unknown. We found that gamma-rays directly induced IFNL1 in human cancer cells. In HT29 cells this induction occurs via the STING−TBK1−IRF1 signaling axis and, to a lesser extent, NF-κB signaling. These findings add another layer of

Purpose: To investigate the induction of type III interferons (IFNs) in human cancer cells by gamma-rays.

Methods and Materials: Type III IFN expression in human cancer cell lines after gamma-ray irradiation in vitro was assessed by reverse transcription−quantitative polymerase chain reaction and enzyme-linked immunosorbent assay. Signaling pathways mediating type III IFN induction were examined by a variety of means, including immunoblotting, flow cytometry, confocal imaging, and reverse transcription−quantitative polymerase chain reaction. Key mediators in these pathways were further explored and validated using gene CRISPR knockout or short hairpin RNA knockdown.

Results: Exposure to gamma-rays directly induced type III IFNs (mainly IFNL1) in human cancer cell lines in dose- and time-dependent fashions. The induction of IFNL1 was primarily mediated by the cytosolic DNA sensors−STING−TBK1−IRF1 signaling axis, with a lesser contribution from the nuclear factor kappa b signaling in HT29 cells. In addition, type III IFN signaling through its receptors serves as a positive feedback loop, further enhancing IFN expression via up-regulation of the kinases in the STING−TBK1 signaling axis.

Reprint requests to: Ruth J. Muschel, MD, PhD, University of Oxford, CRUK/MRC Oxford Institute for Radiation Oncology, Department of Oncology, Old Rd Campus Research Building, Roosevelt Drive, Oxford OX3 7DQ, United Kingdom. Tel: (+44) (0) 1865-225847; E-mail: ruth.muschel@oncology.ox.ac.uk

This study was supported by Cancer Research UK (CRUK; grant number C5255/A15935). J.C. was supported by a MSc Scholarship from Li Ka Shing Foundation Global health Programme at the University of Oxford, a CRUK clinical research training fellowship and a Clarendon Scholarship from University of Oxford. B.M. was supported by a Marie Curie fellowship (No 625631) of the European Unions Seventh Framework Programme (FP7/2007-2013).

Conflict of interest: none.

Supplementary material for this article can be found at www.redjournal.org.

Int J Radiation Oncol Biol Phys, Vol. 101, No. 1, pp. 97−106, 2018
0360-3016/$ - see front matter © 2018 Elsevier Inc. All rights reserved.
https://doi.org/10.1016/j.ijrobp.2018.01.091

complexity to the understanding of irradiation-induced antitumor immunity and may provide novel insights into IFN-based cancer treatment.

Conclusions: Our results suggest that IFNL1 can be up-regulated in human cancer cell lines after gamma-ray treatment. In HT29 cells this induction occurs via the STING pathway, adding another layer of complexity to the understanding of radiation-induced antitumor immunity, and may provide novel insights into IFN-based cancer treatment. © 2018 Elsevier Inc. All rights reserved.

Introduction

It has been increasingly acknowledged that host immunity plays an important role in the therapeutic outcome of radiation therapy (1-5). Irradiated tumor cells release a variety of immunomodulatory factors, including damage associated molecular patterns and cytokines, resulting in an inflammatory microenvironment with the potential to facilitate tumor-specific immunity.

One of the most important mediators in the antitumor immune response is interferons (IFNs), a group of cytokines with the hallmark of antiviral function. Interferons have multiple antitumor effects and have been used to treat a number of malignancies for decades (6). New concepts have emerged suggesting that IFN signaling pathways are involved in enhancing the therapeutic efficacy of radiation treatment through immuno-stimulation. For example, localized radiation treatment not only induced lethal damage in cancer cells but also promoted intratumoral production of type II IFN, IFN-γ, which led to enhanced T-cell infiltration and tumor target recognition (7). Another study found that the efficacy of ablative radiation treatment relied on type I IFN-dependent innate and adaptive immune responses (8). Irradiation of tumors deficient in STING, a component of the pathway mediating type I IFN induction, results in reduced antitumor immunity in the context of immune checkpoint blockade (9). These studies suggest that IFNs could help improve therapeutic efficacy by enhancing tumor-specific immune response.

There are 3 types of IFNs, defined by different receptors, all of which consist of a pair of heterologous subunits. Type I IFNs bind IFN alpha receptor subunit 1&2 and are subdivided into IFN-α (IFNA), -β (IFNB), -ω, -ε, -κ, -δ, -τ, and -ξ. Of them, only IFNA and IFNB are ubiquitously expressed. There is only 1 type II IFN, IFN-γ, which binds to a different receptor complex, IFNGR 1&2. Interferon-γ is expressed by activated immune cells. Type III IFN was first discovered in 2003, and 4 homologous proteins have since been found: IFN-λ 1-4 (IFNL1-4) (10-12). Type III IFNs utilize a receptor complex of IFNLR1, also called interleukin (IL)-28R, together with IL-10R2, a receptor subunit shared with IL-10, IL-22, and IL-26. All cell types are capable of expressing type III IFN.

Induction of type I and II IFNs in irradiated tumors has been extensively documented, whereas the role of type III IFNs in tumors remains unknown (8, 13-15). In this study we found that gamma-rays directly induced type III IFNs in human cancer cell lines in a dose- and time-dependent manner. Induction of IFNL1 in cancer cells was mediated by the cytosolic DNA sensor−STING−TBK1−IRF1 signaling axis and, to a lesser extent, the nuclear factor kappa b (NF-κB) pathway in HT29 cells. In addition, type III IFN signaling through its receptors serves as a positive feedback loop, enhancing IFNL1 expression via up-regulation of the kinases in the STING−TBK1 signaling axis.

Methods and Materials

Cells

Human colorectal cancer cell lines HT29, LOVO, and HCT116 and human cervical cancer cell line HeLa were obtained from American Type Culture Collection. OE21 and OE33 (both human esophageal cancer cell line) were gifts from Dr Ester Hammond (University of Oxford). HT29 cells were grown in Roswell Park Memorial Institute 1640 medium. LOVO, HCT116, OE21, and OE33 were cultured in Dulbecco's Modified Eagle Medium. HeLa cells were maintained in Eagle's Minimum Essential Medium. All mediums were supplemented with 10% (vol/vol) fetal bovine serum and 1% penicillin−streptomycin (all from Sigma-Aldrich, St. Louis, MO). Cells were used with passage number <8. Mycoplasma was routinely tested.

Reagents

ML120B (Bio-techne, Minneapolis, MN) was dissolved in dimethyl sulfoxide at 20 mM and used at 20 μM. Human IFNL1 (PBL, Piscataway, NJ) was used at 1000 U/mL. Human tumor necrosis factor alphas (TNFα, from Bio-techne) were used at 40 ng/mL. Lipofectamine 3000 (Thermo Fisher, Waltham, MA) was used to deliver the following reagents to cells: DNA salt from herring testes (from Sigma-Aldrich), 2′,3′-cyclic guanosine monophosphate-adenosine monophosphate (cGAMP), VACV-70, and Poly I:C HMW (InvivoGen, San Diego, CA). Antibodies used in this study are listed in Table E1 (available online at www.redjournal.org).

Radiation treatment

Cells were seeded in 6-well plates with a density of 0.5 to 5×10^4 cells/cm^2 and maintained at 37°C with 5% CO_2. Twenty-four hours later, cells were treated with gamma-rays at indicated time points. Gamma-ray treatment was delivered using a ^{137}Cs-laboratory irradiator (IBL 637; CIS

bio International, Saclay, France), which produces gamma-rays (0.662 MeV) at a dose rate of 0.81 Gy/min. Fractionated radiation was delivered at 1 fraction per day with a time interval of 24 hours.

Reverse transcription–quantitative polymerase chain reaction

Ribonucleic acid (RNA) was extracted from cells using Trizol (Invitrogen, Carlsbad, CA). Their quality and quantity were measured using a NanoDrop 2000 microvolume spectrophotometer (Thermo Fisher). All RNAs were treated with DNase (Turbo DNA-free Kit, Thermo Fisher) before the complementary DNA (cDNA) synthesis. Approximately 2 μg of RNA for each sample was transcribed into cDNA using the High-Capacity cDNA Reverse Transcription Kit (Thermo Fisher).

Quantitative polymerase chain reaction (qPCR) was performed using SYBR green (Promega, Madison, WI) with specific primers (listed in Table E2; available online at www.redjournal.org) or hydrolysis probes (Taqman primers/probes from Thermo Fisher), including IFIT1, IFI44, and beta-actin (B-Actin). B-Actin was used as a reference gene (Fig. E1; available online at www.redjournal.org). Reactions were run on the Mx3005p QPCR System (Agilent Technologies, Santa Clara, CA) in a final volume of 25 μL, with cDNA equivalent of 10 ng RNA and 400 nM primers. The cycling conditions were as follows: (*1*) 50°C 2 minutes, 1 cycle; (*2*) 95°C 2 minutes, 1 cycle; (*3*) 95°C 15 seconds → 58°C 30 seconds → 72°C 30 seconds, 40 cycles; (*4*) 72°C 10 minutes, 1 cycle.

After the amplication, the threshold cycle (C_t) values for target genes and B-Actin were recorded. The difference of C_t (ΔC_t) between the target gene and B-Actin was calculated. The relative gene expression level of the target gene was equal to $2^{(-\Delta Ct)}$. The difference of ΔCt (ΔΔCt) between the experimental sample and the control sample was calculated as well. The messenger RNA (mRNA) fold induction of the target gene in the experimental samples was then equal to $2^{(-\Delta\Delta Ct)}$. Additional data for quality control of reverse transcription–qPCR (RT-qPCR) can be found in the Supplementary Methods (available online at www.redjournal.org).

Immunoblotting

Immunoblotting was performed as described in the Supplementary Methods (available online at www.redjournal.org).

NF-κB reporter assay

Tumor cells were transfected with Cignal lenti nuclear factor kappa B (NF-κB) hMGFP reporter (10 transducing units per cell) using SureENTRY (Qiagen, Hilden, Germany, final concentration 8 μg/mL) and selected with puromycin (1.5 μg/mL) for 10 to 14 days. Human TNFα was used as a positive control to activate the NF-κB pathway in cells. NF-κB activity of the transfected cells was monitored and quantified using an Attune flow cytometer (Thermo Fisher). The flow cytometry data were analyzed using FlowJo software (FlowJo, Ashland, OR). NF-κB activity was calculated as the percentage of hMGFP-positive cells on a histogram plot of Fluorescein Isothiocyanate filter. Fold change of NF-κB activity was calculated as the ratio of NF-κB activity between experimental sample and control sample.

Gene knockdown using short hairpin RNA

Gene knockdown using short hairpin RNA (shRNA) is described in the Supplementary Methods (available online at www.redjournal.org).

Generation of knockout cell lines using CRISPR

Gene knockout cell lines were generated using the CRISPR technique. Nickase Cas9 plasmids, including pSpCas9n (BB)-2A-GFP (PX461) and pSpCas9n (BB)-2A-Puro (PX462), were obtained from Addgene (Cambridge, MA, plasmids 48140 and 62987). A pair of guide RNA primers for each gene was designed using Feng Zhang laboratory's CRISPR Design (http://crispr.mit.edu/) and cloned into plasmid PX461 and PX462, respectively (Table E3; available online at www.redjournal.org). Plasmid cloning was verified by sequencing. Cells were then transfected with PX461 and PX462 plasmids simultaneously using Lipofectamine 3000. After transfection, cells were selected with puromycin for 24 to 48 hours and processed into single-cell clones by serial dilution. Cells with biallelic gene knockout were selected and validated using immunoblotting or functional assays.

Fluorescent staining and confocal imaging

Fluorescent staining and imaging were performed as described in the Supplementary Methods (available online at www.redjournal.org).

Enzyme-linked immunosorbent assay

The IFNL1 protein level in cell culture supernatants was measured using the human IL-29 ELISA Ready-SET-Go kit (Thermo Fisher).

Results

Induction of type III IFNs in human cancer cell lines after exposure to gamma-rays

We asked which types of IFNs were induced after irradiation of human colorectal cancer HT29 cells in tissue

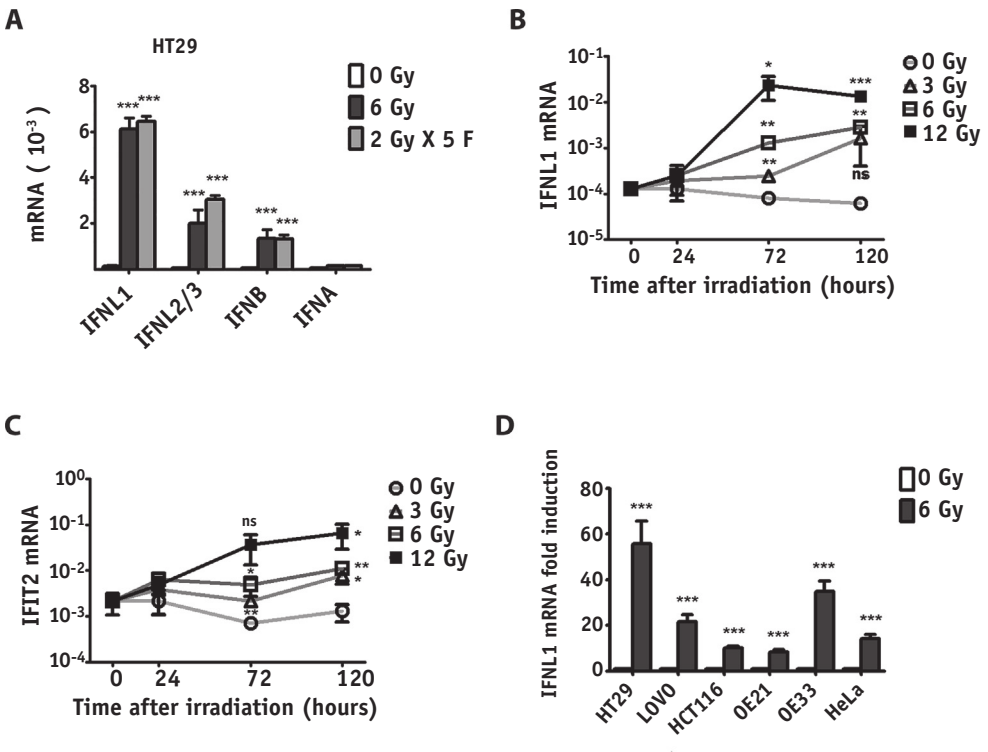


Fig. 1. Induction of type III interferons (IFNs) in human cancer cell lines after exposure to gamma-rays. (A). Interferons messenger RNA (mRNA) expressions in HT29 cancer cells at 120 hours after mock or 6 Gy or 24 hours after 2 Gy × 5 fractions (F) of gamma-rays. HT29 cells were exposed to 0 to 12 Gy of gamma-rays. Cells were harvested at indicated time points for the assessment of IFNL1 (B) and IFIT2 (C) expression. (D) IFNL1 mRNA expression in a variety of cancer cell lines at 120 hours after mock or 6 Gy gamma-ray treatment. All mRNA expression levels were normalized to beta-actin. Gene mRNA fold induction after gamma-ray treatment was normalized to expression level of control. All data in this study represents means and standard deviations of at least 3 values in more than 1 independent experiment. Comparisons were performed using Student *t* test (ns $> .05$, $*P < .05$, $**P < .01$, $***P < .001$).

culture. As shown in Figure 1A, 6 Gy given as a single dose led to robust up-regulation of type I IFN (IFNB) and type III IFN (IFNL1 and IFNL2/3). We also asked whether fractionated administration of gamma-rays at the biologically equivalent dose (the treatment scheme and biologically equivalent dose calculation can be found in the Supplementary Methods, available online at www.redjournal.org) led to a similar pattern of IFN induction. Despite the differences in timing, the patterns of induction were similar between single-dose and fractionated treatments. Enhanced IFNB expression in cancer cells was consistent with previous studies (9, 15), whereas induction of type III IFN in cancer cells after gamma-irradiation has not previously been reported. Induction of IFNL1 and IFIT2, one of the IFN-stimulated genes (ISGs), in HT29 showed dose- and time-dependent patterns (Figs. 1B and 1C). Gamma-ray treatment of several other human cancer cell lines led to significant up-regulation of type III IFN, suggesting that induction of type III IFN by gamma-rays is a more general phenomenon (Fig. 1D).

TBK1 and NF-κB pathways contribute to IFNL1 induction by gamma-rays

The promoters of type III IFN genes have binding sites for both NF-κB transcription factors and IFN regulatory factors (IRFs) (16, 17). The kinases TANK-binding kinase 1 (TBK1) and inhibitor of NF-κB kinase subunit beta (IKKB) mediate activation of these 2 pathways (18). Ionizing radiation is known to induce NF-κB activity (19). We transfected HT29 cells with an NF-κB activity hMGFP reporter plasmid, allowing cellular NF-κB activity to be monitored using flow cytometry (validated in Fig. E2A; available online at www.redjournal.org). After a single dose of 6 Gy gamma-rays, HT29 exhibited gradually increased NF-κB activity (Fig. E2B; available online at www.redjournal.org). The enhanced NF-κB activity in HT29 cells generated by either single-dose or fractionated irradiation with gamma-rays was significantly inhibited using ML120B, an IKKB-specific inhibitor (Fig. 2A). Gamma-ray treatment also resulted in oscillating activation of TBK1 (Fig. 2B). To distinguish the contributions of these 2 pathways to IFN

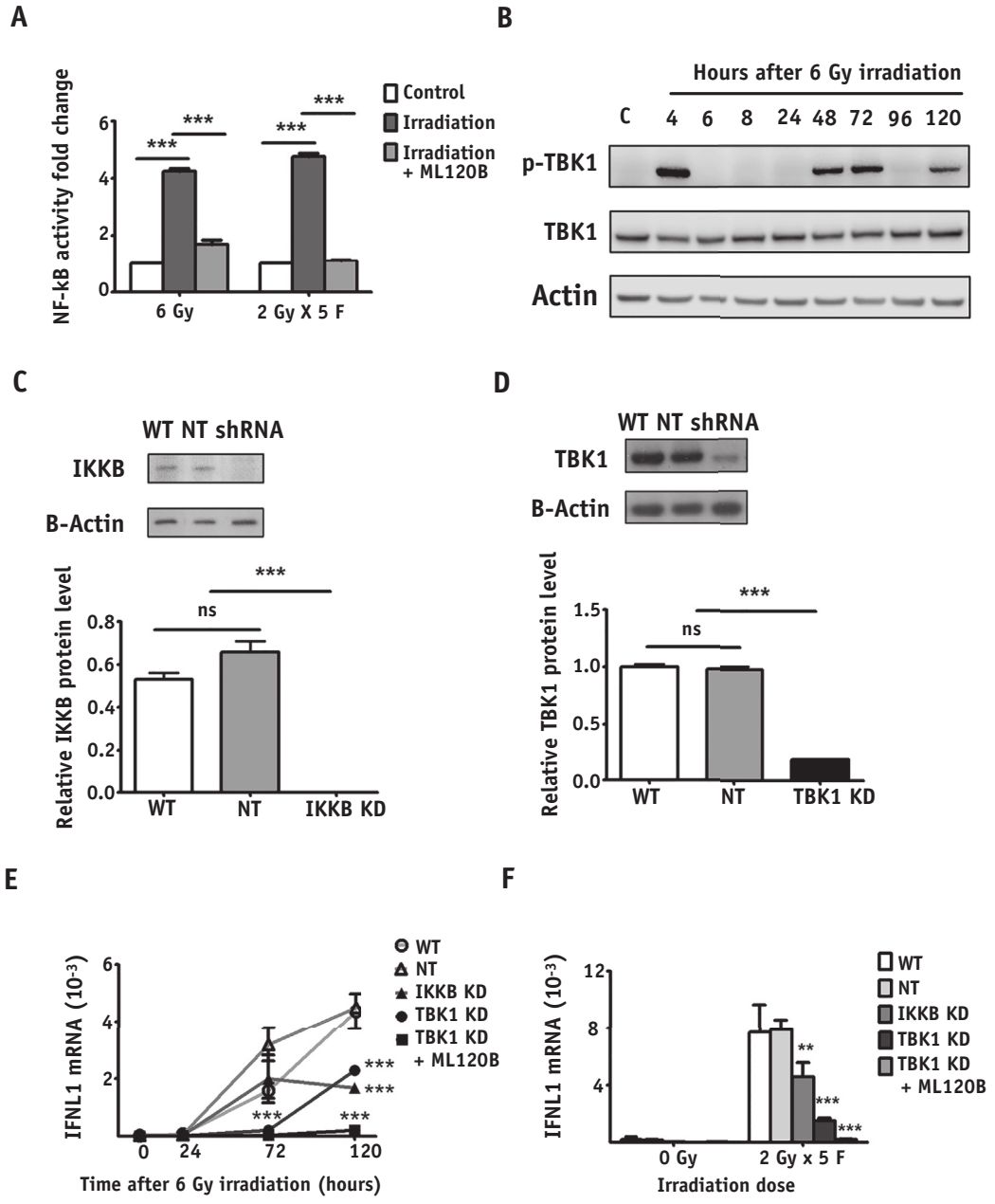


Fig. 2. TANK-binding kinase 1 (TBK1) and nuclear factor kappa B (NF-κB) pathways contribute to IFNL1 induction by gamma-rays. (A) NF-κB activity in HT29 cells at 120 hours after mock or 6 Gy or 24 hours after 2 Gy × 5 F of gamma-rays, with or without ML120B (90 minutes of preincubation and remaining in the medium through the experiment; final concentration 20 μM). Number of replicates (N) for each value = 3. (B) Phosphorylation of TBK1 in HT29 cells after 6 Gy gamma-rays. The knockdown (KD) efficacies of inhibitor of NF-κB kinase subunit beta (IKKB) (C) and TBK1 (D) in HT29 cells were assessed by immunoblotting. N = 3 for (C) and (D). Expression of IFNL1 in a panel of HT29 cells (wild-type [WT] vs nontarget control [NT] vs IKKB KD vs TBK1 KD) after gamma-ray treatment with or without ML120B (E, F). N = 4 for (E) and (F).

induction by gamma-rays, we down-regulated IKKB or TBK1 in HT29 with shRNA (Figs. 2C and 2D). Both reduced IFNL1 induction but to different extents. TBK1 knockdown (KD) significantly down-regulated the expression of IFNL1 at both 72 and 120 hours after gamma-ray treatment, whereas IKKB KD only reduced gamma-ray−induced IFNL1 at the later 120-hour time point (Figs. 2E and 2F). Inhibiting both TBK1 and NF-κB pathways simultaneously completely abolished the induction of IFNL1. Similar results were found in LOVO cells. IFNL1 was mainly mediated by TBK1 and, to lesser extent, the NF-κB pathway (Fig. E3; available online at www.redjournal.org). Thus both pathways play a role in mediating IFN induction, with TBK1 having overall a greater effect.

Cytosolic DNA sensor—STING is the predominant signaling axis in gamma-ray induction of IFNL1

TBK1 can be activated by a variety of sensors (eg, toll-like receptors [TLRs], RIG-I-like receptors, and cytosolic DNA receptors [CDRs]) in cooperation with their relevant adaptors. Of them, TLR3 and RIG-I have been found to mediate type I IFN expression in cancer cells (13, 15, 20). Interestingly, in contrast to previous reports, we found that TLR3 down-regulation actually resulted in more IFNL1 expression in HT29 after gamma-ray treatment (Fig. E4; available online at www.redjournal.org). In the cell lines that we used we could barely detect RIG-I by immunoblot, although its mRNA level increased after a single dose of gamma-rays (data not shown). Thus it is less likely that RIG-I initiates the induction of IFNs after gamma-rays, though its role cannot be totally excluded.

To further delineate the pathways leading to activation of TBK1, we turned to consideration of CDRs, because recently published studies indicated that STING-dependent cytosolic DNA sensing mediated the induction of type I interferon (9, 21, 22). To assess the roles of STING in gamma-ray induction of type III IFN, we eliminated expression of this gene using CRISPR (validated in Fig. E5A; available online at www.redjournal.org). Strikingly, STING KO completely abrogated IFNL1 expression in HT29 after fractionated or single-dose irradiation with gamma-rays (Figs. 3A and 3B). Consistent with our mRNA results, gamma-ray exposure led to substantial induction of IFNL1 protein in the supernatant of irradiated wild-type (WT) HT29. This induction was completed abrogated by knockout of STING (Fig. 3C). Thus, our evidence places STING as an adaptor in gamma-ray—mediated induction of type III IFN. Activation of STING pathway by cGAMP treatment did not enhance NF-κB activity in HT29 cells, indicating that NF-κB pathway is upstream of STING (Fig. E6; available online at www.redjournal.org).

To further explore this signaling pathway, we evaluated the effects of genetic elimination of Cyclic GMP-AMP synthase (cGAS) (validated in Fig. E5B; available online at www.redjournal.org), one of the upstream sensors for STING, which has been implicated in recognition of cytosolic DNA or micronuclei generated as a consequence of radiation (9, 23-25). In HT29 cGAS KO decreased IFNB by 50% or less, indicating that multiple CDRs may be involved (Figs. 3A and 3B).

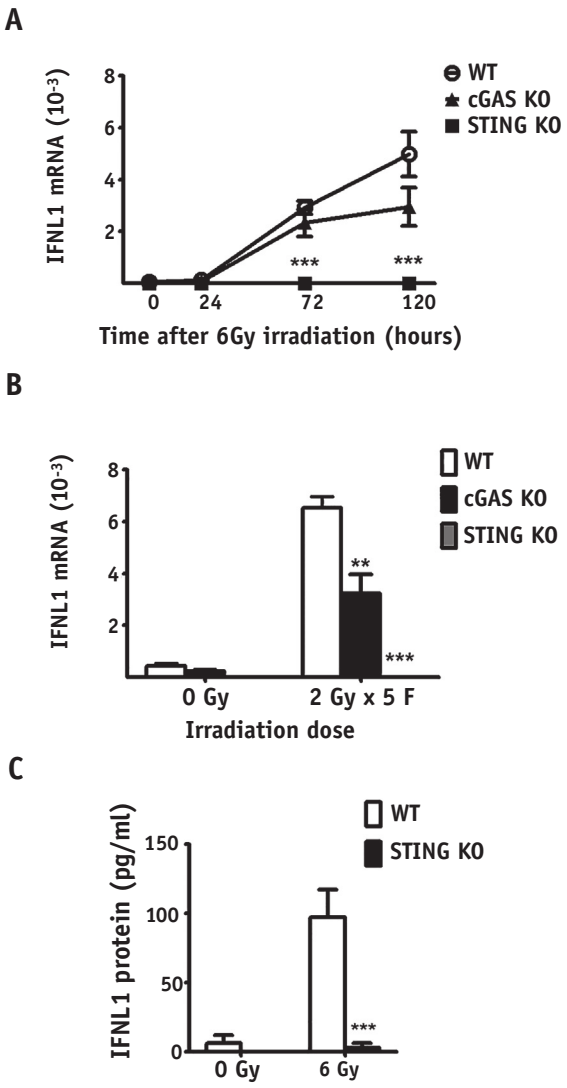


Fig. 3. Cytosolic DNA sensor—STING is the predominant signaling axis in gamma-ray induction of IFNL1. IFNL1 expression in HT29 cells (WT vs cGAS knockout [KO] vs STING KO) at 24, 72, and 120 hours after mock or 6 Gy (A) or 24 hours after 2 Gy × 5 F (B) gamma-rays was assessed by reverse transcription—quantitative polymerase chain reaction (RT-qPCR). N = 3. (C) IFNL1 protein level in tissue culture supernatants of HT29 cells (WT vs STING KO) was measured by enzyme-linked immunosorbent assay (ELISA) at 72 hours after mock or 6 Gy gamma-rays. N = 4.

Gamma-ray induction of IFNL1 in HT29 is mediated by IRF1

We next asked which IRFs are acting in response to gamma-rays to induce IFNL1 transcription. IRFs are mainly localized in the cytoplasm as latent factors and translocate to the nucleus after activation. Of the 9 members of IRFs, IRF1, IRF3, IRF5, and IRF7 positively regulate IFN expression, with only IRF3 and IRF7 shown to be essential (26). To determine the subtypes of IRFs mediating gamma-ray-induction of IFNs, we examined the translocation of IRF1, -3, and -7 from cytoplasm to nucleus in HT29 cells. As shown in Figure 4A, IRF1, but neither IRF3 nor IRF7, translocated to the nucleus after gamma-radiation. Genetic deletion of IRF1 abrogated induction of type III IFN by gamma-rays (Figs. 4B and 4C).

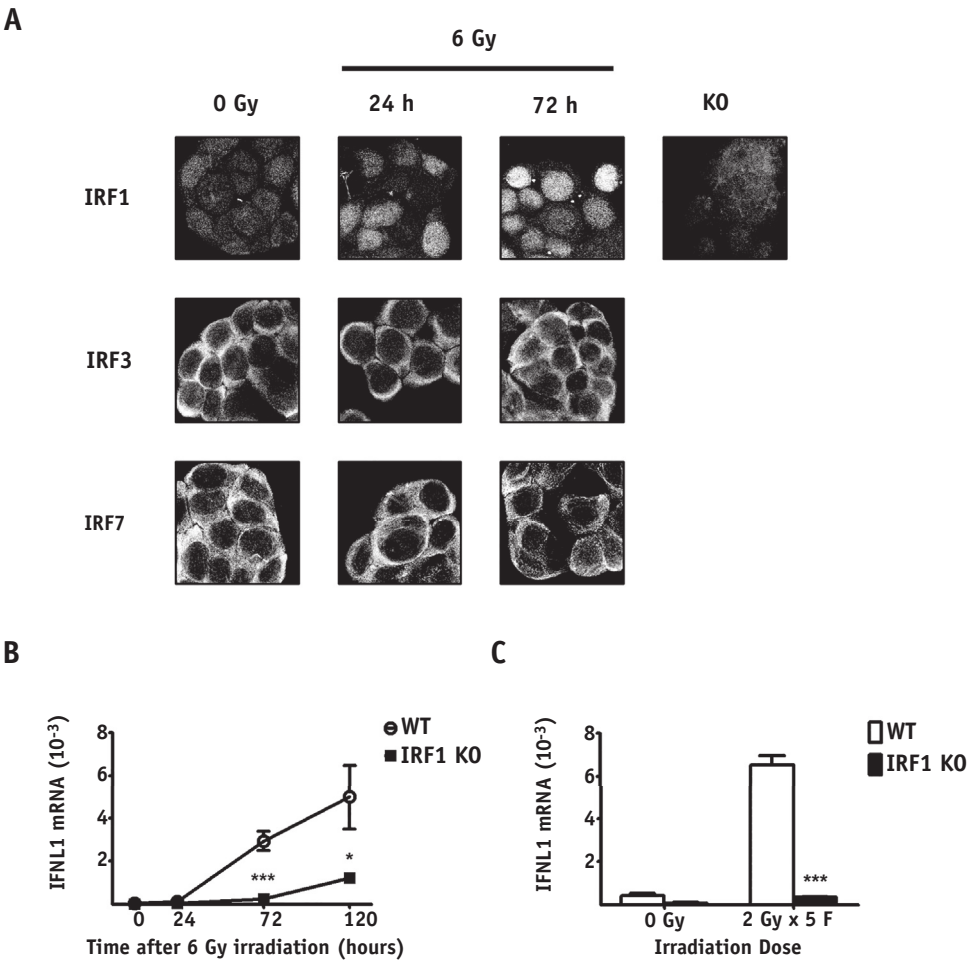


Fig. 4. Gamma-rays induction of IFNL1 is mediated by IFN regulatory factor (IRF)1 in HT29. (A) Distribution of IRF1, IRF3, and IRF7 within HT29 cells after mock or 6 Gy gamma-rays. IRF1 KO was also validated on the right panel. IFNL1 expression in HT29 cells (WT vs IRF1 KO) at 24, 72, and 120 hours after mock or 6 Gy (B) or 24 hours after 2 Gy × 5 F (C) gamma-rays was assessed by RT-qPCR. N = 3.

IL-28R signaling pathways act in a positive feedback loop to enhance induction of IFNL1 after radiation

Binding of IFNs to their receptors in an autocrine or paracrine fashion leads to up-regulation of ISGs. We found robust induction of IFIT2 after gamma-radiation in HT29 cells (Fig. 1C). Activation of type III IFN signaling may further enhance IFN expression by a positive feedback loop. To test this possibility, we genetically eliminated IL-28R (IFNLR) to abrogate type III IFN signaling pathways in HT29 cells (validated in Fig. E5C; available online at www.redjournal.org). Remarkably, we found that IL-28R KO significantly reduced IFNL1 induction at the mRNA and protein levels in HT29 (Fig. 5A-C).

In further experiments, we found that abrogation of the type III IFN signaling pathway significantly reduced the expression of key factors involved in induction of IFNL1, including cGAS, STING, TBK1, and IRFs (Fig. E7; available online at www.redjournal.org). Taken together, these findings document a critical role for positive feedback loops by type III IFN signaling pathways in induction of IFNL1 by gamma-rays.

Model for induction of IFNL1 in human cancer cells by gamma-rays

On the basis of our findings, we propose a model for induction of type III IFNs in cancer cells by gamma-rays. As shown in Figure 6, DNA damage induced by gamma-rays activates STING−TBK1−IRF signaling and the NF-κB pathway as well, leading to induction of type III IFNs. These induced type III IFNs then bind to their relevant receptors. Signaling through type III receptor acts as a feedback loop to further enhance IFNs expression via up-regulation of kinases in the cytosolic DNA signaling pathways.

Discussion

Ionizing radiation-induced type I or II IFNs have been implicated in antitumor immune responses after radiation

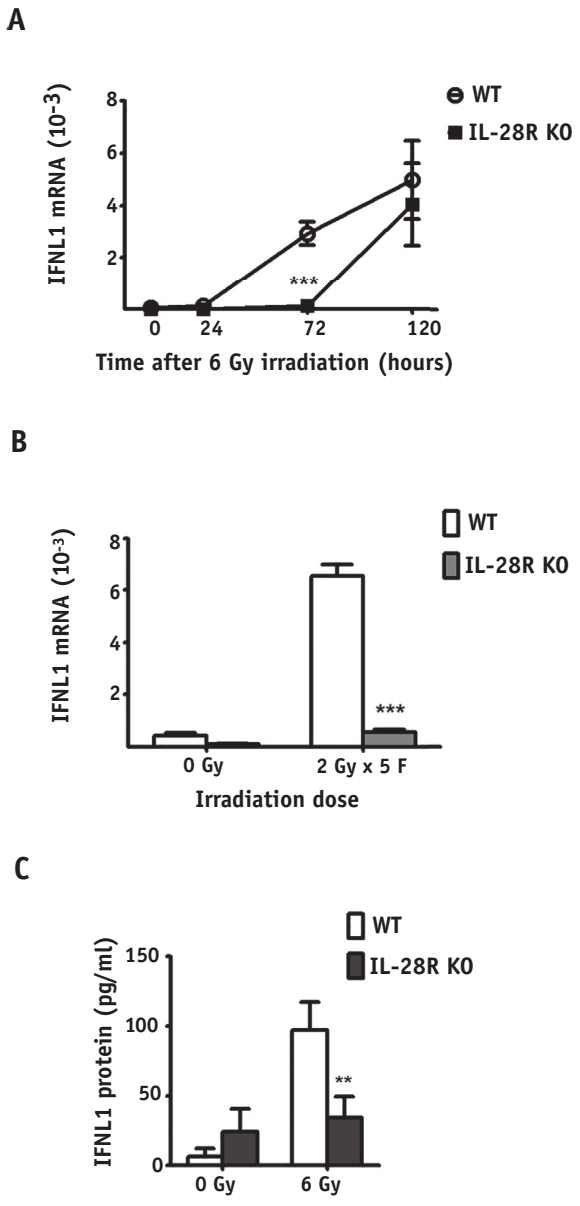


Fig. 5. Interleukin (IL)-28R signaling pathways act in a positive feedback loop to enhance induction of IFNL1 after radiation. IFNL1 expression in HT29 cells (WT vs IL-28R KO) at 24, 72, and 120 hours after mock or 6 Gy (A) or 24 hours after 2 Gy × 5 F (B) gamma-rays was assessed by RT-qPCR. N = 3. (C) IFNL1 protein level in tissue culture supernatants of HT29 cells (WT vs IL-28R KO) was measured by ELISA at 72 hours after mock or 6 Gy gamma-rays. N = 4.

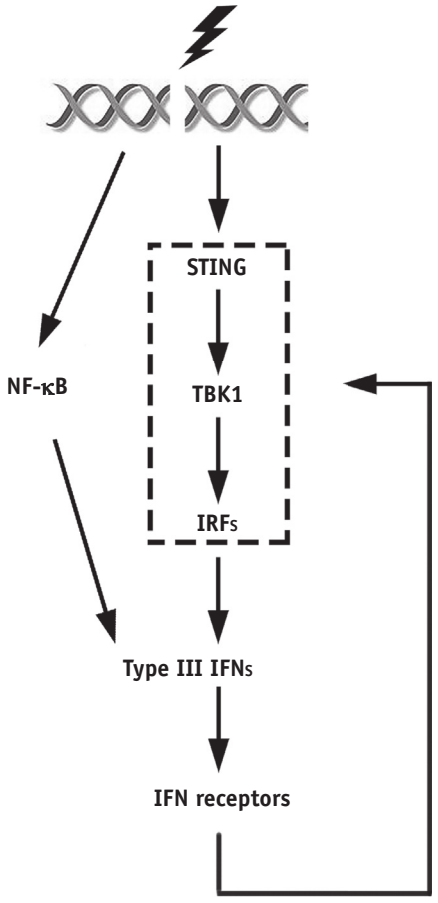


Fig. 6. Model for induction of IFNL in human cancer cells by gamma-rays.

therapy. Here, for the first time, we demonstrate that gamma-rays, a type of ionizing radiation, also led to significant induction of type III IFNs in human cancer cell lines. Moreover, we show that STING−TBK1 signaling and, to a lesser extent, NF-κB mediate type III IFN induction. The induction occurs over days, with maximum levels of mRNA at 3 to 5 days after a single dose of gamma-rays, consistent with recent findings showing a requirement of mitosis after a G2 delay for the formation of micronuclei, an important source of cytosolic DNA (23-25).

Although both STING−TBK1 and NF-κB signaling pathways can trigger type III IFNs, NF-κB proved to have a lesser contribution in the cancer cell lines we tested and at most times. Consistent with our results, Vanpouille-Box Claire et al (9) recently showed that knockdown of cGAS or STING completely abrogated type I IFN induction in several cell lines. Notably, despite our data suggesting that STING is indispensable in induction of type III IFNs after gamma-rays, reduced IFN induction was still found upon inhibition of the NF-κB pathway. No cross-talk was apparent between the NF-κB and the STING pathway in our model, in agreement with a previous study showing that the NF-κB pathway is required for maximum levels of IFNL1 gene expression and could up-regulate type III in an IRF-independent manner (27). Nevertheless, our results suggest that induction of type III IFN in general is mainly driven by STING−TBK1 after radiation, but this is not universal, and redundancy with NF-κB exists.

The STING pathway is triggered by a variety of cytosolic sensors after detection of DNA fragments (14, 28, 29). Potential sources of these DNA fragments include the nuclear genome, mitochondrial DNA, exosomes released by neighboring cells, micronuclei, and uptake of debris after

cell death (22-25, 28, 30, 31). Many cytosolic DNA sensors have been identified, including cGAS, IFI16, DDX41, DNA-PK, and Ku70 (32-36). Although we have not comprehensively sought to identify the cytosolic sensors, cGAS elimination only partially reduced IFN up-regulation in HT29. Clearly multiple redundant mechanisms are present.

Many human colorectal carcinoma cell lines have defective STING signaling (37). These cell lines may rely solely on the NF-κB pathway to express type III IFN in response to gamma-rays and may have relatively less induction. These defects in STING may also lead to reduced antitumor immune responses. Cells with deficiency in key kinases of the DNA damage machinery elicited dramatically increased presence of cytosolic DNA, resulting in type I IFN induction via the STING pathway (14, 38). Under basal conditions, cytosolic DNA can be quickly degraded by Trex1, a master DNA exonuclease in the cytoplasm, and hence would be cleared before activation of the STING pathway (39). Patients with mutated Trex1 exhibit high levels of type I IFN, presumably resulting from the accumulation of cytosolic DNA (40, 41). In the context of inflammation, it has been shown that oxidative modification of DNA by reactive oxygen species confers resistance to Trex1 degradation, resulting in STING-dependent IFN production (42). Further, micronuclei induced by ionizing radiation also trigger cGAS−STING−TBK1. Whether Trex1 has any impact on micronuclei is unknown. These factors will clearly add additional heterogeneity to the induction of IFNs after radiation in cancer cells.

Type III IFN expression could be mediated by a variety of IRFs, depending on the cell type and the activated upstream signaling. Induction via RIG-I or TLR signaling has been suggested to be mediated by both IRF3 and IRF7, whereas IRF1 was also found to play an important role in IFNL up-regulation mediated by peroxisomal MAVS or in human airway epithelial cells in response to RNA virus infection (17, 43-45). Increased type III IFN expression in murine fibroblast cell line after treatment with etoposide, a chemotherapeutic agent that, like gamma-rays, induces DNA double-strand breaks, requires the presence of IRF1 and IRF7 as well (46). In our hands, gamma-rays induced type III IFN in the human cancer cell lines we tested. This induction in HT29 cells was solely mediated by IRF1, and clearly IRF1 is an important downstream mediator of the STING−TBK1 pathway. Consistent with our results, a recently published study indicated that STING-mediated type III IFN production in HEK 293 cells, in response to exogenous DNA, required IRF1, IRF3, and IRF7 (36). Collectively, these results suggest that IRF1 is an important transcriptional factor for cytosolic DNA sensing−mediated type III IFN production.

Type III and I IFNs induce a similar profile of ISGs; however, the induction magnitudes and temporal patterns differ (47, 48). More importantly, whereas almost all cell types respond to type I IFN, response to type III IFN is restricted to epithelial tissues and a subset of immune cells (49, 50). Because our results suggest that type III IFN signaling plays a pivotal role in enhancing induction of type III IFN in a positive feedback loop, the impacts of type III IFN on gamma-ray−induced immune response may be more profound in cancer of epithelial origins. The consequences of gamma-rays−induced type III IFN in cancer cells remain to be determined.

In summary, our results suggest that gamma-rays could significantly up-regulate type III IFNs in human cancer cell lines via the STING pathway, which has added another layer of complexity to the understanding of gamma-rays−induced antitumor immunity and may provide novel insights into IFN-based cancer treatment.

References

1. Apetoh L, Ghiringhelli F, Tesniere A, et al. Toll-like receptor 4-dependent contribution of the immune system to anticancer chemotherapy and radiotherapy. *Nat Med* 2007;13:1050-1059.
2. Lee Y, Auh SL, Wang Y, et al. Therapeutic effects of ablative radiation on local tumor require CD8+ T cells: Changing strategies for cancer treatment. *Blood* 2009;114:589-595.
3. Formenti SC, Demaria S. Systemic effects of local radiotherapy. *Lancet Oncol* 2009;10:718-726.
4. Frey B, Rubner Y, Kulzer L, et al. Antitumor immune responses induced by ionizing irradiation and further immune stimulation. *Cancer Immunol Immunother* 2014;63:29-36.
5. Weichselbaum RR, Liang H, Deng L, et al. Radiotherapy and immunotherapy: A beneficial liaison? *Nat Rev Clin Oncol* 2017;14:365-379.
6. Wadler S, Schwartz EL. New advances in interferon therapy of cancer. *Oncologist* 1997;2:254-267.
7. Lugade AA, Sorensen EW, Gerber SA, et al. Radiation-induced IFN-gamma production within the tumor microenvironment influences antitumor immunity. *J Immunol* 2008;180:3132-3139.
8. Burnette BC, Liang H, Lee Y, et al. The efficacy of radiotherapy relies upon induction of type I interferon-dependent innate and adaptive immunity. *Cancer Res* 2011;71:2488-2496.
9. Vanpouille-Box C, Alard A, Aryankalayil MJ, et al. DNA exonuclease Trex1 regulates radiotherapy-induced tumour immunogenicity. *Nat Commun* 2017;8:15618.
10. Kotenko SV, Gallagher G, Baurin VV, et al. IFN-lambdas mediate antiviral protection through a distinct class II cytokine receptor complex. *Nat Immunol* 2003;4:69-77.
11. Sheppard P, Kindsvogel W, Xu W, et al. IL-28, IL-29 and their class II cytokine receptor IL-28R. *Nat Immunol* 2003;4:63-68.
12. Prokunina-Olsson L, Muchmore B, Tang W, et al. A variant upstream of IFNL3 (IL28B) creating a new interferon gene IFNL4 is associated with impaired clearance of hepatitis C virus. *Nat Genet* 2013;45:164-171.
13. Widau RC, Parekh AD, Ranck MC, et al. RIG-I-like receptor LGP2 protects tumor cells from ionizing radiation. *Proc Natl Acad Sci U S A* 2014;111:E484-E491.
14. Hartlova A, Erttmann SF, Raffi FA, et al. DNA damage primes the type I interferon system via the cytosolic DNA sensor STING to promote anti-microbial innate immunity. *Immunity* 2015;42:332-343.
15. Ranoa DR, Parekh AD, Pitroda SP, et al. Cancer therapies activate RIG-I-like receptor pathway through endogenous non-coding RNAs. *Oncotarget* 2016;7:26496-26515.
16. Onoguchi K, Yoneyama M, Takemura A, et al. Viral infections activate types I and III interferon genes through a common mechanism. *J Biol Chem* 2007;282:7576-7581.

17. Osterlund PI, Pietila TE, Veckman V, et al. IFN regulatory factor family members differentially regulate the expression of type III IFN (IFN-lambda) genes. *J Immunol* 2007;179:3434-3442.
18. Ivashkiv LB, Donlin LT. Regulation of type I interferon responses. *Nat Rev Immunol* 2014;14:36-49.
19. Brach MA, Hass R, Sherman ML, et al. Ionizing radiation induces expression and binding activity of the nuclear factor kappa B. *J Clin Invest* 1991;88:691-695.
20. Sistigu A, Yamazaki T, Vacchelli E, et al. Cancer cell-autonomous contribution of type I interferon signaling to the efficacy of chemotherapy. *Nat Med* 2014;20:1301-1309.
21. Deng L, Liang H, Xu M, et al. STING-dependent cytosolic DNA sensing promotes radiation-induced type I interferon-dependent antitumor immunity in immunogenic tumors. *Immunity* 2014;41:843-852.
22. Woo SR, Fuertes MB, Corrales L, et al. STING-dependent cytosolic DNA sensing mediates innate immune recognition of immunogenic tumors. *Immunity* 2014;41:830-842.
23. Mackenzie KJ, Carroll P, Martin CA, et al. cGAS surveillance of micronuclei links genome instability to innate immunity. *Nature* 2017;548:461-465.
24. Harding SM, Benci JL, Irianto J, et al. Mitotic progression following DNA damage enables pattern recognition within micronuclei. *Nature* 2017;548:466-470.
25. Bartsch K, Knittler K, Borowski C, et al. Absence of RNase H2 triggers generation of immunogenic micronuclei removed by autophagy. *Hum Mol Genet* 2017;26:3960-3972.
26. Honda K, Takaoka A, Taniguchi T. Type I interferon [corrected] gene induction by the interferon regulatory factor family of transcription factors. *Immunity* 2006;25:349-360.
27. Thomson SJ, Goh FG, Banks H, et al. The role of transposable elements in the regulation of IFN-lambda1 gene expression. *Proc Natl Acad Sci U S A* 2009;106:11564-11569.
28. Shen YJ, Le Bert N, Chitre AA, et al. Genome-derived cytosolic DNA mediates type I interferon-dependent rejection of B cell lymphoma cells. *Cell Rep* 2015;11:460-473.
29. Parkes EE, Walker SM, Taggart LE, et al. Activation of STING-dependent innate immune signaling by S-phase-specific DNA damage in breast cancer. *J Natl Cancer Inst* 2017;109.
30. West AP, Khoury-Hanold W, Staron M, et al. Mitochondrial DNA stress primes the antiviral innate immune response. *Nature* 2015;520:553-557.
31. Kitai Y, Kawasaki T, Sueyoshi T, et al. DNA-containing exosomes derived from cancer cells treated with topotecan activate a STING-dependent pathway and reinforce antitumor immunity. *J Immunol* 2017;198:1649-1659.
32. Cai X, Chiu YH, Chen ZJ. The cGAS-cGAMP-STING pathway of cytosolic DNA sensing and signaling. *Mol Cell* 2014;54:289-296.
33. Unterholzner L, Keating SE, Baran M, et al. IFI16 is an innate immune sensor for intracellular DNA. *Nat Immunol* 2010;11:997-1004.
34. Zhang Z, Yuan B, Bao M, et al. The helicase DDX41 senses intracellular DNA mediated by the adaptor STING in dendritic cells. *Nat Immunol* 2011;12:959-965.
35. Ferguson BJ, Mansur DS, Peters NE, et al. DNA-PK is a DNA sensor for IRF-3-dependent innate immunity. *Elife* 2012;1:e00047.
36. Sui H, Zhou M, Imamichi H, et al. STING is an essential mediator of the Ku70-mediated production of IFN-lambda1 in response to exogenous DNA. *Sci Signal* 2017;10.
37. Xia T, Konno H, Ahn J, et al. Deregulation of STING signaling in colorectal carcinoma constrains DNA damage responses and correlates with tumorigenesis. *Cell Rep* 2016;14:282-297.
38. Curtin NJ. DNA repair dysregulation from cancer driver to therapeutic target. *Nat Rev Cancer* 2012;12:801-817.
39. Mazur DJ, Perrino FW. Identification and expression of the TREX1 and TREX2 cDNA sequences encoding mammalian 3'-> 5' exonucleases. *J Biol Chem* 1999;274:19655-19660.
40. Crow YJ, Hayward BE, Parmar R, et al. Mutations in the gene encoding the 3'-5' DNA exonuclease TREX1 cause Aicardi-Goutieres syndrome at the AGS1 locus. *Nat Genet* 2006;38:917-920.
41. Grieves JL, Fye JM, Harvey S, et al. Exonuclease TREX1 degrades double-stranded DNA to prevent spontaneous lupus-like inflammatory disease. *Proc Natl Acad Sci U S A* 2015;112:5117-5122.
42. Gehrke N, Mertens C, Zillinger T, et al. Oxidative damage of DNA confers resistance to cytosolic nuclease TREX1 degradation and potentiates STING-dependent immune sensing. *Immunity* 2013;39:482-495.
43. Odendall C, Dixit E, Stavru F, et al. Diverse intracellular pathogens activate type III interferon expression from peroxisomes. *Nat Immunol* 2014;15:717-726.
44. Siegel R, Eskdale J, Gallagher G. Regulation of IFN-lambda1 promoter activity (IFN-lambda1/IL-29) in human airway epithelial cells. *J Immunol* 2011;187:5636-5644.
45. Ueki IF, Min-Oo G, Kalinowski A, et al. Respiratory virus-induced EGFR activation suppresses IRF1-dependent interferon lambda and antiviral defense in airway epithelium. *J Exp Med* 2013;210:1929-1936.
46. Brzostek-Racine S, Gordon C, Van Scoy S, et al. The DNA damage response induces IFN. *J Immunol* 2011;187:5336-5345.
47. Dumoutier L, Tounsi A, Michiels T, et al. Role of the interleukin (IL)-28 receptor tyrosine residues for antiviral and antiproliferative activity of IL-29/interferon-lambda 1: Similarities with type I interferon signaling. *J Biol Chem* 2004;279:32269-32274.
48. Zhou Z, Hamming OJ, Ank N, et al. Type III interferon (IFN) induces a type I IFN-like response in a restricted subset of cells through signaling pathways involving both the Jak-STAT pathway and the mitogen-activated protein kinases. *J Virol* 2007;81:7749-7758.
49. Sommereyns C, Paul S, Staeheli P, et al. IFN-lambda (IFN-lambda) is expressed in a tissue-dependent fashion and primarily acts on epithelial cells in vivo. *PLoS Pathog* 2008;4:e1000017.
50. Pulverer JE, Rand U, Lienenklaus S, et al. Temporal and spatial resolution of type I and III interferon responses in vivo. *J Virol* 2010;84:8626-8638.

Appendix II Manuscript in preparation

Type I interferon protects cancer cells from CD8 T cell-mediated cytotoxicity after radiation

Abstract

Treatment of tumors with ionizing radiation stimulates an anti-tumor immune response partly dependent on induction of IFNs. These IFNs directly enhance dendritic cell and CD8 T cell activity. Here we show that resistance to an effective anti-tumor immune response is also a result of IFN signaling in a different cellular compartment of the tumor, the cancer cells themselves. We abolished type I IFN signaling in cancer cells by genetic elimination of its receptor IFNAR1. Tumors from cancer cells lacking *Ifnar1* provoked pronounced immune responses after ionizing radiation in tumors from 4 murine model cell lines. This enhanced response depended upon CD8 T cells and was mediated by enhanced susceptibility to T cell mediated killing. Induction of *Serpinb9* proved to be the mechanism underlying control of susceptibility to T cell killing after radiation. *Ifnar1* deficient tumors had an augmented response to anti-PD-L1 immunotherapy with or without radiation. We conclude that type I IFN can protect cancer cells from T cell-mediated cytotoxicity through regulation of *Serpinb9*. This result helps explain why radiation of tumors can stimulate anti-tumor immunity, yet also result in resistance. It further suggests potential targets for intervention to improve therapy and to predict responses.

Introduction

The conflicting effects of type I IFN signaling in the immune response are well recognized. IFNs, both type I IFN and IFNγ (IFNG) facilitate DC and CD8 T cell activity and T cell cross priming. However, IFN can also lead to immunosuppression (1, 2). The role of IFNs in cancer and in response to therapy is similarly complex. In some studies abrogation of IFN signaling in the host or in the cancer cells was shown to diminish localized or systemic immune responses after radiation therapy with or without immune checkpoint blockade (3-5). However, persistent IFN signaling led to resistance to immune checkpoint therapy in other experimental models (6).

Radiotherapy is one of the main treatment modalities for cancer. It is now well accepted that host immunity has a pivotal impact on the therapeutic outcomes of radiotherapy in animal models (7-9). In man addition of an anti-PD-L1 antibody to standard chemoradiotherapy for locally advanced non-small cell lung cancer led to substantially better outcomes although over 50% of the patients still succumbed to their disease (10). Very infrequently localized radiotherapy to one lesion leads to regression of other non-irradiated lesions. This is termed the abscopal effect, which potentially can be enhanced with the addition of immunotherapy (9). Ionizing radiation (IR) boosts the anti-tumor immune response through induction of Types I and III IFNs and immune cell death leading to the release of damage-associated molecular patterns (DAMPs) (2, 5, 11, 12). IR induces DNA strand breakage, which can lead to micronuclei formation (13, 14). These micronuclei release triggers of the STING-TBK1 pathway such as ssDNA leading to induction of IFNs. Although a low level of DNA damage is maintained in many cancer cells leading to chronic activation of this pathway, the DNA damage induced by the doses

of IR used in therapy greatly exceeds this baseline level and should trigger much higher levels of type I and perhaps type III IFNs (5, 12).

IFNs affect the efficacy of radiation therapy in murine models. Type I IFN in particular is a key factor in a radiation-induced immune response (3, 4). Interestingly, activation of type I IFN signaling in tumors can exhibit both beneficial and detrimental effects on the tumor response to radiotherapy. These effects often are mediated by immune responses. Genetic elimination of type I IFN receptors in the murine host or systemic blockade of type I IFN signaling via antibody abrogates the anti-tumor immune response after irradiation (3, 4). IR stimulates immunity through IFN mediated induction of MHC-I on cancer cells (15), activates DCs through IFN signaling (3, 4, 16, 17), releases DAMPS (3, 4), increases the T cell repertoire (18-20), attracts effector T cells by induction of CXCL16 in cancer cells (21), and helps maintain stable interactions between tumor cells and T cells by upregulation of RAE-1 (22); all stimulatory for anti-tumor immunity. Conversely radiation and IFN can lead to resistance to the immune response. There is a growing body of evidence indicating that activation of type I IFN signaling in tumors correlates with worse outcomes in patients and with their resistance to therapies, including radiotherapy (23-26). In some experimental systems, radiation results in resistance to therapy due to expression of PD-L1 that could be mitigated by administration of an antibody blocking PD-L1 (27, 28). In addition STING activation can lead to enhanced myeloid derived suppressor cell infiltration, although this was not directly shown to be IFN based (29). Finally IFN can mediate resistance in the face of immune checkpoint inhibition with anti-CTLA4 or anti-PD-L1 combined with radiation (6). Taken together, these series of results suggest type I IFN signaling in tumors is likely to have opposing effects.

Some of the differing effects of IFN may reflect actions on different cell types in the tumor microenvironment. Since all cells express type I IFN receptors, its effects will depend upon the aggregate response of each cell in the tumor. IFN signaling in DCs and T cells augments the immune response to tumors after radiation (1, 3, 4, 16, 17). The effects of type I IFN signaling in the cancer cell are less well defined, especially in the context of radiotherapy. Accordingly we investigated the effects of type I IFN signaling in cancer cells by genetic elimination of *Ifnar1*. Cancer cells lacking *Ifnar1* gave rise to tumors in murine models, which grew similarly to wild type cells yet had a greatly enhanced response to IR. This response to cancer cells lacking *Ifnar1* depended upon CD8 T cell-based immunity and was mediated by enhanced susceptibility to CD8 T cell mediated killing. We found that downregulation of *Serpinb9,* an interferon inducible gene in *Ifnar1* deficient cells greatly reduced resistance to T cell killing after radiation.

Results

Abrogation of type I IFN signaling in cancer cells enhanced tumor response to IR

To investigate the effects of type I IFN signaling in cancer cells, we prevented this signaling in 4 murine cancer cell lines MC38 (colorectal carcinoma), B16F10 (melanoma), KPC (pancreatic cancer) and LLC (Lewis lung carcinoma). These cell lines vary from provoking a readily detectable immune response with infiltrating T cells (MC38) to intermediate responses (B16F10 and LLC), to those with excluded T cells (KPC). IFNAR, the receptor for type I IFNs is composed of two subunits IFNAR1 and 2. To genetically

abrogate its signaling, we used CRISPR/Cas9 methodology to inactivate *Ifnar1*. The *Ifnar1* KO cell lines failed to respond to exogenous type I IFN by induction of the interferon stimulated genes, *Ifit1* and *Ifi44* (**Figure S1A,B**). There was no difference between growth in culture of *Ifnar1* KO cells and the parental cells in B16F16, KPC and LLC whilst the MC38 *Ifnar1* KO grew faster in tissue culture than its wildtype counterpart MC38 (**Figure S1C-F**). In syngeneic C57BL/6 mice, tumors derived from the parental cells and the *Ifnar1* KO cell lines grew at comparable rates without treatment (**Figure 1**).

We next examined the effect of IR. Clonogenic survival after radiation in tissue culture was equivalent for each *Ifnar1* KO and parental cell line pair (**Figure S1G-J**). The extent of cellular apoptosis and cell cycle delay after radiation was equivalent for MC38 and MC38 *Ifnar1* KO cells (**Figure S1K-L**). In contrast substantial differences were found following IR of tumors. Doses of IR were chosen based on the different radioresistance of each tumor model with 10 Gy for MC38 and LLC, 15 Gy for B16F10 and 20 Gy for KPC. Administration of a single dose of 10Gy IR led to a transient growth delay in WT MC38 tumors with regression followed by recurrence. In comparison, tumors derived from *Ifnar1* KO MC38 cells substantially regressed following radiation and strikingly, 50% of mice remained tumor-free (**Figure 1A**). Kaplan-Meier survival analysis of these data revealed comparable differences (**Figure 1B**, median survival: 44 days vs 24 days, $P < 0.001$). In the three other models, the *Ifnar1* KO tumors displayed significantly greater growth delay after IR compared to WT tumors, but without cure (**Figure 1C-H**). Overall, genetic abrogation of type I IFN signaling in cancer cells enhanced the tumor response to IR.

The enhanced response of *Ifnar1* KO tumors to IR is mediated by CD8 T cells

To evaluate whether an immune response played a role in these responses to IR, we performed an analogous experiment with MC38 tumors in immune incompetent CD1-nude mice. The host immune system is known to supply an important contribution to IR induced tumor control in the MC38 model (4, 16, 30). WT MC38 tumors in CD1-nude mice exhibited growth retardation following IR, although to a lesser extent than in immunocompetent C57BL/6 mice. No significant differences in tumor control or host survival were found between WT and *Ifnar1* KO MC38 tumors in the immunocompromised mice after radiation (**Figure 2A,B)**, implicating the host immune system as a factor affecting the increased sensitivity of *Ifnar1* KO tumors to IR.

Both CD8 T cells and NK cells, the two main populations of anti-tumor effector cells, can mediate the elimination of cancer cells in a tumor. To determine the contribution of these populations to the enhanced radiation response of *Ifnar1* KO tumors, we evaluated the effect of radiation on the growth of MC38 tumors with depletion of either population. Consistent with **Figure 1A**, IR plus isotype control Ab treatment led to significant retardation of tumor growth of both WT and *Ifnar1* KO tumors. With CD8 T cell depletion, the growth delay in response to IR was significantly reduced in WT MC38 tumors and almost completely abolished in *Ifnar1* KO tumors (**Figure 2C,D**; Depletion validated in **Figure S3**). More importantly, no significant differences in tumor radiation response were found between WT and *Ifnar1* KO MC38 tumors in CD8 T cell depleted mice suggesting that CD8 T cells are the main effector cells (**Figure 2E,F**). NK depletion did not have evident effects on *Ifnar1* KO tumors after IR, though there was a minor reduction of tumor response in WT MC38 tumors (**Figure 2C,D**). *Ifnar1* KO tumors in mice wtih NK cell depletion still displayed substantially greater response to IR than WT tumors

(**Figure 2F**). In results similar to those obtained with the MC38 model, CD8 T cell depletion in mice bearing B16F10 or KPC WT or *Ifnar1* KO tumors substantially reduced growth delay of *Ifnar1* KO tumors after IR (**Figure S2E-H**). Collectively, these results suggest that the enhanced response of *Ifnar1* KO tumors to IR is predominantly mediated by CD8 T cell immunity.

We now asked whether mice in which *Ifnar1* KO MC38 tumors had regressed retained systemic anti-tumor immunity to challenge with either WT or *Ifnar1* KO cancer cells. Notably, neither WT nor *Ifnar1* KO MC38 cells grew in mice that had previously rejected *Ifnar1* KO tumors (**Figure 2G**). These data indicate that rejection was a systemic response involving memory. They also suggest that rejection was not due to recognition of a novel antigen presented by the *Ifnar1* KO cells.

CD8 T cells infiltrating *Ifnar1* KO tumors did not have augmented cytotoxic capacity or reduced exhaustion

To understand how abrogation of type I IFN signaling in cancer cells led to better tumor control, we characterized the CD8 T cells in tumors from WT or *Ifnar1* KO MC38 tumors after IR. The percentages of tumor cells and tumor infiltrating CD8 T cells were not markedly different at the time of radiation or 4 days later. By 6 days after radiation the *Ifnar1* KO MC38 tumors had increased infiltration of CD8 T cells and a much smaller percentage of cancer cells, consistent with the decreasing volumes of *Ifnar1* KO tumors at that time (**Figure 1A and 3A,B**). Although the percentages of CD8 T cells infiltrating the different tumors was similar, the *Ifnar1* KO tumors had elevated percentages with Ki67

expression (**Figure 3C,D**), Nonetheless there was only a modest increase in the percentage of Granzyme B positive CD8 T cells compared to those from WT tumors (**Figure 3C,E**). At the later time, the percentage of Granzyme B positive CD8 T cells had decreased in both groups. We evaluated the response of CD8 T cells isolated from the tumors to stimulation (by PMA, Ionomycin and Brefeldin A) in culture. CD8 T cells from WT and *Ifnar1* KO MC38 tumors isolated over a range of times after IR exhibited comparable IFNG induction in response to stimulation. (**Figure 3F,H**). There was a trend of increased Ki67 expression in CD8 T cells from *Ifnar1* KO tumors, but the differences were not statistically significant (**Figure 3F,G**). Although Granzyme B positive CD8 T cells were not as abundant in the other three tumor models as in MC38, there was no significant increase of either Granzyme B or Ki67 positive CD8 T cells after IR in these *Ifnar1* KO tumors (**Figure S3A-D**).

We next examined T cell exhaustion using two markers (PD-1 and TIM-3) in CD8 T cells, whose ligands (PD-L1 and LGALS9) are known to be expressed in some cancer cells from solid tumors. Most of the CD8 T cells were PD-1 positive (75-90%) in WT and *Ifnar1* KO MC38 tumors, with a transient decrease at day 4 after IR in *Ifnar1* KO tumors. In B16F10 and LLC tumors, there were many fewer cells expressing PD-1 than in MC38, but still no significant differences in the percentage of CD8 T cells expressing PD-1 or TIM-3 between WT and *Ifnar1* KO tumors were found (**Figure S3D-F**). The paucity of T cells in the KPC model precluded their analysis. Overall, our experiments uncovered no evidence that *Ifnar1* KO in cancer cells led to consistently increased numbers of CD8 T cells, enhanced expression of markers for cytotoxic capacity or reduced exhaustion in tumor infiltrating CD8 T cells.

Ifnar1 KO cancer cells are more susceptible to CD8 T cell mediated killing

Since we found little alteration in CD8 T cell numbers, or functional markers in *Ifnar1* KO tumors compared to WT, we now asked whether *Ifnar1* KO cancer cells were more susceptible to CD8 T cells. In culture WT and *Ifnar1* KO MC38 cells were incubated with CD8 T cells isolated from either WT or *Ifnar1* KO tumors. The MC38 *Ifnar1* KO cells were substantially more susceptible to killing by both CD8 T cell populations than the WT cells (**Figure 4A)**. Similar results were obtained with B16F10 WT and *Ifnar1* KO cells using CD8 T cells from their tumors **(Figure S4A**). Since irradiation of these cancer cells leads to cell cycle arrest and lack of viability, but only small amounts of apoptosis, and since T cell killing is driven by apoptosis, we used apoptosis as an endpoint to ask whether irradiated *Ifnar1* KO cancer cells were also more susceptible to apoptosis. We found that CD8 T cells isolated from irradiated MC38 tumors generated significantly increased apoptosis of irradiated *Ifnar1* KO MC38 cells than of irradiated WT MC38 cells (**Figure 4B**). Thus *Ifnar1* KO cancer cells were more vulnerable to CD8 T cell-mediated killing in culture.

Next, we asked whether similar susceptibility differences were evident in the immune microenvironment in vivo. GFP-tagged WT MC38 cells and mCherry-tagged *Ifnar1* KO MC38 cells were co-injected into C57BL/6 mice subcutaneously at a 1:1 ratio. As shown in **Figure 4C,D**, these mixed tumors retained the same ratio of cell types after growth in syngeneic mice. In contrast, following IR, *Ifnar1* KO-mCherry cells were almost completely absent from tumors, with WT-GFP cells making up the majority of the CD45 negative cells. To determine whether CD8 T cells contributed to the disparity of *Ifnar1* KO

cell survival after IR, we depleted CD8 T cells with antibody. This partially restored the proportion of *Ifnar1* KO cells to that before radiation. Depletion of NK cells had no effect (**Figure 4E,F**). Similar results were found in the B16F10 model (**Figure S4B,C**). Thus, in vivo as in vitro, *Ifnar1* KO cancer cells displayed greater susceptibility to CD8 T cell-mediated killing than WT cells.

Serpinb9 is the key mediator of enhanced susceptibility of *Ifnar1* KO cancer cells

Cancer cell resistance to CD8 T cell killing can be mediated through a variety of intrinsic mechanisms, including upregulation of immune checkpoints, granzyme inhibitors or anti-apoptotic factors, and downregulation of MHC class I molecules (31-35). To search for candidates underlying the enhanced susceptibility of *Ifnar1* KO cancer cells, we generated a panel of 12 plausible candidates for an initial survey. We stipulated that a suitable candidate would be induced (or suppressed) in cancer cells by IR. **Figure 5** shows that 5 candidates were significantly induced by IR with additional genes excluded due to either failure to be induced or expression in less than 20% of MC38 cells (**Figure S5**). We also stipulated that expression would be reduced in *Ifnar1* KO cells compared to WT for those genes mediating resistance to killing or increased for MHC class I (here *H2-K1*). Of the candidates examined only *Serpinb9* met these criteria in both the MC38 and B16F10 models and thus we concentrated our efforts on *Serpinb9*.

Previous studies have shown that SERPINB9 directly inhibits Granzyme B, a major effector of CD 8 T cell cytotoxicity and leads to resistance to cytolytic T cell killing in cancer cells making it a plausible candidate (32, 36). *SERPINB9* mRNA levels correlated with

IFN gene expression signatures in a variety of cancers in the TCGA database (**Figure 6A**). We confirmed that *Serpinb9* RNA was induced after exposure to type I IFN in the 4 cancer cell lines studied here **(Figure 6B-C)**. IR also led to substantial induction of *Serpinb9* in cancer cells that was approximately 50% less in *Ifnar1* KO cells **(Figure S6, Figure 6E,F)**. Inhibition of JAK1, a downstream effector of IFNAR signaling reduced *Serpinb9* induction by IR to a similar extent as in *Ifnar1* KO cells (**Figure 6E,F, Figure S6**) but did not affect *Serpinb9* induction in *Ifnar1* KO cells. IR can activate STING resulting in activation of interferon transcriptional factors (IRFs) (37, 38), potentially leading to *Serpinb9* transcription. Both IRF1 and 3 were induced by IR in MC38 cells and both IRF1 knockdown and IRF3 KO diminished *Serpinb9* induction after IR but only IRF3 KO affected *Ifnb1* induction **(Figure S6 and 6G, H)**. *Sting* knockout reduced *Serpinb9* induction after radiation. Thus augmented levels of *Serpinb9* after IR may result from induction of type I IFN as well as IFN signaling-independent mechanisms as schematized in **Figure 6I**.

To ask whether induction of *Serpinb9* contributes to resistance to anti-tumor immunity after IR, we used two approaches: genetic elimination of *Serpinb9* via CRISPR/Cas9 (SB9 KO) and *Serpinb9* overexpression in *Ifnar1* KO and *Serpinb9* KO cells (SB9 OE) through lentiviral transfection, which led to *Serpinb9* levels comparable to those after type I IFN induction in the WT **(Figure 7A,B)**. These cells had equivalent clonogenic cell survival after IR in culture **(Figure S7)**. *Serpinb9* KO MC38 tumors spontaneously regressed in C57BL/6 mice after subcutaneous inoculation. Their growth was rescued by CD8 T cell depletion or by re-expression of *Serpinb9*. (**Figure 7C**). The mice that had rejected the MC38 *Serpinb9* tumors also rejected MC38 WT and MC38

Ifnar1 KO cells after rechallenge, suggesting that novel antigens in the KO cells were not responsible for rejection (**Figure 7D**).

In contrast, B16F10 *Serpinb9* KO tumors had equivalent growth to WT (**Figure 7E**). Since *Serpinb9* was not essential for tumor growth in B16F10 cells, we used these tumors to examine the effect of IR. Following IR, *Serpinb9* KO B16F10 tumors had a prolonged tumor growth delay equivalent to that of irradiated B16F10 *Ifnar1* KO tumors (**Figure 7E**). *Serpinb9* KO KPC tumors also exhibited similar enhanced response to IR (**Figure 7F**). Most importantly, reintroduction of *Serpinb9* expression in *Ifnar1* KO cancer cells abrogated their enhanced response to IR. *Serpinb9* restoration did not affect *Ifnar1* KO MC38 or B16F10 tumor growth without treatment (**Figure 7G,H).** Collectively, our results reveal a previously unrecognized link between activation of type I IFN signaling in cancer cells and induction of *Serpinb9*, which protects cancer cells from CD8 T cell-mediated cytotoxicity after irradiation.

Ifnar1 KO tumors exhibited greater response to anti-PD-L1 than WT

PD-L1 is known to be induced by IFNs, although this has been attributed to IFNG (39-42). Our panel of *Ifnar1* KO cancer cells expressed PD-L1 at approximately the extent as their WT counterparts albeit with considerable variation among cell lines (**Figure 5B,C)**. Because anti-PD-L1 antibodies enhance IR-induced anti-tumor immune responses (27, 28), we asked whether addition of anti-PD-L1 to IR would further improve the outcomes of mice bearing *Ifnar1* KO tumors. Despite high percentages of cancer cells in the MC38 model expressing PD-L1, anti-PD-L1 only had a minor, not statistically significant,

additional effect in WT MC38 tumors with or without IR **(Figure 8A,B)**. In contrast, anti-PD-L1 substantially extended the survival of mice bearing *Ifnar1* KO tumors and further improved their outcomes when combined with IR **(Figure 8C,D)**. The majority of mice bearing *Ifnar1* KO MC38 tumors experienced complete regression following IR plus anti-PD-L1 treatment with significant improvement of survival compared with mice with WT tumors. Anti-PD-L1 similarly delayed tumor growth in the B16F10 model, but not in the KPC model (**Figure 8E-J, Figure S8**). Thus, in some but not all experimental models, we observed significantly greater regression of *Ifnar1* KO or *Serpinb9* KO tumors with or without IR in response to anti-PD-L1.

Discussion

The beneficial role of type I IFN signaling in immune cells for the anti-tumor immune response after radiation is well recognized. Less is known about the effect of type I IFN signaling in the cancer cells in the context of radiotherapy. In this study, we found that intact type I IFN signaling in cancer cells was detrimental to tumor control after IR with or without anti-PD-L1 immunotherapy. Abrogation of *Ifnar1* in murine cancer cells resulted in an enhanced anti-tumor response after IR dependent on CD8 T cells. Abrogating this pathway did not generally lead to increased numbers, augmented cytotoxic markers or reduced exhaustion of tumor-infiltrating CD8 T cells, but instead rendered the cancer cells themselves more susceptible to CD8 T cell-mediated killing. We identified *Serpinb9* as a critical component depleted in the *Ifnar1* KO cancer cells. Taken together, our results reveal a previously undiscovered connection between

activation of type I IFN signaling in cancer cells and protection from CD8 T cell-mediated cytotoxicity in irradiated tumors.

Emerging data indicate that IFN signaling has paradoxical effects on tumor control (6, 43, 44). Interferon signaling can enhance the generation of an anti-tumor response with DC and T cells as well recognized targets. Suppressive effects are also recognized including induction of the immune checkpoint mediator PD-L1 (39-42, 45, 46). Radiation, through the induction of type I interferon may amplify these effects. Benci et al. showed that prolonged IFN signaling renders cancer cells more resistant to immune checkpoint blockade with or without radiotherapy (6). Our results suggest that intact type I IFN signaling in cancer cells reduces the benefits from the anti-tumor immune response after radiation, adding another layer of complexity. These results together suggest that activation of type I/II IFN signaling can play a pivotal role in the immune resistance of tumor cells, but with considerable variation depending on the particular conditions.

Serpinb9 was a critical mediator for the enhanced vulnerability of *Ifnar1* KO cancer cells in our study, consistent with its known role as an inhibitor of Granzyme B an important mediator of T and NK cytoxicity including killing of cancer cells (32, 36, 47-49). Pan et al performed a genome-wide CRISPR screen to identify genes whose expression can contribute to cancer cell resistance to cytotoxic T cells (50). This screen uncovered over 100 genes including members of the PBAF transcriptional complex, yet with SerpinB9 as one of the most significant hits. Even within a more comprehensive analysis of a correlative signature for resistance to immune checkpoint blockade in melanoma, *Serpinb9* as a single element correlated with resistance (51). *Serpinb9* expression can be triggered by a variety of mediators, including estrogen, HIF-α2, dsRNA sensing, IFNγ

and various modulators of inflammation (52-56). Induction of *Serpinb9* by type I IFN in normal cells has been reported in the interferome (www.interferome.org). We found induction by type I IFN in cancer cells. *Serpinb9* levels both at baseline as well as after upregulation in response to type I IFN or IR may serve as a common mechanism for cancer cells to survive immune attack.

Blockade of this pathway or targeting *Serpinb9* in cancer cells might be used in the context of radiation therapy to maximize benefits from the anti-tumor immune response. Such an approach would need to be considered carefully since *Serpinb9* plays a role in the protection of cytotoxic effector cells themselves from Granzyme B in the cytotoxic milieu and has been shown to be critical for dendritic cell-mediated antigen cross-presentation (57-61). Further investigations to discriminate between cancer cells and the host in regulation of type I IFN signaling and expression of *Serpinb9* may help develop better stratification and understanding of how *Serpinb9* inhibition might be deployed to yield more effective and specific cancer immunotherapies.

Expression of PD-L1 in tumors was not augmented after IR in our study. Yang et al found that intratumoral type I IFN treatment induced PD-L1 in the tumors and blocking of PD-L1 led to complete eradication of these tumors (45). Benci et al suggest that cancer cell type I and II IFN signaling elicit an immunosuppressive effect attributed mainly to PD-L1 and LGALS9 (6). In our experiments, abrogation of type I IFN signaling in cancer cells did not affect PD-L1 expression in vivo under most of our experimental conditions, perhaps because type II IFN signaling pathways remain intact. Tumor control benefits were consistently observed, however, in *Ifnar1* KO tumors from the addition of anti-PD-L1 treatment. There was little LGALS9 on the surface of the cell lines we examined,

making it less plausible as an important mediator in our experiments. Nonetheless, a contribution of LGALS9 is likely in other settings.

A therapeutic benefit from elimination of type I IFN signaling in cancer cells was evident in vivo following irradiation and immune checkpoint blockade in our experiments. Without IR, the immunosuppressive tumor microenvironment prevailed. How IR reverses the immunosuppressive microenvironment in *Ifnar1* KO tumors remains to be determined. Our findings shed some light on considerations for personalized cancer treatment and combing radiotherapy and immune checkpoint blockade. Radiotherapy with or without anti-PD-L1 may result in a better response in tumors with reduced type I IFN signaling in the cancer cell component and may depend on *Serpinb9* expression.

Methods

Mice

Female C57BL/6 and CD1-nude mice were purchased from Charles River Laboratories (Wilmington, USA). All mice were used at age 6-8 weeks and held under specific pathogen-free conditions with humidity and temperature control. Mice were randomly divided into groups in each experiment. Animal procedures were carried out in accordance with the UK Animal (Scientific Procedures) Act 1986 and local ethics reviews.

Cells

MC38 was a gift from Dr. Lee Gorden (Vanderbilt University, Nashville, TN, USA). KPC was a gift from Dr. Owen Sansom (University of Glasgow, Glasgow, UK). B16F10 and LLC were obtained from American Type Culture Collection. Cells were cultured in DMEM or RPMI 1640 medium supplemented with 10% (v/v) fetal bovine serum, 1% penicillin-streptomycin (all from Sigma-Aldrich, St. Louis, MO) and 25 mM HEPEs (only for B16F10). Cells were used at passage number < 8. Mycoplasma was routinely tested and negative.

Reagents

Universal Type I IFN alpha (PBL) was used at 50 U/ml. Lipofectamine 3000 (Thermo Fisher) was used to deliver 2',3'-cyclic guanosine monophosphate-adenosine monophosphate (cGAMP, from InvivoGen). Ruxolitinib (LC Laboratories) was dissolved in DMSO at 5 mM and then diluted in medium at a final concentration of 2.5 μM.

Antibodies

Abs used in this study are described in **Supplementary Table 1**.

Subcutaneous tumor model

A total number of 2.5 x 10^5 cells were injected subcutaneously on the right flank. For tumor rechallenge, 1 x 10^5 cancer cells were injected on the left flank. Tumor sizes

were measured every other day using calipers. Tumor volumes were calculated using the formula: Length x Width^2/2.

In vivo radiation treatment

Tumors received irradiation when they reached 100 mm^3. Mice under anesthesia were shielded leaving the tumor exposed. X-ray radiation treatment (300 KV, dose rate 2.25 Gy per minute) was delivered to the tumors using a GulmayRS320 irradiation system (Gulmay Medical Ltd, Surrey, UK). Following IR, mice were culled before their tumor size exceeded the ethical limit: 500 mm^3, or 1000 mm^3 in the B16F10 model. Otherwise they were observed for at least two months. Mice whose tumors ulcerated during the experiment were culled and excluded from the analysis. Mice with severe radiation-induced dermatitis (e.g. skin ulceration) and with complete tumor regression were sacrificed, but still included in the analysis.

CD8 T cell or NK cell depletion in C57BL/6 mice

For CD8 T cell depletion experiments, mice received anti-mouse CD8 Alpha (clone 2.43) or Rat IgG2b isotype control (clone LTF-2) Abs at a dose of 10 milligrams per kilogram of mouse body weight (mg/kg) by intraperitoneal injection (i.p.). Anti-mouse NK1.1 (clone PK136) and mouse IgG2a isotype control (C1.18.4) Abs at a dose of 20 mg/kg were used for NK cell depletion experiments. Injections were given on days -1, 2, 5, 8 and 11 (day 0: IR treatment day). The efficacy of cell depletion was validated in C57BL/6 mice bearing MC38 tumors using flow cytometry (**Supplementary Figure 2**).

Anti-PD-L1 treatment in mice

Mice received anti-mouse PD-L1 Rat IgG2b (clone 10F.9G2) or Rat IgG2b isotype control (clone LTF-2) Abs by i.p. injection at 10 mg/kg. Abs were administrated on days -1, 3, 7 and 11.

Flow cytometry profiling of tumors

Tumor samples were cut into small pieces and incubated in Hank's Balanced Salt solution with collagenase 2 (10mg/ml) and DNase I (2 U/ml) (1X protein transport inhibitor cocktail (ThermoFisher) was also included when profiling cytotoxic effector cells) for 30 minutes with regular shaking at 37°C. Cell suspensions were then strained through 50 μm nylon strainers, treated with red blood cell lysis buffer (BioLegend), blocked with anti-mouse CD16/32 antibodies for 5 minutes and incubated with mixed antibodies at 4°C in the dark for 45 minutes. Antibodies used in this study are summarized in **Supplementary Table 1**. Following incubation, cells were washed and fixed using Foxp3/Transcription Factor Fixation/permeabilization working solution (ThermoFisher) for 40 minutes at room temperature. Cells with intracellular markers in the panel were permeabilizated and incubated with antibodies in the dark for 45 min. Subsequently, these cells as well as samples without intracellular markers in the panel were washed, resuspended in PBS and analyzed using LSR II (BD Bioscience) or Attune (ThermoFisher). Data was analyzed using FlowJo software. CD8 T cells were gated as CD45+, CD3ε+ and CD8a+ single live cells for profiling. Cancer cells were

gated as CD45-, CD31- and CD140a- single live cells for assessment of surface marker expression. Fluorescence minus one (FMO) controls were used to discriminate negative and positive signals.

FACS

Single cell suspensions were prepared and stained with mixed antibodies as described above. They were sorted into designed populations using a MoFlo MLS High Speed Cell Sorter (Beckman Coulter Legacy).

Isolation of CD8 T cells from tumors using MACS MicroBeads

CD8 T cells were isolated from tumors using MACS CD8α (Ly-2) MicroBeads according to the manufacturer's protocol. Briefly, single cell suspensions derived from tumors were prepared as described above. 10^7 Cells were resuspended in 90 µl PBS (with 0.5% BSA and 2mM EDTA), incubated with 10 ul of CD8α MicroBeads (Miltenyibiotec) at 4 degree for 15 minutes in the dark. Following washing, cells were resuspended and added to the MACS column in the magnetic field. After washing, cells were flushed from the column and collected for downstream assays. The percentage of CD8 T cells in total live cells was > 90% as assessed by flow cytometry.

In vitro stimulation of CD8 T cells

CD8 T cells were resuspended in RPMI medium supplemented with 10% FBS, 1% penicillian/Streptomycin, 1 mM L-Glutamine and 55 μM 2-mercaptoethanol, and added to 96-well plates. Cells were then incubated with 1X cell stimulation cocktail (ThermoFisher) composed of PMA, ionomycin and Brefeldin A for 4 hours, harvested, stained with antibodies and assessed by flow cytometry.

In vitro killing of cancer cells by tumor-derived CD8+ T cells

Cancer cells were seeded in 96-well plate 24 hours prior to co-culture. The number of cancer cells in the well was re-counted to take account of their proliferation during culture. CD8+ T cells were sorted by FACS from tumors in C57BL/6 mice and added to the plated tumor cells and maintained in the incubator. Tumor cells cultured alone were used as controls. Co-cultured medium was RPMI medium supplemented with 10% of FBS, 1% of Penicillin/Streptomycin, 1mM L-Glutamine, 55 μM 2-mercaptoethanol and IL-2 (30 U/ml). Upon co-culture for 48 hours, culture wells were washed extensively with PBS, fixed with 4% of paraformaldehyde in PBS for 15 minutes and stained with Hoechst (1μg/ml) for 5 minutes. The numbers of remaining cells in the well were then quantified using a Celigo Imaging Cytometer (Nexcelom Bioscience, Massachusetts, USA). The killing percentage was calculated using the following formula: (cell number in control well – cell number in co-cultured well)/cell number in control well x 100.

Imaging assessment of apoptosis in cancer cells upon co-cultured with tumor-derived CD8+ T cells

Cancer cells were tagged with mCherry via lentivirus transfection (vector: pCDH-CMV-MCS-EF1α-Hygro, System Bioscience, Palo Alto, CA, USA) followed by FACS to isolate the bright population. These cells were irradiated with 10Gy IR, immediately seeded in μ-Slide VI 0.4 channel slides (ibidi, Munich, Germany) and returned to the incubator. 48 hs later, CD8+ T cells isolated from WT or IFNAR1 KO MC38 tumors by FACS at day 4 after 10Gy IR, labelled with CMAC dye (ThermoFisher), were added to channel slides in an E: T (effector:tumor cell) ratio of 3:2. The number of cancer cells was evaluated by counting cells seeded in parallel plates to take account of their altered proliferation after IR. Culture media were supplemented with IL-2 (30 U/ml) and Caspase-3/7 Green detection reagent (500 nM, ThermoFisher). Subsequently, channel slides were imaged every 15 minutes for up to 16 hours using Nikon ECLIPSE Ti-E Inverted Microscope. During the whole course of imaging, chamber slides were maintained at 37 °C with 5% CO2. The imaging data was transferred to Imaris station for analysis (Bitplane, Zurich, Switzerland). The percentage of caspase 3/7+ tumor cells was calculated using the following formula: the number tumor cells becoming caspase-3/7+ following interaction with CD8+ T cells/ the number of tumor cells interacted with CD8+ T cells x 100.

IR in tissue culture

In vitro IR was performed as described (12). Briefly, cells were treated with gamma-rays (0.662 MeV) delivered using a 137Cs-laboratory irradiator (IBL 637, CIS bio International, Saclay, France) at a dose rate of 0.81 Gy/minute.

Reverse transcription quantitative PCR (RT-qPCR)

RT-qPCR was performed as described (12). Briefly, RNA was extracted from the cells using Trizol (ThermoFisher) or RNeasy Mini Kit (Qiagen), treated with DNase using Turbo DNA-free™ Kit (Life technologies), or RNase-Free DNase Set (Qiagen), transcribed into cDNA using the High-Capacity cDNA Reverse Transcription Kit (Thermo Fisher Scientific). PCR was performed using SYBR green (Promega) with specific primers (**Supplementary Table 2**) or Taqman primers/probes (Thermo Fisher Scientific, listed in **Supplementary Table 3**). Reactions were run on ABI QuantStudio 5 Real-time PCR System (Thermo Fisher Scientific). The cycling conditions were as follow: a. 50ºC 2 min, 1 cycle; b. 95ºC 10 min, 1 cycle; c.95ºC 15 s -> 60 ºC 60 s, 40 cycles. Following the amplification, the threshold cycle (Ct) values for target genes and the reference gene, *β-actin*, were recorded. The fold induction was calculated using the ΔΔCt method.

Generation of knockout cell lines using CRISPR

Gene knockout using CRISPR/Cas9 in cell lines was performed as described (12). Briefly, a pair of gRNA primers (**Supplementary Table 4**) targeting a region within exons were designed using Feng Zhang lab's CRISPR Design (http://crispr.mit.edu/).

These primers were cloned into Nickase Cas 9 plasmids, pSpCas9n (BB)-2A-GFP (PX461) and pSpCas9n (BB)-2A-Puro (PX462) (gifts from Feng Zhang through Addgene (plasmids # 48140 and # 62987)) respectively according to a published protocol (62). The plasmid cloning was verified by sequencing using the U6 primer (5'-GAGGGCCTATTTCCCATGATTCC-3'). Cells were then transfected with PX461-gRNA-1 and PX462-gRNA-2 plasmids simultaneously using Lipofectamine® 3000 Transfection Reagent (Thermo Fisher Scientific) according to manufacturer's protocol. Following transfection, cells were selected with culture medium containing puromycin (1-2 μg/ml) for 24-48 hours. Cells that remained after selection were used to generate single cell clones via serial dilution or FACS. Single cell clones with gene knockout were selected and validated using western blots or functional assays. Pooled wild type (WT) clones or cells transfected with empty plasmids when WT clones were not available were used as controls.

Gene knockdown (KD) using shRNA

Cells were transfected with non-target shRNA control (SHC016V-1EA) or shRNA targeting mouse IRF1 (SHCLNV-NM_008390 (TRCN0000077441)) lentivirus particles (both from Sigma-Aldrich) using SureENTRY reagent according to the manufacturer's protocol. Transfected tumor cells were selected with puromycin (1.5 μg/ml) for 10-14 days. The efficiency of knockdown was assessed using immunoblot.

***Serpinb9* expression via lentiviral transfection**

Full-length mouse *Serpinb9* cDNA was amplified from the pCMV-SPORT6 vector (Dharmacon; Accession: BC029900; Clone ID: 4925100) using primers (forward, 5'-GCTCTAGAATGAATACTCTGTCTGAAGG-3', reverse, 5'-CGGGATCCTGGAGATGAGAACCTGCCAC-3') and inserted into the XbaI and BamHI sites of pCDH-CMV-MCS-EF1-Hygro vector (System Biosciences). The cloning of vector was validated by sequencing. This vector together with pMD2.G and pCMV-dR8.74 were used for transfection of 293T cells to produce lentiviral particles. Viral particles collected from the culture supernatants were used for transfection of cancer cells using the SureENTRY.

Clonogenic assay

Clonogenic assay was performed as previously described (12).

Cell proliferation assay

Cell proliferation was assessed using WST-1 (Sigma) according to manufacturer's protocol.

Assessment of Caspase 3/7 in cells via flow cytometry

The presence of caspase 3/7 in cells was assessed using CellEvent™ Caspase-3/7 Green Detection Reagent (ThermoFisher) according to manufacturer's protocol.

Assessment of cell cycle in cell using propidium Iodide

The cell cycle distribution in cells was assessed using Propidium Iodide Flow Cytometry kit (Abcam) according to manufacturer's protocol.

ELISA

Cell culture supernatants were collected from MC38 cells at 72 hours after mock or 10Gy IR. Mouse IFNβ protein levels in these supernatants were measured using the mouse IFN-beta ELISA Kit (R & D) according to manufacturer's protocol.

Immunoblotting

Immunoblotting was performed as previously described (12). Antibodies used in this study were listed in **Supplementary Table 1**.

Fluorescent staining and confocal imaging

Fluorescent staining was performed as previously described (12). Antibodies used in this study were listed in **Supplementary Table 1**.

Analysis of gene expression correlation between SERPINB9 and IFN signature in TCGA data

TCGA gene expression data (RNA-seq V2 RSEM) of 10 IFN signature genes (*CSF2RB*, *CD86*, *CD69*, *GBP1*, *BIRC3*, *RUNX3*, *STAT1*, *SERPING1*, *IFI16* and *IRF1*, derived from **Supplementary Table 5**) and *SERPINB9* in 16 different human cancer types was downloaded via cBioPortal (http://www.cbioportal.org/) and log2 transformed. The case numbers for each cancer type were as follows: Prostate Adenocarcinoma(PRAD), n = 498; Breast Invasive Carcinoma (BRCA), n = 1100; Thyroid Carcinoma (THCA), n = 509; Pancreatic Adenocarcinoma (PAAD), n = 178; Kidney Renal Clear Cell Carcinoma (KIRC), n = 446; Lung Adenocarcinoma (LUAD), n = 517; Kidney Renal Papillary Cell Carcinoma (KIRP), n = 291; Brain Lower Grade Glioma (LGG), n = 530; Lung Squamouse Cell Carcinoma (LUSC), n = 501; Bladder Urothelial Carcinoma (BLCA), n = 408; Colorectal Adenocarcinoma (COAD), n = 382; Liver Heptocellular Carcinoma (LIHC), n = 373; Head and Neck Squamouse Cell Carcinoma (HNSC), n = 522; Stomach Adenocarcinoma (STAD), n = 415; Skin Cutaneous Melanoma (SKCM), n = 472; Cervical Squamouse Cell Carcinoma and Endocervical Adenocarcionoma (CESC), n = 306. The correlation between IFN signature generated as the mean expression level of these 10 signature genes and *SERPINB9* was evaluted by Pearson's correlation. Pearson correlation coefficients (r) are indicated. All P values < 0.0001.

Statistics

All values in this study represent means (M) and standard deviations (SD) with the exception that bars in the growth curves of tumors show means and the standard

errors of the mean (SEM). Comparisons were performed using unpaired two-tailed student's t-test when data followed a normal distribution (evaluated using D'Agostino & Pearson omnibus normality test) and the Mann-Whitney U test when they did not or their normality could not be evaluated due to small sample size. Survival time was measured from the beginning of IR treatment until the date of mice being culled. Mice being culled due to radiation-induced dermatitis with complete tumor regression were defined as survival censoring and were counted as tumor-free. The survival curves for different groups of mice were generated using the Kaplan-Meier method. The log-rank test was used to compare the median survival time. P value: NS > 0.05; * P < 0.05; ** P < 0.01; *** P < 0.001. All graphs were plotted using Graphpad Prism 5.

References

1. Minn AJ, and Wherry EJ. Combination Cancer Therapies with Immune Checkpoint Blockade: Convergence on Interferon Signaling. *Cell.* 2016;165(2):272-5.
2. Deng L, Liang H, Fu S, Weichselbaum RR, and Fu YX. From DNA Damage to Nucleic Acid Sensing: A Strategy to Enhance Radiation Therapy. *Clin Cancer Res.* 2016;22(1):20-5.
3. Burnette BC, Liang H, Lee Y, Chlewicki L, Khodarev NN, Weichselbaum RR, et al. The efficacy of radiotherapy relies upon induction of type i interferon-dependent innate and adaptive immunity. *Cancer Res.* 2011;71(7):2488-96.
4. Deng L, Liang H, Xu M, Yang X, Burnette B, Arina A, et al. STING-Dependent Cytosolic DNA Sensing Promotes Radiation-Induced Type I Interferon-Dependent Antitumor Immunity in Immunogenic Tumors. *Immunity.* 2014;41(5):843-52.
5. Vanpouille-Box C, Alard A, Aryankalayil MJ, Sarfraz Y, Diamond JM, Schneider RJ, et al. DNA exonuclease Trex1 regulates radiotherapy-induced tumour immunogenicity. *Nat Commun.* 2017;8:15618.
6. Benci JL, Xu B, Qiu Y, Wu TJ, Dada H, Twyman-Saint Victor C, et al. Tumor Interferon Signaling Regulates a Multigenic Resistance Program to Immune Checkpoint Blockade. *Cell.* 2016;167(6):1540-54 e12.

7. Apetoh L, Ghiringhelli F, Tesniere A, Obeid M, Ortiz C, Criollo A, et al. Toll-like receptor 4-dependent contribution of the immune system to anticancer chemotherapy and radiotherapy. *Nat Med.* 2007;13(9):1050-9.
8. Lee Y, Auh SL, Wang Y, Burnette B, Meng Y, Beckett M, et al. Therapeutic effects of ablative radiation on local tumor require CD8+ T cells: changing strategies for cancer treatment. *Blood.* 2009;114(3):589-95.
9. Ngwa W, Irabor OC, Schoenfeld JD, Hesser J, Demaria S, and Formenti SC. Using immunotherapy to boost the abscopal effect. *Nature Reviews Cancer.* 2018;18(5):313-22.
10. Antonia SJ, Villegas A, Daniel D, Vicente D, Murakami S, Hui R, et al. Durvalumab after Chemoradiotherapy in Stage III Non-Small-Cell Lung Cancer. *N Engl J Med.* 2017;377(20):1919-29.
11. Ranoa DR, Parekh AD, Pitroda SP, Huang X, Darga T, Wong AC, et al. Cancer therapies activate RIG-I-like receptor pathway through endogenous non-coding RNAs. *Oncotarget.* 2016;7(18):26496-515.
12. Chen JZ, Markelc B, Kaeppler J, Ogundipe VML, Cao YH, McKenna WG, et al. STING-Dependent Interferon-lambda 1 Induction in HT29 Cells, a Human Colorectal Cancer Cell Line, After Gamma-Radiation. *Int J Radiat Oncol.* 2018;101(1):97-106.
13. Harding SM, Benci JL, Irianto J, Discher DE, Minn AJ, and Greenberg RA. Mitotic progression following DNA damage enables pattern recognition within micronuclei. *Nature.* 2017;548(7668):466-70.
14. Mackenzie KJ, Carroll P, Martin CA, Murina O, Fluteau A, Simpson DJ, et al. cGAS surveillance of micronuclei links genome instability to innate immunity. *Nature.* 2017;548(7668):461-5.
15. Reits EA, Hodge JW, Herberts CA, Groothuis TA, Chakraborty M, Wansley EK, et al. Radiation modulates the peptide repertoire, enhances MHC class I expression, and induces successful antitumor immunotherapy. *J Exp Med.* 2006;203(5):1259-71.
16. Gupta A, Probst HC, Vuong V, Landshammer A, Muth S, Yagita H, et al. Radiotherapy promotes tumor-specific effector CD8+ T cells via dendritic cell activation. *J Immunol.* 2012;189(2):558-66.
17. Vatner RE, and Janssen EM. STING, DCs and the link between innate and adaptive tumor immunity. *Mol Immunol.* 2017.
18. Twyman-Saint Victor C, Rech AJ, Maity A, Rengan R, Pauken KE, Stelekati E, et al. Radiation and dual checkpoint blockade activate non-redundant immune mechanisms in cancer. *Nature.* 2015;520(7547):373-7.
19. Rudqvist NP, Pilones KA, Lhuillier C, Wennerberg E, Sidhom JW, Emerson RO, et al. Radiotherapy and CTLA-4 Blockade Shape the TCR Repertoire of Tumor-Infiltrating T Cells. *Cancer Immunol Res.* 2018;6(2):139-50.
20. Dovedi SJ, Cheadle EJ, Popple AL, Poon E, Morrow M, Stewart R, et al. Fractionated Radiation Therapy Stimulates Antitumor Immunity Mediated by Both Resident and Infiltrating Polyclonal T-cell Populations when Combined with PD-1 Blockade. *Clin Cancer Res.* 2017;23(18):5514-26.

21. Matsumura S, Wang B, Kawashima N, Braunstein S, Badura M, Cameron TO, et al. Radiation-induced CXCL16 release by breast cancer cells attracts effector T cells. *J Immunol.* 2008;181(5):3099-107.
22. Ruocco MG, Pilones KA, Kawashima N, Cammer M, Huang J, Babb JS, et al. Suppressing T cell motility induced by anti-CTLA-4 monotherapy improves antitumor effects. *J Clin Invest.* 2012;122(10):3718-30.
23. Weichselbaum RR, Ishwaran H, Yoon T, Nuyten DSA, Baker SW, Khodarev N, et al. An interferon-related gene signature for DNA damage resistance is a predictive marker for chemotherapy and radiation for breast cancer. *P Natl Acad Sci USA.* 2008;105(47):18490-5.
24. Boelens MC, Wu TJ, Nabet BY, Xu B, Qiu Y, Yoon T, et al. Exosome transfer from stromal to breast cancer cells regulates therapy resistance pathways. *Cell.* 2014;159(3):499-513.
25. Erdal E, Haider S, Rehwinkel J, Harris AL, and McHugh PJ. A prosurvival DNA damage-induced cytoplasmic interferon response is mediated by end resection factors and is limited by Trex1. *Gene Dev.* 2017;31(4):353-69.
26. Post AEM, Smid M, Nagelkerke A, Martens JWM, Bussink J, Sweep FC, et al. Interferon-stimulated genes are involved in cross-resistance to radiotherapy in tamoxifen-resistant breast cancer. *Clin Cancer Res.* 2018.
27. Deng LF, Liang H, Burnette B, Beckett M, Darga T, Weichselbaum RR, et al. Irradiation and anti-PD-L1 treatment synergistically promote antitumor immunity in mice. *Journal of Clinical Investigation.* 2014;124(2):687-95.
28. Dovedi SJ, Adlard AL, Lipowska-Bhalla G, McKenna C, Jones S, Cheadle EJ, et al. Acquired Resistance to Fractionated Radiotherapy Can Be Overcome by Concurrent PD-L1 Blockade. *Cancer Research.* 2014;74(19):5458-68.
29. Liang H, Deng L, Hou Y, Meng X, Huang X, Rao E, et al. Host STING-dependent MDSC mobilization drives extrinsic radiation resistance. *Nat Commun.* 2017;8(1):1736.
30. Filatenkov A, Baker J, Mueller AMS, Kenkel J, Ahn GO, Dutt S, et al. Ablative Tumor Radiation Can Change the Tumor Immune Cell Microenvironment to Induce Durable Complete Remissions. *Clin Cancer Res.* 2015;21(16):3727-39.
31. Juneja VR, McGuire KA, Manguso RT, LaFleur MW, Collins N, Haining WN, et al. PD-L1 on tumor cells is sufficient for immune evasion in immunogenic tumors and inhibits CD8 T cell cytotoxicity. *Journal of Experimental Medicine.* 2017;214(4):895-904.
32. Medema JP, de Jong J, Peltenburg LTC, Verdegaal EME, Gorter A, Bres SA, et al. Blockade of the granzyme B/perforin pathway through overexpression of the serine protease inhibitor PI-9/SPI-6 constitutes a mechanism for immune escape by tumors. *P Natl Acad Sci USA.* 2001;98(20):11515-20.
33. Lickliter JD, Cox J, McCarron J, Martinez NR, Schmidt CW, Lin H, et al. Small-molecule Bcl-2 inhibitors sensitise tumour cells to immune-mediated destruction. *Br J Cancer.* 2007;96(4):600-8.
34. Zheng P, Sarma S, Guo Y, and Liu Y. Two mechanisms for tumor evasion of preexisting cytotoxic T-cell responses: lessons from recurrent tumors. *Cancer Res.* 1999;59(14):3461-7.

35. Restifo NP, Marincola FM, Kawakami Y, Taubenberger J, Yannelli JR, and Rosenberg SA. Loss of functional beta 2-microglobulin in metastatic melanomas from five patients receiving immunotherapy. *J Natl Cancer Inst.* 1996;88(2):100-8.
36. Bird CH, Sutton VR, Sun JR, Hirst CE, Novak A, Kumar S, et al. Selective regulation of apoptosis: the cytotoxic lymphocyte serpin proteinase inhibitor 9 protects against granzyme B-mediated apoptosis without perturbing the Fas cell death pathway. *Mol Cell Biol.* 1998;18(11):6387-98.
37. Paludan SR, and Bowie AG. Immune sensing of DNA. *Immunity.* 2013;38(5):870-80.
38. Purbey PK, Scumpia PO, Kim PJ, Tong AJ, Iwamoto KS, McBride WH, et al. Defined Sensing Mechanisms and Signaling Pathways Contribute to the Global Inflammatory Gene Expression Output Elicited by Ionizing Radiation. *Immunity.* 2017;47(3):421-34 e3.
39. Blank C, Brown I, Peterson AC, Spiotto M, Iwai Y, Honjo T, et al. PD-L1/B7H-1 inhibits the effector phase of tumor rejection by T cell receptor (TCR) transgenic CD8+ T cells. *Cancer Res.* 2004;64(3):1140-5.
40. Taube JM, Anders RA, Young GD, Xu H, Sharma R, McMiller TL, et al. Colocalization of inflammatory response with B7-h1 expression in human melanocytic lesions supports an adaptive resistance mechanism of immune escape. *Sci Transl Med.* 2012;4(127):127ra37.
41. Spranger S, Spaapen RM, Zha Y, Williams J, Meng Y, Ha TT, et al. Up-Regulation of PD-L1, IDO, and T-regs in the Melanoma Tumor Microenvironment Is Driven by CD8(+) T Cells. *Science Translational Medicine.* 2013;5(200).
42. Garcia-Diaz A, Shin DS, Moreno BH, Saco J, Escuin-Ordinas H, Rodriguez GA, et al. Interferon Receptor Signaling Pathways Regulating PD-L1 and PD-L2 Expression. *Cell Rep.* 2017;19(6):1189-201.
43. Sistigu A, Yamazaki T, Vacchelli E, Chaba K, Enot DP, Adam J, et al. Cancer cell-autonomous contribution of type I interferon signaling to the efficacy of chemotherapy. *Nat Med.* 2014;20(11):1301-9.
44. Katlinski KV, Gui J, Katlinskaya YV, Ortiz A, Chakraborty R, Bhattacharya S, et al. Inactivation of Interferon Receptor Promotes the Establishment of Immune Privileged Tumor Microenvironment. *Cancer Cell.* 2017;31(2):194-207.
45. Yang X, Zhang X, Fu ML, Weichselbaum RR, Gajewski TF, Guo Y, et al. Targeting the tumor microenvironment with interferon-beta bridges innate and adaptive immune responses. *Cancer Cell.* 2014;25(1):37-48.
46. Liu J, Hamrouni A, Wolowiec D, Coiteux V, Kuliczkowski K, Hetuin D, et al. Plasma cells from multiple myeloma patients express B7-H1 (PD-L1) and increase expression after stimulation with IFN-{gamma} and TLR ligands via a MyD88-, TRAF6-, and MEK-dependent pathway. *Blood.* 2007;110(1):296-304.
47. Sun JR, Bird CH, Sutton V, McDonald L, Coughlin PB, DeJong TA, et al. A cytosolic granzyme B inhibitor related to the viral apoptotic regulator cytokine response modifier a is present in cytotoxic lymphocytes. *Journal of Biological Chemistry.* 1996;271(44):27802-9.

48. Cunningham TD, Jiang XG, and Shapiro DJ. Expression of high levels of human proteinase inhibitor 9 blocks both perforin/granzyme and Fas/Fas ligand-mediated cytotoxicity. *Cell Immunol.* 2007;245(1):32-41.
49. Jiang X, Ellison SJ, Alarid ET, and Shapiro DJ. Interplay between the levels of estrogen and estrogen receptor controls the level of the granzyme inhibitor, proteinase inhibitor 9 and susceptibility to immune surveillance by natural killer cells. *Oncogene.* 2007;26(28):4106-14.
50. Pan D, Kobayashi A, Jiang P, Ferrari de Andrade L, Tay RE, Luoma AM, et al. A major chromatin regulator determines resistance of tumor cells to T cell-mediated killing. *Science.* 2018;359(6377):770-5.
51. Jiang P, Gu S, Pan D, Fu J, Sahu A, Hu X, et al. Signatures of T cell dysfunction and exclusion predict cancer immunotherapy response. *Nat Med.* 2018.
52. Kanamori H, Krieg S, Mao CJ, Di Pippo VA, Wang S, Zajchowski DA, et al. Proteinase inhibitor 9, an inhibitor of granzyme B-mediated apoptosis, is a primary estrogen-inducible gene in human liver cells. *Journal of Biological Chemistry.* 2000;275(8):5867-73.
53. Holmquist-Mengelbier L, Fredlund E, Lofstedt T, Noguera R, Navarro S, Nilsson H, et al. Recruitment of HIF-1 alpha and HIF-2 alpha to common target genes is differentially regulated in neuroblastoma: HIF-2 alpha promotes an aggressive phenotype. *Cancer Cell.* 2006;10(5):413-23.
54. Heutinck KM, Kassies J, Florquin S, ten Berge IJM, Hamann J, and Rowshani AT. SerpinB9 expression in human renal tubular epithelial cells is induced by triggering of the viral dsRNA sensors TLR3, MDA5 and RIG-I. *Nephrol Dial Transpl.* 2012;27(7):2746-54.
55. Kannan-Thulasiraman P, and Shapiro DJ. Modulators of inflammation use nuclear factor-B-K and activator protein-1 sites to induce the caspase-1 and granzyme B inhibitor, proteinase inhibitor 9. *Journal of Biological Chemistry.* 2002;277(43):41230-9.
56. Barrie MB, Stout HW, Abougergi MS, Miller BC, and Thiele DL. Antiviral cytokines induce hepatic expression of the granzyme B inhibitors, proteinase inhibitor 9 and serine proteinase inhibitor 6. *J Immunol.* 2004;172(10):6453-9.
57. Zhang M, Park SM, Wang Y, Shah R, Liu N, Murmann AE, et al. Serine protease inhibitor 6 protects cytotoxic T cells from self-inflicted injury by ensuring the integrity of cytotoxic granules. *Immunity.* 2006;24(4):451-61.
58. Ida H, Nakashima T, Kedersha NL, Yamasaki S, Huang M, Izumi Y, et al. Granzyme B leakage-induced cell death: a new type of activation-induced natural killer cell death. *Eur J Immunol.* 2003;33(12):3284-92.
59. Bird CH, Christensen ME, Mangan MS, Prakash MD, Sedelies KA, Smyth MJ, et al. The granzyme B-Serpinb9 axis controls the fate of lymphocytes after lysosomal stress. *Cell Death Differ.* 2014;21(6):876-87.
60. Mangan MS, Vega-Ramos J, Joeckel LT, Mitchell AJ, Rizzitelli A, Roediger B, et al. Serpinb9 is a marker of antigen cross-presenting dendritic cells. *Mol Immunol.* 2017;82:50-6.
61. Mangan MS, Melo-Silva CR, Luu J, Bird CH, Koskinen A, Rizzitelli A, et al. A pro-survival role for the intracellular granzyme B inhibitor Serpinb9 in natural killer cells during poxvirus infection. *Immunol Cell Biol.* 2017;95(10):884-94.

62. Ran FA, Hsu PD, Wright J, Agarwala V, Scott DA, and Zhang F. Genome engineering using the CRISPR-Cas9 system. *Nat Protoc.* 2013;8(11):2281-308.

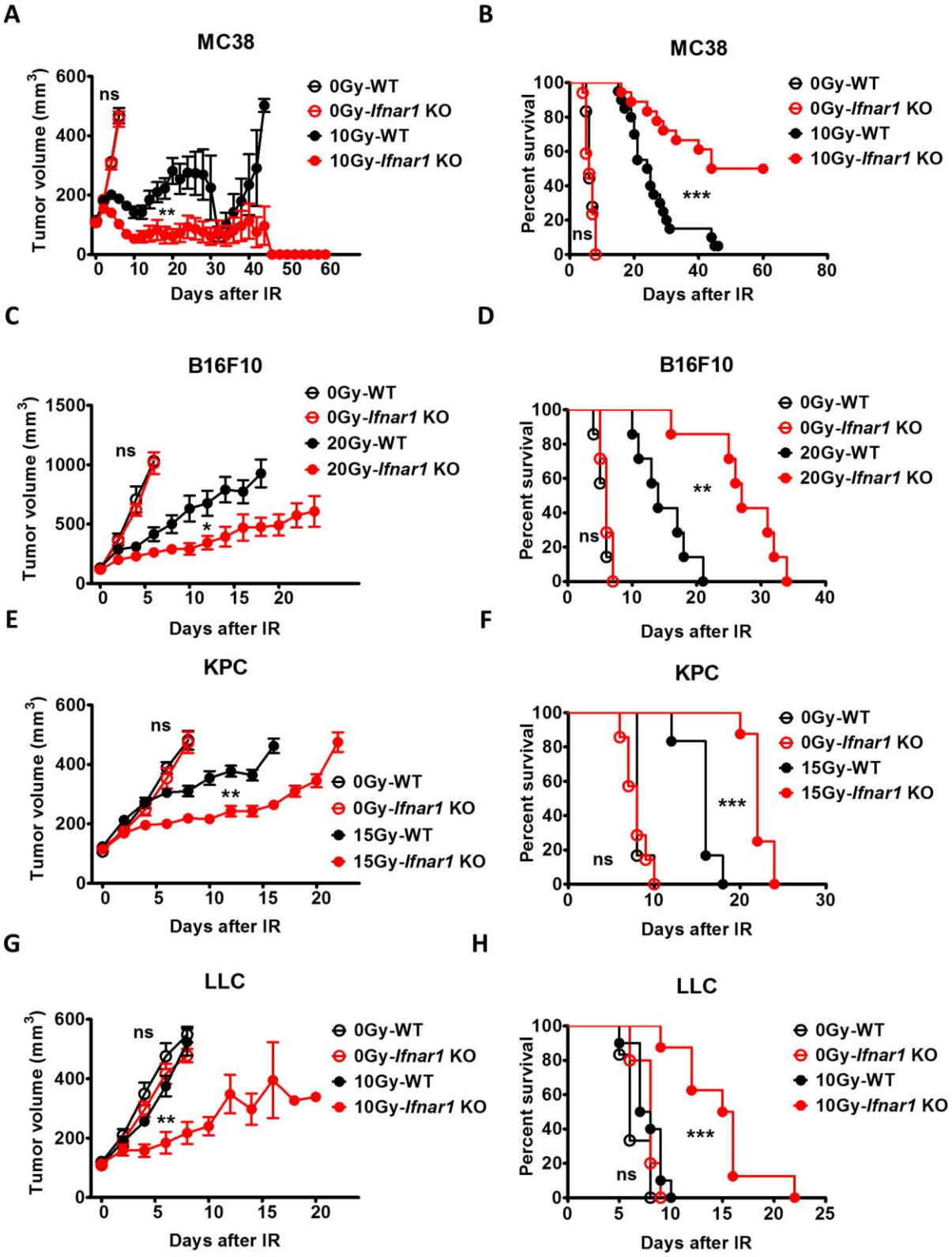

A
MC38
Tumor volume (mm3)
Days after IR
0Gy-WT
0Gy-Ifnar1 KO
10Gy-WT
10Gy-Ifnar1 KO
ns
**
B
MC38
Percent survival
Days after IR
0Gy-WT
0Gy-Ifnar1 KO
10Gy-WT
10Gy-Ifnar1 KO
***
ns
C
B16F10
Tumor volume (mm3)
Days after IR
0Gy-WT
0Gy-Ifnar1 KO
20Gy-WT
20Gy-Ifnar1 KO
ns
*
D
B16F10
Percent survival
Days after IR
0Gy-WT
0Gy-Ifnar1 KO
20Gy-WT
20Gy-Ifnar1 KO
**
ns
E
KPC
Tumor volume (mm3)
Days after IR
0Gy-WT
0Gy-Ifnar1 KO
15Gy-WT
15Gy-Ifnar1 KO
ns
**
F
KPC
Percent survival
Days after IR
0Gy-WT
0Gy-Ifnar1 KO
15Gy-WT
15Gy-Ifnar1 KO
***
ns
G
LLC
Tumor volume (mm3)
Days after IR
0Gy-WT
0Gy-Ifnar1 KO
10Gy-WT
10Gy-Ifnar1 KO
ns
**
H
LLC
Percent survival
Days after IR
0Gy-WT
0Gy-Ifnar1 KO
10Gy-WT
10Gy-Ifnar1 KO
***
ns

Figure 1. *Ifnar1* KO in cancer cells enhanced tumor response to ionizing radiation. Tumors in C57BL/6 mice derived from the indicated cancer cell lines with or without *Ifnar1* KO, including MC38 **(A** and **B)**, B16F10 **(C** and **D)**, KPC **(E** and **F)** and LLC **(G** and **H)** received 0Gy or the indicated single doses of IR. Tumor volumes are summarized in **(A**, **C**, **E** and **G)**. Kaplan-Meier survival curves from the same experiment are plotted in **(B**, **D**, **F** and **H)**. N= 7-18 in control groups and 8-20 in irradiation groups. Error bars are ± SEM. Comparison of two means was performed by the Mann-Whitney U test. Survival comparison between groups were performed using log-rank's test (ns: $P > 0.05$, * $P < 0.05$, ** $P< 0.01$, *** $P< 0.001$).

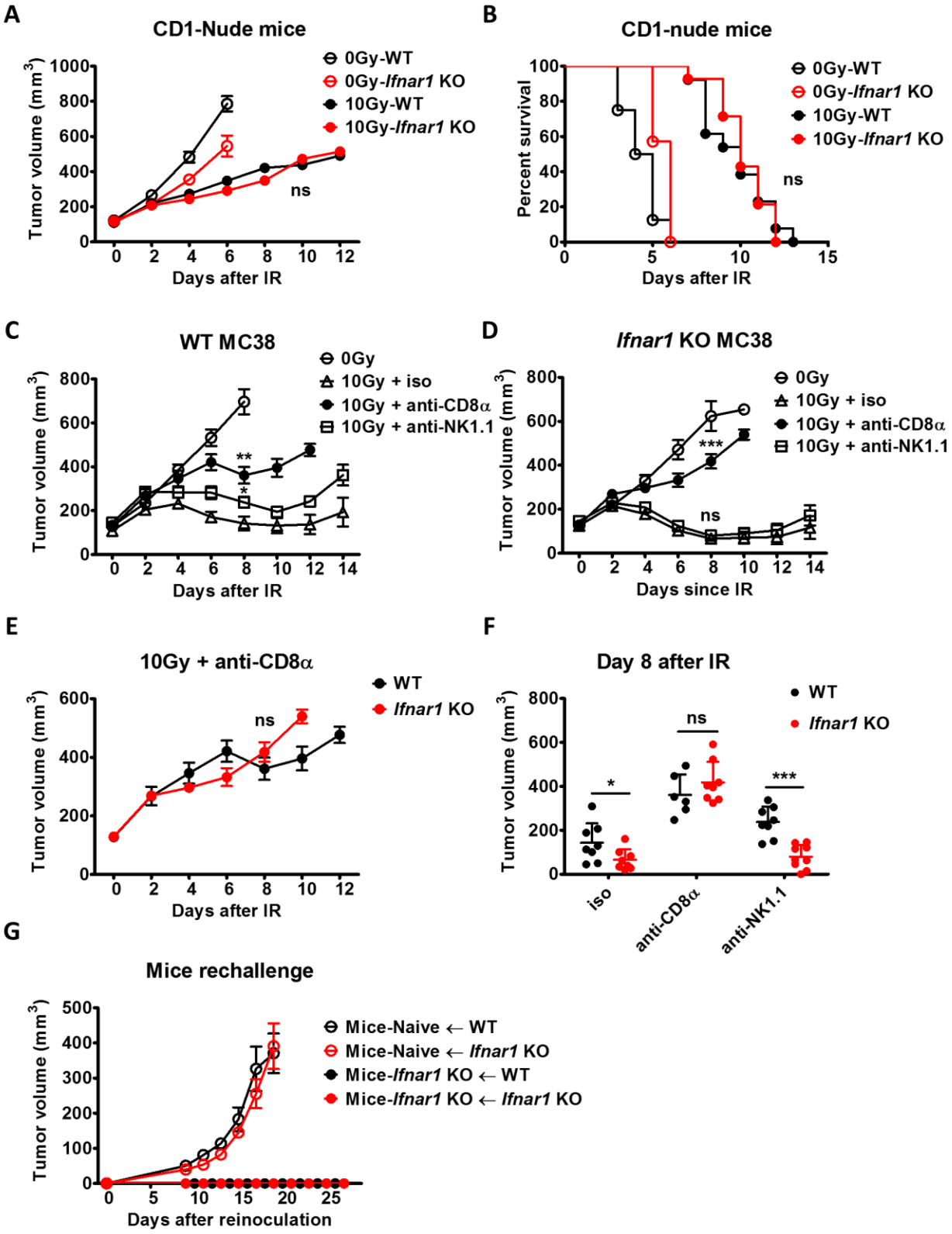

A
CD1-Nude mice
Tumor volume (mm3)
Days after IR
0Gy-WT
0Gy-Ifnar1 KO
10Gy-WT
10Gy-Ifnar1 KO
ns
B
CD1-nude mice
Percent survival
Days after IR
0Gy-WT
0Gy-Ifnar1 KO
10Gy-WT
10Gy-Ifnar1 KO
ns
C
WT MC38
Tumor volume (mm3)
Days after IR
0Gy
10Gy + iso
10Gy + anti-CD8α
10Gy + anti-NK1.1
**
*
D
Ifnar1 KO MC38
Tumor volume (mm3)
Days since IR
0Gy
10Gy + iso
10Gy + anti-CD8α
10Gy + anti-NK1.1
***
ns
E
10Gy + anti-CD8α
Tumor volume (mm3)
Days after IR
WT
Ifnar1 KO
ns
F
Day 8 after IR
Tumor volume (mm3)
WT
Ifnar1 KO
*
ns
***
iso
anti-CD8α
anti-NK1.1
G
Mice rechallenge
Tumor volume (mm3)
Days after reinoculation
Mice-Naive ← WT
Mice-Naive ← Ifnar1 KO
Mice-Ifnar1 KO ← WT
Mice-Ifnar1 KO ← Ifnar1 KO

Figure 2. The enhanced response of *Ifnar1* KO tumors to IR is mediated by CD8 T cell immunity. MC38 tumors (WT and *Ifnar1* KO) grown in CD1-nude mice were treated with 0Gy (N = 7-8) or 10 Gy (N = 13-14) IR. Tumor volumes and mouse survival were assessed and summarized in **(A)** and **(B)**, respectively. C57BL/6 mice bearing subcutaneous WT MC38 **(C)** or *Ifnar1* KO **(D)** MC38 tumors were subjected to the following treatments: (1) 0 Gy IR; (2) 10 Gy IR on day 0 plus isotype control Abs; (3) 10 Gy IR plus anti-CD8α Ab; (4) 10Gy IR plus anti-NK1.1 Ab. Abs were administered on days -1, 2, 5, 8 and 11. N = 8-10. WT **(C)** or *Ifnar1* KO **(D**) tumors with either CD8 T cells or NK cells depleted were compared with tumors receiving isotype control Abs. The growth of WT and *Ifnar1* KO MC38 tumors following 10Gy IR with CD8 T cell depletion were plotted in **(E)**. The mean volume of tumors at day 8 after IR was compared between WT and *Ifnar1* KO **(F)**. C57BL/6 mice, with completely regressed *Ifnar1* KO MC38 tumors after IR were rechallenged with 1 x 10^5 WT or *Ifnar1* KO MC38 cell on the other flank. The growth of tumors following reinoculation was plotted in **(G)**. N = 4-6. Data show mean ± SEM in **(A**-**E)** and **(G)**, and mean ± SD in **F**. Comparison of two means was performed by the unpaired student's t test when data followed a normal distribution and the Mann-Whitney U test when they did not or their normality cannot be evaluated (ns: P > 0.05, * P < 0.05, ** P< 0.01, *** P< 0.001).

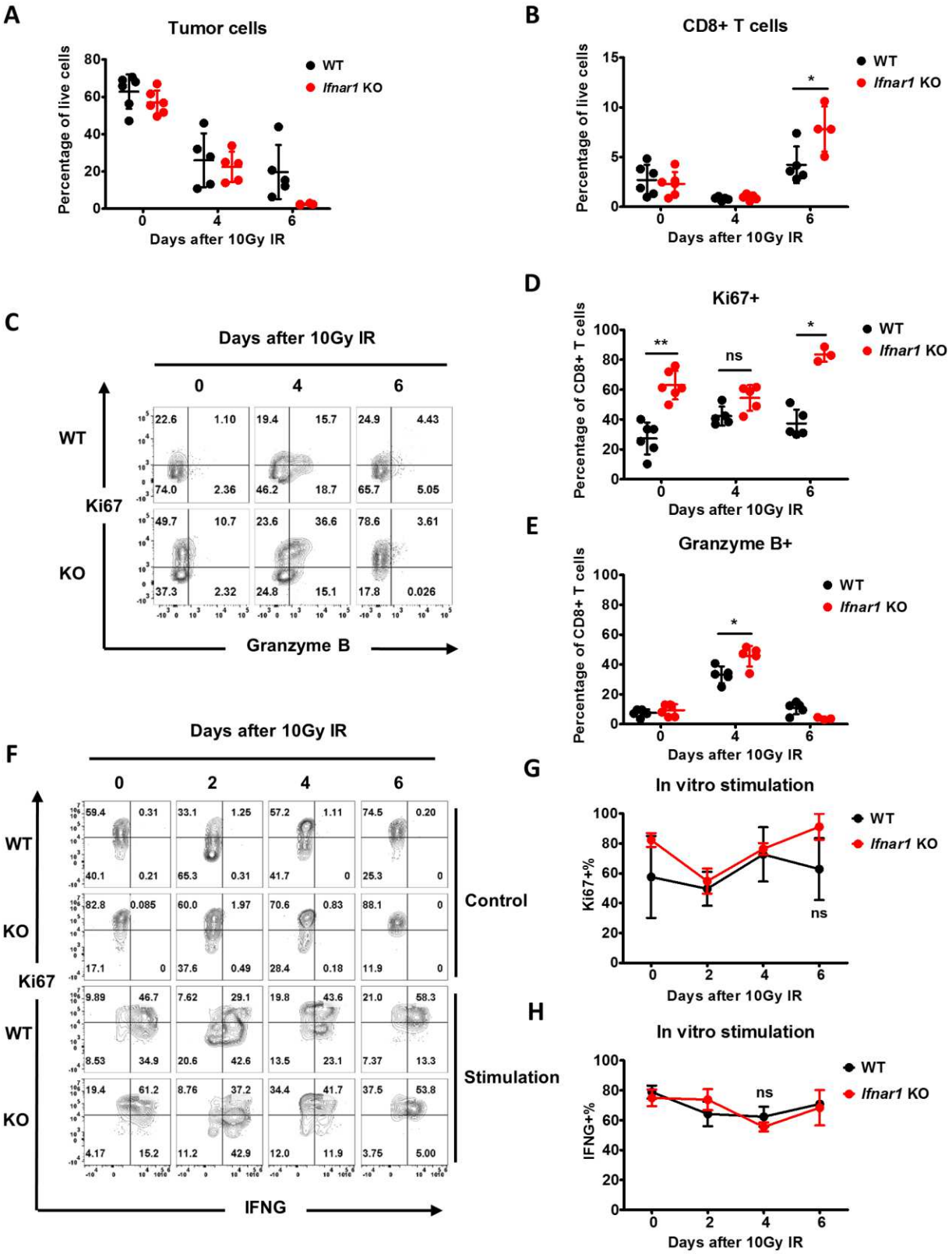

A
Tumor cells
Percentage of live cells
WT
Ifnar1 KO
Days after 10Gy IR
B
CD8+ T cells
Percentage of live cells
WT
Ifnar1 KO
*
Days after 10Gy IR
C
Days after 10Gy IR
0
4
6
WT
Ki67
KO
22.6
1.10
74.0
2.36
19.4
15.7
46.2
18.7
24.9
4.43
65.7
5.05
49.7
10.7
37.3
2.32
23.6
36.6
24.8
15.1
78.6
3.61
17.8
0.026
Granzyme B
D
Ki67+
Percentage of CD8+ T cells
WT
Ifnar1 KO
**
ns
*
Days after 10Gy IR
E
Granzyme B+
Percentage of CD8+ T cells
WT
Ifnar1 KO
*
Days after 10Gy IR
F
Days after 10Gy IR
0
2
4
6
WT
KO
Ki67
59.4
0.31
40.1
0.21
33.1
1.25
65.3
0.31
57.2
1.11
41.7
0
74.5
0.20
25.3
0
82.8
0.085
17.1
0
60.0
1.97
37.6
0.49
70.6
0.83
28.4
0.18
88.1
0
11.9
0
Control
9.89
46.7
8.53
34.9
7.62
29.1
20.6
42.6
19.8
43.6
13.5
23.1
21.0
58.3
7.37
13.3
19.4
61.2
4.17
15.2
8.76
37.2
11.2
42.9
34.4
41.7
12.0
11.9
37.5
53.8
3.75
5.00
Stimulation
IFNG
G
In vitro stimulation
Ki67+%
WT
Ifnar1 KO
ns
Days after 10Gy IR
H
In vitro stimulation
IFNG+%
WT
Ifnar1 KO
ns
Days after 10Gy IR

Figure 3 Characterization of infiltrating CD8 T cells from *Ifnar1* KO MC38 and WT tumors. WT MC38 or *Ifnar1* KO tumors in C57BL/6 mice were subjected to 0 Gy or 10 Gy IR. At day 0, before IR, and days 4 and 6 after IR, tumors were harvested and disaggregated for cell type profiling using flow cytometry. Percentages of tumor cells and CD8 T cells out of the total of live cells are plotted in **(A)** and **(B)**. N = 5-6. Representative flow cytometry plots characterizing gated CD8 T cells are shown in **(C)** with Ki67 on the Y axis displayed against Granzyme B on the X axis. Percentages of Ki67 and Granzyme B positive CD8 T cells in WT or *Ifnar1* KO tumors with or without IR are summarized in **(D)** and **(E)**. N = 5-6. CD8 T cells isolated from WT or *Ifnar1* KO MC38 tumors at day 0, 2, 4, 6 following 10Gy IR, were stimulated with PMA, ionomycin and Brefeldin A for 4 hours, and assessed by flow cytometry (representative plot shown in **(F)**). The percentages of Ki67 or IFNG positive CD8 T cells are plotted in **(G)** and **(H)**. N = 3-4. Data represent mean ± SD. Comparison of two means was performed by the Mann-Whitney U test (ns: $P > 0.05$, * $P < 0.05$, ** $P< 0.01$, *** $P< 0.001$).

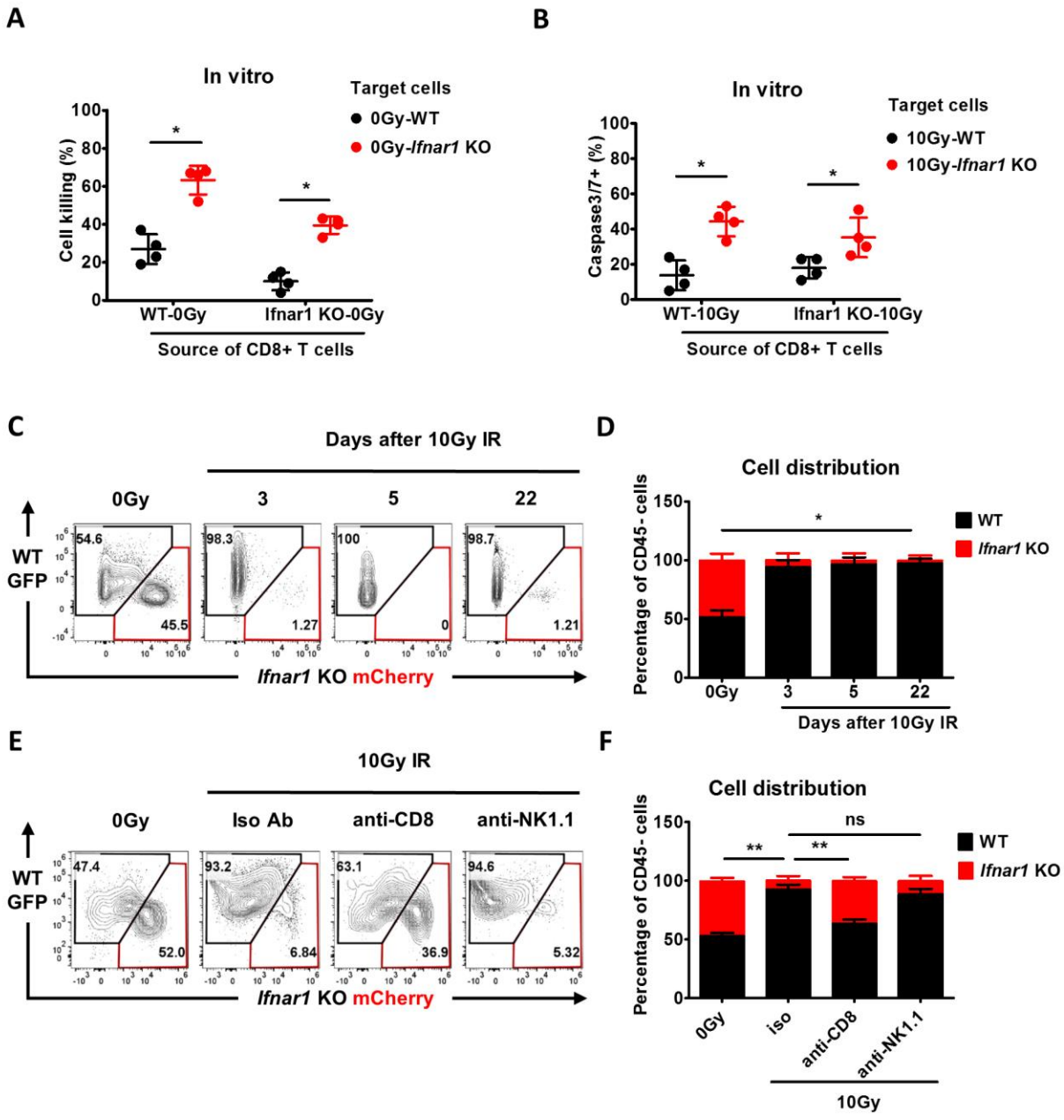
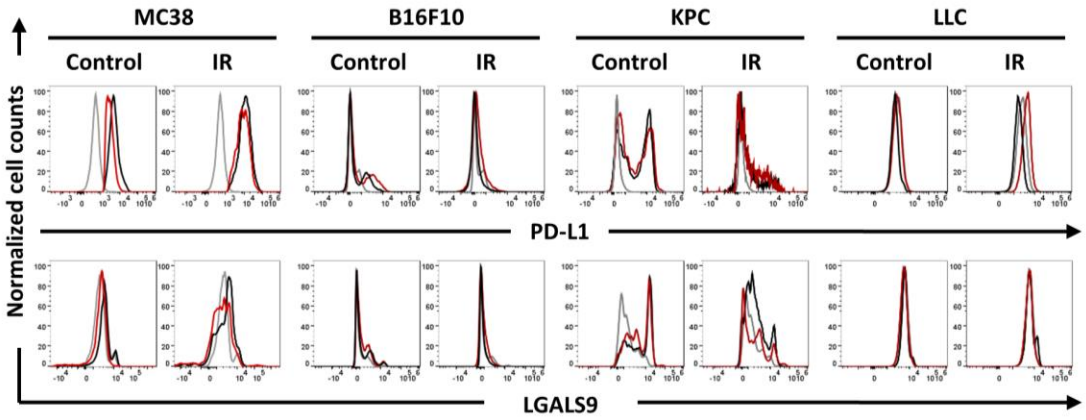

A
In vitro
Target cells
0Gy-WT
0Gy-Ifnar1 KO
Cell killing (%)
WT-0Gy
Ifnar1 KO-0Gy
Source of CD8+ T cells
B
In vitro
Target cells
10Gy-WT
10Gy-Ifnar1 KO
Caspase3/7+ (%)
WT-10Gy
Ifnar1 KO-10Gy
Source of CD8+ T cells
C
Days after 10Gy IR
0Gy
3
5
22
WT GFP
Ifnar1 KO mCherry
54.6
45.5
98.3
1.27
100
0
98.7
1.21
D
Cell distribution
Percentage of CD45- cells
WT
Ifnar1 KO
0Gy
3
5
22
Days after 10Gy IR
E
10Gy IR
0Gy
Iso Ab
anti-CD8
anti-NK1.1
WT GFP
Ifnar1 KO mCherry
47.4
52.0
93.2
6.84
63.1
36.9
94.6
5.32
F
Cell distribution
Percentage of CD45- cells
ns
WT
Ifnar1 KO
0Gy
iso
anti-CD8
anti-NK1.1
10Gy

Figure 4. *Ifnar1* KO MC38 tumor cells are more susceptible to CD8 T cells mediated killing. WT and *Ifnar1* KO MC38 cells were co-cultured with CD8 T cells derived from either WT or *Ifnar1* KO MC38 tumors at a ratio of CD8 T cells: tumor cells of 3:2 for 48 hours. The percentage of cell killing is shown in **(A)**. N = 4. Irradiated MC38 cells (WT or *Ifnar1* KO) were co-cultured with CD8 T cells derived from irradiated WT or *Ifnar1* KO MC38 tumors in a ratio of 3:2. Cells in media supplemented with Caspase-3/7 Green detection reagent were imaged with an epifluorescence microscope. The percentage of tumor cells becoming caspase 3/7+ following interaction with CD8 T cells was evaluated and plotted in **(B)**. N = 4. GFP-tagged WT MC38 cells and mCherry-tagged *Ifnar1* KO MC38 cells at a ratio of 1:1 were injected subcutaneously into C57BL6 mice. Established tumors were subjected to 0 Gy or 10 Gy IR at day 0. At days 3 and 5, and 22 for irradiated tumors, the percentages of GFP and mCherry positive cells in the CD45 negative population were assessed by flow cytometry (representative plot in **(C)** and summary in **(D)**). N =4. Tumors formed from a mixture of cells (MC38 WT-GFP + *Ifnar1*-mCherry 1:1) were subjected to the following: 0Gy, 10 Gy (day 0) + isotype control Abs, 10 Gy + anti-CD8 Ab and 10 Gy + anti-NK1.1 Ab. The distribution of GFP vs mCherry cells in the CD45 negative live population at day 3 was assessed by flow cytometry (representative plot in **(E)** and quantification in **(F)**). N = 5. Data represent mean ± SD. Comparison of two means was performed by the Mann-Whitney U test (ns: $P > 0.05$, * $P < 0.05$, ** $P< 0.01$, *** $P< 0.001$).

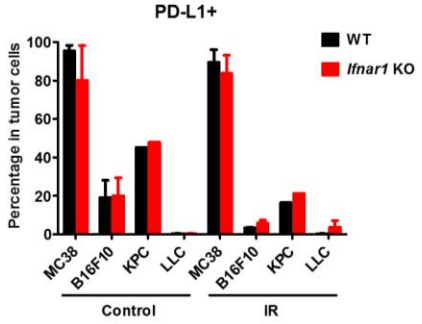
A

Genes	MC38		B16F10	
	IR/control	*Ifnar1* KO/WT	IR/control	*Ifnar1* KO/WT
Serpinb9	1.6 ↑ *	1.5 ↓ *	–	1.5 ↓ *
Serpinb9b	ND	ND	–	ND
Bcl2	1.1 ↑	1.2 ↑	–	1.4 ↑
Bcl2l1	1.3 ↑	1.1 ↑	–	1.1 ↑
Cd274	3.5 ↑ *	1.2 ↑	–	1.9 ↑ *
Lgals9	2.9 ↑ *	1.2 ↓	–	1.5 ↓
Pvr	1.7 ↑ *	1.7 ↓ *	–	1.1 ↑
H2-K1	1.7 ↑ *	1.3↓	–	1.6 ↑

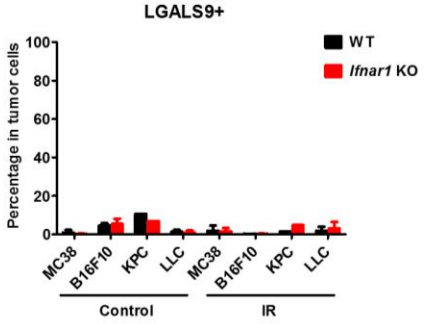
B



C



D



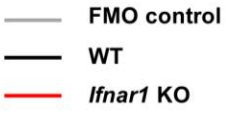


Figure 5 Screening of candidate mediators. Expression of candidate mediators was assessed from cancer cells in tumors. Cancer cells (gating in methods) were sorted from WT or *Ifnar1* KO MC38 or B16F10 tumors 72 hours following 0Gy or IR. RNA from these cells were analyzed by qPCR for *Serpinb9*, *Serpinb9b*, *Bcl2*, *Bcl2l1*, *Cd274*, *Lgals9*, *Pvr*, and *H2-K1*. *Serpinb9b* was not detected (ND). Too few live cells were obtained from irradiated B16F10 tumors for analysis. Gene expression in WT cells from irradiated tumors was normalized to expression in control WT tumors. Gene expression in *Ifnar1* KO cells from control tumors was normalized to expression in WT control tumors. Increases are shown with an upward arrow. Decreased expression is shown as negative reciprocals and a downward arrow. Changes of gene expression are summarized in **(A)** with significance indicated by *. N = 4. The abundance of PD-L1 and LGALS9 on the surface of cells from either WT or *Ifnar1* KO tumors at day 4 following 0Gy or IR was assessed by flow cytometry in tumors from indicated cell lines. Cells stained with Fluorescence Minus One (FMO) were negative controls (grey line), WT cells in black and *Ifnar1* KO in red **(B)**. The percentages of PD-L1 (CD274) and LGALS9 positive cells are summarized in **(C)** and **(D)**. N = 5-6 except KPC where n=1 due to the necessity of pooling samples to obtain sufficient material for analysis. Data represent mean ± SD. Comparison of two means was performed by the Mann-Whitney U test (ns: $P > 0.05$, * $P < 0.05$, ** $P < 0.01$, *** $P < 0.001$).

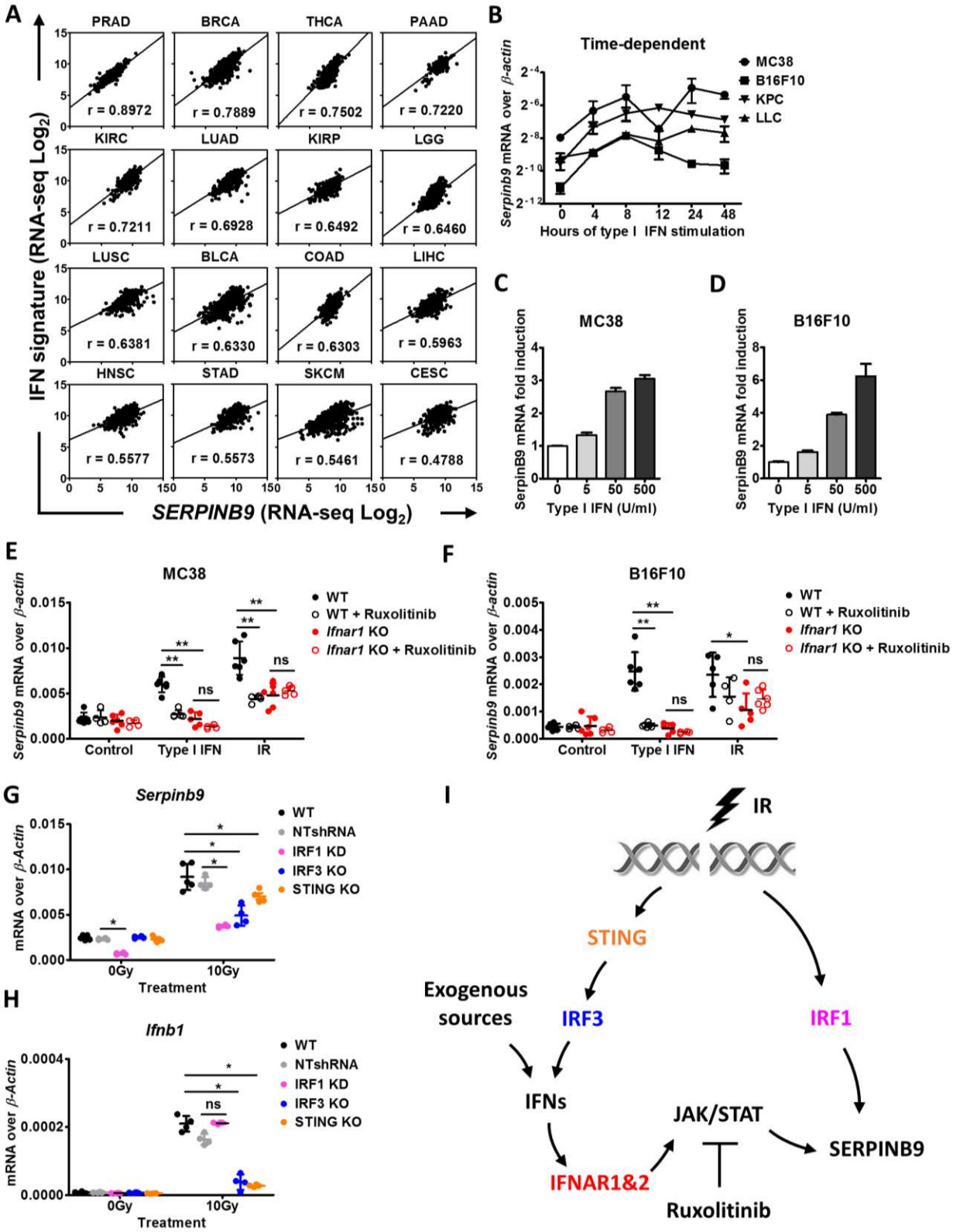

A
PRAD
BRCA
THCA
PAAD
r = 0.8972
r = 0.7889
r = 0.7502
r = 0.7220
KIRC
LUAD
KIRP
LGG
r = 0.7211
r = 0.6928
r = 0.6492
r = 0.6460
LUSC
BLCA
COAD
LIHC
r = 0.6381
r = 0.6330
r = 0.6303
r = 0.5963
HNSC
STAD
SKCM
CESC
r = 0.5577
r = 0.5573
r = 0.5461
r = 0.4788
IFN signature (RNA-seq Log2)
SERPINB9 (RNA-seq Log2)
B
Time-dependent
MC38
B16F10
KPC
LLC
Serpinb9 mRNA over β-actin
Hours of type I IFN stimulation
C
MC38
SerpinB9 mRNA fold induction
Type I IFN (U/ml)
D
B16F10
SerpinB9 mRNA fold induction
Type I IFN (U/ml)
E
MC38
Serpinb9 mRNA over β-actin
WT
WT + Ruxolitinib
Ifnar1 KO
Ifnar1 KO + Ruxolitinib
Control
Type I IFN
IR
F
B16F10
G
Serpinb9
mRNA over β-Actin
WT
NTshRNA
IRF1 KD
IRF3 KO
STING KO
0Gy
10Gy
Treatment
H
Ifnb1
I
IR
STING
Exogenous sources
IRF3
IRF1
IFNs
JAK/STAT
SERPINB9
IFNAR1&2
Ruxolitinib

Figure 6 *Serpinb9* is induced by type I IFN signaling in cancer cells. (A): Correlation of SERPINB9 expression with IFN signature genes in 16 different human cancer types from TCGA database was evaluated by Pearson's correlation. Pearson correlation coefficients (r) are indicated. All P values < 0.0001. **(B)**: *Serpinb9* expression in cancer cells (MC38, B16F10, KPC and LLC) after exposure to type I IFN (50 U/ml) over 48 hours. N = 3. **(C)** and **(D)**: *Serpinb9* expression in MC38 and B16F10 cells after exposure to the indicated concentration of type I IFN (0-500 U/ml) after 4 hours. N = 3. **(E)** and **(F)**: *Serpinb9* expression in MC38 and B16F10 cells (WT vs *Ifnar1* KO) at 4 hours after exposure to type I IFN (50 U/ml) or 72 hours after IR (10Gy for MC38 and 20Gy for B16F10 cells) with or without Ruxolitinib. Dimethyl sulfoxide (final v/v 0.5%) or Ruxolitinib (final concentration 2.5μM) was added to the medium 1 hour before IFN or IR treatment and remained in the medium through the experiment. N = 4-6. **(G)** and **(H)**: *Serpinb9* and *Ifnb1* expression in MC38 (WT, WT cells transfected with non-targeting shRNA lentivirus (NTshRNA), IRF1 knockdown (KD), IRF3 KO and STING KO at 72 hours after 10Gy. N = 4. Gene expression was assessed by RT-qPCR. All mRNA expression levels were normalized to *β-actin*. **(I)** Scheme for induction of *Serpinb9* in cancer cells after type I IFN or IR. Data represent mean ± SD. Comparison of two means was performed by the Mann-Whitney U test (ns: P > 0.05, * P < 0.05, ** P< 0.01, *** P< 0.001).

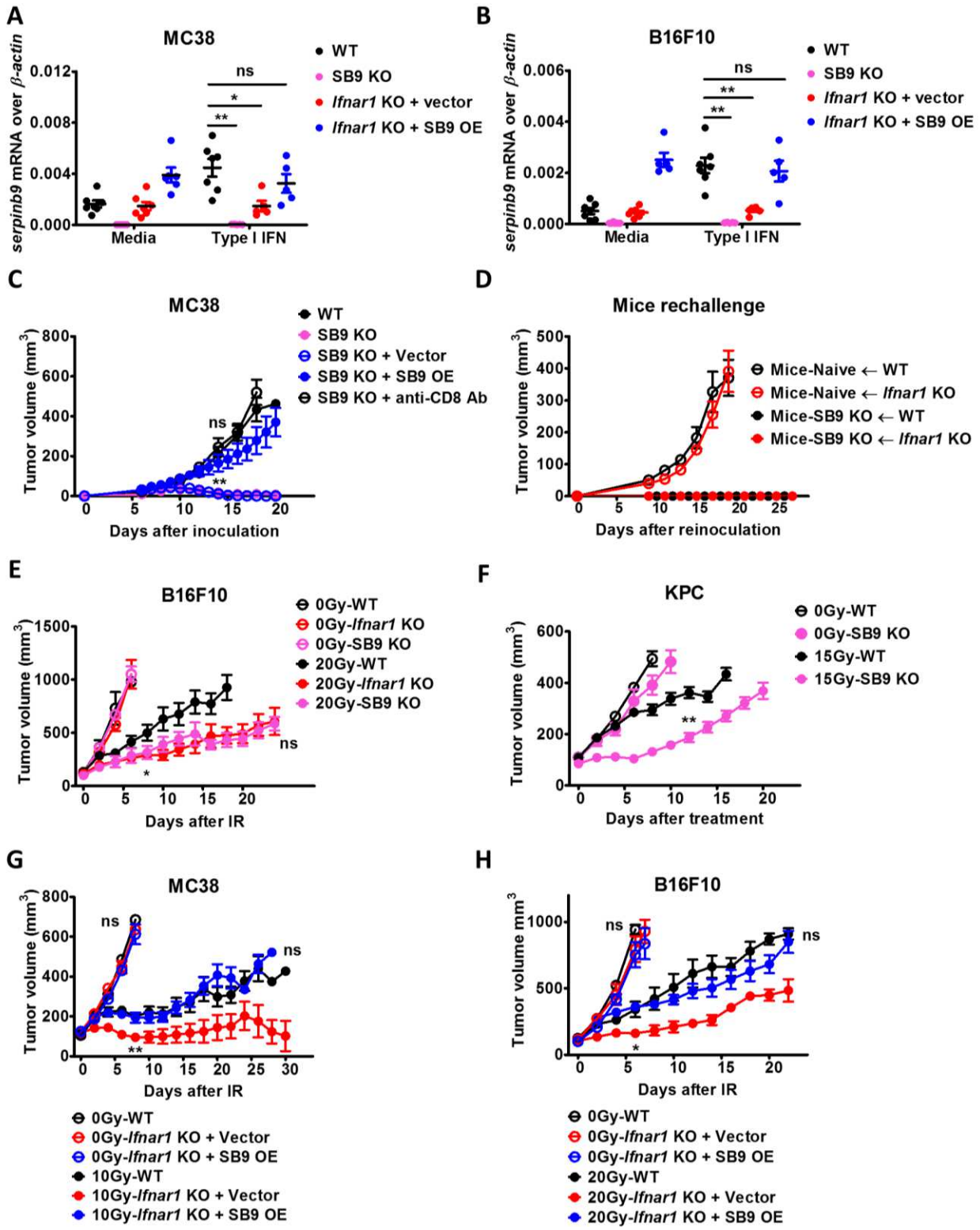

A
MC38
serpinb9 mRNA over β-actin
0.012
0.008
0.004
0.000
ns
*
**
Media
Type I IFN
WT
SB9 KO
Ifnar1 KO + vector
Ifnar1 KO + SB9 OE
B
B16F10
serpinb9 mRNA over β-actin
0.006
0.004
0.002
0.000
ns
**
**
Media
Type I IFN
WT
SB9 KO
Ifnar1 KO + vector
Ifnar1 KO + SB9 OE
C
MC38
Tumor volume (mm3)
800
600
400
200
0
ns
**
0 5 10 15 20
Days after inoculation
WT
SB9 KO
SB9 KO + Vector
SB9 KO + SB9 OE
SB9 KO + anti-CD8 Ab
D
Mice rechallenge
Tumor volume (mm3)
500
400
300
200
100
0
0 5 10 15 20 25
Days after reinoculation
Mice-Naive ← WT
Mice-Naive ← Ifnar1 KO
Mice-SB9 KO ← WT
Mice-SB9 KO ← Ifnar1 KO
E
B16F10
Tumor volume (mm3)
1500
1000
500
0
ns
*
0 5 10 15 20
Days after IR
0Gy-WT
0Gy-Ifnar1 KO
0Gy-SB9 KO
20Gy-WT
20Gy-Ifnar1 KO
20Gy-SB9 KO
F
KPC
Tumor volume (mm3)
600
400
200
0
**
0 5 10 15 20
Days after treatment
0Gy-WT
0Gy-SB9 KO
15Gy-WT
15Gy-SB9 KO
G
MC38
Tumor volume (mm3)
800
600
400
200
0
ns
ns
**
0 5 10 15 20 25 30
Days after IR
0Gy-WT
0Gy-Ifnar1 KO + Vector
0Gy-Ifnar1 KO + SB9 OE
10Gy-WT
10Gy-Ifnar1 KO + Vector
10Gy-Ifnar1 KO + SB9 OE
H
B16F10
Tumor volume mm3
1000
500
0
ns
ns
*
0 5 10 15 20
Days after IR
0Gy-WT
0Gy-Ifnar1 KO + Vector
0Gy-Ifnar1 KO + SB9 OE
20Gy-WT
20Gy-Ifnar1 KO + Vector
20Gy-Ifnar1 KO + SB9 OE

Figure 7. *Serpinb9* is a mediator for the enhanced response of *Ifnar1* KO tumors to IR. MC38 and B16F10 cells (4 phenotypes for each cell line: WT, *Serpinb9* KO, *Ifnar1* KO + vector, *Ifnar1* KO + *SerpinB9* expression (SB9 OE) were stimulated with control media or type I IFN (50 U/ml) for 4 hours. The expression of *Serpinb9* was assessed with data summarized in **(A)** and **(B)**. N = 5-7. The growth of WT, SB9 KO (with or without CD8 T cell depletion), SB9 KO + vector and SB9 KO + SB9 OE MC38 tumors were plotted in **(C)**. N = 6-8. C57BL/6 mice, with complete regression of SB9 KO MC38 tumors, were rechallenged with 1 x 10^5 WT or *Ifnar1* KO MC38 cells on the opposite flank. The growth of tumors following reinoculation was plotted in **(D)** along with growth data of WT and *Ifnar1* KO MC38 tumors in naïve mice from **Figure 2G**. N = 4-6. The volumes of B16F10 tumors (WT, *Ifnar1* KO and SB9 KO) following 0Gy or 20Gy IR are shown in **(E)**. N = 6-7. 20Gy-WT vs 20Gy-SB9 KO: *. 20Gy-*Ifnar1* KO vs 20Gy-SB9 KO: ns. The volumes of KPC tumors (WT and SB9 KO) following 0Gy (n = 5-7) or 15Gy (n = 5-6) are shown in **(F)**. MC38 and B16F10 tumors (WT, *Ifnar1* KO + vector and *Ifnar1* KO + SB9 OE) grown in C57BL6 mice were treated with 0Gy or 10Gy IR for MC38 and 20Gy IR for B16F10. Tumor growth is shown in **(G)** and **(H)**. N = 5-6. Data represent mean ± SD in **(A)** and **(B)**, and mean ± SEM in **(C-H)**. Comparison of two means was performed by the Mann-Whitney U test (ns: $P > 0.05$, * $P < 0.05$, ** $P < 0.01$, *** $P < 0.001$).

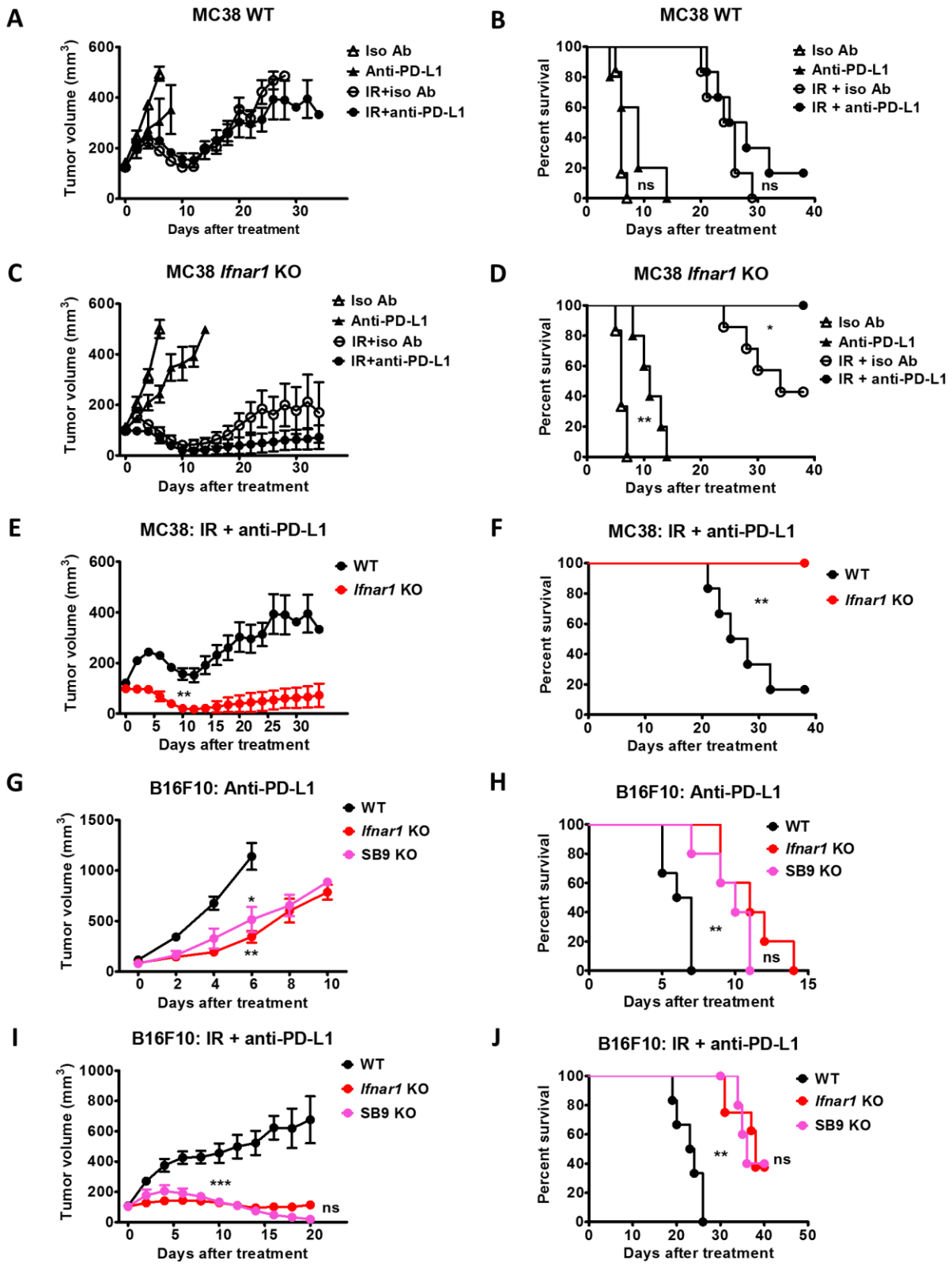

A
MC38 WT
Tumor volume (mm3)
Days after treatment
Iso Ab
Anti-PD-L1
IR+iso Ab
IR+anti-PD-L1
B
MC38 WT
Percent survival
Days after treatment
Iso Ab
Anti-PD-L1
IR + iso Ab
IR + anti-PD-L1
ns
ns
C
MC38 Ifnar1 KO
Tumor volume (mm3)
Days after treatment
Iso Ab
Anti-PD-L1
IR+iso Ab
IR+anti-PD-L1
D
MC38 Ifnar1 KO
Percent survival
Days after treatment
Iso Ab
Anti-PD-L1
IR + iso Ab
IR + anti-PD-L1
*
**
E
MC38: IR + anti-PD-L1
Tumor volume (mm3)
Days after treatment
WT
Ifnar1 KO
**
F
MC38: IR + anti-PD-L1
Percent survival
Days after treatment
WT
Ifnar1 KO
**
G
B16F10: Anti-PD-L1
Tumor volume (mm3)
Days after treatment
WT
Ifnar1 KO
SB9 KO
*
**
H
B16F10: Anti-PD-L1
Percent survival
Days after treatment
WT
Ifnar1 KO
SB9 KO
**
ns
I
B16F10: IR + anti-PD-L1
Tumor volume (mm3)
Days after treatment
WT
Ifnar1 KO
SB9 KO
***
ns
J
B16F10: IR + anti-PD-L1
Percent survival
Days after treatment
WT
Ifnar1 KO
SB9 KO
**
ns

Figure 8. *Ifnar1* KO or *SerpinB9* KO tumors exhibited greater levels of response to anti-PD-L1 with or without IR than WT tumors. C57BL/6 mice bearing subcutaneous WT or *Ifnar1* KO MC38 tumors were subjected to the following treatments: (1) isotype control Ab; (2) anti-PD-L1 Ab (3) 10 Gy IR on day 0 plus isotype control Ab; (4) 10 Gy IR plus anti-PD-L1 Ab. Ab was administrated on days -1, 3, 7 and 11. Tumor volumes are shown in **(A)**, **(C)** and **(E)**; Kaplan-Meier survival curves of mice in **(B)**, **(D)** and **(F)**. N = 5-7. C57BL/6 mice bearing subcutaneous WT, *Ifnar1* KO or *Serpinb9* (SB9) KO B16F10 tumors received anti-PD-L1 Ab on day -1, 3, 7 and 11 with or without 20 Gy IR on day 0. Tumor growth and survival were summarized in **(G)** and **(J)**. N = 5-8. Data represent mean ± SEM. Comparison of two means was performed with the Mann-Whitney U test. Survival comparisons between groups were performed using the log-rank's test (ns: $P > 0.05$, * $P < 0.05$, ** $P < 0.01$, *** $P < 0.001$).